

Interactions of Native and Modified Clupeine with *Escherichia coli* K-12 and
Salmonella enterica serovar Typhimurium 14028 Cells and Model
Biomembranes

by

Marcia Michelle English

Submitted in partial fulfilment of the requirements
for the degree of Doctor of Philosophy

at

Dalhousie University
Halifax, Nova Scotia
November 2017

© Copyright by Marcia Michelle English, 2017

DEDICATION PAGE

'All power, all wisdom, are at our command. We have only to ask' MH pg. 514

Dedicated to Daniel, Nell and Ann

TABLE OF CONTENTS

LIST OF TABLES	viii
LIST OF FIGURES	x
ABSTRACT	xv
LIST OF ABBREVIATIONS AND SYMBOLS USED	xvi
ACKNOWLEDGEMENTS	xviii
CHAPTER 1: INTRODUCTION	1
1.1 The Problem of Antibiotic Resistance	3
1.2 Mechanisms of Bacterial Resistance.....	5
1.3 Cationic Antimicrobial Peptides (CAPs)	7
1.4 Mechanisms of Actions of Cationic Antimicrobial Peptides.....	8
1.5 Clupeine as a Model CAP	11
1.6 Parameters that Determine the Antimicrobial Activity of Clupeine	12
1.6.1 Hydrophobicity	12
1.6.2 Amphipathicity	13
1.6.3 Charge.....	13
1.7 Advantages of CAPs over Conventional Antibiotics.....	14
1.8 Synthesis of Peptides.....	15
1.9 Chemical Modification of Proteins	16
1.10 The Chemical Properties of Protamine	17
1.11 Protamine Modifications	18
1.11.1 Lipophilization of Proteins including Protamine.....	18
1.12 The Reaction of Arginine with CHD	19
1.13 Background on Experimental Techniques	20
1.14 Surface Pressure Measurements.....	21
1.15 Neutron Reflectometry Technique	24
1.16 X-Ray Reflectivity (XRR) Technique.....	30

1.17	Langmuir-Blodgett (LB) and Langmuir-Schaefer (LS) Deposition	33
1.17.1	Porins	35
1.17.2	The Importance of Efflux Pumps.....	39
1.18	Quantitative Real-Time Polymerase Chain Reaction (qPCR)	40
1.19	Research Questions and Objectives	42
1.20	Scope of the Thesis	44
CHAPTER 2: THE CHARACTERIZATION OF NATIVE AND CHD-TREATED CLUPEINE		46
2.1	Abstract	46
2.2	Introduction	47
2.3	Materials and Methods.....	50
2.4	Methods.....	50
2.4.1	Clupeine Modification with CHD.....	50
2.4.2	Detection of Clupeine Modification	51
2.4.3	Determination of the Hemolytic Activity of Clupeine	52
2.4.4	Determination of Minimum Inhibitory Concentration (MIC)	53
2.4.5	Scanning Electron Microscopy.....	54
2.4.6	Amino Acid Analysis of Native and CHD-Treated Clupeine	55
2.5	Results	56
2.5.1	Identification of CHD-Treated Clupeine	56
2.5.2	Cytotoxicity of Native and CHD-Treated Clupeine	58
2.5.3	Morphology of <i>E. coli</i> K-12 and <i>S. enterica</i> Typhimurium 14028 Cells ...	59
	in the Presence of Native and CHD-Treated Clupeine.....	59
2.6	Discussion	61
CHAPTER 3: qPCR AND PROTEOMIC ANALYSIS of <i>E. coli</i> and <i>S. enterica</i> TYPHIMURIUM 14028 CELLS in THE PRESENCE of NATIVE and CHD-TREATED CLUPEINE		68
3.1	Abstract	68
3.2	Introduction	69

3.3	Materials and Methods	73
3.3.1	Strains, Media and Growth Conditions.....	73
3.3.2	Preparation of Cell Cultures for RNA Extraction.....	73
3.3.3	Extraction of Ribonucleic Acid (RNA)	75
3.3.4	Formation of Complementary Deoxyribonucleic Acid (cDNA)	76
	Libraries.....	76
3.3.5	Primer Design	77
3.3.6	Primer Verification	78
3.3.7	Validation of Reference Genes	79
3.3.8	qPCR Linear Dynamic Range and Amplification Efficiencies	80
3.3.9	qPCR.....	82
3.3.10	qPCR Data Analysis	83
3.3.11	Statistical Analysis.....	85
3.3.12	Bacterial Strains, Growth Conditions and Preparation of Cell Envelopes .	85
3.3.13	Preparation of Cells for Porin Extraction.....	85
3.3.14	Outer Membrane Preparation.....	85
3.3.15	Purification of Porin Extracts.....	88
3.3.16	SDS-PAGE	89
3.3.17	In-Gel Digestion for Mass Spectrometry	90
3.3.18	Mass Spectrometry.....	92
3.3.19	Lowry Assay	92
3.4	Results	93
3.4.1	Relative Expression of <i>E. coli</i> Porin Genes in Cells Treated with Native..	93
	or CHD-Treated Clupeine	93
3.4.2	Relative Expression of Porin Genes in <i>S. enterica</i> Typhimurium 14028	
	Cells 95	
	Treated with Native or CHD-Treated Clupeine	95
3.4.3	Porin Protein Profiles Obtained by SDS-PAGE	97
3.5	Discussion	101

CHAPTER 4: INTERACTIONS OF NATIVE AND CHD- TREATED CLUPEINE WITH GRAM-NEGATIVE MODEL MONOLAYERS 112

4.1	Abstract	112
-----	----------------	-----

4.2	Introduction	113
4.3	Materials and Methods	117
4.3.1	Materials	117
4.3.2	Surface Pressure Measurements	117
4.3.3	Neutron Reflectometry Measurements on PE:PG:CL	118
4.3.4	X-Ray Reflectometry Measurements on PE:PG:CL.....	120
4.3.5	Reflectivity Data Analysis	121
4.4	Results	123
4.4.1	Adsorption of native and CHD-Treated Clupeine to PE:PG:CL	123
	(79:17:4 mole %) and DPPG monolayers	123
4.4.2	The Structure of Native and CHD-Treated Clupeine Adsorbed to.....	127
	PE:PG:CL (79:17:4 mole %) Monolayers.....	127
4.5	Discussion	137
CHAPTER 5: INTERACTIONS OF NATIVE AND CHD-TREATED CLUPEINE WITH GRAM-NEGATIVE MODEL BILAYERS		146
5.1	Abstract	146
5.2	Introduction	147
5.3	Materials and Methods	148
5.3.1	Materials	148
5.3.2	Bilayer Deposition and Neutron Reflectometry Measurements	149
5.3.3	Reflectivity Data Analysis	151
5.3.4	Bilayer NR Data Analysis:.....	151
5.4	Results	154
5.5	Discussion	171
5.6	Summary of Biomembrane Experiments	179
CHAPTER 6: CONCLUSION.....		181
6.1	Summary and Conclusions.....	181
6.2	Recommendations for Future Work.....	183
6.3	Final Comments	185

REFERENCES	187
APPENDICES	217
Appendix A: q-PCR	217
Appendix B: Buffers and Reagents for Porin Protein Extraction	221
Appendix C: NR and XRR	224
Appendix D: Bilayer Experiments	229
Appendix E: Data Fitting	233

LIST OF TABLES

Table 1-1 Features of the major outer membrane proteins in <i>E. coli</i> K-12 and <i>S. enterica</i> Typhimurium.....	37
Table 2-1 Percent modification of CHD-treated clupeine and control samples. The absorbance values of the control were subtracted from those of the test samples before the percent modification was calculated.....	57
Table 2-2 Relative abundance of amino acid residues that were different in native and CHD- treated clupeine, determined by amino acid analysis.....	57
Table 2-3 Cytotoxicity of native and CHD-treated clupeine on human red blood cells. The data shown are the averages of three separate experiments and the concentrations shown represent mean values \pm SD (n=3).....	58
Table 2-4 The effect of native and CHD-treated clupeine on the MIC and MBC values of <i>E. coli</i> K-12 cells (strain MG 1655) and <i>S. enterica</i> Typhimurium 14028 cells.....	58
Table 3-1 A summary of the target genes and reference genes (<i>rpoB</i>) used in this study and their corresponding GenBank Accession Numbers and coding regions obtained from the NCBI database.....	77
Table 3-2 Annealing temperatures of the primers used for q-PCR of outer membrane porin (<i>omp</i>) genes in <i>E. coli</i> K-12 (strain MG1655) and <i>S. enterica</i> Typhimurium (strain 14028).....	79
Table 3-3 Summary of <i>E. coli</i> K-12 and <i>S. enterica</i> Typhimurium 14028 porin proteins identified by mass spectrometry. The number of peptides detected in the trypsin gel digests were used as an indicator of the relative abundance of the proteins identified.....	100
Table 3-4 Additional proteins identified by mass spectrometry. The number of peptides detected in the trypsin gel digests were used as an indicator of the relative abundance of the proteins identified.....	101
Table 4-1 Summary of the calculated scattering lengths, scattering length densities, molecular weights, and molecular volumes of the lipids (PE:PG:CL, 79:17:4 mole %) and peptides used in this thesis.....	128
Table 4-2 Structural parameters obtained from a two-layer model fit of a condensed phase d-PE:PG:CL monolayer obtained from simultaneously fitting NR and XRR profiles. The structural parameters described for each layer are the layer thickness (τ), the SLD (ρ) and the corresponding layer roughness. The fits were repeated three times.....	130
Table 4-3 Structural parameters obtained from the three layer model fits of 0.48 μ M native clupeine adsorbed to PE:PG:CL monolayers. The fits were repeated three times.....	134

Table 4-4	Parameters obtained from the best three layer model fits of 0.48 μM CHD-treated clupeine adsorbed to PE:PG:CL monolayers. The fits were repeated three times.	136
Table 5-1	Summary of the calculated scattering lengths, SLDs, molecular weights and molecular volumes and the ratios of PE:PG:CL (79:17:4 mole %) and native and CHD- treated clupeine used in this thesis.	155
Table 5-2	The SLDs of the solvents and solution sub-phases used in this thesis.	155
Table 5-3	Summary of structural parameters obtained for an asymmetrically deposited d-DPPC (inner leaflet) <i>E. coli</i> PE:PG:CL (outer leaflet) bilayer deposited on a silicon surface. These fits were repeated three times.	159
Table 5-4	Parameters derived from fitting the bare h-DPPC:h-PE:PG:CL lipids. These fits were repeated three times.....	161
Table 5-5	Parameters derived from fitting h-DPPC:h-PE:PG:CL lipids in the presence of native clupeine.....	165
Table 5-6	Parameters derived from fitting h-DPPC:h-PE:PG:CL bilayer lipids with CHD-treated clupeine.	165
Table 5-7	Best fit values and error estimates of asymmetrically deposited bare h-DPPC (inner leaflet) <i>E. coli</i> PE:PG:CL (outer leaflet) bilayer deposited on a silicon surface and the bilayer in the presence of native and CHD-treated clupeine.....	170

LIST OF FIGURES

Figure 1-1 Mechanisms used by bacteria to avoid therapeutic antibiotics.	6
Figure 1-2 Number of publications from 2005-2014 in the Web of Science core collection with Cationic Antimicrobial Peptides in the title of the article (http://apps.webofknowledge.com.ezproxy.library.dal.ca).	8
Figure 1-3 The amino acid sequence which is a mixture of the three peptides chains YI, YII and Z. Key: A = alanine; R = arginine; S = serine; T = threonine; G = glycine; V = valine; P = proline; I = isoleucine (Adapted from Ishimura et al., 1991).	12
Figure 1-4 The structure of the major lipids in <i>E. coli</i> and <i>S. enterica</i> Typhimurium. (A) L- α phosphatidylethanolamine, PE, MW = 691.97 g/mol, neutral or Zwitterionic; (B) L- α -phosphatidylglycerol, PG, MW = 744.96 g/mol, anionic; (C) Cardiolipin, Cl, MW = 1285.62 g/mol, anionic. Structures adapted from Avanti Polar Lipids (www.avantilipids.com). The sections of the lipids in the coloured boxes represent the head groups.	23
Figure 1-5 Setup for the formation of monolayers at the air-water interface.	23
Figure 1-6 Surface pressure versus area per molecule of a hypothetical monolayer. Three main phases and level of re-ordering observed at each phase are shown, GE = the gas-extended phase; LE = the liquid-extended and C = the condensed phase. Reprinted from He and Li (2007), (reproduced with permission from Elsevier).	24
Figure 1-7 Schematic showing a pulsed beam of neutrons as it undergoes specular reflection from a sample surface. Reprinted from Clifton et al. (2013a), (reproduced with permission from Springer).	26
Figure 1-8 A simplified neutron reflectivity diagram showing the incident and reflected beams at an interface. In a typical NR experiment, the neutron beam is directed at the interface at an incident angle, θ . The reflectivity of the reflected beam is measured as a function of the momentum change perpendicular to the surface, $Q_z = 4\pi \lambda \sin(\theta)$ and is defined as the ratio of the intensity of the reflected beam to that of the incident beam. The structure across the interface is modeled as a series of layers 0 to n and each layer is usually characterized by its scattering length density (SLD), its thickness, d (Å) and its surface roughness (Å).	27
Figure 1-9 Incident and reflected x-rays on a liquid monolayer.	31

Figure 1-10 Schematic representation of the arrangement of the double crystal deflector (DCD), the diffractometer and the detector (P 100k) used at the 107 beamline at Diamond Light Source (Oxfordshire, UK). The sample is placed on the hexapod located in the center of the diffractometer which then tracks the deflected beam. The DCD uses two different crystals, C1 (111) and C2 (220) to achieve an overall deflection. Rotation of these crystals around the incident beam allows the angle of incidence to be varied. Reprinted from Arnold et al. (2012), (reproduced with permission from the <i>International Union of Crystallography</i>).	32
Figure 1-11 Schematic diagram of the Gram-negative bacterial membrane. LPS represents lipopolysaccharide, PL represents phospholipid and PG represents peptidoglycan. Reprinted from Chatterjee and Chaudhuri (2012), (reproduced with permission from Springer).	34
Figure 1-12 The transfer of a monolayer onto a silicon block (wafer) using the standard Langmuir-Blodgett technique (A) and the standard Langmuir-Schaefer technique (B). Reprinted from Burn et al. (2016), (reproduced with permission from Elsevier).	35
Figure 1-13 Neutron flow cell, with inlet and outlet tubes, used in this study.	35
Figure 1-14 (A) The three-dimensional structure of <i>E. coli</i> OmpF porin (side view); (B), shows a top view of the trimer. Reprinted from Galdiero et al. (2012), (reproduced with permission from <i>Current Protein and Peptide Science</i>).	38
Figure 1-15 Schematic diagram of <i>ompF</i> and <i>ompC</i> porin gene regulation in <i>E. coli</i> and <i>S. enterica</i> Typhimurium. EnvZ is a histidine kinase that modulates the activity of the DNA-binding protein OmpR via phosphorylation. The <i>micF</i> gene is also involved in the post-transcriptional regulation of <i>ompF</i> (Adapted from Pratt et al., 1996).	39
Figure 1-16 Amplification plot showing the accumulation of amplified product as a qPCR reaction progresses. The number of PCR cycles is shown on the x-axis, and the fluorescence intensity, which is proportional to the amount of sample in the tube is shown on the y-axis (http://www.garvan.org.au). ...	42
Figure 2-1 Scheme for the chemical modification of clupeine through the chemical reaction between CHD and the guanido groups of arginine. Reprinted from Potter et al. (2005), (reproduced with Permission from Elsevier).	48
Figure 2-2 Scanning electron micrographs of images of untreated and native clupeine (A) <i>E. coli</i> K-12 and (B) <i>S. enterica</i> Typhimurium 14028 cells.	60
Figure 2-3 Scanning electron micrographs of untreated and CHD-treated (A) <i>E. coli</i> K-12 and (B) <i>S. enterica</i> Typhimurium 14028 cells.	60
Figure 3-1 Work flow for the extraction of porin proteins from <i>E. coli</i> K-12 and <i>S. enterica</i> Typhimurium 14028 cells exposed to native or CHD-treated clupeine (adapted from Garavito and Rosenbusch, 1986).	87

Figure 3-2 Mean relative expression ratios (R values) of <i>ompF</i> expressed in <i>E. coli</i> K-12 cells treated with native clupeine (A) and CHD-treated clupeine (C) and <i>ompC</i> gene in <i>E.coli</i> K-12 cells treated with native clupeine (B) and CHD-treated clupeine (D), (n=3, error bars show the standard deviation) (**P < 0.01; *P < 0.05).....	94
Figure 3-3 Mean relative expression ratios (R values) of <i>ompT</i> gene expressed in <i>E.coli</i> K-12 cells treated with native clupeine (A) and CHD-treated clupeine (B), (n=3, error bars show the standard deviation) (** P < 0.01; * P < 0.05).....	95
Figure 3-4 Mean relative expression ratios (R values) of <i>ompF</i> expressed in <i>S. enterica</i> Typhimurium 14028 cells treated with native clupeine (A) and CHD-treated clupeine (B), (n=3, error bars show the standard deviation) (**P < 0.01; *P < 0.05).....	96
Figure 3-5 Mean relative expression ratios (R values) of <i>ompC</i> in <i>S. enterica</i> Typhimurium 14028 cells treated with native (A) and CHD-treated clupeine (B), (n=3, error bars show the standard deviation) (**P < 0.01; *P < 0.05).	97
Figure 3-6 Outer membrane porin proteins of <i>E. coli</i> K-12 separated on 15% SDS-PAGE. Lane 1, protein marker, lane 2, untreated <i>E. coli</i> ; lanes 3, 4, and 5 proteins from cells treated with 500, 1000 and 1250 µg/mL native clupeine respectively; lanes 6, 7 and 8, proteins from cells treated with 400, 1000 and 1250 µg/mL CHD-treated clupeine, respectively. Lane 9 was the double mutant control. (n=3).....	98
Figure 3-7 Outer membrane porin proteins of <i>S. enterica</i> Typhimurium 14028 separated on 15% SDS-PAGE. Lane 1, protein marker, lane 2, untreated <i>S. enterica</i> Typhimurium 14028; lanes 3, 4, and 5 proteins from cells treated with 500, 1250 and 2500 µg/mL native clupeine respectively; lanes 6, 7 and 8, proteins from cells treated with 500, 1250 and 2500 µg/mL CHD-treated clupeine, respectively. Lane 9 was the double mutant control. (n=3).....	99
Figure 4-1 (A) Surface pressure versus area per molecule plot of a compressed PE:PG:CL mole% (79:17:4) monolayer. (B) Similar plot for a compressed DPPG monolayer. The three main transition phases shown are the gaseous extended (GE), the liquid extended (LE) and the condensed phases.....	125
Figure 4-2 (A) Surface pressure versus time plot for charge-reduced clupeine adsorbed on a DPPG monolayer (control). Two replicates are shown; (B) Stability check for the PE:PG:CL monolayer without the peptide and native and CHD-treated clupeine adsorbed at the air/water interphase of a PE:PG:CL monolayer. These experiments were repeated twice.	126
Figure 4-3 (A) Reflectivity of the d-PE:PG:CL monolayer is plotted against Q_z (\AA^{-1}), the momentum transfer. The continuous black line represents the simulated model data whereas the experimental data are shown in red with error bars. (B) The corresponding real space SLD profile as a function of distance from the interface.....	129

- Figure 4-4** (A) Reflectivity of PE:PG:CL lipid monolayer in NRW with adsorbed native clupeine on the deuterated lipid in (red) and the hydrogenated lipid in (black) is plotted against Q_z (\AA^{-1}), the momentum transfer. The bare lipid with no peptide is shown in blue and the experimental data are represented with error bars whereas the best fit simulated data are represented as continuous lines. The SLD profile as a function of distance from the interface as determined from the fit is shown in (B). 132
- Figure 4-5** (A) Reflectivity of PE:PG:CL monolayer in NRW with adsorbed CHD-treated clupeine on the deuterated lipid in (purple) and the hydrogenated lipid in (black). The bare lipid with no peptide is shown in blue and the experimental data are represented with error bars whereas the best fit simulated data are represented as lines. The SLD profile as a function of distance from the interface as determined from the fit is shown in (B). 133
- Figure 4-6** (A) XRR profile of PE:PG:CL monolayer (black) with adsorbed native clupeine on the deuterated lipid in (green). The data are represented with error bars whereas the best fits are represented as lines. The SLD profile as a function of distance from the interface as determined from the fit is shown in (B). 135
- Figure 4-7** (A) XRR profile of PE:PG:CL monolayer (black) with adsorbed native clupeine on the deuterated lipid (orange). The data are represented with error bars whereas the best fits are represented as lines. The SLD profile as a function of distance from the interface as determined from the fit is shown in (B). 137
- Figure 5-1** The structure of deuterated DPPC showing the alkyl chain region and the lipid head group containing the acyl carbonyls and the phosphate group... 151
- Figure 5-2** (A) The surface pressure area isotherm for DPPC used for the inner layer of the bilayer and (B) represents the surface pressure to area curve for PE:PG:CL mole% (79:17:4) used for the outer layer of the model bilayer prior to clupeine adsorption. The three typical phases shown are the gaseous extended phase (GE), the liquid extended phase (LE) and the condensed (C) phase. 156
- Figure 5-3** The SLD profile obtained from the bare d-DPPC:h-PE:PG:CL lipid contrasts in d-D₂O (black), d-SMW (blue) and d-H₂O (red) and the h-DPPC:h-PE:PG:CL lipid contrasts h-D₂O (orange), h-SMW (aqua blue) and h-H₂O (purple). 156
- Figure 5-4** Reflectivity profile of bare d-DPPC:h-PE:PG:CL bilayer lipids in three contrasts, D₂O (black), SMW (red) and H₂O (blue) and the corresponding fits as lines, D₂O (purple), SMW (black), and H₂O (black). 158
- Figure 5-5** Reflectivity profile of bare h-DPPC:h-PE:PG:CL lipids in three contrasts; D₂O (blue), SMW (red) and H₂O (grey). The corresponding fits are shown as lines; D₂O (black), SMW, (black), and H₂O, (black). 160

Figure 5-6 (A) Reflectivity profile of bare h-DPPC:h-PE:PG:CL bilayer lipids D ₂ O (blue), SMW (red) and H ₂ O (grey) and the corresponding fits all in black. (B) Native clupeine in three contrasts, D ₂ O (gray), SMW (red) and H ₂ O (black). The corresponding fits are shown as lines, D ₂ O (black), SMW (black), and H ₂ O (blue).....	162
Figure 5-7 (A) Reflectivity profile of bare h-DPPC:h-PE:PG:CL bilayer lipids D ₂ O (blue), SMW (red) and H ₂ O (grey) and the corresponding fits, all in black. (B) Reflectivity profile of h-DPPC:h-PE:PG:CL bilayer lipids and CHD-treated clupeine in three contrasts, D ₂ O (gray), SMW (blue) and H ₂ O (pink). The corresponding model fits are shown as lines, all in black.....	163
Figure 5-8 A comparison of the SLD profiles obtained for the bare h-DPPC:h-PE:PG:CL bilayer lipids (A) and in the presence of native clupeine (B)....	166
Figure 5-9 A comparison of the SLD profiles obtained for the bare h-DPPC:h-PE:PG:CL bilayer lipids (A) and in the presence of CHD-treated clupeine (B).	167
Figure 5-10 A comparison of the reflectivity curve obtained for the bare h-DPPC:h-PE:PG:CL bilayer lipids in H ₂ O in the presence of native clupeine in H ₂ O. The data are plotted as points with error bars and the fits are represented as a blue line (A). The corresponding SLD profiles that represent these data are shown in 5-10 (B).....	168
Figure 5-11 A comparison of the reflectivity curve obtained for the bare h-DPPC:h-PE:PG:CL bilayer lipids in H ₂ O in the presence of the CHD-treated clupeine. The data are plotted as points with error bars and the fits are represented as a black line (A). The corresponding SLD profiles that represent these data are show in 5-11 (B).....	169

ABSTRACT

Clupeine, a cationic antimicrobial peptide found in the sperm cells of fish, is of interest as a food additive because of its antimicrobial activity against several foodborne pathogens. However, it has previously been shown that non-specific binding of clupeine to anionic molecules reduces its antimicrobial activity. It has also been shown that the overall positive charge of the native peptide can be reduced by blocking 10% of its arginine residues with 1,2-cyclohexanedione (CHD) to form CHD-treated clupeine. CHD-treated clupeine retains antimicrobial activity but it is not known if the modes of interaction against Gram-negative bacteria remain the same as the native peptide. The focus of this study was to investigate the effect of charge reduction on antimicrobial activity and peptide membrane interactions by comparing the effect of native and CHD-treated clupeine on *Escherichia coli* K-12 and *Salmonella enterica* susp. *enterica* serovar Typhimurium 14028 cells and in model biomembranes.

The minimum inhibitory concentrations (MIC) of the two peptides were determined using the Alamar blue assay. *E. coli* K-12 cells were more susceptible to native (MIC, 500 µg/mL) and CHD-treated (MIC, 400 µg/mL) clupeine than *S. enterica* serovar Typhimurium 14028 cells (MIC, 1250 µg/mL for both peptides). Scanning electron microscopy (SEM) revealed no bacterial cell lysis, however, some cells appeared more elongated in the presence of CHD-treated clupeine. The relative expression of the outer membrane porin gene *ompF* was down-regulated in *E. coli* K-12 cells exposed to native or CHD-treated clupeine, which was in strong contrast to the up-regulation ($P < 0.05$) of this gene observed when *S. enterica* serovar Typhimurium 14028 cells were exposed to minimum bactericidal concentrations (2500 µg/mL) of both peptides. Increased expression of the outer membrane porin protein OmpA, was identified by mass spectroscopy and the oxidative stress-related glyceraldehyde-3-phosphate dehydrogenase (GapA) protein was only observed when test strains were exposed to the CHD-treated peptide.

Model biomembranes composed of lipids used to mimic the inner membrane of *E. coli* (PE, phosphatidylethanolamine: PG, phosphatidylglycerol: and CL, cardiolipin), in the following ratios: PE:PG:CL (79:17:4 mole %) were studied using Neutron Reflectometry (NR) and X-ray reflectometry (XRR). Symmetric bilayers were deposited on silicon blocks applying the Langmuir-Blodgett and Schaefer technique. Some lipid mixing was observed in the inner tail region ($\sim 69 \pm 0.24\%$ DPPC (1,2-dipalmitoyl (d62)-sn-glycero-3-phosphocholine) and $\sim 24 \pm 0.02\%$ PE:PG:CL); and in the outer tail region ($\sim 24 \pm 0.02\%$ DPPC and $\sim 56 \pm 0.01\%$ PE:PG:CL). Native and CHD-treated clupeine were not able to cross the model PE:PG:CL:DPPC bilayer biomembrane, however, CHD-treated clupeine showed increased interactions with the lipid head group.

Although the CHD-treated clupeine interacted differently with the test strains and the model biomembranes compared to the native peptide, a more comprehensive

understanding of the safety and toxicology of these peptide is required before they can be considered for food applications in Canada.

LIST OF ABBREVIATIONS AND SYMBOLS USED

ACMW	Air Contrast Matched Water
AMU	Atomic Mass Unit
ANOVA	One Way Analysis of Variance
BAM	Brewster Angle Microscopy
BLAST	Basic Local Alignment Search Tool
Bp	Base pair
C	Condensed
CAP	Cationic Antimicrobial Peptide
CCD	Charge Coupled Device
CFU	Colony Forming Units
CHD	1,2-Cyclohexanedione
CL	Cardiolipin
cDNA	Complementary Deoxyribonucleic Acid
C _q	Quantification Cycle
DCD	Double Crystal Deflector
DDW	Distilled Deionized Water
DLS	Dynamic Light Scattering
DNA	Deoxyribonucleic Acid
dNTPs	Deoxynucleotides
DPC	Dodecylphosphocholine
DPPC	1,2-dipalmitoyl-sn-glycero-3-phosphocholine
FPLC	Fast Protein Liquid Chromatography
GapA	Glyceraldehyde-3-phosphate dehydrogenase
GE	Gas Extended
G6PDH	Glucose-6-phosphate-1-dehydrogenase
IM	Inner Membrane
InSb	Indium Antimonide
LB	Langmuir-Blodgett
LC/ESI-IT	Liquid Chromatography-Electrospray Ionization-Ion Trap
LC/MS	Liquid Chromatography Mass Spectrometry
LE	Liquid Extended
LOD	Limit of Detection
LOQ	Limit of Quantification
LPS	Lipopolysaccharide
LS	Langmuir-Schaefer
Lu-B	Luria-Bertani
MBC	Minimum bactericidal concentration

MIC	Minimum inhibitory concentration
mRNA	messenger Ribonucleic Acid
MPN	Most Probable Number
MS/MS	Tandem Mass Spectrometry, or Mass Spectrometry/ Mass Spectrometry
MTT	3-[4,5 dimethyliazol-2-yl]-2,5-diphenyl tetrazolium bromide
NA	Nutrient Agar
NAD	Nicotinamide adenine dinucleotide
NB	Nutrient Broth
NR	Neutron Reflectometry
NRW	Non-Reflective Water
OM	Outer Membrane
Omp	Outer Membrane Porin
OsO ₄	Osmium Tetroxide
PBS	Phosphate Buffered Saline
PE	L- α -phosphatidylethanolamine
PG	L- α -phosphatidylglycerol
PS	Peptone Saline
qPCR	Quantitative Real-Time Polymerase Chain Reaction
RNA	Ribonucleic Acid
<i>rpoB</i>	RNA polymerase β -subunit
16S rRNA	16 S ribosomal Ribonucleic Acid
R	Relative Expression Ratio
RT	Reverse Transcriptase
SDS-PAGE	Sodium Dodecyl Sulfate- Polyacrylamide Gel Electrophoresis
SEM	Scanning Electron Microscopy
SLD	Scattering Length Density
TSA	Tryptic Soy Agar
TSB	Tryptic Soy Broth
UV	Ultra Violet
XXR	X-Ray Reflectivity

ACKNOWLEDGEMENTS

First I would like to thank my thesis supervisor Dr. Allan Paulson for his guidance and support throughout my graduate studies. I am also very grateful for the guidance and mentorship that I have received from my other committee members, Dr. Tom Gill and Dr. Paul Gratzner. This has been an exciting journey and I am grateful for all the experiences that I have obtained. I would also like to thank our research collaborators at the University of Reading, Dr. Richard Frazier, Dr. Luke Clifton, Dr. Rebecca Green, Dr. Olga Florek and Dr. Michael Sanders. Thank you for sharing your expertise in neutron reflectometry and x-ray reflectometry and for making my visits to London so successful. Also, thank you Olga for taking the time to answer my many questions about RasCal, your kindness was greatly appreciated. I would also like to thank my external examiner Dr. Darren Korber for your valuable input and time.

Special thanks also to Dr. Cheryl Patten, Dr. Lisbeth Truelstrup Hansen (for reading the manuscript and offering helpful suggestions), Dr. Sue Budge, and Dr. Suzanne Sheffield for your kindness and for always having an open door. Thanks also to Emmalina Corriveau and Dr. Roberto Antueno for helping with the porin expression studies, your help was greatly appreciated. Special thanks to my family and friends for their encouragement and especially to my husband Daniel, my twin sister Ann and my mother Nell, your love and support were invaluable. Finally, thanks to all the other faculty members, graduate students (Emma, Trish, Laura, Helen, Bizu and Marta), and

the staff at Dalhousie University and Saint Francis Xavier University who have contributed in some way to help me get here today. Thank you!

CHAPTER 1: INTRODUCTION

There is a growing research interest into the use of natural cationic antimicrobial agents including peptides for use in food preservation (Pinto et al., 2011; Del Nobile et al., 2009). Long use of antibiotics has led to the development of resistance in some food pathogens (Keymanesh et al., 2009). However, cationic antimicrobial peptides (CAPs) have exhibited broad spectrum inhibitory activity against several foodborne pathogens and there have only been a few reports of developed resistance (Anaya-López et al., 2013). These properties of CAPs have presented an opportunity for considering them as natural food preservatives. In addition, some of these candidate compounds can also be cheaply extracted from waste streams (Gill et al., 2006).

Protamine is a CAP which can be extracted from the milt (sperm) of commercially caught fish including salmon (salmine) and herring (clupeine). Previous work has shown clupeine to be active against a range of food related pathogenic and spoilage bacteria (Islam et al., 1987; Johansen et al., 1995; Truelstrup Hansen and Gill, 2000), but direct applications in foods are made difficult due to non-specific interactions with food components (Truelstrup Hansen and Gill, 2000; Ueno et al., 1988, 1989). However, these non-specific interactions can be overcome by using 1,2-cyclohexandione (CHD) to modify charged arginine guanido moieties of clupeine as shown in milk and ground beef (Potter et al., 2005). Further studies on the mechanism of the CHD-treated clupeine on the bacterial targets are needed as the cause of the increased antimicrobial effect is not known.

Model studies have shown that clupeine is able to enter the cytoplasm in several bacteria without disrupting the cell membrane (Pink et al., 2014). Also, previous computer simulation experiments showed that clupeine would be attracted in a charge-dependent manner to the surface of the Gram-negative cell wall (Pink et al., 2003) but appeared not to permeabilize a model bilayer in electrophysiological experiment or as shown in Monte Carlo computer simulations, despite the fact that clupeine was shown to accumulate in the cytoplasm of challenged intact cells as demonstrated by immunoelectron microscopy (Pink et al., 2014). This observed paradox has led to the hypothesis that for certain Gram-negative bacteria such as *Escherichia coli* (*E. coli*), *Pseudomonas aeruginosa* and *S. enterica* serovar Typhimurium 14028 porins or alternative transport mechanisms might be involved in the internalization of the peptide. In addition, several reports have indicated that some strains of *E. coli* use proteases as a defense mechanism (Stumpe and Bakker, 1997; Truelstrup Hansen and Gill, 2001). The importance of this defense mechanism was investigated when the *E. coli* K-12 test strain used in the present study was exposed to native and CHD-treated clupeine.

Neutron reflectometry (NR) and X-ray Reflectometry (XRR) are complementary biophysical techniques that have been used to investigate peptide-lipid interactions to understand changes in membrane structure in model biomembranes (Dabkowska et al., 2009; Fernandez et al., 2012; Abuillan et al., 2013). At this time, these complementary techniques have not been applied to understand how native and CHD-treated clupeine would interact with mixed lipid mono- and bilayer membranes representing Gram-negative bacteria.

The overall objective of this work was to determine whether native and CHD-treated clupeine (clupeine with 10% of the arginine moieties modified with CHD) have different modes of interaction with two bacteria, *E. coli* K-12 and *Salmonella enterica* subsp. *enterica* serovar Typhimurium 14028 (*S. Typhimurium* 14028). Three types of interactions were investigated in this thesis: (1) the cytotoxicity of the native and modified peptide against the selected bacteria; (2) peptide induced alterations in the expression of the bacterial outer membrane porin (*ompF* and *ompC*) and protease genes (*ompT*) as well as the proteomic profile of outer membrane proteins and; (3) changes in the structure and composition of model biomembranes in the presence of native and CHD-treated clupeine.

This introductory chapter will discuss the importance of cationic antimicrobial peptides (CAPs), will examine some of the physicochemical properties of clupeine, and will conclude with a brief overview of the theory behind the experimental techniques used in this study.

1.1 The Problem of Antibiotic Resistance

Bacteria are of interest to the food and health sectors because of their beneficial and harmful effects. Some beneficial effects include their use as insecticides (*Bacillus thuringiensis* (Bt)) and their use in the manufacture of fermented foods (lactic acid bacteria) such as yoghurt and salami (Doyle et al., 2013). On the other hand, illnesses caused by food-borne pathogens such as *Clostridium botulinum* and *Listeria monocytogenes* are reminders of some of the challenges that still need to be overcome in order to provide safe food. But perhaps one of the greatest challenges that the food and health sector still has to overcome is the problem of increasing antibiotic resistance.

In 1878 when Louis Pasteur presented his Germ Theory of disease, the infectious nature of some micro-organisms including bacteria was only beginning to be understood (Pasteur and Lister, 1996). The isolation of bacteria on solid agar by Robert Koch and the use of aseptic methods by Lister both complemented Pasteur's theory which proposed that micro-organisms may be the cause of some or all diseases (Levy, 2002). The discovery of penicillin by Fleming in 1928 (Davies and Davies, 2010) was another important scientific breakthrough that has contributed to the use of antimicrobial agents in the treatment of bacterial infections. Although the initial use of antibiotics was limited to hospitalized patients, their industrial production made antibiotics more available to the public. The increased availability and widespread use of antibiotics introduced a period that many scientists refer to as the 'antibiotic era' (Greenwood et al., 2003).

For more than 75 years, the use of antibiotics has been the conventional treatment option for both Gram-positive and Gram-negative bacterial infections. Moreover, many of the antimicrobial agents approved for use in humans have also been approved for use in food-producing animals and in plant agriculture (Yan and Gilbert, 2004). However, the emergence of bacterial resistance due to a combination of misuse and overuse of antimicrobial agents as well as the ability of bacteria to adapt under selective pressure has led to the reduced efficacy of some common antimicrobial agents (Neu, 1992). For example, in 1941 nearly all strains of *Staphylococcus aureus* worldwide were susceptible to penicillin G. Today, over 95% of *Staphylococcus aureus* worldwide is resistant to penicillin and methicillin (semi-synthetic penicillin). Consequently, patients in long-term care facilities, such as burn centers, that are treated with β -lactam agents are more likely

to develop methicillin-resistant strains (Neu, 1992). Thus, the impact of antimicrobial resistance on the treatment of bacterial infections is escalating and needs to be addressed.

1.2 Mechanisms of Bacterial Resistance

Bacteria utilize several mechanisms to resist the action of antimicrobials and resistance can be broadly classified as intrinsic or acquired (Normark and Normark, 2002). Intrinsic resistance is mainly the result of some natural property of a bacterial species that renders it naturally resistant, for example, some organisms may be naturally impermeable to some antibiotics due to their cell structure. More specifically, mycoplasmas are resistant to β -lactams due to the lack of peptidoglycan in their cell wall (Neu, 1992; Normark and Normark, 2002). In contrast, acquired bacterial resistance implies that a susceptible organism has developed resistance to an agent to which it was previously susceptible. This phenomenon can occur by mobile genetic elements such as transposons containing resistance genes, or chromosomal mutations that cause bacterial resistance (Normark and Normark, 2002).

Figure 1-1 shows the major mechanisms by which bacteria resist the action of antibiotics and other antimicrobial agents. These include: (1) the bacteria may limit access of antimicrobial agents by decreased membrane permeability of the cell to the drug; (2) the bacteria may cause alterations or change target sites thus rendering the antimicrobial agent inactive; (3) the bacteria may acquire genes that produce enzymes that inactivate antimicrobial agents before they can have an effect; and (4) the bacteria may use efflux pumps to remove the antimicrobial agent from the cell before it can reach a target site (Hawkey, 1998; Tenover, 2006).

In order to ensure the safety of the products that enter the food chain, food antimicrobials including chemical sanitizers may be broadly defined as chemical or natural compounds present in or added directly to food, food packaging, food contact surfaces or food processing environments, to inhibit the growth of (or kill) pathogenic or spoilage microorganisms (Davidson et al., 2005). In addition, antimicrobial drugs are also used in food animals to treat disease, to prevent infection or are used for growth promotion (Health Canada, 2002), thus the food industry is not exempt from the effects of bacterial resistance.

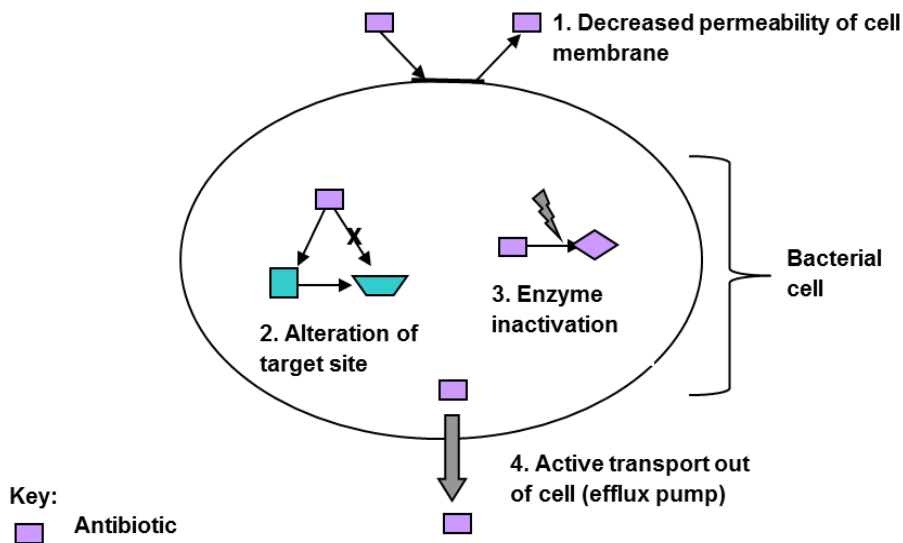


Figure 0-1 Mechanisms used by bacteria to avoid therapeutic antibiotics.

Antimicrobial resistance in food pathogens may also be increased in the presence of biofilms or bacterial stress responses (Verraes et al., 2013). Biofilms are communities of microorganisms that attach to a surface and are usually surrounded by an exopolysaccharide (EPS) matrix. The physical and chemical structure of the latter acts as a physical barrier to the antimicrobial agent reaching its target in food pathogens such as *Listeria monocytogenes* (Mah and O’Toole, 2001).

On the other hand, food pathogens such as pathogenic *E. coli* may undergo stress responses which slow growth and cause other changes in the metabolism of the microbes which in turn enable the microorganism to adapt to unfavourable conditions. As the need for new antimicrobial agents with potential applications as medical therapeutics or food additives that inhibit or kill foodborne pathogens becomes more pressing, more research has focused on cationic antimicrobial peptides, which not only kill a wide variety of microbes but are also less prone to microbial resistance (Hancock, 1997).

1.3 Cationic Antimicrobial Peptides (CAPs)

Plants and animals including fish possess potent broad-spectrum cationic antimicrobial peptides which they use to fend off a wide variety of microbes including bacteria (Zasloff, 2002). The antimicrobial sequence database is very diverse and information on cationic antimicrobial peptides can be found on general biological websites such as GenBank (<http://www.ncbi.nlm.nih.gov/genbank/>) and antimicrobial peptide database (<http://aps.unmc.edu/AP/main.php>). In order for CAPs to be effective they should fulfill several criteria such as: (1) selective toxicity, which refers to the ability of the CAP to kill microorganisms without harming the host cells; (2) rapid bacteriostatic or bactericidal activity; (3) a broad spectrum of antimicrobial activity; and (4) little or no development of resistance to the antimicrobial peptide by the target bacteria (Matsuzaki, 1999).

In recent years, the increased interest in CAPs as possible therapeutic agents and natural antimicrobials for food applications has caused increased research on CAPs (Figure 1-2). Some of the groups of CAPs studied include: (1) defensins, which are commonly found in a variety of mammals and are rich in cysteine and arginine residues; (2) bombinins and

magainins, which are isolated from frog skin and have been well characterized; (3) thionins which are isolated from plants and are often produced in response to infection (Hancock and Fella, 1996); (4) protamines, which are isolated from fish sperm and are basic peptides with little or no secondary structure in aqueous environments but become alpha-helical in hydrophobic environments (Ando et al., 1973).

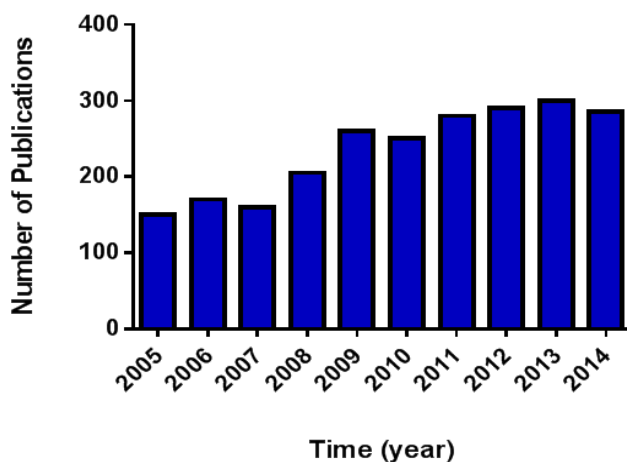


Figure 0-2 Number of publications from 2005-2014 in the Web of Science core collection with Cationic Antimicrobial Peptides in the title of the article (<http://apps.webofknowledge.com.ezproxy.library.dal.ca>).

1.4 Mechanisms of Actions of Cationic Antimicrobial Peptides

Although many studies have addressed the issue of the mechanism of antimicrobial action of CAPs, the subject is not fully understood and continues to be elucidated (Zhang et al., 2001). Using model membrane systems, a variety of techniques such as microscopy, fluorescent staining and circular dichroism have been used to assess the mechanism of action of CAPs (Zhang et al., 2001). Additional studies have also been conducted using whole microbial cells, mainly utilizing membrane potential sensitive

dyes and peptides that are fluorescently labelled (Powers and Hancock, 2003). Together the data from these studies indicate that the mechanism of action of CAPs involves binding to bacterial membranes which may involve membrane disruption or the attack of cytoplasmic targets. In Gram-negative bacteria, the initial association of CAPs with the bacterial membrane occurs through electrostatic interactions between the cationic peptide and the anionic cell envelope (Sloan, 2005).

Three models have been developed to explain the disruption of cell membranes by CAPs: the barrel-stave model, the toroidal model and the carpet model (Powers and Hancock, 2003). In the barrel-stave model, the peptides utilize their amphipathic nature where the hydrophobic peptide regions are aligned into the lipid environment, while the hydrophilic side chains are aligned inward to form trans-membrane pores (Brogden, 2005). It is through these pores that cytoplasmic contents can leak from the cell.

In the toroidal pore model, the peptides insert into the bilayer and cause the lipid bilayer to bend. As a result, phospholipid head groups and polar peptide surfaces line the pore lumen and local aggregations of varied numbers of peptide molecules within the membrane provide a route of passage of ions (Brogden, 2005).

On the other hand, in the carpet model, the peptides align themselves parallel to the membrane surface, and the positively charged peptides are attracted to the negatively charged phosphate groups in the lipid membrane and it is these interactions at various sites around the membrane that form an extensive layer or 'carpet'. The so-called 'carpet' interaction causes the membrane to lose its integrity, with the subsequent leakage of cytoplasmic components (Brogden, 2005). Although different cell membrane disruption

theories exist, there can be little doubt that peptide interaction with the cell membrane is a precursor to bacterial cell death.

In the case of protamine from herring (clupeine), its mode of action is still being elucidated and several theories have been proposed to explain the peptide's mechanism of action. Earlier work by Islam et al. (1984a) reported that protamine inhibition was dependent on the Gram reaction and that Gram-positive organisms were more sensitive to the peptide than Gram-negative organisms. This theory was later revised as both Gram-negative and Gram-positive bacteria were found to be sensitive to protamine (Johansen et al., 1997; Truelstrup Hansen and Gill, 2001).

A second theory about protamine's mechanism of action involved electrostatic forces that govern the initial interactions between the positively charged peptide and the negatively charged bacterial cell envelope (Pink et al., 2003). Johansen et al. (1996) demonstrated that at least for the Gram-positive *L. monocytogenes* and *Shewanella putrefaciens*, protamine caused the poration of the cell envelope followed by complete cell lysis. In addition, Johansen et al. (1997) hypothesized that protamine interacts with anionic cell wall components and anionic phospholipids in the cytoplasmic membrane inducing condensation and resulting in disruption of cell wall layers.

Later, Tolong (2004) used a membrane potential probe, 3,3'-dipropylthiocarbocyanine iodide (disS-C₃(5)) to show that clupeine could translocate the bacterial membrane of *E. coli* and *S. Typhimurium* without cell lysis. In addition, the expression of several outer membrane proteins significantly decreased as *Pseudomonas aeruginosa* acquired resistance to clupeine (Mohan, 2010). Furthermore, Pink and co-workers (2014) investigated the internalization of protamine in three Gram-negative

organisms *E. coli*, *P. aeruginosa* and *S. Typhimurium* and observed that at least for these three organisms, protamine became internalized into the cytoplasm of these bacteria without disrupting the cell envelope. Moreover, transmission immuno-electron microscopy showed most of the clupeine localized at or near the outer membrane of clupeine-resistant *P. aeruginosa*, indicating decreased outer membrane permeability (Mohan, 2010; Pink et al., 2014). On the basis of these observations, a third theory was proposed that outer membrane proteins such as the barrel-like porins may be responsible for clupeine internalization, at least in some Gram-negative bacteria (Pink et al., 2014). One of the objectives of the present work was to test this hypothesis by using clupeine as a model CAP, and a brief introduction to this peptide is presented below.

1.5 Clupeine as a Model CAP

Protamines are small linear peptides commonly isolated from sperm cells of birds, fish and mammals. Industrially, protamine is isolated from the milt of several fish species (Ando et al., 1973). Protamines may be classified into three groups according to the different kinds of basic amino acids present in the peptide, namely, mono-protamines, di-protamines and tri-protamines (Ando et al., 1973). Herring and salmon protamines, clupeine and salmine, respectively, are classified as mono-protamines since they contain only one kind of basic amino acid, arginine.

Clupeine is a mixture of three different peptide chains (YI, YII and Z), each consisting of about 30 residues of which ~66% is arginine on a molar basis (Bonora et al., 1979). The amino acid sequences and the molecular weight (MW) values for each fraction are shown in Figure 1-3. The average molecular weight of clupeine is ~4200 Daltons and its isoelectric point (pI) is in the range 11-13 (Ando et al., 1973).

YI: ARRRSSRPPIRRRRPRRRTRRRRAGRR (MW 4,112)

YII: PRRRTRRASRPVRRRRPRRVSRRRRARRRR (MW 4,049)

Z: ARRRSSRRASRPVRRRRPRRVSRRRRARRRR (MW 4,165)

Figure 0-3 The amino acid sequence which is a mixture of the three peptides chains YI, YII and Z. Key: A = alanine; R = arginine; S = serine; T = threonine; G = glycine; V = valine; P = proline; I = isoleucine (Adapted from Ishimura et al., 1991).

1.6 Parameters that Determine the Antimicrobial Activity of Clupeine

The antimicrobial activity of protamine was discovered by McClean in 1930 who showed that protamine was able to inactivate the *Vaccinia* virus. Although protamine is not currently approved as a food preservative in North America, it is currently used to improve the shelf-life of starch-based foods in Japan (Ueno et al., 1989). In addition, protamine is used in the treatment of heparin overdose and is also used as a carrier in injectable insulin formulations (Horror, 1985; Gottschlich et al., 1988).

1.6.1 Hydrophobicity

The hydrophobicity of clupeine may be defined as the percentage of hydrophobic residues within the peptide (Sloan, 2005). The primary structure of clupeine contains mostly hydrophilic amino acids, with few hydrophobic residues. The hydrophobic residues in the YII fraction are valine (two) and proline (three), whereas the Z fraction also contains two valine residues and one fewer proline residue than YII (Figure 1-3). The YI fraction contains only two hydrophobic amino acids (proline and isoleucine) (Yeaman and Yount, 2003). Although hydrophobicity allows for improved membrane

permeability, too much hydrophobicity can result in the loss of antimicrobial specificity (Yeaman and Yount, 2003) or enhanced cytotoxicity. Clupeine molecules are only moderately hydrophobic, and although its antimicrobial abilities has been proven in some Gram-negative and Gram-positive microorganisms, its cytotoxicity has not been fully characterized (Tolong, 2004).

1.6.2 Amphipathicity

Most CAPs form amphipathic structures upon association with the bacterial outer membrane (Dathe and Wieprecht, 1999). However, clupeine is not amphipathic and lacks secondary structure in aqueous solutions because of the even distribution of positive charge along the peptide backbone (Bonora et al., 1979). Indeed, the amphipathic structure is ideal for interacting with the membrane surface because the hydrophobic residues interact with the membrane while the hydrophilic residues are oriented toward the aqueous phase.

1.6.3 Charge

As noted, clupeine is a positively charged antimicrobial peptide with a pI between 11 and 13, and the cationic nature at pH values below the pI of clupeine is due to the high proportion (~66%) of arginine in the peptide's structure (Suzuki and Ando, 1972). Some researchers believe that the positive charge of the peptide helps to modulate its antimicrobial activity (Sloan, 2005). For example, the positively charged clupeine is believed to be responsible for the electrostatic attraction to the negatively charged phospholipid membrane of susceptible bacteria. However, the strong cationic nature of the peptide has been shown to be undesirable in complex food systems since non-specific

binding of clupeine to anionically charged food proteins reduces its antimicrobial activity (Potter et al., 2005).

1.7 Advantages of CAPs over Conventional Antibiotics

Protamine has exhibited antimicrobial activity on some food-borne pathogenic Gram-positive and Gram-negative bacteria. For example, Johansen et al. (1995) have reported such bactericidal activity on the Gram-positive bacteria *Staphylococcus aureus*, in addition to a prolonged lag phase on the Gram-negative food spoilage organism *Sh. putrefaciens*. But as with any class of antimicrobial agents, a key issue is whether or not resistance to cationic antimicrobial peptides can be provoked.

One of the major motivations for the increased interest in CAPs such as clupeine is that bacteria appear to not easily develop resistance to these agents. In a review by Peschel and Sahl (2006), the authors discuss several host-pathogen adaptations with regard to the production of CAPs, and proposed that the latter have co-evolved with microbial resistance. Some interesting examples were used to support their hypothesis. For example, it was proposed that defensins form intra-molecular disulphide bridges which stabilize their secondary structure and make the CAPs more resistant to bacterial proteolysis (Peschel and Sahl, 2006).

Nevertheless, there are some reported bacterial cationic antimicrobial peptide resistance mechanisms. For example, some bacteria (*Streptococcus pyogenes*) produce inhibitory proteins that bind CAPs and prevent them from reaching the bacterial cell membrane while others (*St. aureus* and *L. monocytogenes*) reduce the net anionic charge of the bacterial cell envelope, reducing its affinity for CAPs (Peschel and Sahl, 2006). In addition, simple linear or α -structures such as clupeine are susceptible to proteolysis and

are targeted by several microbial proteases. Indeed, work by Truelstrup Hansen et al. (2001) has shown this to be true for several bacteria including *Bacillus cereus* and proteolytic *Clostridium botulinum* strains. The authors explained that this susceptibility to trypsin-like proteases was due to the high arginine content of clupeine.

While this may seem to weaken the evidence in support of the efficacy of clupeine, it should be pointed out that although *E. coli* has been reported to possess a clupeine degrading enzyme, this bacterium is still inhibited and killed by clupeine (MIC 500 to 1000 µg/mL) Truelstrup Hansen and Gill (2000). Clearly, a better understanding of how and why antimicrobial agents work and don't work is needed in order to fully combat bacterial resistance.

1.8 Synthesis of Peptides

In order to fully investigate cationic antimicrobial peptides as new therapeutic and preservative agents, their mode of action must be known and understood. A variety of strategies have been adapted to synthesize peptides including: (a) chemical synthesis, either in the solution phase, coupled to a solid phase or a combination of both; (b) enzymatic synthesis; and (c) recombinant DNA technology (Hancock and Lehrer, 1998).

Generally the size of the peptide determines the most suitable technology for its production but currently, chemical synthesis is the most widely used approach for peptide synthesis (Vlieghe et al., 2010). Chemical peptide synthesis has the advantage that non-natural or chemically modified amino acids can be simply introduced to generate a diversity of amino acid sequences. In this regard, synthetic peptides have been very useful in improving our understanding of the mechanism of action of CAPs. For the production of naturally occurring peptides with isotopic labels (such as ^{15}N , ^{13}C , and or

²H) successful recombinant expression of the antimicrobial peptide LL-37 has been reported by Moon et al. (2006).

There are several barriers to the development of antimicrobials as new pharmaceutical drugs, such as the high cost of synthesizing and screening the peptides and lack of sufficient studies to validate safe and effective doses (Marr et al., 2006). Other drawbacks include their low oral bioavailability (injection is generally required), their short half-life due to susceptibility to proteolytic enzymes and their poor ability to cross physiological barriers due to their hydrophilic nature (Vlieghe et al., 2010).

1.9 Chemical Modification of Proteins

For many years, the chemical modification of proteins has been widely used to study protein structure and function. More importantly, chemical modification can be used as a tool for improving the functional properties of proteins by altering their structures (Means and Feeney, 1971). Protein modifications can occur naturally or synthetically. For example, in a cell, in order to generate specific biological functions, proteins undergo various natural modifications after translation such as glycosylation, phosphorylation and amino acid side-chain modifications (Rucker, 1993). In contrast, the synthetic modification of proteins involves the intentional addition of a chemical reagent to the protein.

Today some of the many reasons for chemically modifying proteins include: (1) determining the reactivity of side groups; (2) investigating structure-function relationships; (3) monitoring protein activity *in vitro* and *in vivo* through fluorescent or affinity tags; and (4) changing the physical properties of the protein (Means and Feeney, 1998). Modifying clupeine to change its physical properties and investigating how the

peptide's structure is related to its function is one of the main objectives of this thesis. This modification was achieved by reducing native clupeine's charge by blocking 10% of the arginine residues with 1,2-cyclohexanedione (CHD). This particular modification was chosen since it has been shown that charge plays an important role in the antimicrobial activity of clupeine (Potter et al., 2005).

However, when the aim of chemical modification is to establish structure-function relationships, several structural peptide properties can be related to functional properties (Means and Feeney, 1971). For example, properties such as molecular size, shape and flexibility can be related to viscosity and gelation. Similarly, properties such as the balance of hydrophobic and hydrophilic groups distributed on the surface of the protein and steric properties can be related to solubility, foaming and emulsification (Means and Feeney, 1998).

1.10 The Chemical Properties of Protamine

Protein modification reactions are usually classified based on the type of reagent used, and some of the most frequently used reactions include: acylation; succinylation; alkylation; esterification; amidation and oxidation (Nakai and Modler, 1996). One way of categorizing reagents used for chemical modification is by their specificity; the first type of specificity may be for a particular amino acid side chain whereas the second type may be for a particular site on the protein (Kito, 1996).

Most chemical modification reactions are with the basic form of an amino acid reacting as a nucleophile. Lysine residues are among the most common target sites because of their exposure and relatively high reactivity for nucleophilic substitution (Means and Feeney, 1971). The rate of reaction of any of these amino acids will decrease

as the group is protonated, thus the rate of chemical modification is pH dependent (Kito, 1996).

Protamine is strongly basic due to the presence of guanidine groups on the arginine residues. In addition, the basicity of the guanidine group of arginine is due to the large resonance stabilization of the protonated form; since arginine is protonated under all circumstances, arginine does not react as a nucleophile (Brown and Poon, 2005). The chemical modification of protamine is not trivial as it contains no lysine residues and is made up of approximately 66% arginine residues. However, several modifications of protamine have been reported: (1) the lipophilization of clupeine with fatty acid chlorides (Buttimor, 2005), and (2) the blocking of arginine residues in clupeine with CHD (Potter et al., 2005). These protamine modifications will be discussed in the next section.

1.11 Protamine Modifications

1.11.1 Lipophilization of Proteins including Protamine

Lipophilization is one kind of chemical modification and refers to the binding of lipid components to the proteins with a general increase in protein hydrophobicity. There are many ways of covalently attaching hydrophobic groups to proteins, such as: acylation by fatty acids and N-hydroxysuccinimide esters; acylation by acetic and succinic anhydrides, and reductive alkylation (Roussel-Philippe et al., 2000). In addition, fatty acid chlorides have also been used to covalently modify proteins and increase their hydrophobicity (Buttimor, 2005). For example, work by Smith and Yada (1991) and Roussel-Philippe et al. (2000) achieved lipophilization of proteins by utilizing fatty acid chlorides; however both research groups used proteins that contained lysine residues and these amino acids were the specific sites of modification.

When Buttamor (2005) lipophilized protamine using fatty acid chlorides, the site of attachment was not a lysine residue but rather an N-terminal proline. Attachment to an N-terminal proline occurs because of two reasons: (1) none of the other amino acids in protamine have a reactive primary amine, and (2) lysine residues are absent in protamine (Ando et al., 1973). Indeed, the literature shows that lipophilization can improve the functional properties of proteins. For example, Wong et al. (2006) lipophilized casein glycomacropeptide (GMP) and the emulsification activities of GMP were improved, while Smith and Yada (1991) lipophilized *Mucor miehei* aspartyl proteinase (MMP) and observed increased conformational stability of MMP.

1.12 The Reaction of Arginine with CHD

Arginine is considered a basic amino acid because of the guanidine side chains. The guanido group has a $pK_a > 12$, which gives the group a positive charge at pH values < 12 (Brown and Poon, 2005). Prior to the work done by Toi et al. (1967) arginine specific reagents were uncommon, but since then several methods have been developed for the modification of arginine. The method developed by Toi et al. (1967) used CHD in 0.2 M NaOH, but although the method is specific for arginine, there is some concern that the alkaline conditions used are too harsh for some proteins (Means and Feeney, 1971).

Although the arginine residues in protamine are less reactive than free arginine, due to the steric hindrance of the guanido groups of adjacent arginine residues (Brown and Poon, 2005), the arginine groups in clupeine were successfully modified using 0.05 M CHD in a 0.2 M boric acid buffer (pH 8.5) (Potter et al., 2005). The reaction of the dicarbonyl CHD with clupeine is a condensation reaction and the arginine residues

modified can be quantified using the Sakaguchi reaction (Sakaguchi, 1950; Wang et al., 2008).

The above discussion has described the problem of antibiotic resistance and has examined the physiochemical properties of CAPs and in particular native and CHD-treated clupeine. It is hypothesized that the interactions with model bacterial cell membranes and antimicrobial effects on Gram-negative model organisms can be modulated by reducing the overall surface charge of clupeine by chemical modification with CHD. In order to test this hypothesis several techniques were employed; the section that follows provides a basic introduction to the theory of these techniques.

1.13 Background on Experimental Techniques

The techniques used in this study can be separated into two main groups: (1) techniques that probe lipid binding at the air/liquid interface in Gram-negative model biomembranes (monolayer and Langmuir-Blodgett (LB)/Langmuir-Schaefer (LS) model systems); surface pressure measurements, x-ray reflectometry (XRR) and neutron reflectometry (NR); and (2) techniques such as quantitative real-time polymerase chain reaction (qPCR), sodium dodecyl sulfate polyacrylamide gel electrophoresis (SDS-PAGE) and mass spectrometry (MS) that can be used to determine changes in gene expression, protein expression and peptide recovery, respectively, during exposure to native and CHD-treated clupeine.

This section provides a brief overview of the theory behind the experimental techniques and the methods used to obtain the surface pressure, NR and XRR data obtained in this thesis. Surface pressure studies, NR and XRR are all complementary

techniques that together can be used to provide insights into the interaction of peptides in monolayer and bilayer model membrane systems. In addition, a brief description of RT-qPCR is also outlined.

1.14 Surface Pressure Measurements

Interfaces refer to the boundary regions between two phases in equilibrium, for example, liquid-liquid and liquid-gas, and at the interface there is usually a transition between the composition and properties of the two bulk phases which it separates (Maget-Dana, 1999). Pure water has a surface tension of 72.8 mN m^{-1} at 20°C , which is equivalent to a surface pressure of zero. However, if a lipid is spread on the air/pure water surface, the lipid forms a monolayer (or Langmuir film) at the interface and the presence of the monolayer reduces the surface tension of water at the interface. Surface pressure may be defined as the reduction in surface tension at the interface from that of the pure bulk at equilibrium (Langmuir, 1933; Petty, 1996). A simple equation describing this relationship is shown in equation 1-1:

$$\text{Equation 0-1} \quad \pi (\text{mN m}^{-1}) = \gamma_0 - \gamma$$

Where π represents the surface pressure, γ_0 represents the surface tension of the pure water and γ represents the surface tension of the lipid-covered surface (Petty, 1996).

Lipid monolayers at an air/water interface provide a simple sensitive model for mimicking biological membranes and this technique has been used to study membrane insertion of proteins and peptides (Zhang et al., 2001; Lad et al., 2007; Clifton et al., 2012). The structures of the main lipids used in the thesis are shown in Figure 1-4. The Langmuir troughs used in this work were fitted with Teflon™ movable barriers, and surface pressure was used to control the formation of lipid monolayers at the air-liquid

interface (Figure 1-5). The characteristics of a monolayer can be studied by measuring changes in the surface tension when the monolayer is compressed between two barriers (Figure 1-5).

The reduction in surface tension is measured as an increase in surface pressure using a Wilhelmy plate which consists of a strip of chromatographic paper attached to the arm of an electronic microbalance that is connected to a computer. As the monolayer is compressed, the lipid molecules re-order themselves to form three main phases (Figure 1-6) and the phases formed will depend on the lipid used. In the first phase, known as the gas-extended (GE) phase, the surface pressure is usually below 0.5 mN m^{-1} and the molecules are far enough apart such that there is little or no interaction between the molecules.

Further compression of the monolayer results in an increase in surface pressure and the gas-extended phase gives way to the second phase, the liquid-extended (LE) phase. However, unlike the GE phase, molecular interactions in the LE phase are increased and the hydrocarbon chains are randomly oriented (Petty, 1996; Kaganer, Möhwall and Dutta, 1999). At a surface pressure of $\sim 25 \text{ mN m}^{-1}$ the final compressible phase, the condensed phase forms. Here, the molecules are closely packed and the hydrocarbon chains are uniformly oriented away from the water surface (Girard-Ergot and Blum, 2007).

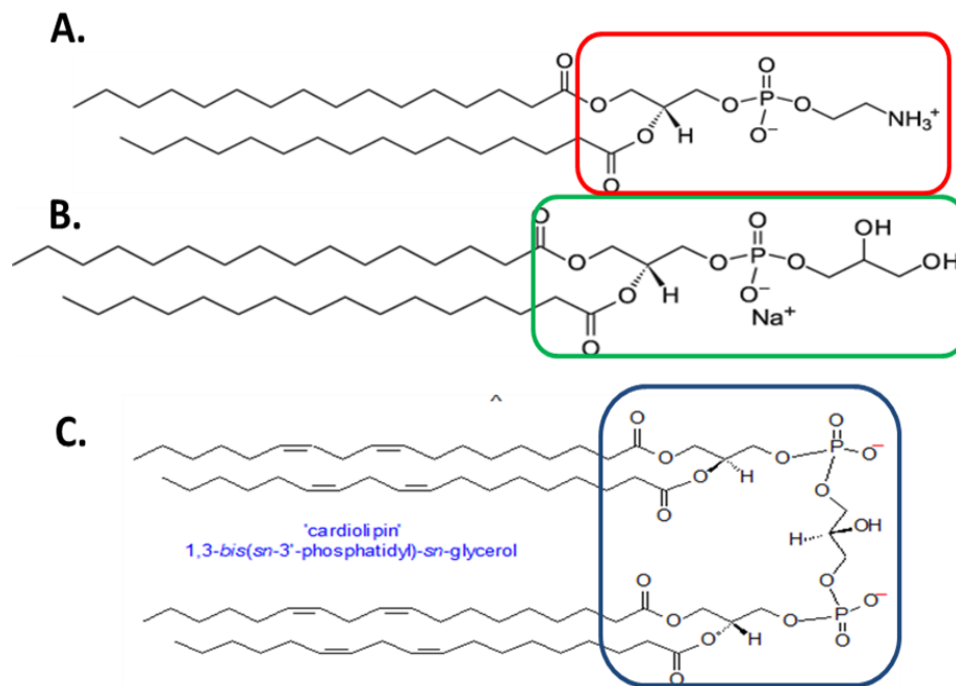


Figure 0-4 The structure of the major lipids in *E. coli* and *S. enterica* Typhimurium. (A) L- α phosphatidylethanolamine, PE, MW = 691.97 g/mol, neutral or Zwitterionic; (B) L- α -phosphatidylglycerol, PG, MW = 744.96 g/mol, anionic; (C) Cardiolipin, Cl, MW = 1285.62 g/mol, anionic. Structures adapted from Avanti Polar Lipids (www.avantilipids.com). The sections of the lipids in the coloured boxes represent the head groups.

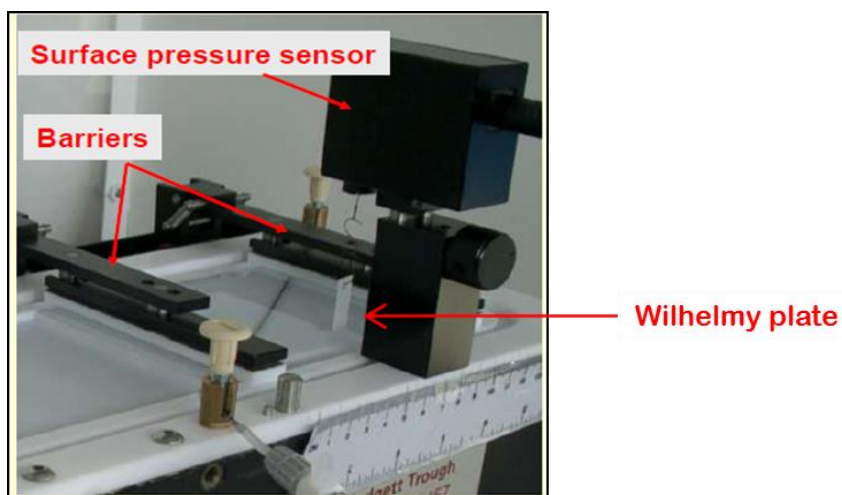


Figure 0-5 Setup for the formation of monolayers at the air-water interface.

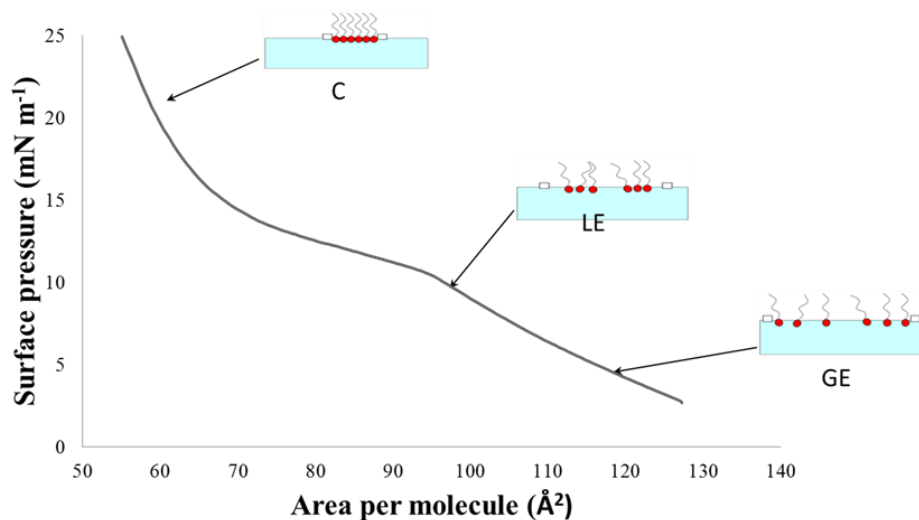


Figure 0-6 Surface pressure versus area per molecule of a hypothetical monolayer. Three main phases and level of re-ordering observed at each phase are shown, GE = the gas-extended phase; LE = the liquid-extended and C = the condensed phase. Reprinted from He and Li (2007), (reproduced with permission from Elsevier).

1.15 Neutron Reflectometry Technique

A neutron is an atomic particle with a mass equivalent to 1.675×10^{-27} kg (1,839 times greater than that of an electron), and has a lifetime of about ~ 1000 seconds as a free particle (Lefmann, 2007). Neutrons also have no charge and have greater penetrating power through materials than charged particles such as electrons (Pynn, 2009; Lopez-Rubio and Gilbert, 2009). Neutrons may be produced from reactor sources or from spallation sources. Reactor sources produce neutrons through the nuclear fission of uranium atoms whereas spallation sources produce neutrons by bombarding a heavy metal target with high energy protons (Lefmann, 2007). The spallation source used in this work was the ISIS spallation source in Oxfordshire, UK. Neutrons may be scattered coherently or incoherently (Lopez-Rubio and Gilbert, 2009). Coherent scattering occurs

when the neutron interacts with all the nuclei in the sample in a coordinated fashion and yields information on structure (Pynn, 1990).

On the other hand, incoherent scattering arises when the neutron interacts independently with each nucleus in the sample. Whether a system will scatter coherently or incoherently will depend on the scattering length of each nucleus in the system. To clarify this point, if the scattering cross section of a nucleus is pictured as a circle, then the radius of that circle is what is termed the scattering length (Jeffries et al., 2016). The total scattering length density (SLD) of a film is an additive quantity that is directly related to the chemical composition, coherent scattering length and volume fraction of each isotopic component of the film (Pambou et al., 2016).

In terms of operating principles, a neutron reflectometer requires several parameters in order to function (Figure 1-7) such as: (1) a neutron source (reactor-based or by spallation in accelerator-based neutron sources); (2) a beam chopper that defines the correct neutron wavelength range required; (3) slits for collimating the incoming beam; (4) monitors for assessing the neutron wavelength; (5) a sample stage for the accurate positioning of the sample; and (6) a detector to record the reflected beam (Clifton et al., 2013a).

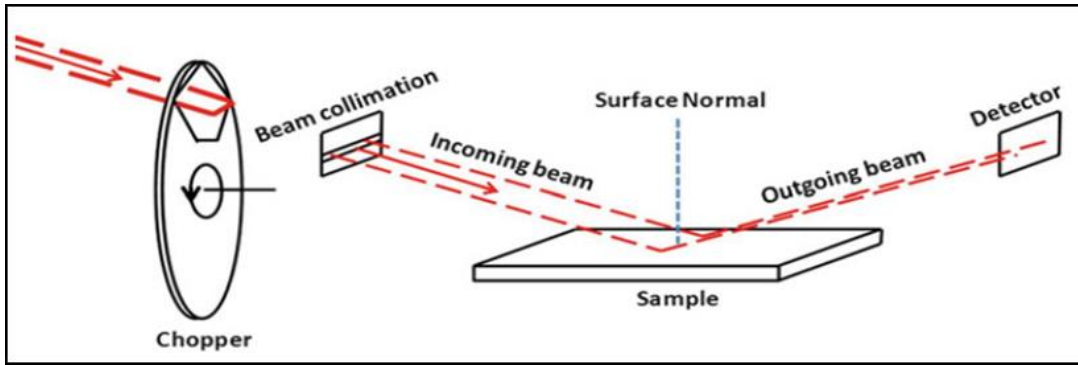


Figure 0-7 Schematic showing a pulsed beam of neutrons as it undergoes specular reflection from a sample surface. Reprinted from Clifton et al. (2013a), (reproduced with permission from Springer).

In a neutron reflectometry experiment, a neutron beam is reflected from a surface and the intensity of the reflected beam is measured by the monitor (as a function of the angle of incidence, Figure 1-8), and the reflected intensity is measured at the detector (Kwaambwa et al., 2010). Once the reflected intensity is divided by the incident intensity, reflectivity as a function of wavelength is obtained. Using equation 1-2, the units are converted from wavelength into Q_z , where:

$$\text{Equation 0-2} \quad Q_z = \frac{4\pi}{\lambda} \sin(\theta)$$

In this equation, Q_z is the wave vector transfer, λ is the neutron wavelength, and θ is the incident angle of the beam (Clifton et al., 2013a).

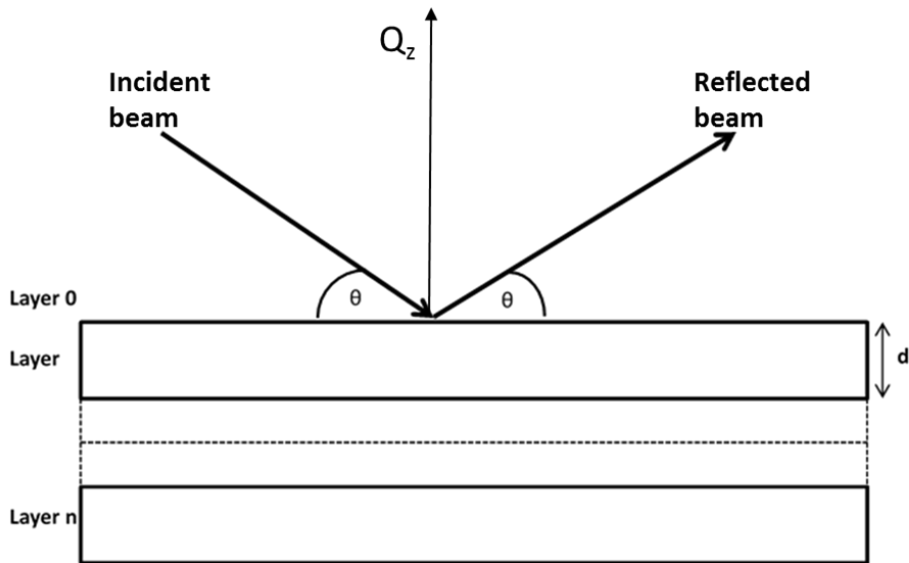


Figure 0-8 A simplified neutron reflectivity diagram showing the incident and reflected beams at an interface. In a typical NR experiment, the neutron beam is directed at the interface at an incident angle, θ . The reflectivity of the reflected beam is measured as a function of the momentum change perpendicular to the surface, $Q_z = \frac{4\pi}{\lambda} \sin(\theta)$ and is defined as the ratio of the intensity of the reflected beam to that of the incident beam. The structure across the interface is modeled as a series of layers 0 to n and each layer is usually characterized by its scattering length density (SLD), its thickness, d (Å) and its surface roughness (Å).

This process of converting the raw data collected during the experiment to true reflectivity values is known as data reduction. It is important to note that the only change in wave vector transfer is along the z axis, which is perpendicular to the interface, and that the reflected intensity decays as a function of Q to the fourth power (Penfold and Thomas, 1990). Because the instruments are not 100% efficient, it is necessary during the data reduction process to use a scale factor to correct for non-ideal responses to the detector and monitor.

The scale factor used for this study was obtained from a clean deuterium oxide (D_2O) surface. In summary, raw NR data are reduced or converted to true reflectivity

values by: (1) reducing the data from the D₂O sample; (2) obtaining the scale factor for the D₂O sample and (3) reducing the data for each sample run using this scaling factor. These reduced data files are now ready for analysis; the procedure used to analyze and fit the data is outlined in the methods section of Chapter 4 and in Appendix E.

In NR, the signal depends on differences in scattering length density (SLD) that the beam encounters (Green et al., 2000). Because the scattering power of neutrons does not increase linearly with increasing atomic number, light atoms such as hydrogen (deuterium) can be distinguished in the presence of heavier ones (Demkowicz and Majewski, 2016). This property of nuclear reflectivity also allows isotopes of the same element to have different scattering lengths for neutrons; a common example in the literature is that of hydrogen (¹H) and deuterium (²H) which have different SLDs, $-0.56 \times 10^{-6} \text{ \AA}^{-2}$ and $6.35 \times 10^{-6} \text{ \AA}^{-2}$, respectively (Singh and Basu, 2004; Clifton et al., 2013a). In the present study, in order to observe peptide-lipid interactions at the interface, contrast variation (also called isotopic substitution) was employed to label different components of the lipid samples and the solvents used.

In this way significant changes were made to the SLD of the samples and solvents while their other chemical properties had negligible changes (Heberle et al., 2015). Moreover, contrast matching makes it possible to change the SLD of a given material so that it either dominates or is removed from the total scattering (Lopez-Rubio and Gilbert, 2009). In addition, the substitution of deuterium for hydrogen in lipid tails and the use of “air contrast matched water” (ACMW) or non-reflective water (NRW) (8% D₂O:92% H₂O) in solvent mixtures helps to clearly resolve signals from the interface. Since NRW

has a SLD of zero, similar to that of air, the reflectivity measured would arise directly from the interface with no contribution from the bulk phase (Green et al., 2000).

In a number of NR studies, Clifton et al. (2011) and Lad et al. (2007) used hydrogenated lipids in deuterated solutions (D_2O) and deuterated lipids in hydrogenated solutions containing water to prepare a number of isotopic contrasts. These mixtures were valuable in identifying protein and the lipid contribution at the interface. For example, the isotopic contrasts containing deuterated lipids and hydrogenated protein in NRW provided information about changes in the lipid component, whereas contrasts containing hydrogenated lipids and hydrogenated proteins in NRW provided information about the protein component. In addition, these authors used contrasts containing deuterated lipids and hydrogenated protein in D_2O , which provided information on both the lipid and protein components. In this study similar isotopic contrasts to these were prepared to illustrate how native and CHD-treated clupeine interact with model biomembranes.

The reflectivity profiles are then analyzed using data fit procedures described in detail by Born and Wolf (1970) and Clifton et al. (2013a). These are explained more fully in Section 4.3.6, thus only the general principle will be mentioned here. In this approach, a model of the distribution of the lipid and peptide components at the interface is generated as a series of layers, and each layer is defined by its SLD, thickness and roughness (Dabkowska et al., 2009). These parameters are then adjusted or fitted to the least number of layers until there is good agreement between the calculated reflectivity curve and the measured data (Dabkowska et al., 2009; Clifton et al., 2011).

1.16 X-Ray Reflectivity (XRR) Technique

X-ray reflectivity is a non-destructive method that has been successfully used to characterize peptide/lipid interactions at the air/water interface and has helped to provide information on the spatial location of the protein and lipid components at these interfaces (Clifton et al., 2012; Danauskas, 2009). All x-ray studies in this thesis were performed at the I07 beamline at Diamond Light Source (Oxfordshire, UK), which is an x-ray diffraction beamline that uses a synchrotron light source. A detailed overview of the system is described in Arnold et al. (2012) so only a brief account is given here.

To generate x-rays, three conditions must be met. First, there must be a source of electrons because x-rays interact with electrons in matter, that is, they are scattered by the electron cloud in atoms. Second, the electrons must be accelerated at high speed; higher speed gives higher intensity x-ray beams with an electromagnetic spectrum reaching shorter wavelength. And third, a target material is needed to receive the impact of the electrons and interact with them. X-rays are produced when the free electrons cause energy to be released as they interact with atomic particles in the target (<https://www.nde-ed.org>).

In reflectivity experiments, the incident and reflected beams are symmetrically arranged, therefore, the momentum transfer has only a vertical component, Q_z , normal to the reflectivity surface (Figure 1-9). Reflectivity is therefore measured as a function of the wave vector transfer (Q_z) and is normal to the liquid surface, (Equation 1-2), where λ denotes the wavelength of the radiation and θ is the angle between the surface and the x-ray beam.

The I07 beamline has the capacity for XRR techniques due to a ‘double-crystal-deflector’ (DCD), (indium antimonide (InSb), 111 and 220) scheme which is arranged to satisfy Bragg geometry. This means that when an x-ray beam encounters a layer, reflection occurs only when the conditions for constructive interference are fulfilled. The DCD is also designed so that both crystals are mounted on the same rotating stage which is aligned with the incoming beam. The incoming beam is first deflected by the (111) crystal and then back in the opposite direction by the (220) crystal (Figure 1-10). This produces an overall beam deflection, $2\Delta\theta$, where $\Delta\theta$ is equal to the difference in Bragg angles of these two lattice planes (Arnold et al., 2012).

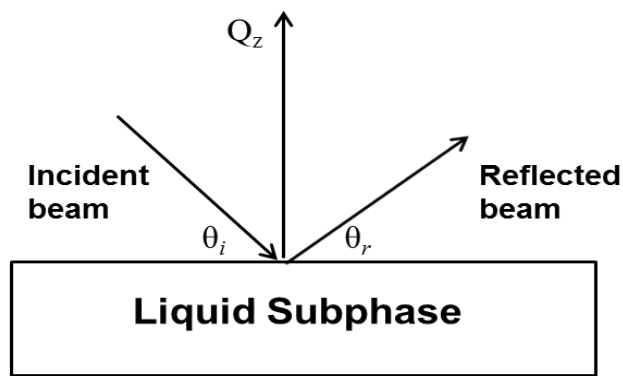


Figure 0-9 Incident and reflected x-rays on a liquid monolayer.

Bragg’s Law refers to equation 1-3 and explains the reflection of x-ray beams at certain angles of incidence:

$$\text{Equation 0-3} \quad 2d \sin\theta = \lambda$$

In this equation, d represents the space between layers in a sample, θ is the incident angle, and λ is the wavelength of the incident x-ray beam (Arnold et al., 2012). Both the 111 and 220 crystals are mounted on the same rotating stage with its axis aligned to the incoming beam. The crystals can be rotated around this axis, which allows the beam path to be moved and the angle of incidence to be varied without changing the sample position

(Arnold et al., 2012). The vertical incidence angle, α , may be obtained using equation 1-4.

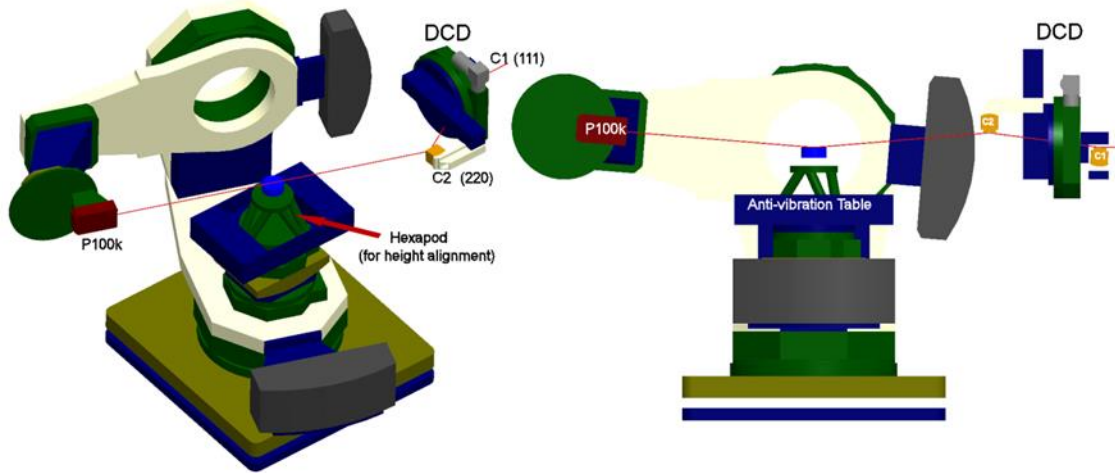


Figure 0-10 Schematic representation of the arrangement of the double crystal deflector (DCD), the diffractometer and the detector (P 100k) used at the 107 beamline at Diamond Light Source (Oxfordshire, UK). The sample is placed on the hexapod located in the center of the diffractometer which then tracks the deflected beam. The DCD uses two different crystals, C1 (111) and C2 (220) to achieve an overall deflection. Rotation of these crystals around the incident beam allows the angle of incidence to be varied. Reprinted from Arnold et al. (2012), (reproduced with permission from the *International Union of Crystallography*).

$$\text{Equation 0-4} \quad \sin \alpha = \sin \psi \sin 2\Delta\theta$$

Where: ψ represents the angle of rotation about the incoming beam axis. When ψ is 90° , α is at its maximum value of $2\Delta\theta$ which corresponds to a maximum possible momentum transfer ($> 2.54 \text{ \AA}^{-1}$) for all energies (Arnold et al., 2012).

The reflectivity, R , is given as the ratio of the specularly scattered intensity to the intensity of the incident x-ray beam. Due to the rapid decrease in reflectivity with increasing Q_z , reflectivity data are often plotted as R/R_F versus Q_z , (or RQ^4 versus Q) where R_F is the Fresnel reflectivity of an ideally flat interface (Evers et al., 2012). Since

x-rays interact with electrons rather than neutrons, XRR probes the electron density profile (EDP) of a sample, and the EDP is described as a series of layers which are defined by their SLD, thickness and roughness (Dabkowska et al., 2009). These parameters are then fitted to model reflectivity curves as shown in Chapter 4.

1.17 Langmuir-Blodgett (LB) and Langmuir-Schaefer (LS) Deposition

Gram-negative bacteria are surrounded by two lipid bilayer membranes (Figure 1-11): (1) an inner cytoplasmic membrane which is composed of phospholipids, mainly phosphatidylethanolamine (70-80%), phosphatidylglycerol and cardiolipin, and (2) an outer asymmetric membrane which is composed of outer membrane proteins, lipopolysaccharides (LPS) and phospholipids (Chatterjee and Chaudhuri, 2012).

The outer membrane (OM) functions as a size-selective permeability barrier and protects the bacteria from harmful compounds in the environment, a property which makes Gram-negative bacteria more intrinsically resistant to most antibiotics than Gram-positive bacteria (Hancock and Rozek, 2002). However, it has been shown that antimicrobial cationic peptides such as macrophage cationic proteins (MCP-1 and MCP-2), can use a separate antibiotic pathway, known as self-promoted uptake across the outer membrane, a strategy which often works as well or better against Gram-negative than Gram-positive bacteria (Sawyer et al., 1988).

The asymmetric bilayer of Gram-negative bacteria can be prepared using the standard Langmuir-Blodgett (LB) and Langmuir-Schaefer (LS) techniques. In the LB technique a hydrophilic, solid block (or wafer) made of silicon dioxide (SiO_2) is raised vertically from the subphase through the monolayer (Figure 1-12 A) while keeping the pressure constant. However, it has been shown that antimicrobial cationic peptides such

as macrophage cationic proteins (MCP-1 and MCP-2), can use a separate antibiotic pathway, known as self-promoted uptake across the outer membrane, a strategy which often works as well or better against Gram-negative than Gram-positive bacteria (Sawyer et al., 1988). The monolayer adsorbs to the solid substrate and a well-organized lipid layer is deposited on the solid substrate (Hughes et al., 2008). By contrast, in the LS technique, the solid wafer is pushed horizontally through the monolayer to deposit the latter on the wafer, thus the substrate is parallel to the interface (Figure 1-12 B).

Figure 1-13 shows a photograph of a neutron flow cell used in this study with inlet and outlet tubes that allow easy exchange of different solutions for each isotopic contrast used. Figure D-5 (Appendix D) shows the neutron flow cell setup for a NR experiment. In this arrangement the neutron beam is incident on the neutron wafer and is reflected from the liquid interface region.

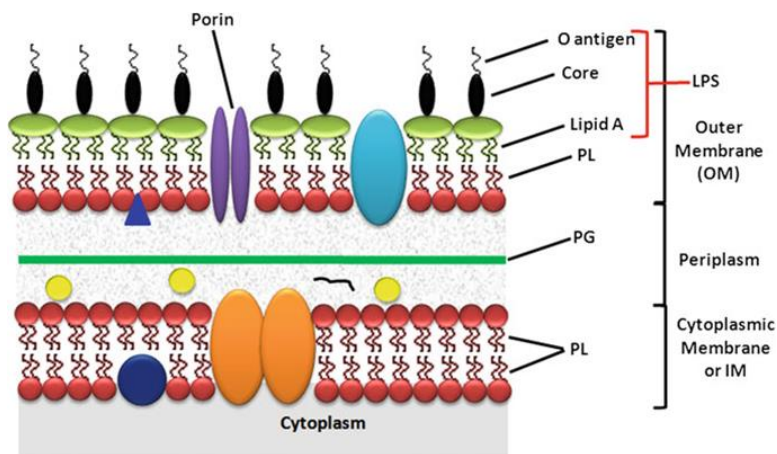


Figure 0-11 Schematic diagram of the Gram-negative bacterial membrane. LPS represents lipopolysaccharide, PL represents phospholipid and PG represents peptidoglycan. Reprinted from Chatterjee and Chaudhuri (2012), (reproduced with permission from Springer).

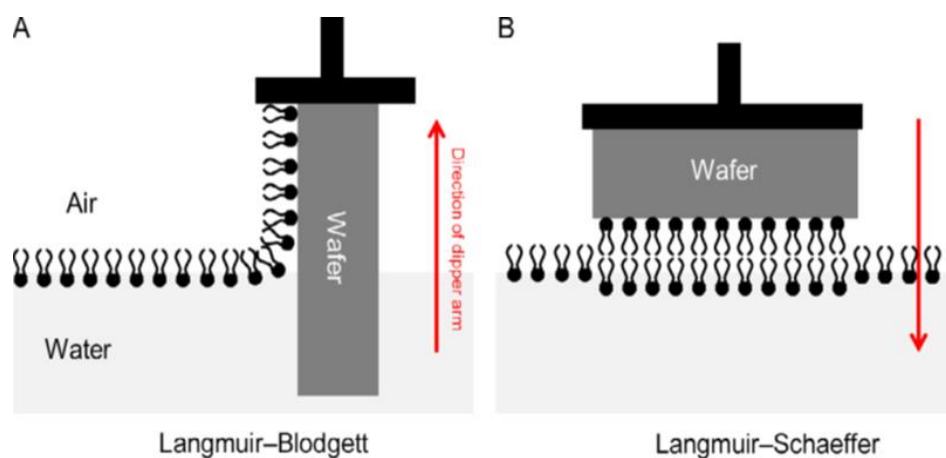


Figure 0-12 The transfer of a monolayer onto a silicon block (wafer) using the standard Langmuir-Blodgett technique (A) and the standard Langmuir-Schaeffer technique (B). Reprinted from Burn et al. (2016), (reproduced with permission from Elsevier).

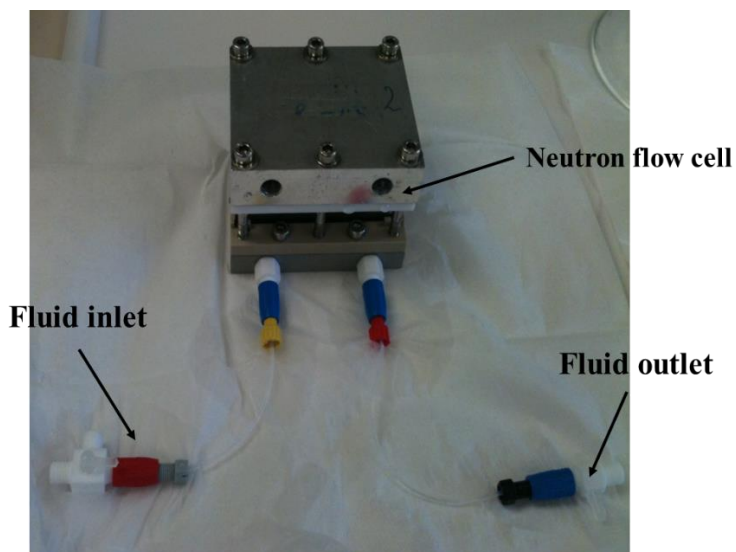


Figure 0-13 Neutron flow cell, with inlet and outlet tubes, used in this study.

1.17.1 Porins

A major component of Gram-negative bacterial membranes consists of protein channels called porins (Nakae, 1976; Puente et al., 1989). These β -barrel porin proteins

span the outer membrane and are largely responsible for the uptake of nutrients while limiting access to toxic substances (Mizuno et al., 1983; Pagès et al., 2008). In 1979, Reeves proposed a nomenclature system for the outer membrane proteins in *E. coli* and *S. Typhimurium*. In this system, the outer membrane proteins were named after their structural genes; e.g., OmpF is the product of the *ompF* gene and Omp means outer membrane protein (Reeves, 1979; Benz, 1985). *E. coli* produces the following porins, OmpF, OmpC and PhoE, whereas the outer membrane of *S. Typhimurium* contains OmpF, OmpC and OmpD (Benz, 1985; Singh et al., 1996). Another major porin identified in both *E. coli* and *S. Typhimurium* cells is OmpA (Smith et al., 2007). The OmpA from *S. Typhimurium* is nearly identical (94%) to *E. coli* OmpA (Singh et al., 2003).

In *E. coli* the outer membrane porins OmpF and OmpC show preferential acceptance for cations (Table 1-1), whereas PhoE selects inorganic phosphate and anions. This preference in selectivity has been proposed to be related to the nature of the amino acid residues lining the channel wall (Nikaido, 2003). In addition, the OmpF porin forms a slightly larger pore (1.2 nm diameter) as compared to OmpC (1.1 nm; Table 1-1); the slightly larger pore diameter is believed to allow for more rapid diffusion through the OmpF than the OmpC pore (Nikaido and Vaara, 1987). Porin channels contain three cylinder-shaped monomers which together are known as trimers (Figure 1-14 B) and each monomer forms a distinct channel (Nikaido, 1994; Jap and Walian, 1996). Each monomer is a β -sheet cylinder that consists of 16 strands which are connected by extraplasmic loops. These loops contribute to the structural integrity of the trimer and also determine the functional properties of the pore (Cowan et al. 1992). For example,

one of these loops, Loop 3, plays a unique role by folding back into the barrel and forming a constriction zone which divides the channel into three main regions, an external mouth or vestibule, a constriction zone and an inner periplasmic mouth or vestibule (Kumar et al., 2015).

Table 0-1 Features of the major outer membrane proteins in *E. coli* K-12 and *S. enterica* Typhimurium.

Source of Porins	Selectivity for anions or cations	Function	Pore Diameter (nm)	Molecular Weight (kDa)
<i>E. coli</i>				
OmpF	cationic ^a	porin	1.2	38
OmpC	cationic ^a	porin	1.1	37
OmpA	non-specific	structural/porin	1.0	37
Pho E	anionic	porin	1.2	36
<i>S. Typhimurium</i>				
OmpF	cationic	porin	1.4	39
OmpC	cationic	porin	1.4	40
OmpD	cationic ^c	porin	1.2	35.5
OmpA	non-specific	structural/porin	1.0	38

^a Kim et al. (2012) and Nikaido (1994), ^b Vandeputte-Rutten et al. (2001) ^c Singh et al. (1996), n/a means not applicable.

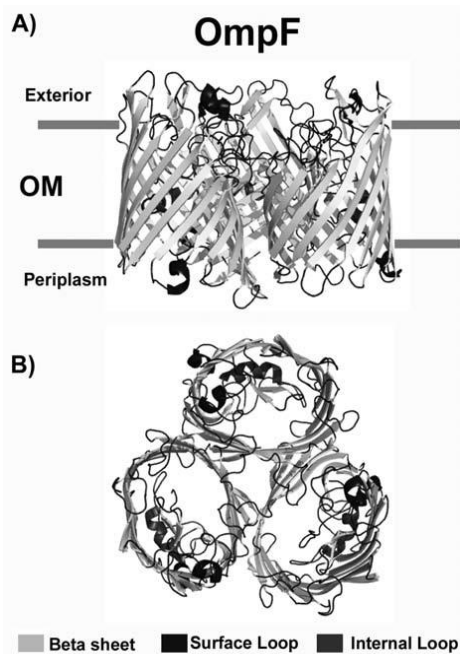


Figure 0-14 (A) The three-dimensional structure of *E. coli* OmpF porin (side view); (B), shows a top view of the trimer. Reprinted from Galdiero et al. (2012), (reproduced with permission from *Current Protein and Peptide Science*).

It has been postulated that the external mouth and the constriction zone contain amino acids with positively or negatively charged residues, whereas the internal vestibule is an uncharged area that is restricted only by the β -strands of the wall (Kumar et al., 2015). The functional mechanisms used to describe the permeation of solutes through porins owe their significance to a combination of experimental and computational studies. For example, liposome swelling assays in *E. coli* and *S. Typhimurium* determined that the OmpF porin has an exclusion limit of ~ 600 nm (Nikaido et al., 1983 and Nikaido, 1994).

Later electrophysiological studies using porin-mediated ion current in planar lipid bilayers were instrumental in determining the selectivity of porin proteins (Benz et al. 1985). Furthermore, computational studies have shown that charged porin residues interact with permeating ions through electrostatic interactions, which rules out the notion of simple diffusion patterns (Im and Roux, 2002 and Im, 2002).

The expression of the major porins OmpF and OmpC in *E. coli* and *S. enterica* Typhimurium is regulated by a two component system (Figure 1-15) consisting of EnvZ and OmpR, and RNA anti-sense regulators, MicF and MicC (Head et al., 1998; Pagès et al., 2008). EnvZ is a trans-membrane-bound histidine kinase that acts as an osmosensor by monitoring changes in external osmolarity and modulates the activity of the DNA-binding protein OmpR by phosphorylation or dephosphorylation (Frost et al., 1989; Benz, 2004a). When phosphorylated, OmpR binds to the promoters of the porin genes and is

responsible for controlling transcriptional expression of genes such as the outer membrane porin protein genes *ompF* and *ompC* (Joo et al., 2013).

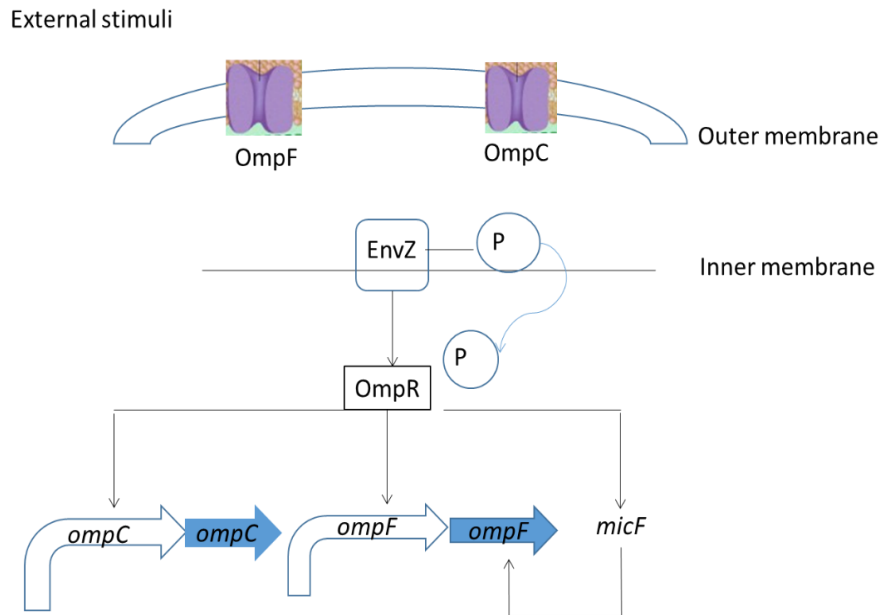


Figure 0-15 Schematic diagram of *ompF* and *ompC* porin gene regulation in *E. coli* and *S. enterica* Typhimurium. EnvZ is a histidine kinase that modulates the activity of the DNA-binding protein OmpR via phosphorylation. The *micF* gene is also involved in the post-transcriptional regulation of *ompF* (Adapted from Pratt et al., 1996).

For example, in growth media of low osmolarity and poor carbon sources, EnvZ relays this information to OmpR and the latter is phosphorylated and activates transcription of the *ompF* gene and represses the *ompC* gene. On the other hand, in growth media of high osmolarity and good carbon sources, the reverse is true where *ompF* transcription is repressed and *ompC* transcription is activated (Mizuno et al, 1988).

1.17.2 The Importance of Efflux Pumps

Efflux pumps are active transporters that move toxic compounds including cationic antimicrobial peptides out of bacterial cells (Band and Weiss, 2015). Several studies have shown that Gram-negative bacteria use these complexes to mediate

resistance against antibiotics and antimicrobial agents (Weatherspoon-Griffin et al., 2014; Weatherspoon-Griffin et al., 2011; Buckley et al., 2006). An example of these efflux pump complex is the *E. coli* and *Salmonella* CpxR/CpxA two-component signal transduction system. CpxA (a histidine kinase) and its response regulator CpxR, regulate gene expression in response to periplasmic stress (Weatherspoon-Griffin et al., 2011).

1.18 Quantitative Real-Time Polymerase Chain Reaction (qPCR)

Real-time polymerase chain reaction is a modification of the standard PCR that is used to generate many identical copies of a specific deoxyribonucleic acid (DNA) sequence. Unlike standard PCR that uses agarose gels to detect the amplified DNA product at the end of the reaction, in real-time PCR amplified deoxyribonucleic acid (DNA) can be measured and detected as the reaction progresses, which is in ‘real-time’ (Bio-Rad Laboratories, 2006). Real-time PCR techniques can be devised to result in either qualitative (presence or absence of a sequence), quantitative (number of copies of DNA) or have “relative quantification” (relative change in gene expression) data (Bio-Rad Laboratories, 2006).

In quantitative real-time Polymerase Chain Reactions (qPCR), a DNA-binding dye or a fluorescent probe is added to the reaction tubes which make the real-time detection of PCR products possible. Quantification is achieved by measuring the amount of amplified product at each stage of the PCR cycle. As shown in Figure 1-16, there is little change in fluorescence at the baseline stage of the reaction, but during the exponential phase there is theoretical doubling of the DNA product. At the plateau stage

of the reaction, the reaction components are limiting and no more fluorescence is produced (Bio-Rad Laboratories, 2006).

Enough PCR product needs to accumulate before a detectable fluorescent signal is obtained, and the cycle number at which this occurs is the quantification (or C_q), cycle (Guénin et al., 2009). This fluorescence level that distinguishes relevant amplification from background signal (little change in fluorescence) is called the threshold level (Figure 1-16). The C_q value is also dependent on the amount of target DNA present at the start of the qPCR reaction and the amount of DNA produced during the PCR cycle. If more target DNA is present at the start of the reaction or produced during the PCR cycle, fewer cycles will be required for detectable fluorescence and an earlier or a lower C_q value is obtained. By contrast, if the amount of target DNA at the start of the reaction and the amount of DNA produced during the PCR cycle is low, then amplification is observed in later cycles and a larger C_q value is obtained. The manufacturers of the qPCR instrument used in this study suggest a C_q range of 8-35 is desirable (Applied Bio-Systems, CA, USA).

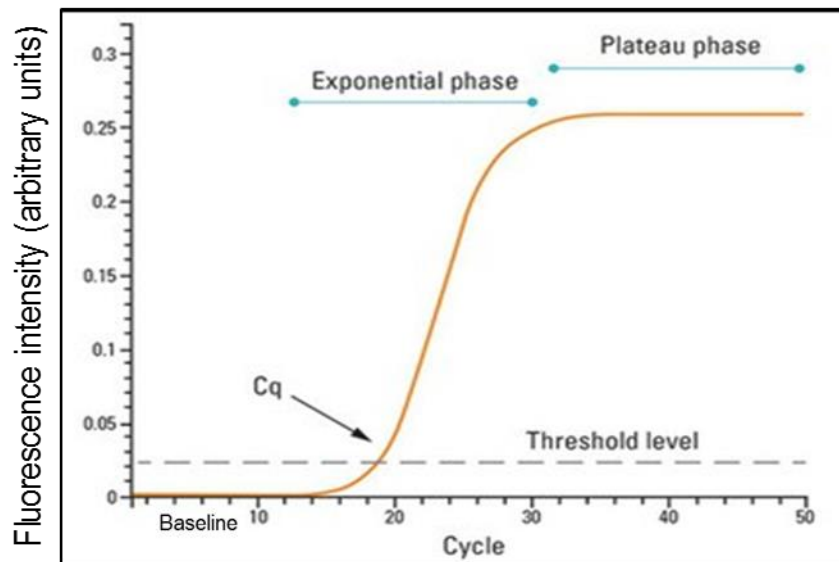


Figure 0-16 Amplification plot showing the accumulation of amplified product as a qPCR reaction progresses. The number of PCR cycles is shown on the x-axis, and the fluorescence intensity, which is proportional to the amount of sample in the tube is shown on the y-axis (<http://www.garvan.org.au>).

Quantitative real-time PCR has had many applications in recent years. For example, Saikaly et al. (2007) used qPCR to monitor the fate and transport of the surrogate biological warfare agents *Bacillus atrophaeus* and *Serratia marcescens* in building debris and leachate from landfills with the aim of assessing alternatives for the safe disposal of biocontaminants. More recently qPCR has been applied to quantify pathogenic bacteria in food, for example *St. aureus* in cheese (Ablain et al., 2009) and *L. monocytogenes* in different food products (Rantsiou et al., 2008).

In addition, qPCR can also be used to quantify gene expression levels of bacteria used in the food industry, such as bacteria used in the ripening of cheese (*Lactobacillus paracasei*, Faletti et al., 2010) and bifidobacteria in fermented oat drink (Lahtinen et al., 2006). Moreover, Dumas et al. (2006) used qPCR for the analysis of antimicrobial resistance gene expression in *Pseudomonas aeruginosa* and reported that the method was fast and sensitive. In the present study, qPCR was used to compare the expression of outer membrane porin genes in untreated *E. coli* K-12 and *S. enterica* Typhimurium 14028 cells and cells exposed to native or CHD-treated clupeine.

1.19 Research Questions and Objectives

Interest in CAPs such as clupeine is increasing due to their potential role as substitutes for antimicrobial agents (Pink et al., 2014). Clupeine has exhibited antimicrobial activity toward some food-borne pathogenic Gram-negative bacteria (Johansen et al., 1997; Truelstrup Hansen et al., 2001) but its method of internalization in

at least some strains of Gram-negative bacteria is still unclear. The experiments used in the present study to address these research questions involve a unique multidisciplinary approach involving chemical modification and physiochemical and microbiological analyses.

Neutron reflectometry and x-ray reflectometry were used to ascertain the manner in which the CHD-treated and native peptides interact with bacterial model surfaces. In this thesis it was hypothesized that a small reduction in charge of native clupeine (10% arginine modification) to from CHD-treated clupeine could result in different interactions in *E. coli* model membranes and in Gram-negative target bacteria. It is anticipated that the results from this work will not only lead to a better understanding of the initial steps involved in clupeine interaction with *E. coli* K-12 and *S. enterica* Typhimurium 14028 cells but may also contribute to the development of more cost-effective antimicrobials. Accordingly, a series of research questions will be addressed:

- 1) Do native and CHD-treated clupeine have different cytotoxic and hemolytic activity against the selected bacteria and human red blood cells?
- 2) Does exposure to native and CHD-treated clupeine change the morphology of *E. coli* K-12 and *S. enterica* Typhimurium 14028 cells?
- 3) Is the relative expression of the outer membrane porin genes *ompF* and *ompC* and the proteomic profiles different in *E. coli* K-12 and *S. enterica* Typhimurium 14028 cells exposed to native and CHD-treated clupeine, and are these responses concentration dependent?
- 4) Is the relative expression of the protease gene *ompT* increased when *E. coli* K-12 cells are exposed to MIC concentrations of native and CHD-treated clupeine?

- 5) Are there differences in the structure and composition of model *E. coli* monolayer and bilayer systems in the presence of native versus CHD-treated clupeine?

1.20 Scope of the Thesis

Chapter 1 introduces the problem of bacterial resistance and the merits of the CAP clupeine. An overview on the methods used to study peptide-lipid interactions is given and the chapter ends with an outline of the research objectives and rationale for this work. Chapter 2 begins with an overview of the chemical modification of clupeine and the determination of the peptide's minimum inhibitory concentration (MIC) and minimum bactericidal concentrations (MBC). The hemolytic activities of native and CHD-treated clupeine were determined in human red blood cells. In addition, the effects of native and CHD-treated clupeine on the morphology of *E. coli* K-12 and *S. enterica* Typhimurium 14028 cells are also presented.

In Chapter 3, data obtained from quantitative real-time PCR (qPCR) and Sodium Dodecyl Sulfate Polyacrylamide Gel Electrophoresis (SDS-PAGE) experiments are presented. Here the changes in the relative expression ratios of outer membrane porin (omp) genes (*ompF* and *ompC*) are described when *E. coli* K-12 and *S. enterica* Typhimurium 14028 cells are exposed to minimum inhibitory concentrations of native and CHD-treated clupeine. Protein bands selected from SDS-PAGE gels were identified by mass spectrometry and changes in the relative expression of the *E. coli* protease gene *ompT* were also investigated.

In Chapter 4, surface pressure measurements, neutron reflectometry and x-ray reflectivity techniques are applied to provide a more detailed picture of the interfacial activity of native and CHD-treated clupeine in monolayer membranes and in Chapter 5

bilayer model systems were used to determine the peptide-lipid interactions in a system that more closely represents the symmetry of the Gram-negative inner membrane. The model membranes were formed by: (1) preparing lipid monolayers at the air-liquid interface and (2) preparing Langmuir-Blodgett/Langmuir-Schaefer bilayer model systems which more closely represents the symmetry of the Gram-negative inner membrane. These studies provided an opportunity to collaborate with researchers at the University of Reading, the Diamond Light Source and the Rutherford Appleton Laboratory (Harwell Science and Innovation Campus, Didcot, Oxfordshire, UK).

In Chapter 6, the results of Chapters two to five are summarized and the potential future directions of this research are outlined. Detailed descriptions of selected parts of the analyses are described in Appendix E.

CHAPTER 2: THE CHARACTERIZATION OF NATIVE AND CHD-TREATED CLUPEINE

2.1 Abstract

Bacterial resistance is of major importance to the food and medical sectors, consequently new approaches to overcome this problem are always of interest. One way to manage bacterial resistance is by the use of cationic antimicrobial peptides (CAPs) as commercial antimicrobial agents if their efficacy can be shown. The aim of the present study was to chemically modify the charge of native clupeine with 1,2-cyclohexanedione (CHD) (10% arginine modification) as a means to investigate the effect of peptide charge reduction on the cytotoxic and hemolytic activities of both peptides. The cytotoxic and hemolytic activities of the native and CHD-treated peptide were investigated against *E. coli* K-12 and *S. enterica* Typhimurium 14028 cells and human red blood cells, respectively. Minimum inhibitory concentration (MIC) values determined by the Alamar blue assay showed that the *E. coli* strain was more susceptible to CHD-treated clupeine and the native peptide (400 $\mu\text{g}/\text{mL}$ and 500 $\mu\text{g}/\text{mL}$ respectively), and minimum bactericidal concentration (MBC) values of 700 and 635 $\mu\text{g}/\text{mL}$, for the native and CHD-treated peptides, respectively. On the other hand, the *S. Typhimurium* strain which had similar MIC and MBC values of (1250 $\mu\text{g}/\text{mL}$ and 2500 $\mu\text{g}/\text{mL}$ respectively, for both peptides). The percent hemolysis observed in the presence of the native peptide ($0.36\% \pm 0.01$) was significantly ($P < 0.05$) lower than in the presence of the CHD-treated peptide ($0.45\% \pm 0.01$). The small increase in the relative abundance of the hydrophobic amino acids alanine and proline in CHD-treated clupeine may have contributed to this effect. Scanning electron microscopy (SEM) revealed no visible signs of cell lysis in the

bacterial strains, following peptide treatment, although fewer flagella were observed in *S. enterica* Typhimurium 14028 cells with increasing concentrations of both peptides. These results suggest that changes in the charge and the structure of the CHD-treated clupeine may account for the different effects observed in the tested cells.

2.2 Introduction

Food antimicrobials are natural or chemical agents that are used to ensure the safety of our food supply by inhibiting or preventing the growth of foodborne pathogens (Davidson et al., 2005). Unfortunately, the increased emergence of microbial resistance limits the usefulness of some antimicrobial agents, thus, there is increased interest to identify potential alternative antimicrobial agents to use as food preservatives. Cationic antimicrobial peptides (CAPs) are good potential candidates for food applications due to their broad spectrum of antimicrobial activity and their low tendency to develop bacterial resistance (Wang et al., 2016).

Although most CAPs have similar physical properties such as: (1) net positive charge of +2 to +9; (2) small polypeptides (12 to 50 amino acid residues); and (3) amphiphilic nature, their antibacterial activity is often difficult to predict because of the variability in their amino acid sequences and 3-D structures (Yeaman and Yount, 2003; Haney, 2011). Indeed, other researchers (Bals and Wilson, 2003; Jenssen et al., 2006) have shown that even when CAPs have similar secondary structures, they can exhibit very different antimicrobial effects. Thus, when any CAP is modified it cannot be assumed that the mechanism of action will remain the same; each must be examined individually to evaluate its merits.

Clupeine was chosen as a model CAP for this study because it has shown antimicrobial activity toward some food-borne pathogenic Gram-negative and Gram-positive bacteria (Johansen et al., 1997; Truelstrup Hansen et al., 2001). However, non-specific binding of the peptide to anionic food surfaces limits the availability of the peptide to interact with the anionic surfaces of target bacteria. For this reason, Potter et al. (2005) reduced the alkalinity of native clupeine by blocking some of the guanido groups of arginine residues using CHD. In addition, unlike the native peptide, CHD treated clupeine has shown significant reduction of Gram-negative spoilage bacteria (*Enterobacteriaceae*) in ground beef (Potter et al., 2005). During the chemical modification of clupeine, the surface charge can be reduced by using a mild treatment with a low (0.05 M) concentration of CHD at pH 8.5 (Figure 2-1), (Means and Feeney, 1971; Potter et al., 2005).

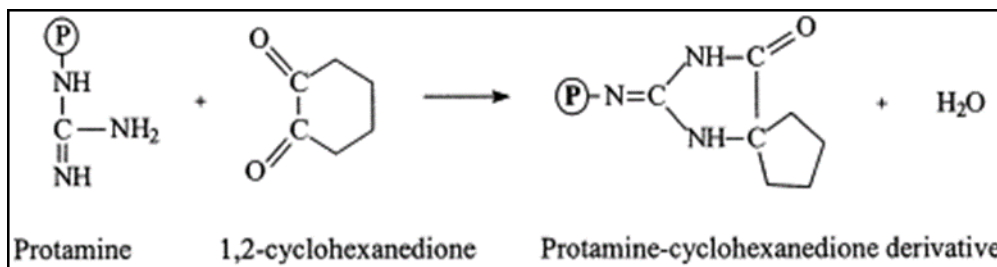


Figure 0-1 Scheme for the chemical modification of clupeine through the chemical reaction between CHD and the guanido groups of arginine. Reprinted from Potter et al. (2005), (reproduced with Permission from Elsevier).

Most of the earlier studies on clupeine focused on the interactions of native clupeine with Gram-positive organisms whereas Gram-negative organisms were believed to be less susceptible to native clupeine (Islam et al., 1984a; Johansen et al., 1995). However, other studies have since proved that some Gram-negative organisms are more

sensitive to clupeine than previously proposed (Truelstrup Hansen et al., 2001; Johansen et al., 1997). This study also helps to contribute to the understanding of the interaction of the native and CHD-treated clupeine with Gram-negative organisms.

Some of the more recent studies using native clupeine have shown that different factors can either improve or weaken the efficacy of the peptide. For example, Truelstrup Hansen et al. (2001) reported on a synergistic or bactericidal effect of clupeine in the presence of EDTA against several foodborne pathogens. In addition, Pink et al. (2003) reported on the decreased antimicrobial activity of clupeine against *Pseudomonas* PAO1 and *E. coli* in the presence of magnesium (Mg^{2+}) and calcium (Ca^{2+}) ions.

Chemical modification of proteins has also been reported to play an important role in determining the functionality of proteins (Kito, 1986; Wong et al., 2006). Accordingly, in the present study, a small reduction in charge (10% arginine modification) of native clupeine was carried out with 1,2 cyclohexanedione (CHD) to address whether native and CHD-treated clupeine have different cytotoxic and hemolytic activities. The cytotoxic activities of the native and CHD-treated peptide, measured as MIC and MBC were compared in two Gram-negative bacteria, *E. coli* K-12 and *S. enterica* Typhimurium 14028 cells. On the other hand, the hemolytic activities of the peptides were determined using human red blood cells. Also, changes in the morphology of the bacterial strains exposed to native and CHD-treated clupeine were investigated using scanning electron microscopy (SEM). Finally, the amino acid composition of the native and CHD-treated peptides were also analyzed to determine if charge reduction had any effect on this property.

2.3 Materials and Methods

The following reagents were obtained from Sigma-Aldrich (Oakville, Canada): protamine sulfate from Atlantic herring (*Clupea harengus*), L-arginine HCL solution, CHD, 8-hydroxyquinoline, sodium hydroxide, liquid bromine, and HPLC grade chloroform.

2.4 Methods

2.4.1 *Clupeine Modification with CHD*

The surface charge of arginine was reduced by adding CHD (a compound that reacts with the guanido groups of arginine) to native clupeine in a modified version of the method described by Means and Feeney (1971). In each of six large Erlenmeyer flasks, 2.8 g of CHD was dissolved in 500 mL of 0.2 M boric acid buffer (pH 8.5) then 2.5 g of native protamine sulphate from herring (Sigma-Aldrich, Oakville, Canada) was added and the contents of each flask stirred for 20 s. The flasks were covered to prevent photo-oxidation of the CHD and were then placed in a covered shaking water bath at 37°C. Two flasks were removed after 1, 2.5 and 7.5 min and after each time point, the reaction was quenched by adding 500 mL of ice cold 5% (v/v) acetic acid to each flask. Control samples were prepared in a similar manner except that no CHD was added to the reaction flasks.

The volume of the content in each flask was reduced to 200 mL using a Prep/Scale Millipore Model P34404 ultrafiltration apparatus (Millipore, Toronto, Canada) with 900 cm², 1000 Da tetrafluoroethylene (TFE) filters (110 rpm). The reduced volumes were then washed with 1 L of 1% (v/v) acetic acid and 2 L of distilled, deionised water (DDW) and concentrated once again to 200 mL. Finally, the purified modified

clupeine samples were frozen at -30°C and then freeze dried the following day in a freeze-dryer (Labconco, Missouri, USA). Stock solutions of each of the freeze-dried clupeine samples were prepared by first dissolving 0.1 g of the powder in 40 mL of 1% (v/v) acetic acid. Working solutions were then prepared by diluting the stock solutions 1:50 with DDW.

2.4.2 Detection of Clupeine Modification

2.4.2.1 Modification with CHD

The average absorbance at 494 nm from the Sakaguchi reaction (Sakaguchi, 1950; Potter et al., 2005), which is specific for arginine, was used to determine the unmodified arginine residues in the CHD-treated clupeine. The percent modification of arginine residues was then determined using an arginine-HCl standard curve and taking into account that ~20 of the 30 amino acid residues in clupeine are arginine (Ando et al., 1973).

For the Sakaguchi reaction, three sets of test tubes for three replicates were prepared as follows: the tubes for samples contained 4 mL DDW and 1 mL CHD-treated clupeine sample; the tubes for the negative control samples contained 4 mL DDW and 1 mL of negative control (clupeine samples that were exposed to modification solvents without the addition of CHD); and the blank tubes contained 5 mL of DDW. The control clupeine samples were used to account for inherent substances that would affect the absorbance of the modified samples. Thus, the absorbance value of the negative control was subtracted from the absorbance values of the CHD-treated samples.

To each set of tubes the following reagents were added 1.0 mL of 0.2% (w/v) 8-hydroxyquinoline, followed by 1.0 mL of 10% NaOH (final concentration of 0.028%

(w/v) 8-hydroxyquinoline). All the tubes were then vortexed and placed on ice for exactly 3 min after which 0.5 mL of cold sodium hypobromite (0.4% w/v) was added to develop the colour, and the tubes were vortexed for 30 s. After vortexing, 1.0 mL of 40% (w/v) urea was quickly added and mixed to destroy excess hypobromite and to prevent the colour from fading (Hua et al., 2008). Absorbance readings at 494 nm in a UV/Visible spectrophotometer (Pharmacia Ultraspec 2000) were then obtained within 2 min of adding sodium hypobromite.

To generate the arginine standard curve, a stock solution of arginine-HCL was prepared by dissolving 100 mg of arginine in 100 mL of DDW. Standard solutions were then prepared by diluting the stock solution to obtain a range of concentrations from 0 - 20 $\mu\text{g/mL}$. A blank reaction tube was prepared in a similar manner as the standard solutions except that none of the arginine solution was added. For the standard curves, absorbance readings were measured at 494 nm (Hua et al., 2008). The linear regression equation of the line was used to determine the percent modification of the arginine residues of the original 20 residues per clupeine molecule.

2.4.3 Determination of the Hemolytic Activity of Clupeine

2.4.3.1 Hemolytic assay

The cytotoxicity of native and CHD-treated clupeine against human red blood cells was determined by a hemolytic assay, performed as outlined by Andrä et al. (2008). Briefly 20 μL of human red blood cells (5×10^8 cells/mL) were washed in 10 mM PBS (pH 7.4) and incubated with 80 μL of native and CHD-treated peptide (concentrations between 10 and 100 $\mu\text{g/mL}$ in 10 mM PBS, pH 7.4) for 30 min at 37°C. After incubation, intact red cells were removed by centrifugation for 10 min at 1000 x g, and

the supernatant diluted 10 fold with 10 mM PBS, pH 7.4. Absorbance at 405 nm was measured to determine the amount of released hemoglobin (hemolysis) as:

Equation 0-1

$$\%hemolysis = \left\{ \frac{A_{sample} - A_{buffer}}{A_{max} - A_{buffer}} \right\} \times 100$$

Where:

A = absorbance

A_{max} = maximum lysis

Maximum lysis (A_{max}) was achieved by adding the same volume of distilled DDW, to the cells instead of the peptide.

2.4.4 Determination of Minimum Inhibitory Concentration (MIC)

The MIC, i.e., the lowest concentrations of native and CHD-treated clupeine required to inhibit the growth of *E. coli* K-12 MG1655 (American Type Culture Collection, ATCC, Manassas, VA, USA), and *S. enterica* Typhimurium strain 14028 (ATCC, Manassas, VA, USA), were determined by the Alamar Blue broth dilution assay. The protocol used was adapted from Baker et al. (1994) and Truelstrup Hansen et al. (2001) and the redox dye resazurin (Acros Organics) was incorporated in the assay. In the presence of resazurin, active, living cells cause reduction of the dye from blue (its oxidized form) to pink (the reduced form). MIC tests were performed to determine the concentrations with which to treat the test bacteria for gene expression studies, and for electron microscopy.

Stock solutions of native and CHD-clupeine were prepared by dissolving 100 mg in 1 mL of 0.1% sterile Tween 80 surfactant (Sigma) in distilled water. Working

solutions (7.8 mg/mL) were then prepared by adding 0.78 mL of antimicrobial stock to 9.22 mL of tryptic soy broth (TSB, Oxoid, 30 g/L, pH 7.0) to obtain an initial maximum concentration of 5000 µg/mL. The 5000 µg/mL solutions were serially diluted with TSB to obtain concentrations of 500, 1000, 1250 and 2500 µg/mL of native and CHD-treated clupeine.

A single colony of each test organism grown on Tryptic Soy Agar (TSA) plates was used to inoculate a volume of 30 mL of TSB. The tubes were then placed overnight in a shaking incubator set at 250 rpm and 37°C to obtain mid log-phase, (confirmed in preliminary experiments). The overnight bacterial cultures (*E. coli* K-12 and *S. enterica* Typhimurium 14028) were diluted with peptone saline (PS, 0.1% peptone (Oxoid); 0.85% sodium chloride (Fisher)) to $\sim 10^4$ cfu/mL and used to inoculate wells were in sterile 96-well polypropylene microtitre plates.

All tests were done in triplicate, with wells containing 125 µL of TSB with 0 (control), to 2500 µg/mL of native or CHD-treated peptide, 50 µL of bacterial dilution and 20 µL of resazurin. The plates were incubated for 24 h at 37°C and the lowest concentrations of native and CHD-clupeine required to inhibit the growth (i.e., no colour change) was recorded as the MIC. The minimum bactericidal concentration (MBC) was determined by surface-inoculating the entire contents of wells that remained blue after 24 h onto Tryptic Soy Agar (TSA, Oxoid, 40g/L) plates. The plates were incubated at 37°C overnight and observed for the presence or absence of growth.

2.4.5 Scanning Electron Microscopy

To observe the effect of native and CHD-treated clupeine on the morphology of *E. coli* K-12 (strain MG1655) and (*S. enterica* Typhimurium 14028) cells, SEM was

performed. All bacterial strains for SEM were grown overnight in TSB at 37°C and then diluted in PS to obtain an $A_{450 \text{ nm}}$ reading of 1 to reach a cell count of $\sim 1.0 \times 10^9$ CFU/mL, which was confirmed by spread plating on TSA plates. The bacterial cultures were placed in 6-well plates (Millipore, Sigma), and coverslips that were previously coated with Poly-L-Lysine (Electron Microscopy Sciences, EMS) were added to the plates to encourage attachment of bacteria to the coverslips. The cultures were treated with the following concentrations of native and CHD-treated clupeine; for *E. coli*, 500 $\mu\text{g/mL}$ (400 $\mu\text{g/mL}$ for CHD-treated clupeine), 1000 $\mu\text{g/mL}$, 1250 $\mu\text{g/mL}$, and for (*S. enterica* Typhimurium 14028) 500 $\mu\text{g/mL}$, 1250 $\mu\text{g/mL}$ and 2500 $\mu\text{g/mL}$, for 30 min at 37°C. Untreated controls (no peptide) were also prepared for each bacterium.

Following incubation, the cells were washed once with 0.5 mL of sterile PBS and then primary fixation was carried out overnight with 2.5% (w/v) glutaraldehyde (in DDW). The next day, the cover slips were washed with three changes of DDW and then post-fixed in 1% (w/v) OsO_4 (Electron Microscopy Sciences, Hatfield, PA, US) for 20 min. The coverslips were washed in DDW to remove excess OsO_4 and then dehydrated in increasing concentrations of ethanol (25% to 100%). The dried cover slips were mounted on stubs, sputter-coated with gold-palladium (27 nm), and stored under vacuum. Microscopy was performed at the Scientific Imaging Suite, Dalhousie University, using a Hitachi S-4700 FEG Scanning Electron Microscope (Hitachi High Technologies Canada, Toronto, Canada). Representative images were taken using an electron energy of 3.0 kV and a magnification range of 500 to 30,000 x.

2.4.6 Amino Acid Analysis of Native and CHD-Treated Clupeine

Amino analysis was performed at the Hospital for Sick Children, Peter Gilgan Centre for Research & Learning (SPARC BioCentre, Toronto, Canada). The analysis was performed using a Waters Acquity UPLC System (Milford, Massachusetts, USA). Peptide samples (0.01 g) were hydrolyzed with 6 N hydrochloric acid with 1% phenol and using the Waters Pico-Tag Workstation, air was removed from the reaction vial, replaced with pre-purified nitrogen and sealed under nitrogen. The reaction vial was placed in the block heater to hydrolyze for 24 h at 110°C. After hydrolysis, the samples were dried by a Tomy CC-181 Centrifugal Concentrator with a Sargent-Welch Model 8821 vacuum pump and the excess HCl was also removed during this process.

After drying, the samples were treated with a redrying solution consisting of methanol: water: triethylamine (2:2:1), then mixed and dried under vacuum for 15 min. The samples were then derivatized for 20 min at room temperature with a derivatizing solution made up of methanol: water: triethylamine: phenylisothiocyanate (PITC) (7:1:1:1). After 20 minutes, the derivatizing solution was removed under vacuum and the samples were dissolved in a sample phosphate buffer (pH 7.4) and an aliquot (4 µL) injected into the column (UPLC BEH C18, 2.1 x 100 mm), running on a modified PICO-TAG gradient. The column temperature was 48°C and the derivatized amino acids were detected at 254 nm using a TUV Detector Module. Data were collected and processed using Waters Empower 3 Chromatography software.

2.5 Results

2.5.1 *Identification of CHD-Treated Clupeine*

Table 2-1 shows the percent arginine modified achieved by exposing native clupeine to CHD for up to 7.5 min. Overall, the percent arginine modification increased

with time, and after 7.5 min 48% modification had been accomplished (Table 2-1). The CHD-treated clupeine with 10% of the arginine residues being modified was chosen for further experiments because it had been previously reported that moderate reductions in charge led to slightly improved antimicrobial efficacy (Potter et al., 2005). When comparing the amino acid compositions of the CHD-treated and native clupeine samples it was observed that the CHD-treated clupeine had a modest decrease (~6%) in the relative abundance of arginine and marginal increases in the relative abundance of the hydrophobic residues alanine (0.9%) and proline (1.4%) (Table 2-2). The decrease in the relative abundance of arginine may be because the modified arginines could not be derivatized and therefore were not detected in the amino acid analysis. No differences were observed in the other amino acid residues.

Table 0-1 Percent modification of CHD-treated clupeine and control samples. The absorbance values of the control were subtracted from those of the test samples before the percent modification was calculated.

Incubation time (min)	Average Absorbance Values (494 nm)	% Modification
0 (control)	0.021	-
1	0.028	3
2.5	0.071	10 *
5.0	0.157	23
7.5	0.319	48

*The (10% arginine modified) CHD-treated clupeine (corresponding to 2 modified arginine residues per molecule) was used in this study.

Table 0-2 Relative abundance of amino acid residues that were different in native and CHD- treated clupeine, determined by amino acid analysis.

Amino Acid Residue	Relative Abundance % Native	Relative Abundance % CHD-treated
Arginine	66.4	61.4
Proline	6.0	7.4
Alanine	3.9	4.8

2.5.2 Cytotoxicity of Native and CHD-Treated Clupeine

The presence of the CHD-treated clupeine caused release of an average of 0.45% \pm 0.01 hemoglobin, which was significantly ($P < 0.05$) higher than the release from cells exposed to the native peptide (average 0.36% \pm 0.01) (Table 2-3). Increasing peptide concentrations had no effect ($P > 0.05$) on the hemolytic activity which demonstrates the peptides' specificity for prokaryotic versus eukaryotic cells.

Table 0-3 Cytotoxicity of native and CHD-treated clupeine on human red blood cells. The data shown are the averages of three separate experiments and the concentrations shown represent mean values \pm SD (n=3).

Concentration of Peptide ($\mu\text{g/mL}$)	% Hemolysis (Native)	% Hemolysis (CHD-treated)
0	-	-
10	0.35 \pm 0.006	0.43 \pm 0.001
50	0.37 \pm 0.001	0.48 \pm 0.001
100	0.38 \pm 0.002	0.46 \pm 0.002
500	0.35 \pm 0.005	0.44 \pm 0.006

Table 0-4 The effect of native and CHD-treated clupeine on the MIC and MBC values of *E. coli* K-12 cells (strain MG 1655) and *S. enterica* Typhimurium 14028 cells.

Bacteria	Cationic Peptide	MIC ($\mu\text{g/mL}$)	MBC ($\mu\text{g/mL}$)
<i>E. coli</i> K-12	Native	500	700
	CHD-treated	400	635
<i>S. Typhimurium</i> 14028	Native	1250	2500
	CHD-treated	1250	2500

Table 2-4 shows the MIC and MBC values determined against the test strains in the presence of native and CHD-treated clupeine. The MIC and MBC values showed that *E. coli* K-12 was more sensitive to the CHD-treated peptide as compared to the native peptide. In contrast, *S. enterica* Typhimurium 14028 cells showed similar sensitivity to the presence of the native and CHD-treated peptides and the same MIC and MBC values (1250 $\mu\text{g/mL}$ and 2500 $\mu\text{g/mL}$, respectively) were observed in the presence of native clupeine and CHD- treated clupeine.

2.5.3 Morphology of *E. coli* K-12 and *S. enterica* Typhimurium 14028 Cells in the Presence of Native and CHD-Treated Clupeine

Overall, the native (Figure 2-2) and CHD-treated clupeine (Figure 2-3) caused minor changes in the morphology of *E. coli* K-12 (strain MG1655) cells and *S. enterica* Typhimurium 14028 cells. SEM showed that the *E. coli* cells appeared intact and smooth with no lysis or signs of rupture in the presence of both peptides; however, the shape of the cells appeared more elongated in the presence of 400 $\mu\text{g/mL}$ CHD-treated clupeine compared to the untreated cells.

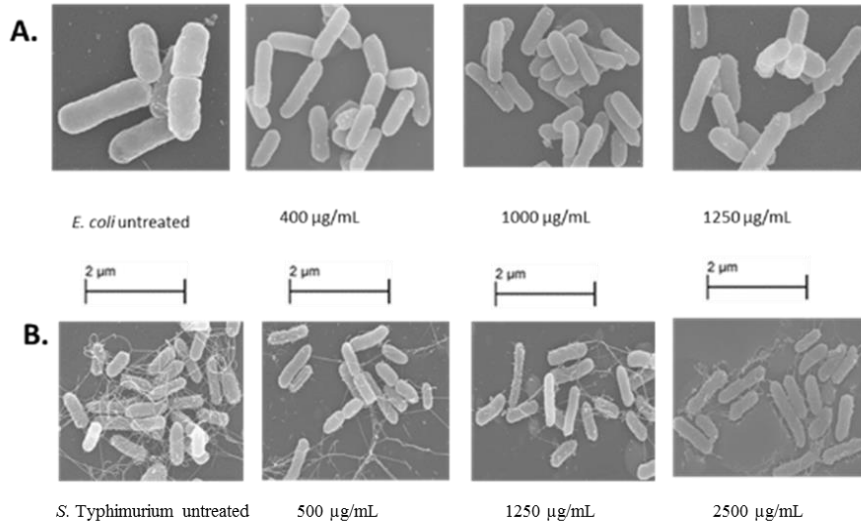


Figure 0-2 Scanning electron micrographs of images of untreated and native clupeine (A) *E. coli* K-12 and (B) *S. enterica* Typhimurium 14028 cells.

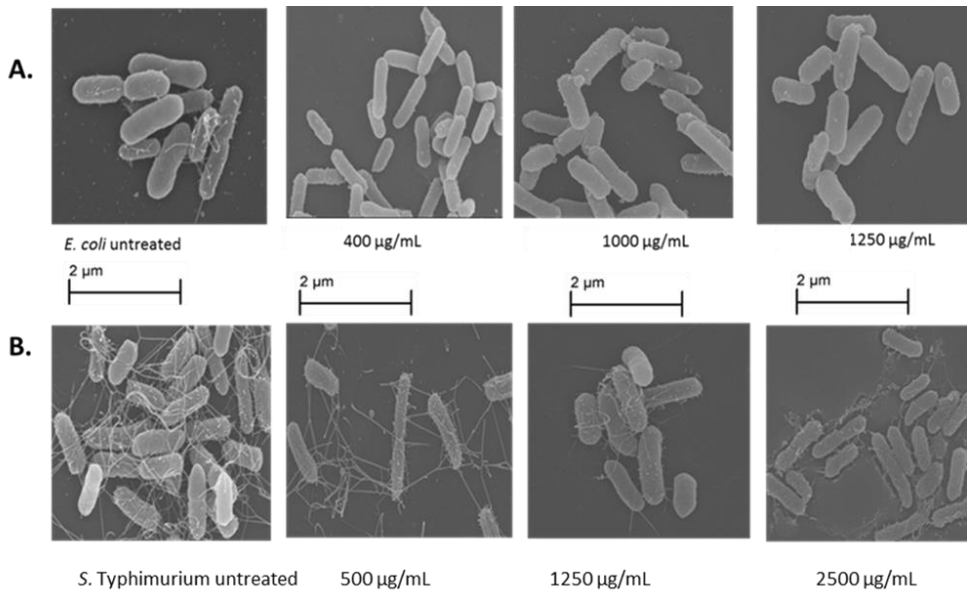


Figure 0-3 Scanning electron micrographs of untreated and CHD-treated (A) *E. coli* K-12 and (B) *S. enterica* Typhimurium 14028 cells.

Similarly, the *S. enterica* Typhimurium 14028 cells also showed no signs of lysis however, fewer flagella were observed on the cells with increasing concentrations of the native and CHD-treated peptide. In an earlier study, the presence of clupeine resulted in considerable cell membrane lysis and cytoplasmic leakage in both Gram-positive (*L. monocytogenes*) and Gram-negative (*S. putrefaciens*) cells as observed with light microscopy (Johansen et al., 1996). In the latter study, clear evidence of cell envelope damage was observed for *S. putrefaciens* in the presence of 100 µg/mL protamine, whereas protamine concentrations of 500 and 1000 µg/mL resulted in nearly complete cell damage. These findings suggests at the very least, that different Gram-negative bacteria have different susceptibilities to clupeine.

2.6 Discussion

Clupeine modified by CHD (10% arginine modification) (Figure 2-1 and Table 2-1) was initially hypothesized to have different interactions with the tested cells as compared to the native peptide. To begin to characterize the peptides' antimicrobial activity, their MICs were determined for two Gram-negative bacteria (Table 2-4). Although the Alamar blue assay does not differentiate between the modes of action of the peptide, i.e., whether it is bactericidal or bacteriostatic (Wiegand et al., 2008), this method was appropriate to measure the MIC because it measures bacterial metabolic activity and therefore cell clumping often observed in clupeine treated bacteria had no effect on the assay (Johansen et al., 1995). For the present study no autoaggregation assays were performed.

The MIC obtained for *S. enterica* Typhimurium 14028 cells in this study is in agreement with other studies that used native clupeine (Potter et al., 2005; Pink et al.,

2014) and CHD-treated clupeine (Potter et al., 2005). However, the higher value observed (1250 µg/mL) in the presence of *S. enterica* Typhimurium 14028 compared to *E. coli* K-12 cells (400 µg/mL and 500 µg/mL in the presence of the CHD-treated and the native peptide respectively) suggests that the *E. coli* K-12 strain tested was more susceptible to the presence of the peptides under the experimental conditions used. Although Potter et al. (2005) reported a lower MIC for *E. coli* 25922 (313 µg/mL) it is still comparable to what was observed in this study for 10% CHD-treated clupeine. This finding therefore supports the argument that *S. enterica* Typhimurium 14028 cells appears more ‘tolerant’ to native and CHD-treated clupeine than *E. coli* K-12 cells.

The differences in the MIC values for the tested strains may be explained by the findings from a study by Witherspoon-Griffin et al. (2014). These authors showed that the CpxR/CpxA two-component system facilitates *Salmonella* and *E. coli* resistance to cationic antimicrobial peptides including protamine from salmon, by activating transcription of two gene loci (*amiA* and *amiC*) that encode two peptidoglycan amidases. However, other factors such as the environmental pH in which the organisms are present may impact the MIC. For example, in an agar-dilution assay *Listeria monocytogenes* showed different levels of susceptibility to clupeine based on the pH of the environment; MICs decreased from 500 µg/mL to 50 µg/mL when pH was increased from 7 to 7.5 and 8.0 (Truelstrup Hansen and Gill, 2000).

Melo et al. (2009) discussed several properties of CAPs including their charge, hydrophobicity, conformation and amphipathicity that may influence their interaction with bacterial membranes. Clupeine consists of approximately 31 amino acids, 20 of which are arginine, a property which contributes to the peptide’s high positive charge

when the 'environmental' pH is below its pI of 11. Higher positive charge is believed to favour electrostatic interactions with the negatively charged Gram-negative membrane (Melo et al. 2009). Indeed, bacterial surface charge (measured as electrophoretic mobility) was reported to be statistically correlated with the antimicrobial activity of native clupeine against 21 test strains (Potter et al., 2005). Unlike other CAPs that are amphipathic, clupeine is not because the positive charges are evenly distributed along its backbone, and thus clupeine lacks the secondary structure which is found in other CAPs (Pink et al., 2014). The presence of secondary structure in CAPs is significant as it is believed to be involved in the antimicrobial mechanism of action of most CAPs (Wu et al., 1999).

Earlier reports by Rathinakumar and Wimley (2008), Rathinakumar et al. (2009) and Wimley (2010), have shown that the antimicrobial activity of CAPs may rely on their interfacial activity, which is dependent on an appropriate balance of hydrophobic and electrostatic interactions between peptides, water and lipids (Wimley, 2010). However, it should be noted that the interfacial activity theory may not be applicable to clupeine since it has no hydrophobic functional domains while in solution (Pink et al., 2014). Nevertheless, it cannot be ruled out that the change in charge and structure helped to improve the antimicrobial activity of the peptide, at least in the presence of the *E. coli* K-12 strain tested; this effect was not evident in the presence of the *S. enterica* Typhimurium 14028 cells. Potter et al. (2005) also reported that in most cases the CHD modification of clupeine did not lower the MIC and the MBC values for a larger panel of Gram-negative and Gram-positive bacteria in comparison to native clupeine.

Another important feature of many but not all CAPs is their ability to selectively destroy bacterial cells without causing harm to human cells. There was no effect of peptide concentration on the hemolytic activity ($P > 0.05$), but, there was significantly greater hemolysis with CHD-treated clupeine ($P < 0.05$). Although it should be noted that the percent hemolysis was extremely low, i.e., less than 0.5% of the red cells releasing hemoglobin ($0.36\% \pm 0.01$ and $0.45\% \pm 0.01$ for native and CHD-treated clupeine respectively). It is possible that the difference in the amino acid composition of the two peptides may be related to the mild hemolytic activity observed since the relative abundance of the hydrophobic amino acids alanine and proline were increased by about 23% in CHD-treated clupeine (Table 2-2). The preferential targeting of CAPs for microbial cells as opposed to human cells has been attributed to differences in lipid composition of prokaryotic (bacterial) versus eukaryotic (human) cells (Yeaman and Yount, 2003). For example, mammalian membranes have a neutral charge because they have a rich presence of phosphatidylcholine (PC) and phosphatidylethanolamine (PE) and sphingomyelin (SM) (Yeaman and Yount, 2003). In addition, the presence of cholesterol inside the mammalian cell membrane is another factor which leads to weaker interaction with these membranes and CAPs (Bacalum and Radu, 2015).

In contrast, bacterial membranes are usually negatively charged due to the presence of acidic phospholipids such as phosphatidylglycerol (PG) and the presence of lipopolysaccharide (LPS), which consists of three main regions in Gram-negative bacteria: (1) a lipid A region; (2) a region of charged core sugar molecules with free phosphate groups; and (3) a region consisting of a polysaccharide side chain composed of variable repeating sugar units (Epanand and Vogel, 1999) and teichoic acids which are

characteristics of Gram-positive surfaces (Omardien et al., 2016). The hemolytic assay in this chapter was designed so that the concentration of erythrocytes used in the *in vitro* assay was close to the actual physiological levels of erythrocytes in humans.

In order to identify different morphological changes in the bacterial cells in the presence of the peptides, SEM studies were performed. Overall the cells showed no visible signs of cell lysis, however, the *S. enterica* Typhimurium 14028 cells showed fewer flagella with increasing concentrations of both peptides, and although actual values were not obtained from image analysis, the cells appeared smaller in size (Figures 2-2 and 2-3). The lack of cell lysis observed in this study was in agreement with previous work reported by Aspedon and Groisman (1996), who tested native clupeine against *S. enterica* Typhimurium 14028s and hypersensitive strains of *S. enterica* Typhimurium. Pink et al. (2014) also reported no cell lysis of *E. coli* strain 29522, *S. enterica* Typhimurium 14028 and *Pseudomonas aeruginosa* strain PAO1 27853 in the presence of native clupeine.

Although informative, there are limitations to using SEM which must be acknowledged as compared to using a high-resolution technique such as Transmission Electron Microscopy (TEM) to examine changes in bacterial cells in the presence of peptides. First, SEM scans low-resolution images of the surface of the sample, whereas TEM captures a two-dimensional, high-resolution image of the cell structure. Consequently, when the cell membrane is the target of the peptide-bacterial cell interaction, as was the case in this study, important structural details are likely to be missed when the cells of interest are exposed to the native or CHD-treated clupeine. This limitation reduces the possibility of linking the changes observed in the model

biomembranes (Chapters 4 and 5) with those observed in the bacterial cells. Nevertheless, the initial observations obtained from the SEM data may serve as useful starting points for future studies.

It is noteworthy that Hartmann et al. (2010) used both SEM and TEM to study the interaction of two antimicrobial peptides, the β -stranded gramicidin S and the α -helical peptidyl-glycylleucine-carboxamide (PGLa) with *E. coli* ATCC 25922 and *St. aureus* ATCC 25923. SEM revealed changes such as shortening and swelling of the cells along with the formation of blisters (*E. coli*) and holes and craters (*St. aureus*). In contrast, TEM identified the formation of intracellular structures in both strains and morphological changes in the DNA region of *St. aureus* (Hartmann et al. 2010). In addition, Johansen et al. (1996) used Atomic Force Microscopy (AFM) to examine the surface topography and immuno-TEM to study the ultrastructural changes of *L. monocytogenes* and *S. putrefaciens* cells exposed to concentrations of 0 - 2000 $\mu\text{g/mL}$ or 0 - 1000 $\mu\text{g/mL}$ of native clupeine (for AFM and TEM studies, respectively). In both experiments the cells were incubated for 8 to 12 h at 25°C. These experiments showed that native clupeine was able to form holes (AFM) in the cell envelope of *S. putrefaciens* cells using 2000 $\mu\text{g/mL}$ native clupeine, which was lethal to these cells; at concentrations of 100 $\mu\text{g/mL}$ evidence of cell envelope damage was observed with TEM. In a similar way, data from the present study could be strengthened by applying microscopic techniques complementary to SEM such as: (1) TEM to further characterize peptide membrane interactions, and, (2) AFM, which unlike SEM and TEM, AFM allows real-time nano-scale imaging of the surfaces of living cells under physiological environments

(Johansen et al., 1996) and would help to provide a more complete picture of the effects of CHD-treated clupeine on *E. coli* K-12 and *S. enterica* Typhimurium 14028 cells.

In summary, different MIC values were observed for *E. coli* cells in the presence of CHD-treated clupeine. The modest increase in the hydrophobic amino acid composition of CHD-treated clupeine may have contributed to the small increase in hemolytic activity of this peptide. These observations suggest that the CHD-treated peptide is perhaps slightly more toxic to human cells than the native peptide, however, further tests would be required to fully establish the degree of toxicity. SEM images showed no visible signs of cell lysis in either bacterium, however, the *S. enterica* Typhimurium 14028 cells showed fewer flagella and appeared smaller in size with increasing concentrations of both peptides.

CHAPTER 3: qPCR AND PROTEOMIC ANALYSIS of *E. coli* and *S. enterica* TYPHIMURIUM 14028 CELLS in THE PRESENCE of NATIVE and CHD-TREATED CLUPEINE

3.1 Abstract

In Gram-negative bacteria, the levels of two outer membrane porin proteins (Omps), OmpF and OmpC are regulated in response to a variety of environmental parameters including the presence of cationic antimicrobial peptides (CAPs). However, the relative expression of these proteins has not been fully characterized when *E. coli* K-12 and *S. enterica* Typhimurium 14028 cells are exposed to native clupeine and to clupeine with 10% arginine modified by 1,2 cyclohexanedione (CHD-treated clupeine). In the present study, the changes in *omp* gene expression and the proteome profiles of the two test strains exposed to various concentrations of native or CHD-treated clupeine were examined. For the *E. coli* K-12 cells, it was also determined whether exposure to native and CHD-treated clupeine up or down-regulated *ompT* gene expression.

In *E. coli* K-12 cells, the relative expression of *ompF* was decreased whereas the expression of the *ompC* gene was increased in the presence of native clupeine. Conversely, the expression of both genes was down-regulated in the presence of CHD-treated clupeine. On the other hand, little or no effect on *ompF* expression was observed at or below MIC levels of native and CHD-treated clupeine in *S. enterica* Typhimurium 14028 cells. This was in strong contrast to the up-regulation ($P < 0.05$) of *ompF* observed at the highest concentration of both peptides used (2500 $\mu\text{g/mL}$). An interesting finding in both test strains was the presence of the OmpA porin protein,

where increased protein expression was identified in *E. coli* K-12 cells in the presence of 1000 µg/mL native and CHD-treated clupeine (43% and 27%, respectively). In addition, the expression of the metabolism and oxidative stress-related glyceraldehyde-3-phosphate dehydrogenase (GapA) protein appeared to be concentration dependent, where the greatest expression (6%) observed was at 1000 µg/mL concentrations of CHD-treated clupeine. However, similar expressions (4%) were observed at MIC and MBC concentrations of CHD- treated clupeine (1000 and 1250 µg/mL, respectively). The relative expression of the *ompT* gene was also up-regulated only when *E. coli* K-12 cells were exposed to MIC concentrations of CHD-treated clupeine. Taken together, these findings suggest that *E. coli* K-12 and *S. enterica* Typhimurium 14028 cells respond differently to the presence of native or CHD-treated clupeine.

3.2 Introduction

Prolonged use of antibiotics at sub-lethal levels has accelerated the development of resistance in some food pathogens which has increased the search for alternative antimicrobial agents (Saeed et al., 2009; Rai et al., 2016). Among alternative candidate compounds, particular attention has been paid to cationic antimicrobial peptides (CAPs) because they have exhibited broad spectrum antimicrobial activity against several foodborne pathogens, and have also shown a lower tendency to induce bacterial resistance (Keymanesh et al., 2009; Anaya-López et al., 2013).

The CAP clupeine has demonstrated antimicrobial activity against several foodborne pathogens, however, its mode of interaction with Gram-negative bacteria is still being elucidated. Tolong's work (2004) with native clupeine showed that the peptide

does not affect all Gram-negative cells in the same way. Furthermore, Pink et al. (2014) used immune-TEM to demonstrate that native clupeine was able to translocate both the outer and inner membranes of *E. coli* 25922 and *S. enterica* Typhimurium 14028 cells and concentrate in the cytoplasm. Because there was no permanent disruption of the membranes, it was suggested that clupeine's internalization was likely mediated by cation-selective barrel-like porin proteins (Pink et al., 2014). This was an interesting report as some of the earlier studies on native clupeine's interaction with other Gram-negative bacteria were more focused on the peptide's effectiveness as an antimicrobial agent against foodborne pathogens, not the peptide's mode of internalization (Truelstrup Hansen and Gill, 2000; Truelstrup Hansen et al., 2001). In addition, Potter et al. (2005) showed that charge reduction improved the antimicrobial activity of the clupeine, however, the molecular details of these interactions are still not clearly defined.

Bacterial environments are also constantly changing, and central to their survival is their ability to sense and respond to these changes. In the Gram-negative bacterial outer membrane are β -barrel porin proteins that span the outer membrane and allow the passage of small polar molecules (Pagès et al., 2008). In 1979, Reeves proposed a nomenclature system for the outer membrane proteins in *E. coli* and *S. enterica* Typhimurium. In this system, the outer membrane proteins (Omps) were named after their structural genes; e.g., OmpF is the product of the *ompF* gene (Reeves, 1979; Benz, 1985). *E. coli* produces three major trimeric porins, OmpF, OmpC and PhoE, whereas the outer membrane of *S. enterica* Typhimurium contains three different porin proteins, OmpF, OmpC and OmpD (Benz, 1985). OmpA is another major outer membrane protein found in both *E. coli* and *S. enterica* Typhimurium cells (van der Heijden et al., 2016;

Confer, and Ayalew, 2015; Santiviago et al., 2003). In *E. coli*, the outer membrane porins OmpF and OmpC show a slight preference for cations and allow passage of these molecules, whereas PhoE preferentially allows the passage of anions (Table 1-1). In addition, the OmpF porin forms a slightly larger pore (1.2 nm) as compared to OmpC (1.1 nm) (Table 1-1); this difference in pore size is believed to allow for more rapid diffusion of solutes through the OmpF than the OmpC pore (Nikaido and Vaara, 1987).

The *ompF* and *ompC* genes are structural genes that encode for the OmpF and OmpC porin proteins, respectively (Pratt, 1996), thus, the production of these proteins is related to the expression of the RNA transcripts. Similar to the *ompF* and *ompC* genes, as the osmolarity of the medium increases, OmpF production decreases while OmpC production increases so that the total amount of OmpF and OmpC proteins ($\sim 10^5$ copies) per cell remain constant (Mizuno et al., 1983; Luckey, 2008; Kefala et al., 2010).

Additionally, studies using OmpF and OmpC mutants have provided strong evidence to support a role for these outer membrane porins in bacterial resistance to different antibiotics. Using moxalactam, a broad-spectrum β -lactam antibiotic against Gram-negative bacteria, Komatsu et al. (1981) showed that *E. coli* K-12 mutants that lacked the OmpF porin showed moderate β -lactam resistance, which was attributed to lower penetration of the antibiotic in the mutant as compared to the wild-type strain. In addition, Mortimer and Piddock (1993) showed that in the presence of the antibiotics tetracycline, cefoxitin and cephalothin, *E. coli* cells that lacked the *ompF* gene (*ompF* mutants) had increased resistance due to restricted intracellular accumulation of the drugs. In a similar experiment, Lin et al. (2012) showed that the loss of *ompC* in *E. coli* also resulted in improved resistance in the presence of cephalothin and cefoxitin. Taken

together, the results from these studies show an important role for *ompF* and *ompC* in the rate of entry of antibiotics into *E. coli* cells and thus antibiotic resistance.

Another gene of interest that was examined was the *ompT* gene. The rationale for selecting this gene was based on a study by Strumpe et al. (1998) who identified OmpT as the protease responsible for another defence mechanism namely the degradation of protamine by exposed *E. coli* KS272 cells. OmpT is a 35.5 kDa aspartic protease which could potentially be used by *E. coli* to destroy invading CAPs (McCarter et al., 2004).

Quantitative PCR (qPCR) is a technique that allows us to evaluate changes in gene expression that occur when bacteria are exposed to antimicrobial agents (Wong and Medrano, 2005; Dowd et al., 2008; Alemu, 2014). QPCR can be used to measure the relative changes in gene expression ($\Delta\Delta C_q$ method, Pfaffl, 2000) between treated and untreated (control) cells. A similar strategy was also used in this study to measure the changes in protein expression, except that mass spectrometry (MS) and sodium dodecyl sulfate polyacrylamide gel electrophoresis (SDS-PAGE) techniques were applied. The aim of the work in this chapter is to investigate the role of porin genes and porin proteins in the Gram-negative bacterial response to native and CHD treated clupeine. To study these genetic changes, *E. coli* K-12 and *S. enterica* Typhimurium 14028 cells were grown to late exponential phase in a low osmolarity M9 medium supplemented with 0.4% sucrose followed by exposure to native or CHD-treated clupeine. For the gene expression studies, target genes were normalized to the reference gene *rpoB*, and in the two types of experiments, an *E. coli* double mutant strain ($\Delta ompF \Delta ompC$) was also used as a negative control. Taken together, data from this study will help to define some of the

molecular responses used by *E. coli* K-12 and *S. enterica* Typhimurium 14028 cells to counter the antimicrobial action of native and CHD-treated clupeine.

3.3 Materials and Methods

3.3.1 Strains, Media and Growth Conditions

Cultures of *E. coli* K-12 strain MG1655 (American Type Culture Collection, (ATCC, Manassas, VA, USA) and *S. enterica* Typhimurium strain 14028 (ATCC, Manassas, VA, USA) were used in this study. These bacteria were chosen to compare the changes in gene/protein expression in pathogenic (*S. enterica* Typhimurium 14028) and non-pathogenic (*E. coli* K-12) Gram-negative bacteria.

An *E. coli* double mutant strain ($\Delta ompF/\Delta ompC$) was obtained from the Coli Genetic Stock Center (CGSC), (CS 484, # 6067). All strains were cultured at 37°C in 30 mL Tryptic Soy Broth (TSB 30 g/L; Difco, Fisher Scientific) and then stored at -80°C in 1 mL stock cultures containing TSB and 20% w/v glycerol. Working cultures were prepared by inoculating 100 μ L stock cultures in 30 mL of fresh TSB (Oxoid) and incubating overnight at 37°C. The overnight cultures were then streaked on TSA, (Oxoid) plates and an isolated colony from each strain was transferred to a 50 mL sterile centrifuge tube and subcultured in 30 mL of TSB overnight in a shaking incubator (250 rpm) set at 37°C prior to use. This method produced cells in the late exponential phase, which were used because it has been previously reported that slowly growing cells are better at surviving adversity than rapidly growing cells (Brown and Williams, 1985; Brown et al., 1990).

3.3.2 Preparation of Cell Cultures for RNA Extraction

Overnight cultures, which had been precultured as described above, were diluted to ~1000 cfu/mL followed by the addition of 1-mL aliquots to four, 250 mL Erlenmeyer flasks each containing 50 mL of M9 glucose minimal salts media (160 mM Na₂HPO₄, 80 mM KH₂PO₄, 40 mM NaCl, 72 mM NH₄Cl, 0.8 mM MgSO₄·7H₂O, 0.4% (w/v) filter sterilized glucose, 2 µg/mL thiamine and 0.008% (w/v) biotin). This medium was chosen to ensure that the same medium used for the protein studies would also be used for the gene expression studies. Because concentrations of cations (Ca²⁺ and Mg²⁺) can affect clupeine's activity (Pink et al., 2003) a very low concentration of magnesium sulfate was used and no calcium ions were used. This low osmolarity medium supports the growth of *E. coli* and *S. enterica* Typhimurium cells (Varik et al., 2016; McLeod and Spector, 1996), however, growth is slow, therefore the cells were grown for 3 days in a shaking incubator (250 rpm) set at 37°C to achieve late exponential phase (confirmed by optical density readings). After the growing period the cells were pooled and pelleted by centrifugation (5,000 x g for 10 min) at 4°C. A typical culture of 200 mL (4 flasks of 50 mL of media) yielded about 1 g wet weight of cell pellet. The cell pellet was washed twice in Peptone Saline (0.1% PS and 0.85% NaCl) and then re-suspended in 4 mL of M9 glucose minimal salts media.

The cell suspension was then evenly divided into four separate sterilized tubes and treated with different concentrations of native or CHD-treated clupeine for 1 h. Working solutions of each peptide (5000 µg/mL) were made up in M9 minimal media and *E. coli* K-12 cells were exposed to the following concentrations (µg/mL) of native clupeine: 0 (control), 500 (MIC), 1000 or 1250; whereas the following concentrations (µg/mL) of the CHD-treated peptide were used, 400 (MIC), 1000 and 1250. The *S.*

enterica Typhimurium 14028 cells were exposed to 500, 1250 or 2500 µg/mL native and CHD-treated clupeine. Four flasks containing the *E. coli* negative control, (($\Delta ompF/\Delta ompC$)) were also prepared and the same concentrations of native and CHD-treated clupeine used for the *E. coli* K-12 cells were also used to treat the mutant cells. All the flasks were incubated for 1 h at 37°C after which the cells were pelleted by centrifugation at 5,000 x g for 10 min. The pelleted and treated cell suspensions (including controls not exposed to the peptides) were used for the RNA extraction described below.

3.3.3 Extraction of Ribonucleic Acid (RNA)

Total RNA was extracted from cell suspensions (Section 3.3.2) following the manufacturer's instruction (RNeasy mini kit, Qiagen, Germany). Briefly, the pelleted cells were treated with 2 volumes of RNAprotect (Qiagen) and then centrifuged at 5000 x g for 5 min. The cells obtained were lysed with lysozyme (1 mg/mL; Sigma-Aldrich) in TE buffer (10 mM Tris-HCl, 1 mM EDTA; pH 8.0) for up to 10 min. Then 350 µL of buffer RLT containing β-mercaptoethanol was added to the cells to degrade intracellular RNases released during cell lysis. The cells were then centrifuged for 2 min at 13,400 x g and 250 µL of ethanol was added to the lysate.

The lysate including any precipitate formed was then transferred to a 2 mL collection tube which was centrifuged for 15 s at 13,400 x g. The flow-through was discarded and the material bound to the column (which included the RNA) was treated with DNase I (28 U) for 15 min at 25°C (RNase-Free DNase 1 set, Qiagen) to remove residual DNA. The RNA-containing material was first washed with a stringent buffer, RW1 (700 µL) to remove biomolecules bound to the membrane and then washed with a

mild buffer (RPE, 500 μ L) to remove traces of salt still bound to the column. The RNA samples were eluted in 40 μ L RNase-free water and their purity and concentration determined spectrophotometrically at 260 nm (Nano-Photometer®-P330, Implen, Germany). Finally, the integrity of the samples was checked by agarose (1.5%) gel electrophoresis before being reverse-transcribed into complementary DNA (cDNA). The RNA samples were reverse transcribed on the same day they were extracted and RNA extraction was carried out in an RNase-free environment using RNaseZAP (Sigma) decontamination solution.

3.3.4 Formation of Complementary Deoxyribonucleic Acid (cDNA) Libraries

Total RNA extracted from *E. coli* K-12, *S. enterica* Typhimurium 14028 and *E. coli* $\Delta omp/\Delta ompC$ cells was reverse transcribed with 75 U/ μ L of iScript RNase H⁺ Reverse Transcriptase (Bio-Rad). For the cDNA reaction, 1 μ g of RNA was mixed with 4 μ L of the iScript mix which contained random hexamer primers and oligonucleotides, 1 μ L reverse transcriptase (RT) was added, and RNase-free water was added to a final volume of 20 μ L. The reaction was carried out in a Biometra Tgradient thermocycler (Biometra, Göttingen, Germany) in the following stages, 90°C for 5 min (priming), then 30 min at 42°C (reverse transcription) and 5 min at 95°C to inactivate the RT. The RT reaction was carried out in triplicate and a no-RT control was also set up to confirm that the samples were not contaminated with genomic DNA. The appropriate cDNA samples were pooled and their concentrations determined spectrophotometrically at 260 nm (Nano-Photometer®-P330, Implen, Germany) before they were aliquoted (15 μ L) and stored -20°C for later use.

3.3.5 Primer Design

The coding regions for each of the target genes of interest were retrieved from the complete genomes for *E. coli* K-12 MG1655 (GenBank accession number NC_000913) and *S. enterica* Typhimurium 14028 (GenBank accession number NC_016856) located on the NCBI database (www.ncbi.nlm.nih.gov). The target genes along with their accession numbers and their locations in the genome are outlined below in Table 3.2

Primer design was based on the target gene sequences and was performed using Primer3 (http://biotools.umassmed.edu/bioapps/primer3_www.cgi), a computer-based program; all primers were designed for this study (Table 3.3), except the primers for *ompT* which were obtained from Vinson et al. (2010). Once the primers were designed, a Basic Local Alignment Search Tool, BLAST (<http://blast.ncbi.nlm.nih.gov>) search was done to determine that the sequence source of the significant hits for *E. coli* would be from the *E. coli* K-12 MG1655 genome or closely related species. Similar BLAST searches were done for the *S. enterica* Typhimurium 14028 primers, with the expectation that the sequence source of the significant hits would be *S. enterica* Typhimurium 14028 or closely related species. All primer sequences were manufactured (Sigma-Aldrich; customdna@sial.com) on a 0.025 mg synthesis scale and using a reverse-phase cartridge purification step (RP1).

Table 0-1 A summary of the target genes and reference genes (*rpoB*) used in this study and their corresponding GenBank Accession Numbers and coding regions obtained from the NCBI database.

Gene of Interest	Accession Number	Coding Region in Genome
------------------	------------------	-------------------------

***E. coli* K-12**

<i>ompF</i>	NC000913	985120...986202
<i>ompC</i>	NC000913	2311646...2312749
<i>ompT</i>	From Vinson et al. (2010)	4181245...4185273
<i>rpoB</i>	NC000913	

***S. Typhimurium* 14028**

<i>ompF</i>	NC016856	1048140...104923
<i>ompC</i>	NC016856	2416996...2418132
<i>rpoB</i>	NC016856	4379489...4383517

3.3.6 Primer Verification

All primers were validated for primer dimers and hairpin structures with the Sigma-Aldrich online tool, OligoEvaluator™ (<http://www.oligoevaluator.com>). The specificity of each primer was first tested *in silico* using the CLC Main Workbench sequence analysis software (CLC Main Workbench 7.0.3 <http://www.clc.bio.com>), and then verified experimentally by PCR, to ensure each set of primers would only amplify the target gene. A master mix was prepared containing 1 µL of each respective primer (10 µM) 0.5 µL of Takara *LA Taq*™ DNA Polymerase (Clontech, Laboratories Inc., CA, USA) 5 µL of 10X LA Buffer II (25 mM Mg²⁺; Clontech, Laboratories Inc., CA, USA), and 8 µL of deoxynucleotide triphosphates (dNTPs; 2.5 mM each; Clontech, Laboratories Inc., CA, USA), and the appropriate volume of sterile water to make a volume of 49 µL. The master mix was transferred to the reaction tubes and 1 µL of 10 ng/µL of cDNA template was added to each tube to make a final volume of 50 µL.

Target cDNA samples were amplified in a Biometra thermocycler and the cycling conditions were as follows: 94°C for 10 min for denaturation, 39 cycles of (95°C for 15 s,

60 °C for 30 s, 72°C for 30 s) to repeat denaturation, annealing and extension and a 10 min final elongation step at 72°C. All PCR products were run on a 1.5% agarose gel and a 100 base pair (bp) Takara DNA ladder (Takara Bio Inc.) was used as the DNA marker in all the gels.

3.3.7 Validation of Reference Genes

Two reference genes were chosen from the literature, 16S ribosomal Ribonucleic Acid (16S rRNA) and RNA polymerase β -subunit (*rpoB*). Preliminary relative expression data (Δ Cq) values were applied to (<http://www.leonxie.com/referencegene>), an online program that used the BestKeeper method (Pfaffl et al., 2004), an Excel (Microsoft Inc.) based tool, to determine the most stable gene under the given experimental conditions.

Table 0-2 Annealing temperatures of the primers used for q-PCR of outer membrane porin (*omp*) genes in *E. coli* K-12 (strain MG1655) and *S. enterica* Typhimurium (strain 14028).

Primers ^a	Sequence (5'→3')	Annealing temp. (°C)	Amplicon size (base pair, bp)
<i>E. coli</i> K-12			
<i>ompF</i> -F	TTAACTTTGCCTACAGGGAC	55.5	199
<i>ompF</i> -R	TGGCTTATTACAGCATTGGT		
<i>ompC</i> -F	GAACACGAAACCGACTTTAC	54	192
<i>ompC</i> -R	GTGCTGAACGATATCTCACT		
<i>ompT</i> -F ^b	TCCTCAACGAACCCAATTACC	63	198
<i>ompT</i> -R ^b	TTCCAGTCAAGCCAATGTAGG		
<i>rpoB</i> -F	GTATCCGGGTGAAGCAGGTA	63	237
<i>rpoB</i> -R	TCGGATACGAGGATGGAGTC		
<i>S. Typhimurium</i>			
14028			

<i>ompF</i> -F	AACTCTCAGAATGGCGATGG	64.2	185
<i>ompF</i> -R	GCAGCCAGGTAGACGTTGTT		
<i>ompC</i> -F	ACGCTCGCCTGTATGGTAAC	63.9	163
<i>ompC</i> -R	GCAAAACCGTAAGAGGTGGA		
<i>rpoB</i> -F	CGGTCTGATCAACTCCCTGT	64.2	183
<i>rpoB</i> -R	ACAAAGTGGCCTTCGTCATC		

^aThe primers were named after the target genes *ompF*, *ompC* and *ompT* and the reference gene *rpoB*.

^bThe *ompT* primers were obtained from Vinson et al. (2010); all other primers were designed in this study.

Of the two reference genes tested, *rpoB* had the lowest standard deviation of quantification cycle (C_q) values and was chosen as the reference gene. The *rpoB* gene also produced similar C_q values for the starting template amount of 0.2 $\mu\text{g}/\mu\text{L}$ under all the different treatment conditions, which confirmed its stability under the given experimental condition.

3.3.8 qPCR Linear Dynamic Range and Amplification Efficiencies

To ensure that there was a logarithmic change in response for the target and reference genes a dilution series was set up for each primer set using the following dilution series: 1000, 500, 100, 50 and 10 $\text{ng}/\mu\text{L}$ cDNA. This experiment for the primers was done once, and the samples were run in triplicate and included a no-template control (NTC). In order to determine the PCR efficiencies, standard curves were set up for each target gene and the reference gene using cDNA prepared in previous validation experiments. The cDNA template was diluted with RNase/DNase free water in a 5-fold series covering 7 log cycles starting with 200 ng cDNA /well.

Each PCR efficiency experiment was repeated three times on three separate plates to determine the inter-assay reproducibility ($n=3$) and using three technical replicates

(repeated measures of the same sample) in order to determine the intra-assay reproducibility (Saikaly et al., 2007). The standard curves were evaluated for linearity and all C_q values for the treated and untreated samples fell within the linear quantifiable range. No-template controls were also included in all experiments to rule out reagent contamination and primer dimer formation. Using the slope of the line relating C_q to input cDNA concentration, the q-PCR efficiency was calculated from the following equation (Rasmussen et al., 2001):

Equation 0-1

$$E = 10^{[-1/\text{slope}]}$$

The calculated efficiency values ranged from 1.89 to 2.1. From the standard curve, the dynamic range was defined as the highest cDNA concentration that did not inhibit the reaction to the lowest cDNA concentration that did not inhibit the reaction. This cDNA range was 200 ng to 0.0126 ng.

The cDNA samples generated from the treated and untreated cells were diluted 1/10 (working concentration 100 ng/ μ L) in order to have results in the confidence interval of the technique (Eleaume and Jabbouri, 2004) and because the sample volume was limited to 10% of the total reaction volume (i.e., 2 μ L/ reaction). As a result, no C_q values generated from outside of the linear dynamic range were used in the relative gene expression calculations. The limit of quantification (LOQ) was defined as the lowest amount of cDNA that could be accurately quantified on the linear dynamic range of the standard curve (Ruggirello et al. 2014; Kubista, 2014). In these experiments, the LOQ for the diluted cDNA samples was 0.0126 ng/mL cDNA. For normalization, the endogenous control *rpoB* was used to normalize the target genes. In addition, the same amount of

RNA (1 $\mu\text{g}/\mu\text{L}$) was used for cDNA synthesis and all the samples were diluted 1/10 (working concentration 100 $\text{ng}/\mu\text{L}$).

3.3.9 qPCR

Quantitative real-time PCR was performed in 20 μL reaction volumes. At first, 4 different master mix concentrations (200 nM, 250 nM, 300 nM and 400 nM) were tested to determine which concentration resulted in the highest melt curve peak. The optimal master mix concentration (400 nM) was prepared for the target gene as well as the reference gene and each master mix contained 10 μL GoTaq qPCR 2X master mix (Promega, A6001), which contains BRYT Green®, a DNA-binding dye, 0.8 μL of the forward and reverse primers (10 μM) for the appropriate target or reference gene, and 0.2 μL of a reference dye (Promega).

Each sample well contained 18 μL of master mix and 2 μL of cDNA template for a final volume of 20 μL , and a no-template control was set up for each gene using 2 μL of RNase/DNase free water instead of the cDNA template. All amplifications were carried out in Micro Amp® Fast Optical® 96-well reaction plates (Applied Biosystems®) and once the wells were loaded the plates were sealed with optical adhesive covers (Applied Biosystems) before they were placed in the cycler.

Real-time quantification was performed using a StepOnePlus™ Real-Time PCR system (Applied Biosystems®; CA, USA) operated by RQ Manager software version 1.2. Cycling conditions were as follows: 95°C for 10 min, and 40 cycles of 95°C for 15 s and annealing at 52°C – 66°C (depending on the primers used, Table 3-3) for 1 min. To test the specificity of the qPCR products, a melt curve was performed starting at 60° for 1 min up to 95°C for 15 sec. The cDNA generated from three independent RNA extractions

were analyzed and for each qPCR run, three technical replicates were set up for each gene. The specificity of the qPCR products was also confirmed by running the products on 1.5% agarose gels.

3.3.10 qPCR Data Analysis

Data collection was performed using instrument software (Applied Biosystems, CA, USA). The relative change in gene expression levels of *ompF*, *ompC* and *ompT* genes from *E. coli* and *ompF* and *ompC* for *S. enterica* Typhimurium 14028 cells exposed to native and CHD-treated clupeine were compared to control samples with no exposure to clupeine. Because the q-PCR efficiencies were different, but still close to one another, quantification for each target gene was determined by the efficiency correction method using the reference gene *rpoB*.

The Efficiency Correction Equation (Equation 3-2) is an adaptation of the Livak method that incorporates differences in PCR efficiencies and has been previously used to calculate relative gene expression (Pfaffl et al., 2001),

Equation 0-2:

$$R = \frac{E_{target} \Delta C_q target (control-treated)}{E_{reference} \Delta C_q reference (control-treated)}$$

Where: R, is the relative expression ratio (or fold change); E_{target} , is the qPCR efficiency of the target genes (*ompF*, *ompT* and *ompC*); $E_{reference}$ is qPCR efficiency of the reference gene (*rpoB*); $\Delta C_q target$ is the mean C_q of the target gene in the untreated sample minus the mean C_q of the target gene in the treated sample; $\Delta C_q reference$ is the mean C_q of the reference gene in the untreated sample minus the mean C_q of the reference gene in the treated samples.

The first step in the data analysis involved removing outliers and calculating a C_q mean of the technical replicates for all samples and genes. In the second step, the ΔC_q of each target gene was calculated by subtracting the C_q mean of the target gene in the treated samples from the C_q mean of the target gene in the untreated samples.

Equation 0-3:

$$\Delta C_{q \text{ target}} = (C_{q \text{ mean untreated}} - C_{q \text{ mean treated}})$$

This step was then repeated for the reference gene in the same samples,

Equation 0-4:

$$\Delta C_{q \text{ ref}} = (C_{q \text{ mean untreated}} - C_{q \text{ mean treated}})$$

The third step of the analysis involved correcting the target assay from deviation from 100% efficiency. Here the target efficiency was raised to the power of the ΔC_q of the target gene for the treated and untreated samples, which was calculated in the previous step. The same calculations were applied to the reference gene, and efficiency correction was also done for the reference gene in the treated and untreated samples. In the final step, the relative expression ratio (or fold change, R) was calculated by dividing the target correction by the reference correction. The untreated sample was expected to have an R value of 1 as all the other samples were expressed relative to this sample.

To confirm the accuracy and reproducibility of the q-PCR data, intra-assay variations were determined between the triplicate C_q values for each of the treatments as outlined in the MIQE (minimum information for publication of quantitative real-time experiments) guidelines (Bustin et al., 2009). This variation was expressed as the mean $C_q \pm$ the standard deviation (SD). Each experiment was repeated 3 times and on 3

separate plates, however the inter-assay variation was not determined since C_q values regenerated from different runs are subject to inherent variation (Bustin et al., 2009).

3.3.11 Statistical Analysis

Bar graphs showing $R \pm SD$ were generated using GraphPad Prism® (GraphPad Prism® Software Inc., version 7, San Diego, CA, USA). Statistical significance was established at a 95% confidence interval (CI) relative to the control using a one way analysis of variance (ANOVA) with Dunnett's post-test (GraphPad Prism®). A difference in mean values between groups was considered to be significant when P was ≤ 0.05 .

3.3.12 Bacterial Strains, Growth Conditions and Preparation of Cell Envelopes

E. coli K-12 strain MG1655 and *S. enterica* Typhimurium strain 14028 were used in this study. An outer membrane protein control was obtained from the Coli Genetic Stock Center (CGSC), CS 484 ($\Delta ompF / \Delta ompC$, # 6067). A detailed description of strains and cell culturing is found in section 3.3.1.

3.3.13 Preparation of Cells for Porin Extraction

Overnight cultures, which have been described in Section 3.3.1 were diluted to 1000 cfu/mL followed by the addition of 1 mL aliquots to four, 250 mL Erlenmeyer flasks each containing 50 mL of M9 minimal media. The cells were treated as described in Section 3.3.2.

3.3.14 Outer Membrane Preparation

A flow chart of the main steps involved in the preparation of the membrane proteins is shown in Figure 3-1, which was adapted from Garavito and Rosenbusch (1986). Bacterial cells (~1 g, wet weight) exposed to native or CHD-treated clupeine were suspended in 5 mL lysis buffer containing 10 mM Tris-HCl, 5% sucrose, 0.1 M NaCl, 3 mM sodium azide (NaN₃), 100 μL deoxyribonuclease (DNase, 1 mg/mL), and 10 μL of each of the protease inhibitors aprotonin, pepstatin, and leupeptin (all 1 mg/mL), and frozen overnight at -20°C.

On the following day, the cell solutions were thawed and physically disrupted by passing them through a French Press twice at 14,000 pascal. Unbroken cells were removed by centrifugation (5000 x *g* for 10 min) and the crude membranes were recovered by centrifuging at 29,000 x *g* for 1 h at 4°C. The crude membranes were incubated in a buffer (10 mM Tris-HCl containing DNase and ribonuclease, Sigma) for 1 h at 60°C to digest unwanted DNA and RNA. The crude membranes containing the membrane proteins were then collected by centrifuging at 29,000 x *g* for 1 h at 4°C.

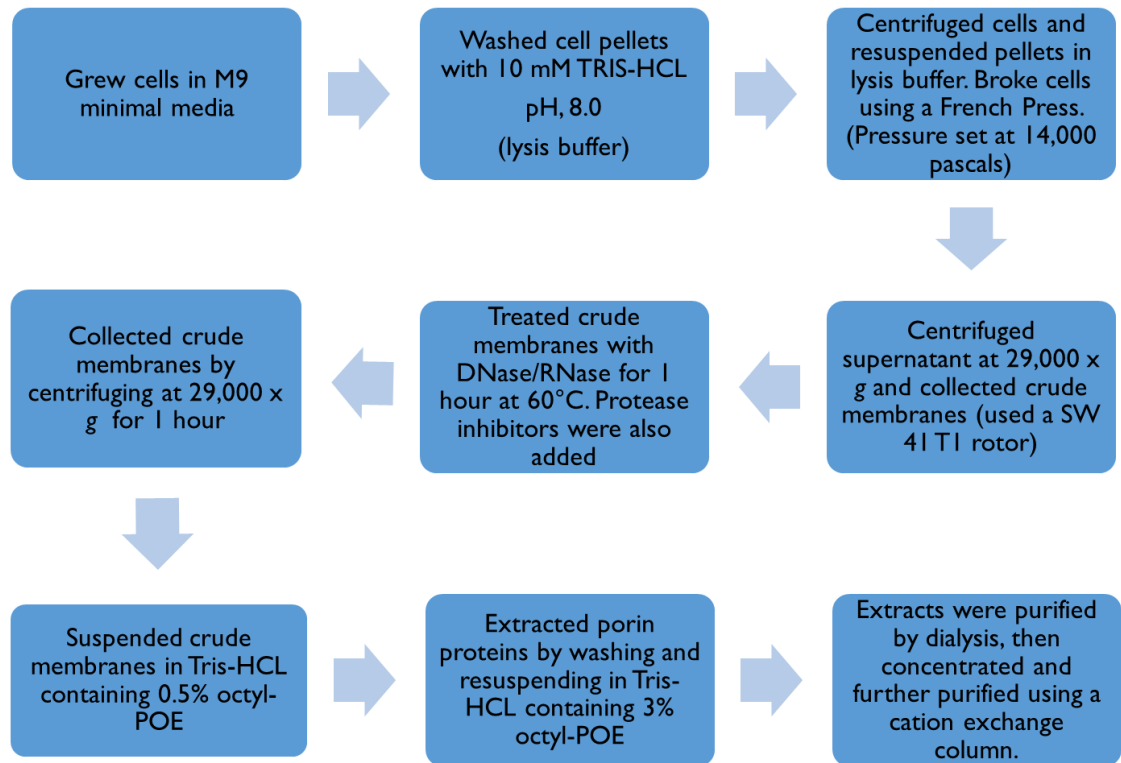


Figure 0-1 Work flow for the extraction of porin proteins from *E. coli* K-12 and *S. enterica* Typhimurium 14028 cells exposed to native or CHD-treated clupeine (adapted from Garavito and Rosenbusch, 1986).

In order to solubilize the outer membrane proteins and to remove phospholipids, the crude membranes were washed twice with a pre-extraction buffer containing 10 mM Tris-HCl, 3 mM NaN₃; 1 mM ethylenediaminetetraacetic acid (EDTA), 3 mM DL-dithiothreitol (DDT); 0.5% of the detergent octyl-oligooxyethylene (or octyl-POE), pH 8.0 and centrifuged for 1 h at 29,000 x g at 4°C. Porins were then extracted by re-suspending the pellet in 5 mL of extraction buffer (10 mM Tris-HCl; 3 mM NaN₃; 1 mM EDTA; 3 mM DDT and 3% octyl-POE; pH 8.0) and incubating at 4°C overnight.

Finally, the solutions were centrifuged at 29,000 x g for 1 h at 4°C and the supernatants retained as the porin extracts.

3.3.15 Purification of Porin Extracts

To purify the porin samples, the extracts were dialyzed at 4°C overnight against 4 L of a buffer containing 10 mM HEPES, 150 mM NaCl, 5 M NaOH, and 0.7% octyl-POE. The purpose of the dialysis step was not only to purify the porins but also to adjust the composition of the detergent octyl-POE to that of the start buffer used for cation exchange. After dialysis, the samples were concentrated using an Amicon Ultra-4 Centrifugal Filter Unit (EMD Millipore Corporation Billerica, MA, USA) which had a 10,000 Da molecular weight cut-off. The porin samples were centrifuged in the centrifugal filter units for 5 min at 5000 x g and approximately 500 µL of retentate was collected and the supernatant discarded for each sample.

The retentate from the filtration step was further purified using a Hi-Trap Sepharose cation exchange column (GE Healthcare, 17-1151-01, 1 mL). The column was prepared by running 5 mL of starting buffers 1 and 2 through followed by 10 mL of buffer 1. Immediately following this step, the porin sample was run through the column. The pH of these starting buffers was adjusted to 3.46; ~ 1 pH unit below the pI of OmpF (pI 4.65) (GE Healthcare, 2014) to facilitate binding of the porin to the Hi-Trap column. After the sample was loaded, buffer 3 was used to wash away unbound sample components from the column. The increased pH (4.8) and ionic strength (1 M NaCl) of buffers 5 and 6 were then used to elute the bound porin from the column. During the purification process, the flow rate of the peristaltic pump was adjusted to 1 mL/min and

eluants were collected for 30 s each. The compositions of all the buffers used are outlined in Appendix B.

3.3.16 SDS-PAGE

Discontinuous Sodium Dodecyl Sulfate-Polyacrylamide Gel Electrophoresis (SDS-PAGE), first described by Laemmli (1970), was used to verify the presence of porin proteins in the untreated cells and in the cells challenged with native or CHD-treated clupeine. The porin samples (12.5 μ L, 0.2 μ g protein/ μ L stock), plus water (7.5 μ L) and a protein sample buffer (5 μ L, 1 M Tris-HCl (pH 6.8)), containing 5% SDS, 50% glycerol, 0.5% bromophenol blue and 10% β -mercaptoethanol were heated for 10 min. The combination of heat and β -mercaptoethanol denatured the porin proteins without breaking peptide bonds and allowed SDS to coat the proteins giving them a negative charge.

The samples were cooled and loaded into a stacking gel (6% acrylamide) and resolved on a 15% acrylamide running gel. A prestained protein marker with a range of 7 kDa to 175 kDa (P7708S; BioLabs) was used to compare the positions of the protein sample bands. The gels were run in a Mini-PROTEAN Tetra Cell (Bio-Rad) filled to the appropriate position with a 1x running gel buffer containing 0.025 M Tris, 0.192 M glycine and 0.1% SDS, pH 8.3 . The gels were run at 175 V, 300 mA for 90 min and were stopped when the bromophenol blue tracking dye reached the bottom of the gel. The gels were run in triplicate with equal protein loading in each lane.

To visualize the positions of the proteins, the gels were stained with a silver staining protocol similar to the method described by Shevchenko et al. (2006) but with some modifications. First the gel slabs were fixed in a solution containing 40% ethanol,

12% acetic acid and 0.05% formaldehyde for 20 min. The gel slabs were then washed in 50% ethanol in water, three times for 20 min. A sensitization step in 0.02% sodium thiosulfate (Sigma-Aldrich) was carried out for 1 min followed by staining with silver nitrate in the dark at room temperature for 20 min. After staining, the gel slabs were washed twice in water and then developed to the desired intensity with a 6% sodium carbonate solution containing 0.05% formaldehyde and 0.0004% sodium thiosulfate. The development was stopped by washing the slabs with a 40% ethanol, 12% acetic acid solution containing 0.05% formaldehyde. The gel slabs were then washed in 50% methanol for 20 min and stored in a 30% methanol solution at 4°C until analyzed.

Photographs of the gels were taken with a Canon compact digital camera and the images were analyzed using myImage Analysis software (version 1.1; Thermo Fisher Scientific). Standard curves were generated by plotting Relative front (R_f) values (the distance a band in the protein standard had migrated divided by the total length of the lane) versus the log of their known molecular weights. The apparent molecular weights of the porin protein present in each sample were determined by using the R_f values obtained from myImage Analysis software and interpolation using the standard curve. The actual molecular weights were determined by mass spectrometry.

3.3.17 In-Gel Digestion for Mass Spectrometry

Proteins of interest were selected based on the apparent molecular weights of the untreated samples (~30 kDa). The bands of interest were excised from the gel slabs and in-gel digestion with trypsin was carried out as described by Shevchenko et al. (2006). The cut bands were transferred to micro-centrifuge tube, and in-gel reduction, alkylation

and destaining were carried out. At first the gel pieces were shrunk by adding 500 μL of acetonitrile (HPLC grade, Fisher Scientific) and incubated at room temperature for 10 min. Then, the gel pieces were centrifuged using a benchtop centrifuge (5000 x g for 3 min) to remove the liquid. Fifty microliters of a 10 mM DL-dithiothreitol (Sigma-Aldrich) solution in 100 mM ammonium carbonate (Sigma-Aldrich) was then added to each tube to completely cover the gel pieces, which were incubated in DTT for 30 min at 56°C in a water bath.

After removal from the water bath the gels were cooled to room temperature on ice. Five hundred microliters of acetonitrile were added and the tubes incubated for 10 min at room temperature. After this, 50 μL of 55 mM iodoacetamide (Sigma-Aldrich) in 100 mM ammonium bicarbonate was added to the gel pieces and incubated for 20 min in the dark at room temperature. Following this step the gel pieces were shrunk once more in acetonitrile for another 10 min at room temperature.

The gel pieces were then swollen by adding 50 μL of a digestion buffer containing 12.5 ng/ μL of trypsin (N-tosyl-L-phenylalanyl chloromethyl ketone, TPCK treated; Sigma-Aldrich) in 10 mM ammonium bicarbonate (pH 8.5) containing 10% (v/v) of acetonitrile, for 2 h in an ice bucket. After the first 30 min, the tubes were checked and another 50 μL of trypsin was added to ensure all the gel pieces were covered in the buffer. The gel pieces were incubated for another 90 min with trypsin and then 20 μL of ammonium bicarbonate buffer (pH 8.5) was added to the centrifuge tubes. Following this saturation step with trypsin, the gel pieces were digested for 30 min at 55°C.

The digested peptide products were then extracted by adding 100 μL of an extraction buffer containing 1:2 of 5% (v/v) formic acid/acetonitrile, to each tube and

incubating for 15 min at 37°C in a shaking water bath. Following digestion, the supernatant was removed and placed in a clean tube and stored at -4°C until analyzed.

3.3.18 Mass Spectrometry

The tryptic digests were purified using Oasis Solid Phase Extraction columns (Waters Oasis HLB Extraction Cartridges PN: WAT094226) and characterized by liquid chromatography mass spectrometry (LC MS/MS), and the main sequences found were identified by searching against a Uniprot Basic Alignment database. The number of peptides detected in trypsin gel digests was taken as an indicator of the relative abundance of the proteins in the strains tested (Zhu et al., 2009; Gautam et al., 2011).

3.3.19 Lowry Assay

The protein concentrations of the purified porin samples were determined by a modified Lowry Assay known as the Bio-Rad DC (detergent compatible) Protein Assay. Two separate standard curves were made, one with a 1.4 mg/mL bovine serum albumin (BSA) solution for the untreated porin samples and one with a 1.4 mg/mL clupeine solution for the native and CHD-treated porin samples. The appropriate protein standard solutions ranging from 0-80 µg/mL were used to generate two standard curves.

Clean tubes were used for each concentration, and to each tube the appropriate volume of standard solution was added plus 250 µL of the alkaline copper tartrate solution (Reagent A and S mixture); finally, 2 mL of a dilute Folin reagent (Reagent B) was added to each tube. The contents of each tube were vortexed and incubated at room temperature for 15 min, and the absorbance of each sample was read at 750 nm.

Sample tubes were prepared in a similar way to the standards; however, 30 µL of each sample was used, plus 250 µL of reagent A+S mixture and 2 mL of reagent B. The

sample tubes were also vortexed and incubated at room temperature for 15 min and absorbance measurements were taken at 750 nm. A blank tube was prepared using 30 μ L of water instead of the porin samples.

3.4 Results

3.4.1 *Relative Expression of E. coli Porin Genes in Cells Treated with Native or CHD-Treated Clupeine*

E. coli K-12 cells in the presence of native clupeine showed decreased expression of the *ompF* gene and a corresponding increase in expression of the *ompC* gene (Figure 3-2A and Figure 3-2B). In the case of the *ompC* gene, a significant ($P < 0.05$) increase in the relative expression ratio was observed at concentrations of 500 and 1000 μ g/mL of the native clupeine (Figure 3-2B). On the other hand, in the presence of CHD-treated clupeine the relative expression ratios of both the *ompF* (Figure 3-2C) and the *ompC* (Figure 3-2D) genes were down-regulated. Increasing concentrations of the CHD-treated peptide resulted in a progressive reduction in the relative expression ratio of *ompF* significant ($P < 0.01$; Figure 3-2C).

The relative expression ratio of the *ompT* gene was down-regulated at each concentration of native clupeine ($P < 0.01$; Figure 3-3A) but for CHD-treated clupeine, *ompT* was significantly down-regulated only at 1250 μ g/mL ($P < 0.01$; Figure 3-3B).

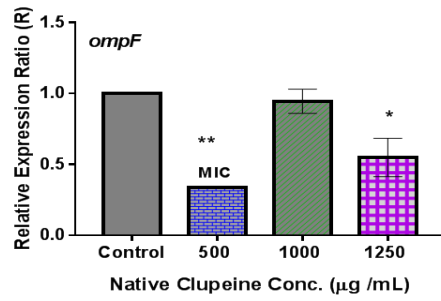
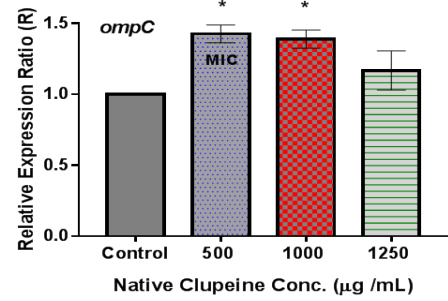
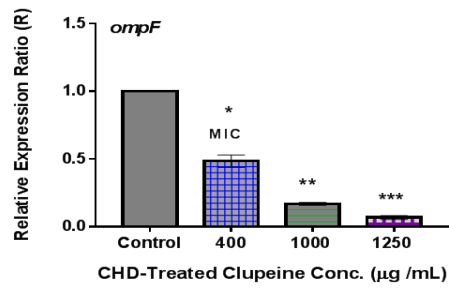
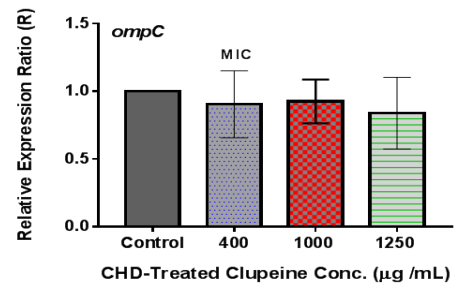
A.**B.****C.****D.**

Figure 0-2 Mean relative expression ratios (R values) of *ompF* expressed in *E. coli* K-12 cells treated with native clupeine (A) and CHD-treated clupeine (C) and *ompC* gene in *E. coli* K-12 cells treated with native clupeine (B) and CHD-treated clupeine (D), (n=3, error bars show the standard deviation) (***P < 0.001, **P < 0.01; *P < 0.05).

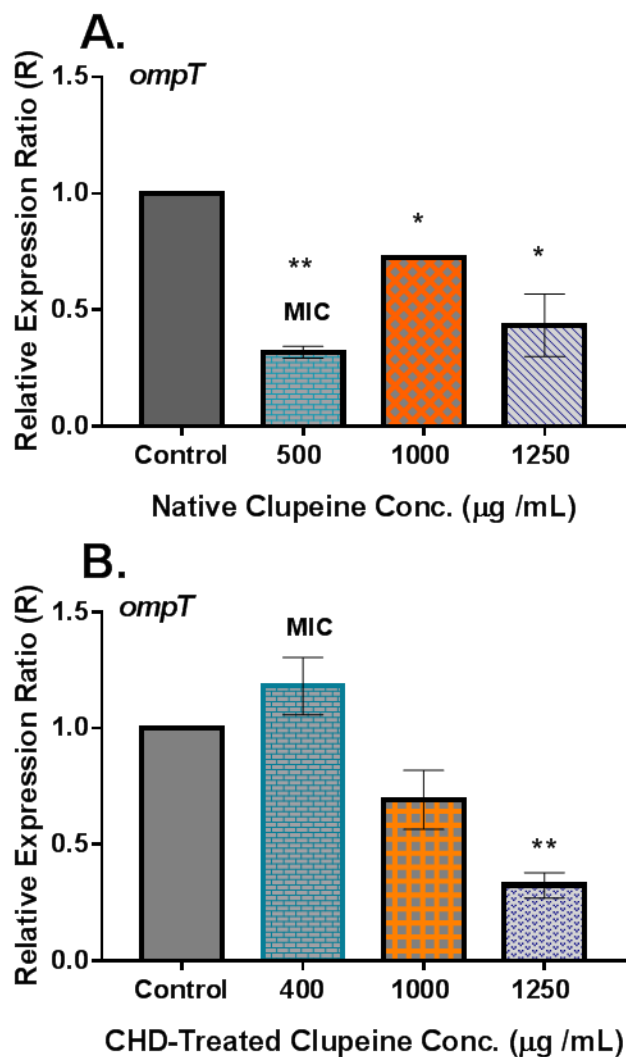


Figure 0-3 Mean relative expression ratios (R values) of *ompT* gene expressed in *E.coli* K-12 cells treated with native clupeine (A) and CHD-treated clupeine (B), (n=3, error bars show the standard deviation) (** P < 0.01; * P < 0.05).

3.4.2 Relative Expression of Porin Genes in *S. enterica* Typhimurium 14028 Cells Treated with Native or CHD-Treated Clupeine

In the case of *S. enterica* Typhimurium 14028 cells, *ompF* expression was greatly up-regulated in the presence of 2500 µg/mL native clupeine (P < 0.001), with no effect at lower concentrations (P > 0.05; Figure 3-4A), whereas with CHD-treated clupeine, *ompF*

was down-regulated at the MIC (400 $\mu\text{g/mL}$) ($P > 0.05$) but was up-regulated at 2500 $\mu\text{g/mL}$ ($P < 0.001$; Figure 3-4B). Interestingly, *ompC* gene expression was down-regulated with increasing concentrations of native clupeine, especially at the highest concentrations (1250 and 2500 $\mu\text{g/mL}$; Figure 3-5A), whereas it was up-regulated at the highest concentrations (1250 and 2500 $\mu\text{g/mL}$) of CHD-treated clupeine ($P < 0.05$; Figure 3-5B).

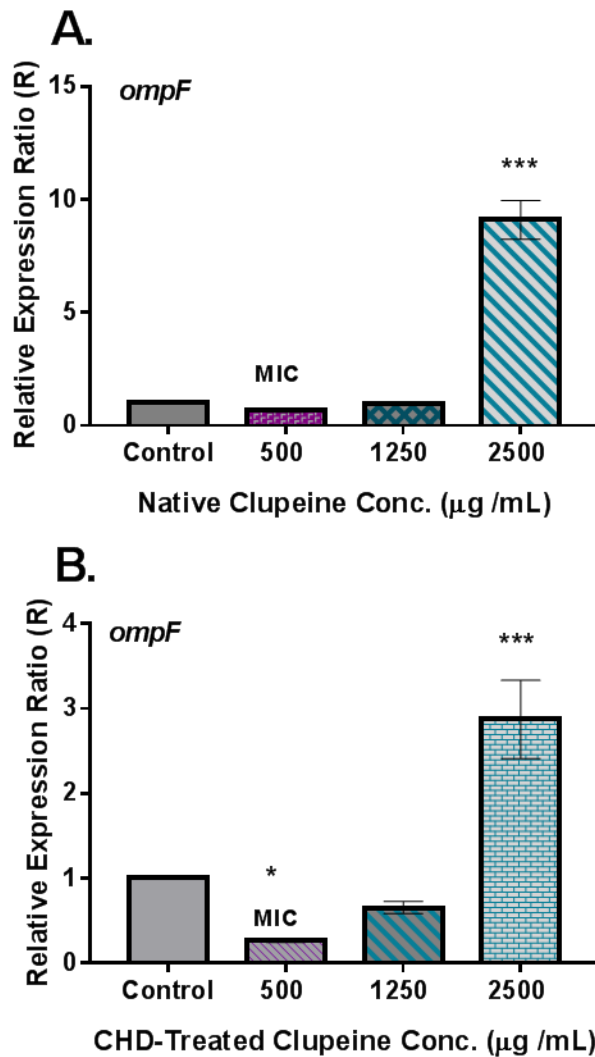


Figure 0-4 Mean relative expression ratios (R values) of *ompF* expressed in *S. enterica* Typhimurium 14028 cells treated with native clupeine (A) and CHD-treated clupeine (B), ($n=3$, error bars show the standard deviation) (***) $P < 0.001$; *) $P < 0.05$).

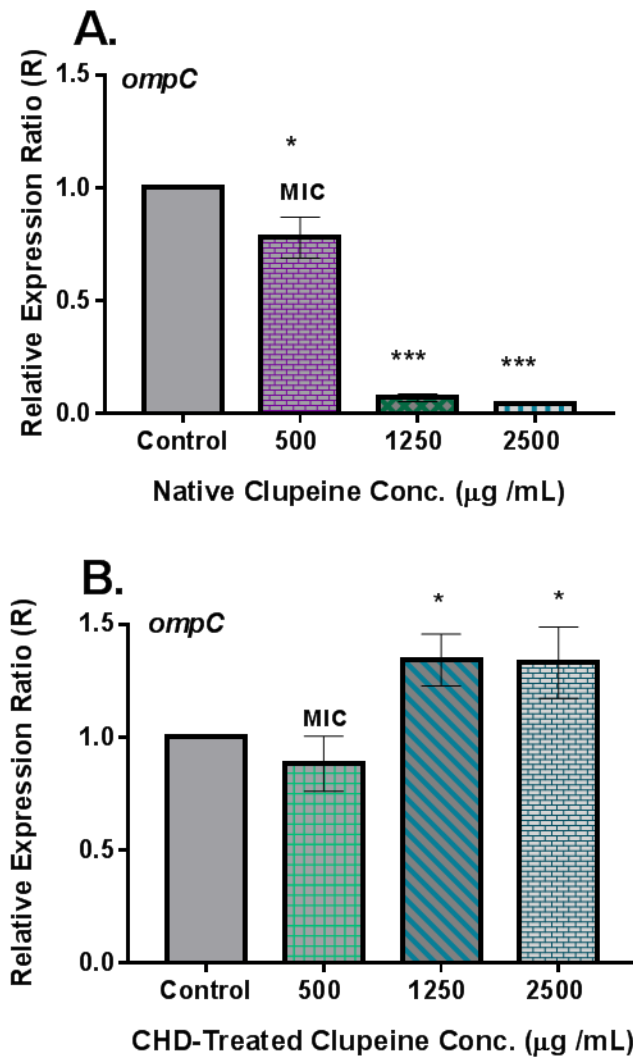


Figure 0-5 Mean relative expression ratios (R values) of *ompC* in *S. enterica* Typhimurium 14028 cells treated with native (A) and CHD-treated clupeine (B), (n=3, error bars show the standard deviation) (***) $P < 0.001$; *) $P < 0.05$).

3.4.3 Porin Protein Profiles Obtained by SDS-PAGE

SDS-PAGE was carried out on the protein extracts obtained from the treated and untreated *E. coli* K-12 and *S. enterica* Typhimurium 14028 cells, and comparative

profiles are shown in Figure 3-6 and Figure 3-7, respectively. A single band was observed in the untreated *E. coli* K-12 and *S. enterica* Typhimurium 14028 cells (Figures 3-6 and 3-7, lane 2) and was identified by mass spectrometry as OmpA, (MW 37.2 kDa). Protein bands with similar apparent molecular weights as the untreated control were selected for in-gel digestion, and the peptides obtained were identified using a UniProt Basic Local Alignment Search Tool (BLAST).

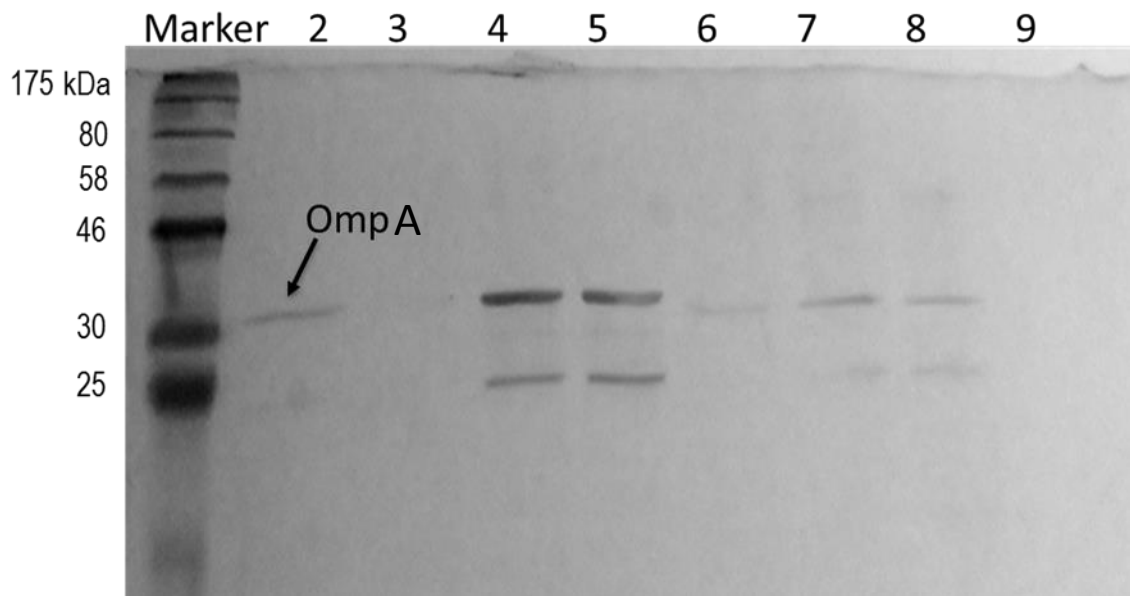


Figure 0-6 Outer membrane porin proteins of *E. coli* K-12 separated on 15% SDS-PAGE. Lane 1, protein marker, lane 2, untreated *E. coli*; lanes 3, 4, and 5 proteins from cells treated with 500, 1000 and 1250 $\mu\text{g}/\text{mL}$ native clupeine respectively; lanes 6, 7 and 8, proteins from cells treated with 400, 1000 and 1250 $\mu\text{g}/\text{mL}$ CHD-treated clupeine, respectively. Lane 9 was the double mutant control. (n=3)

At all concentrations of native and CHD-treated clupeine used, OmpA was the main protein identified among outer membrane proteins isolated from *E. coli* K-12 cells (Table 3-3). However, OmpC and OmpF porin proteins were also identified in the

presence of CHD-treated clupeine (Table 3-3). In addition, only at MIC concentrations of the CHD treated peptide (400 $\mu\text{g}/\text{mL}$) was the OmpT protein identified.

In outer membrane protein preparations from *S. enterica* Typhimurium 14028 cells challenged with native clupeine, OmpA was also the main protein identified. In contrast, only OmpC porin protein was identified in *S. enterica* Typhimurium 14028 cells exposed to the CHD-treated peptide (Table 3-3).

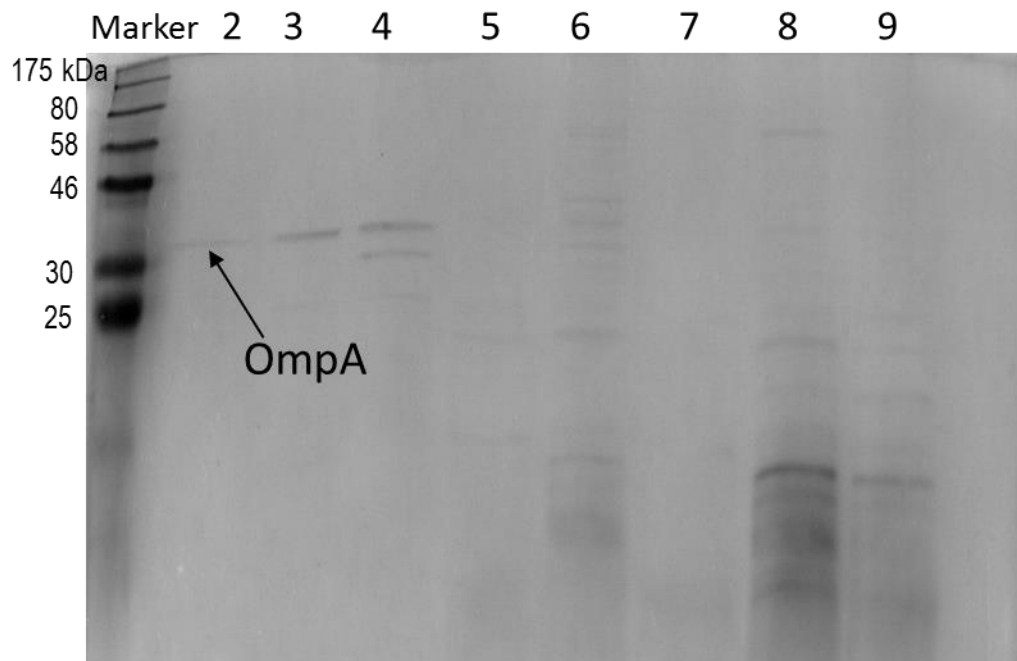


Figure 0-7 Outer membrane porin proteins of *S. enterica* Typhimurium 14028 separated on 15% SDS-PAGE. Lane 1, protein marker, lane 2, untreated *S. enterica* Typhimurium 14028; lanes 3, 4, and 5 proteins from cells treated with 500, 1250 and 2500 $\mu\text{g}/\text{mL}$ native clupeine respectively; lanes 6, 7 and 8, proteins from cells treated with 500, 1250 and 2500 $\mu\text{g}/\text{mL}$ CHD-treated clupeine, respectively. Lane 9 was the double mutant control. (n=3).

Along with the porin proteins expressed, the protein glyceraldehyde-3-phosphate dehydrogenase (GapA) was also identified in both *E. coli* K-12 and *S. enterica* Typhimurium 14028 cells that were exposed to CHD-treated clupeine. It is noteworthy

that this protein was not identified in the preparation from cells that were exposed to the native peptide (Table 3-4).

Table 0-3 Summary of *E. coli* K-12 and *S. enterica* Typhimurium 14028 porin proteins identified by mass spectrometry. The number of peptides detected in the trypsin gel digests were used as an indicator of the relative abundance of the proteins identified.

Samples	Molecular Weight (kDa)	Relative Abundance of Target Protein Expressed (%)	Proteins identified
<i>E. coli</i> K-12			
Untreated	37.2	12	OpmA
500 µg/mL N-Clu	37.2	9	OmpA
1000 µg/mL N-Clu	37.2	43	OmpA
1250 µg/mL N-Clu	37.2	35	OmpA
400 µg/mL CHD-Clu	37.2	22	OmpA
	41.2	9	OmpC
	39.3	12	OmpF
	35.5	6	OmpT
1000 µg/mL CHD-Clu	37.2	27	OmpA
	41.2	10	OmpC
	39.3	2	OmpF
1250 µg/mL CHD-Clu	37.2	25	OmpA
	41.2	10	OmpC
	39.3	2	OmpF
<i>ΔompF / ΔompC</i>			*
<i>S. Typhimurium</i> 14028			
Untreated	37.5	27	OmpA
500 µg/mL N-Clu	37.5	32	OmpA
1250 µg/mL N-Clu	37.5	39	OmpA
	37.5	15	OmpC
2500 µg/mL N-Clu	37.5	18	OmpA
	41.2	5	OmpC

500 µg/mL CHD-Clu			*
1250 µg/mL CHD-Clu	41.2	5	OmpC
2500 µg/mL CHD-Clu	41.2	11	OmpC
<i>ΔompF/ΔompC</i>			*

* No porin protein was identified in these samples.

Table 0-4 Additional proteins identified by mass spectrometry. The number of peptides detected in the trypsin gel digests were used as an indicator of the relative abundance of the proteins identified.

Samples	Relative Abundance of Protein Expressed (%)	Proteins Identified
<i>E. coli</i> K-12		
Untreated	10	b
500 µg/mL N-Clu	-	-
1000 µg/mL N-Clu	-	-
1250 µg/mL N-Clu	-	-
400 µg/mL CHD-Clu	4	a
1000 µg/mL CHD-Clu	6	a
1250 µg/mL CHD-Clu	4	a
<i>S. Typhimurium</i> 14028		
Untreated	-	-
500 µg/mL N-Clu	-	-
1250 µg/mL N-Clu	-	-
2500 µg/mL N-Clu	-	-
500 µg/mL CHD-Clu	-	-
1250 µg/mL CHD-Clu	5	a
2500 µg/mL CHD-Clu	4	a

a glyceraldehyde-3-PO₄-dehydrogenase present

b glucose-6-PO₄-dehydrogenase present

“-“ this means a and b were not identified

3.5 Discussion

The best understood model used to describe porin regulation in Gram-negative organisms involves the EnvZ/OmpR two-component regulatory system (Liu and Ferenci, 1998). However, the role of porin genes and porin proteins in the bacterial response to native and CHD-treated clupeine (10% arginine modified) is not clearly defined. To

study these interactions, *E. coli* K-12 and *S. enterica* Typhimurium 14028 cells grown to late exponential phase were challenged with various concentrations of native or CHD-treated clupeine. In *E. coli* K-12 cells exposed to 500 and 1250 µg/mL native clupeine, the relative expression of the *ompF* gene was decreased, whereas the expression of the *ompC* gene was increased at all concentrations. In contrast, the expression of the *ompF* gene was down-regulated in the presence of the CHD-treated peptide, while *ompC* expression was unaffected at any concentration (Figure 3-2).

In addition to the EnvZ/OmpR osmoregulation of *ompF* and *ompC* genes shown in Figure 1-15, *micF* also plays a role in the osmoregulation of the *ompF* gene. Indeed, Ramani et al. (1994) reported that when *E. coli* cells are grown in Luria-Bertani broth supplemented with 0 to 6% sucrose (low to medium osmolarity), increased *micF* RNA (an antisense RNA) results in destabilization of *ompF* mRNA or inhibition of OmpF translation. Ultimately these events resulted in reduced expression of the OmpF porin protein. According to the EnvZ/OmpR model, *ompF* expression is expected to increase in low osmolarity media, yet, the data from the present study showed an overall decrease in *ompF* transcripts in *E. coli* cells exposed to either peptide (Figure 3-2). Although the levels of *micF* RNA were not measured in this study, the observation of decreased *ompF* transcripts suggests that a possible role for *micF* osmoregulation cannot be ruled out since *micF* works at the transcriptional as well as the translation level (Mizuno et al., 1983; Anderson et al., 1989).

On the other hand, when gene expression was compared in *S. enterica* Typhimurium 14028 cells, little or no effect on *ompF* expression was observed at lower peptide concentrations (Figure 3-4). This was in strong contrast to the significant ($P <$

0.05) up-regulation of *ompF* observed at the highest concentration of peptide used (2500 µg/mL). Moreover, in *S. enterica* Typhimurium 14028 cells, the highest concentration of native and CHD-treated clupeine had opposite effects on *ompC* gene expression (Figure 3-5). The differences in the MIC values for the tested strains may be explained by the findings from a study by Witherspoon-Griffin et al. (2014). These authors showed that the CpxR/CpxA system facilitates *Salmonella* and *E. coli* resistance to cationic antimicrobial peptides including protamine from salmon, by activating transcription of two gene loci (*amiA* and *amiC*) that encoding two peptidoglycan amidases. In addition, Foster and Spector (1996) also proposed that microbial resistance is required for virulence in *Salmonella* species. These authors also noted that the growth phase of the organism is another factor that directly impacts virulence efficiency. Consequently, the potential of the growth media and the growth phase of the cells to modulate gene/porin expression should not be underestimated.

The M9 minimal media used in this study was a mixture of inorganic salts plus 0.4% glucose as a carbon source. Although this media is known to satisfy the growth of *E. coli* and *S. enterica* Typhimurium 14028 cells, the growth rate is slower than in nutrient-rich media such as Luria–Bertani (Gray et al., 2006; Warry et al., 2008; Carrica et al., 2011). In nature bacteria must encounter many challenges such as nutrient limitation and toxic compounds, thus the rationale for the growth conditions chosen for these studies is two-fold. First, slowly growing cells (late exponential phase) tend to survive adversity better than those growing quickly (early to mid-log phase cells) (Brown et al., 1990), and second, the expression of the *ompF* gene and the OmpF porin is osmoregulated by the EnvZ/OmpR two-component regulatory system and *micF* (Ramani

et al., 1994). One limitation of this experimental design is that the inherent complexity makes it difficult to conclusively distinguish between the effect of growth conditions and cell phase from the effect of the presence of the peptides on the individual gene expression profiles obtained. For example, a characteristic response of cells growing in adverse environments is to slow down growth rate (Brown et al., 1990), however, the cells may undergo different physiological changes that may affect gene expression levels independent of the presence of the peptides.

For future studies, additional information may be obtained by performing experiments where single *E. coli* K-12 and *S. enterica* Typhimurium 14028 mutants (e.g., $\Delta ompF$ or $\Delta ompC$) and their parent strains are grown in a rich medium such as TSB in the presence of either native or CHD-treated clupeine. These conditions would allow the effect of the peptides on gene expression to be observed independent of the EnvZ/OmpR osmoregulation system which occurs in low or high osmolarity media. As well, using cells that are mid log phase may provide additional information as suggested by the observations of Brown et al. (1990), who emphasized that the physiological state of the organisms used in studying antimicrobial interactions greatly affect the outcome of such studies. Within this context, changes in cell properties (such as porin proteins) in the presence of the peptides could be determined several generations before the cells enter stationary phase. Nevertheless, the results from the present study indicate that overall, different gene expression profiles were obtained for the two organisms tested under the experimental conditions used.

In order to determine if the porin expression data were related to the gene expression studies, SDS-PAGE and mass spectrometry were performed on similar cell

preparations that were exposed to native or CHD-treated clupeine. Unlike the down regulation of the *ompF* gene observed (Figure 3-2A) some OmpF and OmpC porin proteins (12% and 9% relative protein expression, respectively) were identified when *E. coli* K-12 was exposed to MIC concentrations of CHD-treated clupeine (Table 3-3). However, Vogel and Marcotte (2013) reported that the expression level of mRNA (the direct product of DNA transcription) only explains a fraction (~40%) of the variation in protein abundance and that the latter may be affected by post-transcriptional regulation of genes independently of their up or down-regulation. Therefore, although not all the protein bands observed on the SDS-PAGE gels (Figures 3-6 and 3-7) were identified, based on the protein expression data (Table 3-3), there is an argument to be made that native clupeine and CHD-treated clupeine elicit different responses in *E. coli* K-12 cells challenged with varying concentrations of these peptides. Indeed, reduced amounts of OmpF in *E. coli* have been previously linked to resistance to various antibiotics including the β -lactams, tetracycline and chloramphenicol (Cohen et al., 1988). Based on the proposition made by Pratt et al. (1996) it seems likely that the bacterial cells made a trade-off in the presence of increasing concentrations of native clupeine. In *E. coli*, this trade-off meant decreasing the expression of the permeability properties of the larger more efficient porin at the cost of optimal nutrient access.

An interesting finding in this study was the higher proportion of OmpA identified in untreated *S. enterica* Typhimurium 14028 cells (27% relative protein expression) compared to untreated *E. coli* K-12 cells as well as in the latter exposed to native or CHD- treated clupeine (43% and 27% relative protein expression, respectively) (Table 3-

3). It should be noted that the OmpA porin protein was not identified in the double mutant control used in this study.

The up-regulation of OmpA observed may be related to the function of this protein in the bacterial cells of interest. OmpA provides structural integrity to the membrane (Wang, 2002) and also functions in active and passive ion transport (Khalid et al., 2008), however, there has been an ongoing debate in the literature surrounding the pore-formation ability of OmpA and the native conformation of the protein (Pautsch and Schultz, 2000; Hong et al., 2006; Smith et al., 2007). In addition to the protein's well-known structural role, Gautam et al. (2011) proposed a possible role for OmpA in drug resistance based on the total OmpA peptide recovery in two different strains of *E. coli*. They used an antimicrobial susceptible strain of *E. coli*, and observed that upon digestion with trypsin the total OmpA peptide recovery was 15 peptides; this number increased to 22 when a multi-drug resistant strain of *E. coli* was used.

In a similar way, in the present study, peptide recovery was taken as an indicator of the relative abundance of proteins identified by mass spectrometry and was used to compare differences in the expression of the OmpA porin protein. This approach is possible because an increase in protein abundance typically results in an increase in the number of its identified unique peptides (Zhu et al., 2009). However, when using this approach two assumptions were made: (1) an equal amount of enzyme (trypsin) was used to generate peptides from the gel bands, and (2) the protein extraction efficiencies were the same for all the samples investigated. Table 3-3 shows increased peptide recovery observed in *E. coli* K-12 cells exposed to native and CHD-treated clupeine as compared

to untreated *E. coli* K-12 cells. Considering the increased levels on OmpA, the latter may satisfy an alternative channel requirement (Lu and Ferenci, 1998).

Additional support for OmpA's role in membrane permeability may be garnered from a recent study by van der Heijden et al. (2016) who proposed that *S. Typhimurium* 12023 cells lacking catalase and peroxidase activity were able to regulate the opening and closing of OmpA and OmpC pores by using a stress response mechanism. They also demonstrated that during periods of low osmotic stress in the *S. Typhimurium* 12023 cells, the OmpC porin was preferentially used to facilitate the diffusion of hydrogen peroxide into the cells. However, when oxidative stress within the cells increased (redox potential value above -290 mV), the OmpC porins were closed and the OmpA porin facilitated diffusion of hydrogen peroxide into the cells. The switch in the expression of porins was attributed to a unique structure in the OmpA porin; an extensive periplasmic domain that contains two cysteines. These cysteines were able to form a disulfide bond in the presence of oxidative stress and therefore act as a regulatory switch. Unlike the OmpA porin this periplasmic domain is absent from the OmpC porin (van der Heijden et al., 2016).

It is also noteworthy that in the presence of MIC concentrations of CHD-treated clupeine, other porin proteins were identified in *E. coli* K-12 cells, more specifically, OmpF, OmpC and OmpT (12%, 9% and 6%, respectively). However, in the virulent *S. Typhimurium* 14028 strain, only OmpC porin protein was identified and expressed at MIC (1250 µg/mL) and MBC (2500 µg/mL) concentrations of CHD-treated clupeine (Table 3-3). These observations suggest an important role for clupeine concentration in these experiments.

In this study, glyceraldehyde-3-phosphate dehydrogenase (GapA) which is a known target of oxidative stress was also identified by MS (Table 3-4). GapA is a glycolytic enzyme which catalyzes the conversion of glyceraldehyde 3-phosphate to 1, 3-diphosphoglycerate using the co-factor nicotinamide amide dinucleotide (NAD), which is reduced to NADH (Tunio et al., 2010). In addition to its metabolic function, GapA displays various non-glycolytic roles in different subcellular locations including membrane fusion and covalent modifications that are linked to oxidative stress (Aguilera et al., 2009). GapA was identified in all cells exposed to CHD-treated clupeine except for *S. enterica* Typhimurium 14028 cells exposed to 500 µg/mL CHD-treated clupeine (Table 3-4), no other Omps were identified from this in-gel digest. It is possible that in the latter, the sample may have been recovered during the preparation process for MS. The amount of GapA observed appeared to be dependent on the concentration of CHD-treated clupeine, where the greatest expression (6%) observed was at 1000 µg/mL concentrations of CHD-treated clupeine. However, similar expressions (4%) were observed at 1000 and 1250 µg/mL concentrations of CHD-treated clupeine (Table 3-4).

The connection with increased expression of different proteins associated with oxidative stress is in agreement with previous studies which demonstrated that CAPs as well as antibiotics induce reactive oxygen species in bacterial cells (Belenky and Collins, 2011; Dwyer et al., 2015). However, the response to oxidative stress does not always result in increased expression of GapA. For example, Weber et al. (2004) studied the oxidative response of *St. aureus* cells exposed to 100 mM of hydrogen peroxide over a time period of 5, 10, 20 and 40 min. One of the key findings of this study was the identification of GapA after 5 min of incubation. Under oxidative stress conditions, the

active site of the enzyme (cysteine residues) was oxidized which inactivated the enzyme and resulted in decreased adenosine triphosphate (ATP) in the cell and reduced growth. In contrast to the increased GapA expression observed in the presence of CHD-treated clupeine, and the defective GapA observed in the Weber et al. (2004) study, no GapA was identified in the cells exposed to native clupeine, although glucose-6-phosphate 1-dehydrogenase (G6PDH) was identified in the untreated *E. coli* cells (Table 3-4). Glucose-6-phosphate 1-dehydrogenase is a key enzyme involved in the distribution of carbon between glycolysis and the pentose phosphate pathway (Stanton, 2012).

It was also interesting to note the down-regulation of the *ompT* gene which codes for the OmpT protease enzyme. An earlier report by Stumpe et al. (1998) identified OmpT as the protease responsible for the degradation of protamine from salmon (salmine) exposed to *E. coli* KS272 cells. In addition, Truelstrup Hansen and Gill (2000) also observed degradation of protamine from herring (clupeine) in the presence of *E. coli* 25922 cells. The protamine used in the work by Stumpe et al. (1998) was protamine from salmon (salmine), however in the present study, protamine from herring (clupeine) was used.

Although there are structural differences between these two types of protamines, they were both degraded by proteases in the studies described above. As noted in Chapter 1 (Figure 1-3), clupeine is a mixture of three different variants (YI, YII and Z), whereas salmine is made up of two variants (S-A and S-B) (Islam et al., 1985). These two heterogeneous protamines also contain certain variations in their amino acid primary sequence. For example, clupeine contains more threonines (2, versus none in salmine) and 6 prolines as compared to 3 in salmine), whereas salmine has 21 arginines compared

to clupeine with 19 (Swiss-prot <http://us.expasy.org/sprot/>). Nevertheless, in this study, up-regulation of the *ompT* gene and the presence of the OmpT protein was only observed in the presence of MIC concentrations of CHD-treated clupeine, which indicates that the concentration of the peptide may be important in the relative expression of the *ompT* gene and its corresponding protein. Unlike the *ompF* and *ompC* genes that are regulated by the EnvZ/OmpR regulatory system, the *ompT* gene is not. However, not all proteases are associated with degrading CAPs. For example, clupeine and salmine were able to inhibit the proteolytic activity of the arginine-specific cysteine protease (RC-protease) from *Porphyromonas gingivalis*, a Gram-negative bacteria implicated in periodontal disease (Knotani et al., 1999).

In contrast, a study by Thomassin et al. (2012) compared the OmpT protease activity of two foodborne pathogens, enterohemorrhagic *Escherichia coli* (EHEC) and enteropathogenic *E. coli* (EPEC) against the α -helical antimicrobial peptides C18G and LL-37, and found that EHEC OmpT readily degraded and inactivated the antimicrobial peptides which promoted bacterial survival while the EPEC OmpT had a more marginal role in antimicrobial peptide degradation. The faster degradation of the EHEC OmpT was attributed to a high expression of the *ompT* gene and high levels of the OmpT protein in the outer membrane of EHEC as compared to EPEC.

In summary, different gene expression profiles were obtained for *E. coli* K-12 and *S. enterica* Typhimurium 140208 cells exposed to native and CHD-treated clupeine. An interesting finding from the study was an increased proportion of OmpA porin identified in both test strains and the expression of GapA only in the cells exposed to CHD-treated clupeine. In addition, the relative expression of the *ompT* gene was only up-regulated at

MIC concentrations of the CHD-treated peptide, which suggest that the presence of the peptide may be modulating *ompT* gene expression since the latter is not known to be regulated by the EnvZ/OmpR osmoregulatory system.

CHAPTER 4: INTERACTIONS OF NATIVE AND CHD-TREATED CLUPEINE WITH GRAM-NEGATIVE MODEL MONOLAYERS

4.1 Abstract

Concern about bacterial resistance has increased research in understanding the interactions of cationic antimicrobial peptides (CAPs) such as clupeine with Gram-negative bacteria. Clupeine is of interest because it has exhibited antimicrobial activity against some foodborne pathogens, however, the structural details that occur in these cells remains to be elucidated. In this study, the interactions of native clupeine and clupeine modified (10% charge reduced) with 1,2-cylcohexanedione (CHD-treated clupeine), were studied in model monolayer membranes that mimic the inner membrane of *E. coli*. Model membranes were prepared using the following lipids: DPPE (1,2-dipalmitoyl--glycero-3-phosphoethanolamine), DPPG (1,2-dipalmitoyl-sn-glycero-3-[phosphor-rac-1-glycerol]) and CL (1,1'2,2'-tetramyristoyl cardiolipin) in the following ratios PE:PG:CL (79:17:4 mole %). Complementary techniques neutron reflectometry (NR) and X-ray reflectometry (XRR) along with surface pressure measurements were used to study these interactions.

Unlike the native peptide that showed a 2.3% decrease in surface pressure, in the presence of the CHD-treated peptide, there was a 4.6% increase in surface pressure. Surface excess in the presence of native clupeine was 0.67 mg/ m^2 where 55% ($0.364 \pm 0.02 \text{ mg/m}^2$) was found in the peptide layer of the model. In contrast, in the presence of CHD-treated clupeine, 61% ($0.59 \pm 0.14 \text{ mg/m}^2$) of the total peptide surface excess

(0.969 mg/m²), was found in the peptide layer of the model. In the presence of both peptides, there was a general decrease in scattering length density (SLD), in the presence of the native peptide (~3%), compared to a 2% decrease in the presence of the CHD-treated peptide, this decrease in SLD was attributed to greater hydration of the outer lipid head group.

In addition, the lipid volume fraction of the monolayer also decreased in the presence of the peptides, a 38% decrease in lipid volume fraction from 0.97 to 0.59 ($P < 0.001$) was observed with native clupeine whereas a 28% decrease in lipid volume fraction from 0.97 to 0.69 ($P < 0.05$) occurred in the presence of the CHD-treated peptide. These observations suggest that the peptides are able to remove lipid content from the surface during their interaction with the monolayer.

4.2 Introduction

The widespread resistance of pathogenic bacteria to antibiotics and antimicrobial agents was postulated by Fleming as early as 1945 (Rosenblatt-Farrell, 2009). Acquired antimicrobial resistance may be defined as the survival of bacteria after exposure to an agent at a concentration to which it was originally sensitive (Jepson, 2014). Due to the biochemical and structural differences in their cell wall structures, bacteria may be classified into two main groups based on the Gram stain technique, Gram-positive and Gram-negative. Gram positive bacteria have a cell membrane and a thick cell wall of peptidoglycan, whereas Gram-negative bacteria have an inner membrane, periplasm, cell wall and an outer membrane (Ruiz et al., 2005). Both Gram-positive and Gram-negative bacteria have evolved to exhibit antimicrobial resistance although the mechanism might be different.

One potential approach to replace antimicrobial agents that are no longer effective is the use of cationic antimicrobial peptides (CAPs). CAPs are ubiquitous in nature (Zasloff, 2002) and range in size from 20 to 40 amino acids, and studies have demonstrated their broad spectrum of antimicrobial activity and their non-sensitivity to host cells (Hancock and Rozek, 2002). Much of the work on CAPs has shown that their cationic and hydrophobic composition make them well suited for bacterial membrane interactions (Brogden, 2005; Wimley, 2010). Two common peptide interactions with bacterial membranes include (a) disrupting the bacterial membrane barrier and (b) affecting specific membrane functions. An example of the latter is pyrrolicorin, a membrane-bound enzyme that binds to DnaK, a heat-shock protein and reduces its ATPase activity (Epan and Epan, 2011; Brogden, 2005 and Shai, 1999).

Among these peptides, clupeine, a CAP found in the sperm cells of herring, has demonstrated antimicrobial activity toward some food-borne pathogenic Gram-negative and Gram-positive bacteria, with previous research suggesting that Gram-positive organisms are generally the most protamine-susceptible bacteria (Johansen et al., 1997; Truelstrup Hansen et al., 2001). The amphipathic nature of CAPs has been shown to be important in the electrostatic interactions that facilitate the binding of these peptides with anionic phospholipid head groups (Zhu et al., 2015). But, unlike most CAPs, clupeine is not amphiphilic and lacks secondary structure due to the even distribution of positive charges along the peptide's backbone (Bonora et al., 1979).

Two common techniques that have been used to examine peptide-membrane interactions of CAPs include liposome leakage assays and membrane potential assays. Liposome leakage assays involve the incorporation of a fluorophore and a second

molecule in a lipid vesicle (liposome), and the role of the second molecule is to quench the fluorescence of the fluorophore at high concentration (Schibli et al., 2002; Rathinakumar et al., 2009). On the other hand, membrane potential assays are usually carried out in living cells, and although the dyes are unable to penetrate intact cell membranes, an increase in fluorescence is observed when membrane permeabilization allows entry of the dye in bacterial cells (Rathinakumar et al., 2009). One main advantage of these techniques is that they help to determine whether antimicrobial activity may be attributed to membrane permeabilization. However, one limitation is that details of the initial interaction of the peptide with the lipid is not determined, only the outcome of the interaction is observed. In order to gain a better understanding of the mechanism of action of clupeine its initial interactions with lipid membranes must first be understood. This formed the basis of the rationale for choosing to use NR and XRR techniques in the present study.

NR and XRR are complementary techniques that have been used to study peptide lipid interactions by using model membranes in the form of monolayers or bilayers (Barker et al., 2016). Among Gram-negative bacteria, *E. coli* is considered an ideal model organism and several researchers have used model membranes composed of fatty acid mixtures that represent either the inner or outer *E. coli* membrane to study peptide-lipid interactions (Broniatowski et al., 2015). Lipid composition is an important factor that affects peptide-lipid interactions (Wimley, 2010) and CAPs such as clupeine which are more cationic than hydrophobic will require more anionic lipids for peptide binding. In this study monolayers were constructed using the lipids PE: PG: CL (79:17:4 mole %), which are mostly anionic (PG and CL) or zwitterionic (PE) in nature (Figure 1-4). In

addition, this unique lipid ratio was specifically designed to mimic the *E. coli* inner membrane (Morein et al., 1996).

Both NR and XRR techniques can be used to provide structural details that elucidate the physical basis for the manner in which peptides interact with cell membranes (Barker et al., 2016). For example, Clifton et al. (2012) used NR and XRR to determine the interaction of the plant defence proteins α 1- and α 2-purothionin with 1,2-Dipalmitoyl-sn-glycero-3-phosphorylglycerol (DPPG) monolayers and these authors were able to determine both the lipid area per molecule and the protein coverage after interaction with the model membrane (Baker et al., 2016). These outcomes show that NR can be used as a suitable tool to provide structural information at the sub-molecular unit length scale for model bacterial membranes (Barker et al., 2016).

Figure 1-5 shows the basic setup for a monolayer film, and the NR setup used in this study is shown in Figure A2-2. The main objective of the NR and XRR experiments was to help answer the following questions: (1) what is the influence of native and CHD-treated clupeine on the surface pressure of the lipid membrane? (2) To what extent are native and CHD-treated clupeine inserted in the hydrophobic lipid layer or, are the peptides only adsorbed to the lipid-head group interface. (3) What is the influence of native and CHD-treated clupeine on the lipid monolayer thickness and the electron density profile of the lipid head group? (4) What is the extent of the contribution of native and CHD-treated clupeine to the NR and XRR reflectivity signal? Taken together, the answers to these questions should help provide a better understanding of the initial steps in the mechanism of action of native and CHD-treated clupeine with *E. coli* inner model membranes.

4.3 Materials and Methods

4.3.1 *Materials*

DPPE, 1,2-dipalmitoyl--glycero-3-phosphoethanolamine, MW 691.97 (zwitterionic and synthetic purity > 99%); DPPG, 1,2-dipalmitoyl-sn-glycero-3-[phosphor-rac-1-glycerol] (anionic sodium salt), MW 744.96; and 1,1',2,2'-tetramyristoyl cardiolipin (anionic sodium salt), MW 1,285.62 were all purchased from Avanti Polar Lipids (Alabaster, AL, USA). Stock solutions of all the lipids were prepared using a 3:1 mixture of HPLC grade chloroform to methanol (Sigma-Aldrich, Oakville, ON, Canada) in a ratio of PE:PG:CL (79:17:4 mole %) and stored at -20°C. All the lipid samples were brought to room temperature before use.

Native clupeine (MW 4112 Da) was obtained from Sigma (clupeine sulfate, P4505, Sigma, Oakville, ON, Canada) and was used without further purification. The preparation of CHD treated clupeine was prepared as outlined in Chapter 2. The peptide solutions were made using a 0.02 M phosphate buffer solution (pH 7) and were diluted to a final concentration of 0.48 μM by adding the concentrated peptide solution to the 80- cm^3 buffer subphase of the Langmuir trough.

4.3.2 *Surface Pressure Measurements*

Surface pressure measurements on a Langmuir trough (model 611 Nima Technology, Coventry, England) interfaced with a computer data acquisition system were carried out by the Wilhelmy plate method and was carried out as described by Lad et al. (2007). Before the start of each experiment, the trough was first cleaned with chloroform

then with several changes of ultra-high quality (UHQ) grade water. The clean trough was filled with 80 mL of 0.02 M phosphate buffer (pH 7), and 20 μ L of the lipid solution in chloroform was spread dropwise using a Hamilton syringe, (Hamilton Company, Reno, NV) on the surface of the buffer to form a monolayer.

After allowing five minutes for the chloroform to evaporate, the lipid monolayer was compressed by reducing the area within the barriers and fixing the barriers when a target surface pressure of $\sim 25 \text{ mN m}^{-1}$ was achieved. Control checks were carried out for $\sim 4.2 \text{ h}$ on the bare PE:PG:CL monolayers to determine their stability. For each experiment, the compressed film was relaxed for twenty minutes at $\sim 25 \text{ mN m}^{-1}$ prior to the addition of 1 mL of native or CHD-treated clupeine solution to the subphase (final peptide concentration of $0.48 \mu\text{M}$). The peptide solutions were added with a long needle which allowed the rapid insertion into the subphase and prevented disruption of the monolayer. Compression isotherms were recorded as surface pressure (π) - area (A) curves prior to the addition of the peptides and on addition of the peptide to the subphase, and plots of surface pressure versus time were recorded to follow adsorption of the peptides to the lipid layer. All compressions were repeated until a reproducible trace was obtained and the final surface pressure values had a standard deviation of $\pm 1 \text{ mN m}^{-1}$. Similar experiments were carried out using the negatively charged phospholipid, DPPG, as a control.

4.3.3 Neutron Reflectometry Measurements on PE:PG:CL

Neutron reflectivity (NR) measurements were carried out using the white beam SURF reflectometer at the Rutherford Appleton Laboratory (Didcot, Oxfordshire, UK),

using neutron wavelengths from 0.5 to 6.5 Å. The beam intensity was calibrated with respect to a clean D₂O surface. The sample preparation and method were carried out with some modifications as described by Green et al. (2000), Lad et al. (2007) and Clifton et al. (2011) and is outlined below.

All the NR experiments were performed at room temperature and the lipid films were prepared by spreading the PE:PG:CL (79:17:4 mole %) lipid mix (from the stock solution) in a large 200 x 400 mm Langmuir trough (Nima Technology Ltd, Coventry, UK) containing a 20 mM phosphate buffer (pH 7.0). After evaporation of the solvent, the films were compressed to a surface pressure of 23 mN m⁻¹ to reduce the volume of the subphase from ~ 380 mL to ~ 100 mL. The compressed films were relaxed for twenty minutes at 23 mN m⁻¹ prior to the addition of native or CHD-treated clupeine solutions (0.48 μM) to the lipid monolayer, and neutron reflectivity curves were recorded at two angles of incidence ($\theta = 1.5$ and 0.8°) to yield a momentum transfer range of ~0.01 – 0.6 Å⁻¹ both before and after the addition of native or CHD-treated clupeine.

NR was measured under multiple isotopic contrasts and this was achieved by using hydrogenated and deuterated lipids in NRW (8% D₂O, 92% H₂O) and D₂O. Measurements using h-lipids on NRW were done to observe protein binding since the h-lipid will be largely non-reflecting ($\rho(h - lipid) = -0.39 \times 10^{-6} \text{Å}^{-2}$), where ρ represents the Scattering Length Density (SLD). Repeat experiments using isotopic contrasts with d-lipid ($\rho(d - lipid) = 7.5 \times 10^{-6} \text{Å}^{-2}$) on NRW were also done to reveal any changes in lipid layer structure caused by the interaction. Contrasts of h-lipid on D₂O were also done to enable differentiation between peptide adsorbed beneath the interface and the lipid head group (Clifton et al., 2013a).

4.3.4 X-Ray Reflectometry Measurements on PE:PG:CL

X-ray reflectivity experiments were performed at the I07 beamline at the Diamond Light Source (Harwell Science and Innovation Campus, Didcot, Oxfordshire, UK). The sample preparation and method described by Clifton et al. (2012, 2015) was carried with some modifications and is outlined below.

Experiments were performed at room temperature and the lipid films were prepared by spreading the PE:PG:CL (79:17:4 mole %) lipid mix (from the stock solution) in a large 200 x 400 mm Langmuir trough (Nima Technology Ltd, Coventry, UK) containing a 20 mM phosphate buffer (pH 7.0). After evaporation of the solvent, the films were compressed to a surface pressure of 23 mN m⁻¹ to reduce the volume of the subphase from ~ 380 mL to ~100 mL. The compressed films were relaxed for twenty minutes at 23 mN m⁻¹ prior to the addition of native or CHD-treated clupeine solutions (0.48 μM) to the lipid monolayer.

A monochromatic x-ray wavelength of 0.992 Å (corresponding to a photon energy, E of 12.5keV) was used and a fast shutter was applied to avoid over-exposure to the x-ray beam. The experiments were also performed in a helium atmosphere to reduce background scattering and to prevent oxidative damage. The reflectivity profiles were measured in a Q_z range of 0.01 to 0.8 Å⁻¹ and data were collected on a Dectris Pilatus 100 k detector. XRR data were reduced by performing a normalisation and a “footprint correction” step. There were three parts to the normalisation, the first part involved dividing by the incident flux since this varies with the incident angle. The second part involved stitching the three regions together; this was done by overlapping points at the

extremes of each region. Finally, the third part involved scaling the data so that reflectivity at the critical edge was equal to one. The detector also used two ‘regions of interest’, (ROI) to simultaneously measure the signal, and this background was subtracted from all the data sets (Clifton et al., 2012).

4.3.5 Reflectivity Data Analysis

NR and XRR data were analyzed using a Matlab version of RasCal (version 1.1.2, Hughes, A., ISIS Spallation Neutron Source, Rutherford, Appleton Laboratory) a program which uses Abeles layer models to fit reflectivity data. In RasCal, structures across the interface are modeled as a series of layers and each layer is described by three main parameters: its thickness (τ), its SLD (ρ), and its roughness (Clifton et al., 2013a). The SLD of the lipids (head groups and tails), solvents and peptides were calculated depending on their chemical composition using the equation:

Equation 0-1

$$\rho = \frac{\sum b}{V}$$

Where b represents the scattering length for each element and V represents the molecular volume (Lad, 2006). The XRR and NR data were first fitted individually (Appendix D) then fitted simultaneously as described by Nelson (2006) and Clifton et al. (2012) to place restrictions on the NR fit. The thickness and roughness parameters were linked in a single model and the scattering length densities and background values were allowed to vary (Nelson, 2006).

Bare lipid monolayers with no peptides were divided into two layers, the first, a lipid chain layer containing CH_3 and CH_2 groups and the second, a head group layer

containing the lipid head groups (Dabkowska et al., 2009). This classification was based on two assumptions: (1) the first layer contains only lipid component and that layer two contains only the head group; (2) the second assumption is related to the area per molecule and assumes that this value is the same for both the lipid head group and the tail region (Clifton et al., 2011). However, in order to measure peptide binding to the monolayer, a third layer was included in the model to represent the presence of the peptides below the lipid monolayer (Saunders et al., 2013).

A set of reflectivity profiles measured under the three isotopic contrasts (hydrogenated (h)-lipid in NRW; h-lipid in D₂O and deuterated (d)-lipid in NRW) were fitted together and the large difference between the SLD of hydrogen ($-0.56 \times 10^{-6} \text{ \AA}^{-2}$) and deuterium ($6.35 \times 10^{-6} \text{ \AA}^{-2}$) was used to detect the location of different components in the monolayer. The parameters of the measured data were then fitted to the theoretical model until the best fit or the lowest Chi Square value (χ^2) was achieved. The quality of the fit was also assessed visually.

The fitted SLD for each isotopic contrast was related to the volume fraction of each component using equations 4-2 and 4-3:

Equation 0-2

$$\rho(h) = \rho(h - lipid)\Phi(h - lipid) + \rho(peptide)\Phi(peptide) + \rho(water)\Phi(water)$$

Equation 0-3

$$\rho(d) = \rho(d - lipid)\Phi(d - lipid) + \rho(peptide)\Phi(peptide) + \rho(water)\Phi(water)$$

Where Φ is the volume fraction and ρ = the scattering length density. Because the subphase consisted of NRW which has a SLD of zero, $\rho(water)\Phi(water)$ was eliminated from equations 4-2 and 4-3. The volume fraction of the lipid and peptides were then determined by subtracting equation 4-2 from equation 4-3 to give:

Equation 0-4

$$\Phi (\text{lipid}) = \frac{\rho(D) - \rho(H)}{\rho(D-L) - \rho(H-L)}$$

Where $\rho_{(D)}$ and $\rho_{(H)}$ are the fitted scattering length densities and $\rho_{(D-L)} - \rho_{(H-L)}$ are the calculated scattering length densities. The SLDs and the molecular volume for the native and CHD-treated peptides were calculated using a Biomolecular Scattering Length Density Calculator (<http://psldc.isis.rl.ac.uk/Psldc/>). To calculate the SLD for the lipid mixture of PE:PG:CL (79:17:4 mole%), the SLD of each individual lipid head and tail was calculated and then multiplied by its fraction in the mixture (Table 4-1, C-1 to C-3). The molecular volumes of the lipid components were calculated using the Molinspiration Property Calculator (<http://www.molinspiration.com/cgi-bin/properties>). The area per molecule (A) occupied by the peptide and the lipid in each layer and the surface excess (Γ) for each component in the system were calculated using the following equations:

Equation 0-5

$$A = \frac{\sum b}{\tau \phi \rho}$$

Equation 0-6

$$\Gamma = \frac{MW}{A * 6.02}$$

Where b is the scattering length and τ is the layer thickness obtained from the model fit (Clifton et al., 2011).

4.4 Results

4.4.1 Adsorption of native and CHD-Treated Clupeine to PE:PG:CL (79:17:4 mole %) and DPPG monolayers

The main aim of the surface pressure experiments was to help define whether the peptide mode of binding at the air/liquid interface was the same in native versus CHD-treated clupeine in model PE: PG: Cl (79:17:4 mole %) monolayers representing the inner membrane of *E. coli*. Figure 4-1 B shows a typical surface pressure isotherm for a compressed DPPG monolayer which was used as a control for these experiments. In the gas extended phase (GE) phase, the DPPG isotherm showed a gradual increase in surface pressure from ~ 3.5 to ~ 8 mN m⁻¹ when the area per molecule decreased from 95 to ~ 70 Å² (Figure 4-1 B). The surface pressure continued to rise as the monolayer was compressed and at ~ 50 Å² the pressure reached a maximum of ~ 25 mN m⁻¹ in the final compressible phase, the condensed phase. This result was consistent with previous work performed by Lad et al. (2005) who also reported increased SP when the protein lysozyme was adsorbed onto monolayers made from stearic acid and phosphocholine. Contrary to the DPPG isotherm, the PE:PG:CL isotherm showed no increase in surface pressure in the GE phase where the molecules are far enough apart so that there is little interaction, however, the surface pressure increased from 0 to ~ 5 mN m⁻¹ in the LE phase where the molecules interact more than the GE phase (Figure 4-1 A). The maximum surface pressure of ~ 25 mN m⁻¹ was achieved when the monolayer was compressed to an area per molecule of ~ 30 Å.

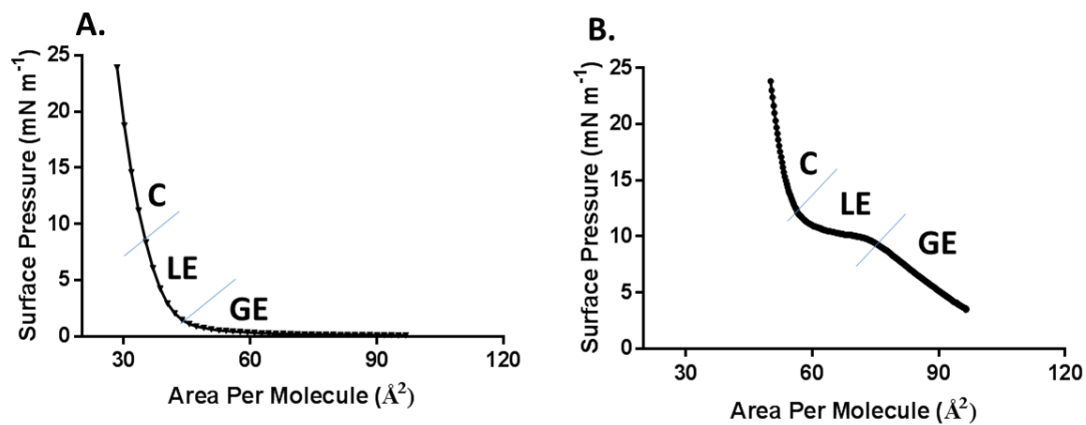


Figure 0-1 (A) Surface pressure versus area per molecule plot of a compressed PE:PG:CL mole% (79:17:4) monolayer. (B) Similar plot for a compressed DPPG monolayer. The three main transition phases shown are the gaseous extended (GE), the liquid extended (LE) and the condensed phases.

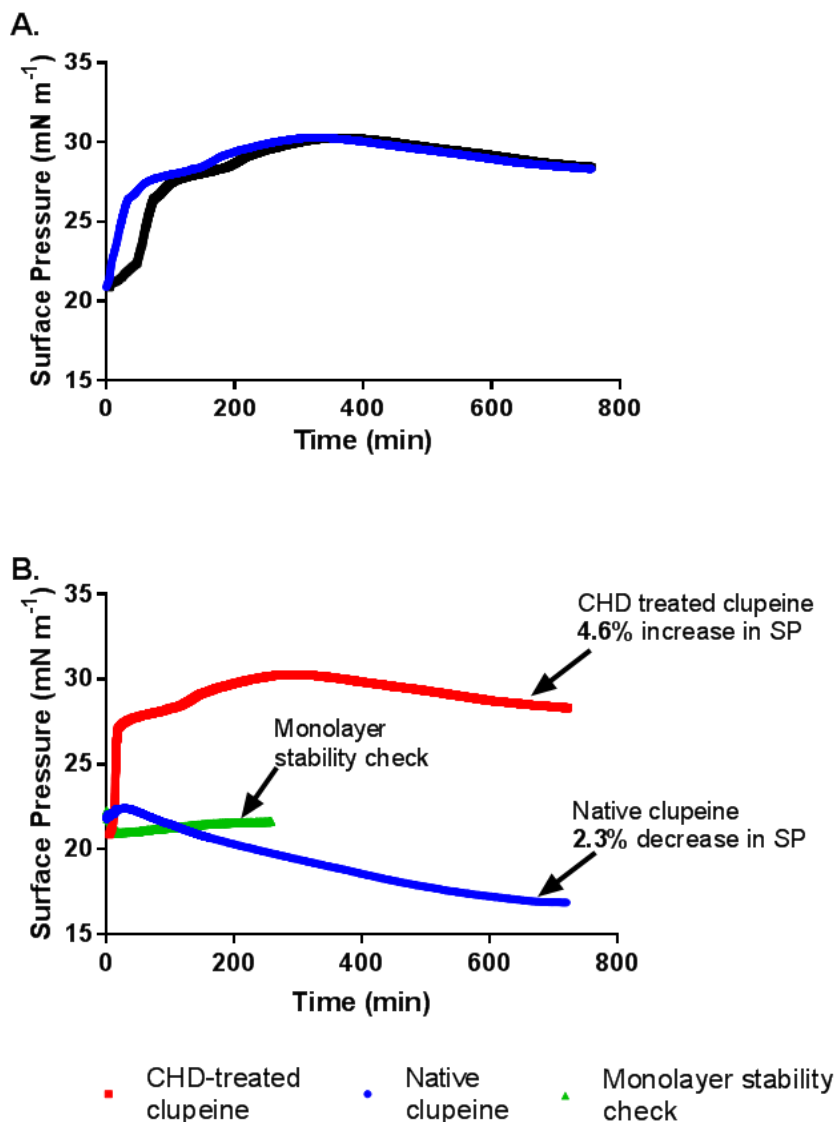


Figure 0-2 (A) Surface pressure versus time plot for charge-reduced clupeine adsorbed on a DPPG monolayer (control). Two replicates are shown; (B) Stability check for the PE:PG:CL monolayer without the peptide and native and CHD-treated clupeine adsorbed at the air/water interphase of a PE:PG:CL monolayer. These experiments were repeated twice.

Unlike the native peptide that showed a 2.3% decrease in surface pressure when the peptide was injected below the lipid monolayer, in the presence of the CHD-treated peptide, there was a 4.6% increase in surface pressure (Figure 4-2 B). A stability curve,

containing the pure monolayer with no added peptide is also shown in Figure 4-2 B. Although the stability curve does not extend for the full length of the experiment, after 200 min the decrease in surface pressure observed in the presence of the native peptide was not observed. The final peptide concentrations used for the monolayer studies were less than the MIC values reported in Chapter 2, however, these concentrations have been used previously to examine the lipid binding interactions of antimicrobial peptides using NR (Clifton et al., 2011).

4.4.2 The Structure of Native and CHD-Treated Clupeine Adsorbed to PE:PG:CL (79:17:4 mole %) Monolayers.

NR and XRR reflectivity data were fitted simultaneously to provide more details about the interaction of native and CHD-treated clupeine with model monolayers of *E. coli* inner membrane. Table 4-1 provides a summary of the calculated scattering lengths and SLDs of the lipid and peptide components used in this thesis.

Isotopic substitution was used to generate multiple contrast in NRW by combining water (92%) and D₂O (8%) (SLDs; $-0.56 \times 10^{-6} \text{ \AA}^{-2}$ and $6.35 \times 10^{-6} \text{ \AA}^{-2}$ respectively). The contrasts used to obtain more detailed information about the structure of the bare monolayer (with no peptide) were the d-PE:PG:CL on an NRW phosphate buffer subphase (NR) and the h-PE:PG:CL on a H₂O phosphate buffer subphase using XRR. The reflectivity profile obtained for the bare d-PE:PG:CL monolayer is shown in Figure 4-3 A and the scattering length density across the interface that this fit describes is shown in Figure 4-3 B.

Table 0-1 Summary of the calculated scattering lengths, scattering length densities, molecular weights, and molecular volumes of the lipids (PE:PG:CL, 79:17:4 mole %) and peptides used in this study.

Parameters	Scattering length Σb (10^{-3}\AA)	SLD (10^{-6}\AA^{-2})	Molecular Weight (g/mol)	Molecular Volume (\AA^3)
h-PE:PG:CL (head + tail)	0.339	0.300	720	1128
h-PE:PG:CL (hd. group)	0.598	2.059	273	288
d-PE:PG:CL tail	6.236	7.488	496	838
h-PE:PG:CL tail	-0.326	-0.394	434	838
Native clupeine in NRW	29.02	2.023	4200	
CHD-treated clupeine in NRW	29.02	2.023	4200	

As in the other reflectivity profiles, the points with the associated error bars represent the experimental data whereas the solid lines represent the reflectivity that was calculated from the best-fit model of the interface. A two layer model was used to fit the data which means the lipid monolayer was divided into two regions, layers one and two (Table 4-2). Layer 1 represents the acyl chain region and has a thickness (τ) of 15 ± 0.64 \AA and a volume fraction (Φ_L) of 0.97 ± 0.01 , whereas layer 2 represents the lipid head group of the condensed PE:PG:CL monolayer and this layer has a (τ) of 12.93 ± 1.21 \AA (Table 4-2). There is no minimum in the reflectivity data (a smooth curve) which suggests the film thickness remains the same (Figure 4-3A). Changes in thickness would result in interfacial fringes due to interference between neutrons reflected from the top and bottom of the interfacial layer (Clifton et al., 2013).

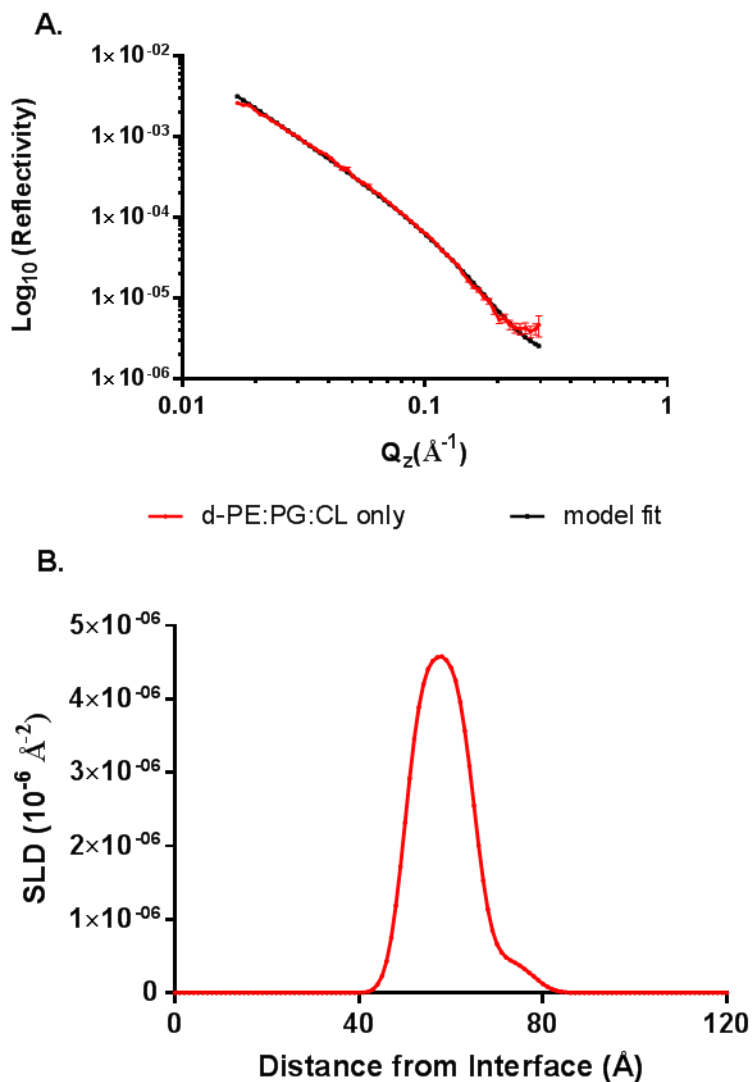


Figure 0-3 (A) Reflectivity of the d-PE:PG:CL monolayer is plotted against Q_z (\AA^{-1}), the momentum transfer. The continuous black line represents the simulated model data whereas the experimental data are shown in red with error bars. (B) The corresponding real space SLD profile as a function of distance from the interface.

Table 0-2 Structural parameters obtained from a two-layer model fit of a condensed phase d-PE:PG:CL monolayer obtained from simultaneously fitting NR and XRR profiles. The structural parameters described for each layer are the layer thickness (τ), the SLD (ρ) and the corresponding layer roughness. The fits were repeated three times.

Parameters	Thickness τ (Å)	SLD (10^{-6}Å^{-2})	Layer roughness (Å)	Lipid volume fraction (Φ_L)
Layer 1, acyl chain				
d-PE:PG:CL, NR	15.0 ± 0.64	7.28 ± 0.76	3.93 ± 1.09	0.97 ± 0.02
h-PE:PG:CL, XRR	15.0 ± 0.64	9.55 ± 0.49		
Layer 2, head group				
d-PE:PG:CL, NR	12.93 ± 1.21	0.46 ± 0.25		
h-PE:PG:CL, XRR	12.93 ± 1.21	13.2 ± 0.07		

τ , represents layer thickness and Φ_L , represents lipid volume.

In order to determine the structural changes after peptide addition it was necessary to fit the data using a three layer model. Moving from air to the solution, layer 1 in the model was described as the lipid acyl chain with or without native or CHD-treated clupeine; layer 2 (the middle layer) was composed of the head group with the peptides and some water; and layer three represented the adsorbed protein layer and some water. The rationale for using this model was based on two reasons: (1) an unusually thick head group (layer 2) and (2) poor fitting of the reflectivity curves. The parameters obtained from the simultaneous fitting of the NR and XRR data sets are shown in Tables 4-3 and 4-4.

As shown in Figure 4-4 A, the three layer model proposed for native clupeine adsorbed to the condensed phase PE:PG:CL monolayer, fitted the data well. In addition, the hydrogenated contrasts in NRW proved to be informative in identifying the contribution of the peptide to the monolayer. For example, the calculated SLD of the h-PE:PG:CL (head and tail) was $0.30 \times 10^{-6}\text{Å}^{-2}$ (Table 4-1), and it was assumed that any

change in reflectivity would be caused by the addition of the peptide. In the presence of the native peptide, the largest SLD value for the h-PE:PG:CL contrast was observed in the head group region, layer 2 ($1.07 \pm 0.06 \times 10^{-6} \text{ \AA}^{-2}$), whereas the lowest SLD value was observed in the acyl chain region, layer 1 ($-0.37 \pm 0.01 \times 10^{-6} \text{ \AA}^{-2}$) (Table 4-3). Similarly, in the presence of the CHD-treated peptide, the lipid head group region showed the largest SLD ($1.69 \pm 0.05 \times 10^{-6} \text{ \AA}^{-2}$), whereas the acyl chain region showed the lowest SLD ($-0.37 \pm 0.01 \times 10^{-6} \text{ \AA}^{-2}$) (Table 4-4). The complementary SLD profile for the monolayer in the presence of native clupeine is shown in Figure 4-4 B, whereas Figure 4-5 B shows the SLD profile in the presence of the CHD-treated peptide.

Additional evidence for peptide adsorption was determined from the calculation of the total peptide surface excess (Γ) or the amount of clupeine at the air/water interface. Surface excess in the presence of native clupeine was 0.67 mg/ m^2 where 55% ($0.364 \pm 0.02 \text{ mg/m}^2$) was found in the peptide layer. In contrast, in the presence of CHD-treated clupeine, 61% ($0.59 \pm 0.14 \text{ mg/m}^2$) of the total peptide surface excess (0.969 mg/m^2), was found in the peptide layer (Table 4-4). The increases in layer thickness also supports the surface excess data. In particular, more peptide was incorporated in the peptide layer, in the presence of the CHD-treated peptide (thickness (τ), $17.56 \pm 0.05 \text{ \AA}$) as compared to the native peptide (thickness (τ), $15.27 \pm 0.07 \text{ \AA}$), Table 4-3 and Table 4-4 respectively.

In addition to the increases in the head group region and the peptide layer thickness, a general decrease in lipid volume fraction (Φ_L) was also observed when the peptide samples were added to the monolayer (Tables 4-2 to 4-4).

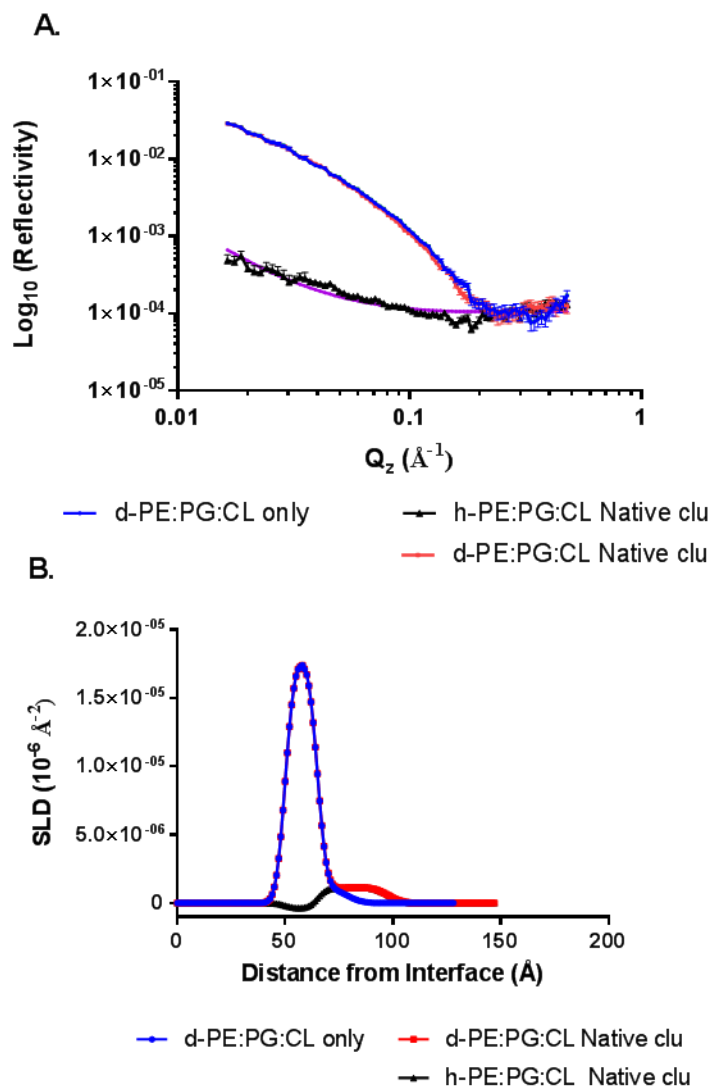


Figure 0-4 (A) Reflectivity of PE:PG:CL lipid monolayer in NRW with adsorbed native clupeine on the deuterated lipid in (red) and the hydrogenated lipid in (black) is plotted against Q_z (\AA^{-1}), the momentum transfer. The bare lipid with no peptide is shown in blue and the experimental data are represented with error bars whereas the best fit simulated data are represented as continuous lines. The SLD profile as a function of distance from the interface as determined from the fit is shown in (B).

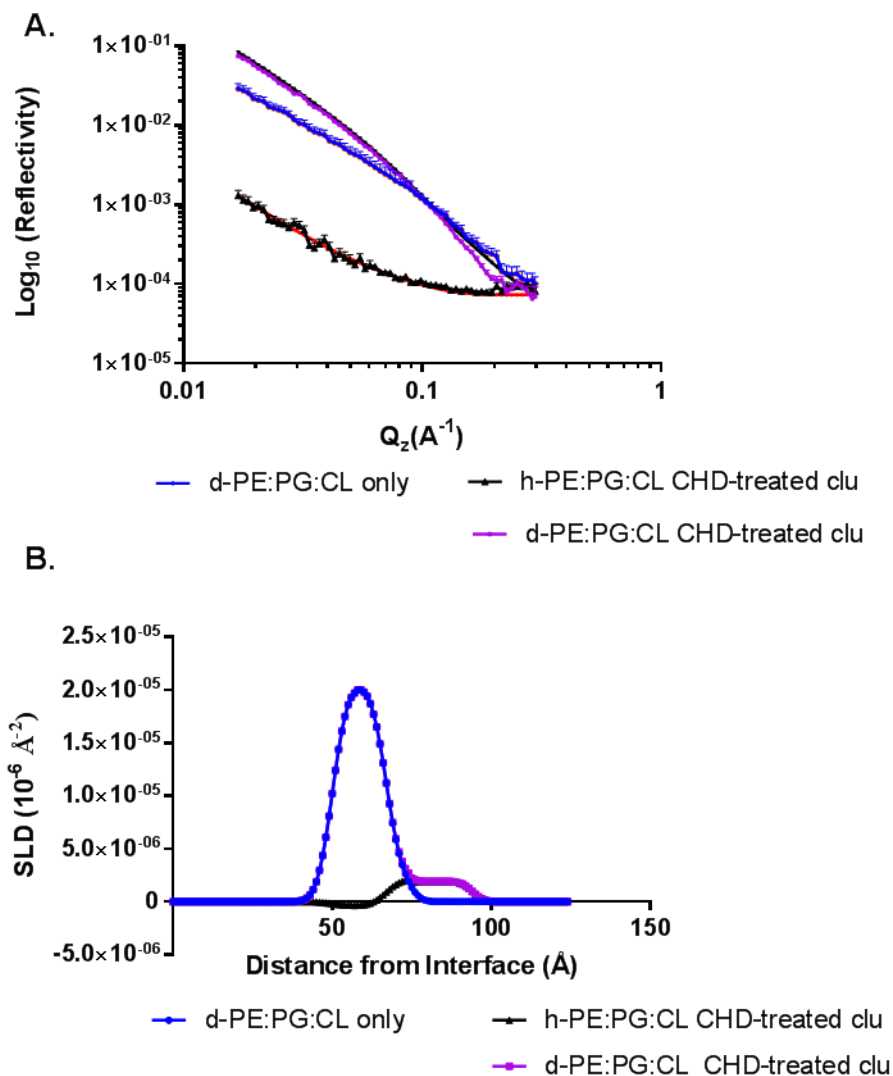


Figure 0-5 (A) Reflectivity of PE:PG:CL monolayer in NRW with adsorbed CHD-treated clupeine on the deuterated lipid in (purple) and the hydrogenated lipid in (black). The bare lipid with no peptide is shown in blue and the experimental data are represented with error bars whereas the best fit simulated data are represented as lines. The SLD profile as a function of distance from the interface as determined from the fit is shown in (B).

For example, in the presence of native clupeine, there was a 38% decrease in lipid volume fraction (Φ_L) from 0.97 to 0.59 ($P < 0.001$), and a 28% decrease from 0.97 to 0.69 ($P < 0.05$) in the presence of the CHD-treated peptide. These observations suggest

that the peptides are able to remove lipid content from the surface during their interaction with the monolayer.

Table 0-3 Structural parameters obtained from the three layer model fits of 0.48 μM native clupeine adsorbed to PE:PG:CL monolayers. The fits were repeated three times.

Parameters	Thickness τ (\AA)	SLD (10^{-6}\AA^{-2})	Layer roughness (\AA)	Γ Surface excess (mg/m^2)	(Φ_L) Lipid volume fraction
Layer 1, acyl chain					
d-PE:PG:CL, NRW	15.0 \pm 0.01	4.27 \pm 0.01	3.51 \pm 0.15	0.005 \pm 0.02	0.59 \pm 0.02
h-PE:PG:CL, NRW	15.0 \pm 0.01	-0.37 \pm 0.01			
h-PE:PG:CL, XRR	15.0 \pm 0.01	9.69 \pm 0.03			
Layer 2, head group					
d-PE:PG:CL, NRW	12.72 \pm 0.01	1.07 \pm 0.06		0.297 \pm 0.02	
h-PE:PG:CL, NRW	12.72 \pm 0.01	1.07 \pm 0.06			
h-PE:PG:CL, XRR	12.72 \pm 0.01	12.87 \pm 0.40			
Layer 3, peptide layer					
d-PE:PG:CL, NRW	15.27 \pm 0.07	1.00 \pm 0.09	3.88 \pm 0.32	0.364 \pm 0.02	
h-PE:PG:CL, NRW	15.27 \pm 0.07	1.00 \pm 0.01			
h-PE:PG:CL, XRR	15.27 \pm 0.07	10.9 \pm 0.01			

τ , represents layer thickness; Γ , represents, surface excess; and Φ_L represents lipid volume fraction.

Figures 4-6 and 4-7 show the XRR reflectivity profiles and corresponding electron density profiles for native and CHD-treated clupeine on the monolayer, respectively. The XRR data were fitted simultaneously with the NR data, and similar to the NR data a three layer model was used. In addition, each layer in the model was characterized by a thickness and electron density profile.

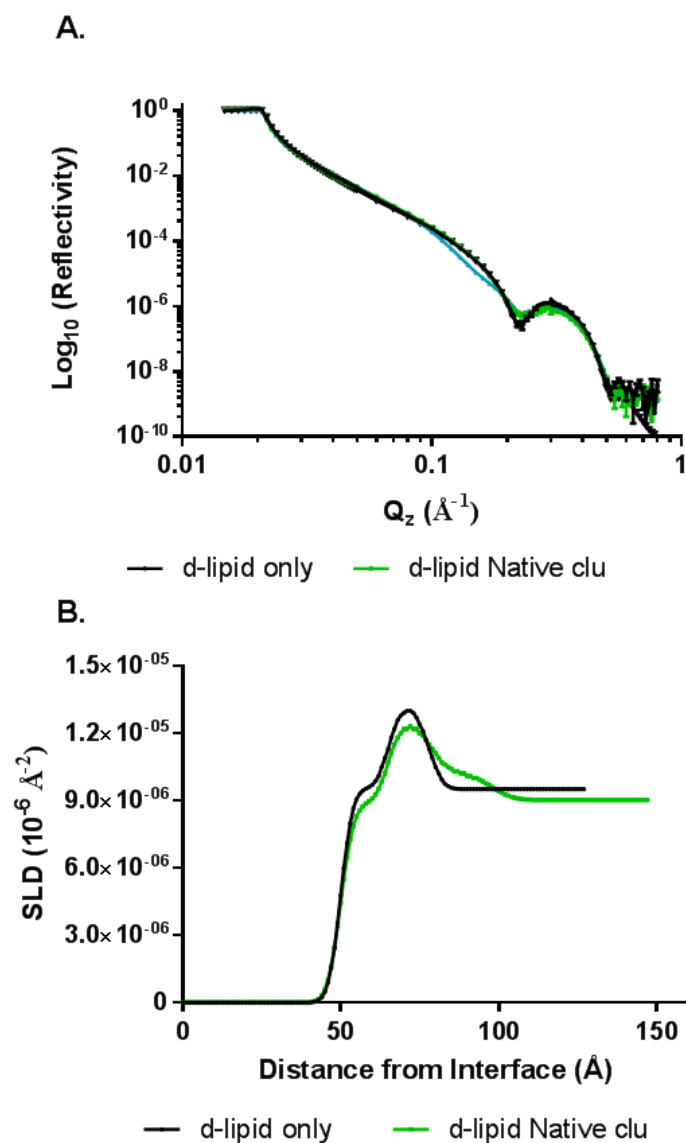


Figure 0-6 (A) XRR profile of PE:PG:CL monolayer (black) with adsorbed native clupeine on the deuterated lipid in (green). The data are represented with error bars whereas the best fits are represented as lines. The SLD profile as a function of distance from the interface as determined from the fit is shown in (B).

Table 0-4 Parameters obtained from the best three layer model fits of 0.48 μM CHD-treated clupeine adsorbed to PE:PG:CL monolayers. The fits were repeated three times.

Parameters	τ (\AA)	SLD (10^{-6}\AA^{-2})	Layer roughness (\AA)	Γ peptide (mg/m^2)	(Φ_L) Lipid volume fraction
Layer 1, acyl chain					
d-PE:PG:CL, NRW	16.49 \pm 0.14	5.08 \pm 0.05	3.83 \pm 0.06	0.007 \pm 0.03	0.69 \pm 0.03
h-PE:PG:CL, NRW	16.49 \pm 0.14	-0.37 \pm 0.01			
h-PE:PG:CL, XRR	16.49 \pm 0.14	8.64 \pm 0.01			
Layer 2, head group					
d-PE:PG:CL, NRW	8.27 \pm 0.06	1.69 \pm 0.05		0.372 \pm 0.03	
h-PE:PG:CL, NRW	8.27 \pm 0.06	1.69 \pm 0.05			
h-PE:PG:CL, XRR	8.27 \pm 0.06	12.46 \pm 0.06			
Layer 3, peptide layer					
d-PE:PG:CL, NRW	17.56 \pm 0.05	1.42 \pm 0.44	3.50 \pm 0.44	0.59 \pm 0.14	
h-PE:PG:CL, NRW	17.56 \pm 0.05	1.22 \pm 0.25			
h-PE:PG:CL, XRR	17.56 \pm 0.05	9.25 \pm 0.05			

τ , represents layer thickness; Γ , represents, surface excess; and Φ_L represents lipid volume fraction.

In the presence of the peptides, the changes in the acyl region were variable. For example, in the presence of the native peptide, there was an increase in the SLD of the acyl region from $9.55 \pm 0.01 \times 10^{-6} \text{\AA}^{-2}$ (Table 4-2) to $9.69 \pm 0.01 \times 10^{-6} \text{\AA}^{-2}$ (Table 4-3), whereas in the presence of the CHD-treated peptide, the SLD of the acyl region decreased from $9.55 \pm 0.01 \times 10^{-6} \text{\AA}^{-2}$ to $8.64 \pm 0.01 \times 10^{-6} \text{\AA}^{-2}$ (Table 4-3). On the other hand, for the head group region, a general decrease in SLD was observed when either peptide was added to the monolayer.

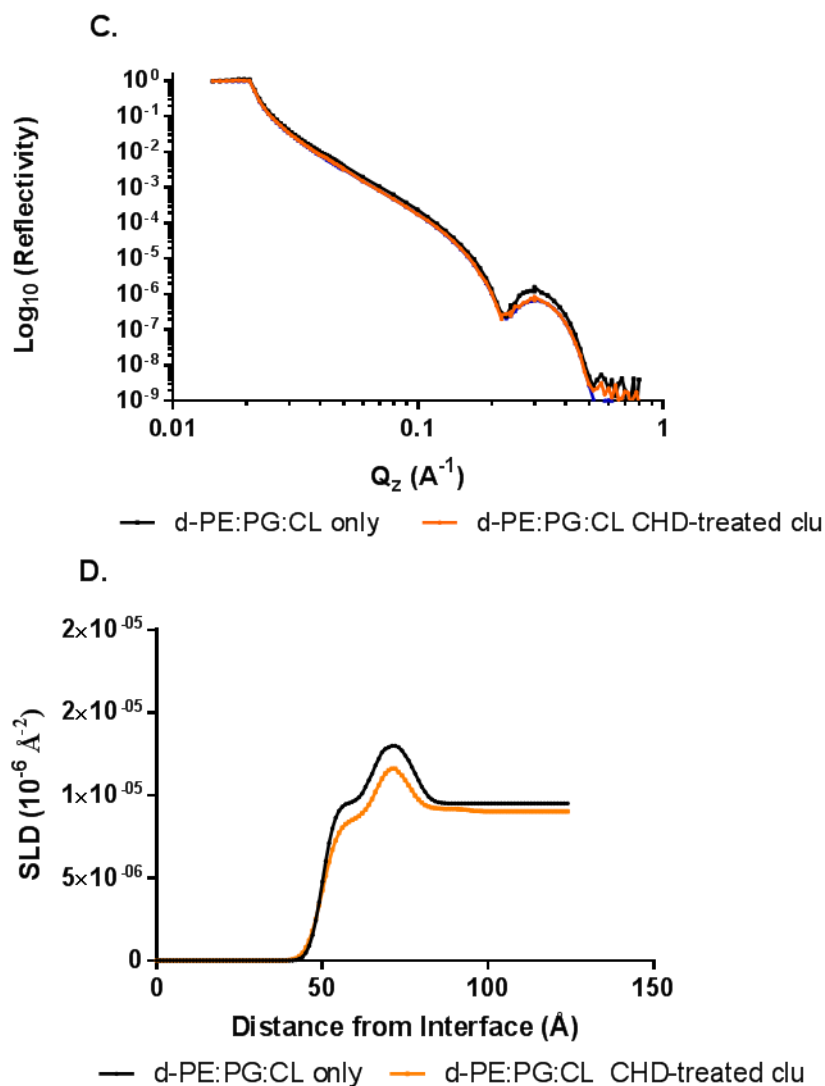


Figure 0-7 (A) XRR profile of PE:PG:CL monolayer (black) with adsorbed native clupeine on the deuterated lipid (orange). The data are represented with error bars whereas the best fits are represented as lines. The SLD profile as a function of distance from the interface as determined from the fit is shown in (B).

4.5 Discussion

In the present study, a small reduction in charge of native clupeine (10% arginine modification) to form CHD-treated clupeine was hypothesized to result in different interactions with *E. coli* PE:PG:CL model membranes. Both isotherms in Figure 4-1

showed steep slopes in the condensed phase, however, this observation was more distinct in the PE:PG:CL isotherm (Figure 4-1 A) which indicates that lipid composition affected the re-ordering of the molecules and increased the complexity of the interaction of the lipid components when the monolayer was compressed. In addition, different lipid head group composition has also been reported to affect the area per molecule values at which different phase transitions occur in lipid monolayers (Ciunac et al., 2017).

The surface pressure data showed an increase in the presence of CHD-treated clupeine and a decrease in the presence of the native peptide, however for both peptides the peptide surface excess (Γ) calculated from the NR data showed evidence of peptide interaction with the monolayer, albeit more in the presence of the CHD-treated peptide (Table 4-3). In these experiments, adsorption of peptides to the monolayer would be expected to decrease the surface tension and the latter is measured as an increase in surface pressure using a Wilhelmy plate. If this proposition is true, then the discrepancy in the decrease in surface pressure and the surface excess calculated from the NR data for native clupeine may be explained by the loss of lipid from the monolayer in the presence of the peptide. For example, there was a 38% decrease in lipid volume fraction (0.97 to 0.59; $P < 0.001$), in the presence of the native peptide as compared to a 28% decrease in lipid volume fraction (0.97 to 0.69; $P < 0.001$) in the presence of the CHD-treated peptide.

The interaction of native clupeine with lipopolysaccharide (LPS) monolayers was studied by Abuillan et al. (2013), using grazing incidence x-ray fluorescence (GIXF). The authors reported that in calcium-free buffer, surface pressure increased from 24 mN m^{-1} to 50 mN m^{-1} along with a corresponding increase in the carbohydrate head group

thickness (from $26.4 \pm 0.7 \text{ \AA}$ to $31.1 \pm 5.1 \text{ \AA}$). In a similar study, Oliveira et al. (2009) also studied the interaction of native clupeine on LPS monolayers. Here surface pressure values remained zero in the presence of Hepes buffer (containing Ca^{2+}) to which 1 mg/mL native clupeine was added. However, on calcium free buffer, there was a rapid increase in surface pressure, which was attributed to native clupeine moving towards the air/water interface rather than adsorbing to saccharide head group surfaces. In addition, the GIXF data showed no change in the electron density profile of LPS Ra (LPS that lacks the O-antigen) monolayers after the addition of native clupeine. The increase in surface pressure in the presence of native clupeine reported by Abuillan et al. (2013) was not observed in the present study, but supports the data obtained in the presence of the CHD-treated clupeine. However, the surface pressure data from the present study should be interpreted cautiously since not many experimental runs were performed and stability checks were not performed for the entire run of the experiment. Thus it cannot be ruled out that the monolayer might not have been perfectly stable for the duration of the experiment.

In addition to the clupeine studies described above, Pink et al. (2014) used a combination of planar bilayer studies and Monte Carlo (MC) simulations (using 65:35 and 75:25 PE:PG molar ratio bilayers) to study the interaction of native clupeine with model Gram-negative inner membranes. The planar bilayer studies showed that different native clupeine concentrations were not able to induce a change in current flow through the bilayer, and both the inner and outer membranes remained intact. MC simulation data also confirmed the planar lipid results and predicted that native clupeine does not

approach the surface, and theoretically, the closest distance between the bilayer membrane and native clupeine's center of mass would be 7 nm.

The apparent contradiction between the findings of Pink et al. (2014) and the surface excess data reported in the present study may be a consequence of differences in the lipid composition (Tables 4-3, 4-4). The lipid mix used in this study, (PE:PG:CL) consisted of the zwitterionic lipid (DPPE) and the two anionic lipids (DPPG and CL) whereas for the planar studies, Pink et al. (2014), used DPhPC (diphytanoyl phosphatidylcholine) and (PE:PG:DPG). DPhPC, is one of the common lipids used in electrophysiological studies because it is thought to form stable bilayers (Hsieh et al., 1997). However, the polymorphic nature of DPhPC and the sensitivity of its head group orientation to hydration are factors that may affect bilayer stability and peptide lipid interactions (Hsieh et al., 1997). In addition, the contrasting results observed between the planar lipid studies from the Pink et al. (2014) study and the surface excess data calculated from the present study may also be a consequence of differences in the physical properties probed by the two techniques which also demonstrates the advantage of using complementary techniques, (in this case NR and XRR) to study peptide-membrane interactions. An inherent limitation of using monolayer models in the present study to examine peptide-lipid interactions is that the monolayer represents half a bilayer and does not fully replicate the complexity of the interactions of peptides with Gram-negative bacterial membranes.

In the present study, both NR and XRR data sets were fitted simultaneously in a single model using multiple contrasts and the SLD, thickness of head group and acyl regions along with the background values were allowed to vary (Nelson, 2006). Using

multiple contrasts and constraining the fits with the XRR data is a strategy that is often applied to resolve some of the ambiguity in fitting NR data and to obtain a more accurate model structure (Nelson, 2006; Clifton et al., 2012). Other important points to note during the fitting of the data include; first, assuming that layer 1 contained only the lipid component whereas layer 2 contained the lipid head group and some water. This model is a common convention that is used in NR studies (Clifton et al., 2011; Ciumac et al., 2017) and it provided an acceptable fit of the data in the absence of the either peptide. In addition, when fitting the bare d-PE:PG:CL and h-PE:PG:CL monolayers, the roughness parameters were linked for all the layers on the XRR and NR contrasts, this was done to reduce the number of parameters in the model. On the other hand, in the presence of the peptides, a separate roughness parameter was assigned to the peptide layer. It should be noted that for d-PE:PG:CL and h-PE:PG:CL monolayers in the presence and absence of peptides, the SLD and thickness parameters were fitted individually.

In fitting NR data it is also advantageous to obtain an adequate description of the data with a minimum number of parameters (Nelson, 2006). However, in the presence of native or CHD-treated clupeine it was necessary to include a third peptide layer because using the two layer model resulted in an unusually thick head group and poor fitting of the reflectivity curves. The inability of a two layer model to provide satisfactory fits to either DPPC or DPPG monolayers in the presence of a short cationic peptide, G-(IIKK)4I-NH₂ has been reported by Ciumac et al.(2017). In this particular case, more physically realistic fits were obtained when a three layer model was applied. Similarly in the present study, a three layer model was used to characterize the peptide-lipid interactions and the lipid head group region and the peptide layer was also assumed to

contain some water. Ciumac et al. (2017) estimated the number of water molecules associated with DPPC and DPPG head groups by comparing the fitted SLD values and the thickness from the D₂O contrasts, however, in the present study this was not done for the monolayer experiments as the data were fitted without using the hydration parameter. Although this may seem to weaken the assumptions of the model, in the bilayer systems studied in Chapter 5 the amount of water associated with the lipid head groups was considered.

In order to improve confidence in the data interpretation it is also important to justify the limits of the parameters used. For example, the SLD values were set to be within the theoretical calculated ranges (Table 4-1). In addition, initial parameters were set from similar experiments in the literature (Clifton et al., 2011; Clifton et al., 2012). It is useful to comment that for the theoretical calculation of the CHD-treated SLD in the different contrasts, there was some uncertainty about the exact number of protons exchanged, and thus it was assumed that not all the exchangeable protons were replaced for each isotopic contrast. Therefore, the theoretical SLD of the CHD-treated peptides was calculated neglecting the effect of hydrogen/deuterium exchange on the peptide and was assumed to be the same as that of the native peptide (Table 4-1). The obvious limitation with this assumption is accepting that the theoretical or ‘dry’ SLD value of the CHD-treated peptide would not change in different contrast solutions (H₂O, NRW and D₂O). Thus any differences in the ‘dry’ SLD which might have occurred with modifying the native clupeine to form CHD-treated clupeine would not have been accounted for in the calculations. Despite this limitation, the model to data fits seem reasonable and there were no significant divergence in the fits with the current models used.

As shown in Table 4-3, peptide binding in the presence of native clupeine showed minimal adsorption in the lipid layer (surface excess (Γ), 0.005 ± 0.02), but more interaction with the lipid head group region (Γ , 0.297 ± 0.02) and a thickening of the peptide layer (τ , increased from $15.0 \pm 0.01 \text{ \AA}$ to $15.27 \pm 0.07 \text{ \AA}$). On the other hand, the amount of peptide interaction with the lipid head group region was greater (surface excess (Γ), 0.372 ± 0.03) in the presence of the CHD-treated peptide, and the peptide layer was also thicker ($17.56 \pm 0.05 \text{ \AA}$; $P < 0.05$), Table 4-4. The use of contrast matching (or isotopic substitution) to change the reflectivity of the solvents in the system was also advantageous in helping to identify changes in the SLD. There was an overall decrease in SLD in the presence of both peptides, and a greater decrease was observed in the presence of the native peptide ($\sim 3\%$) compared to a 2% decrease in the presence of the CHD-treated peptide.

The lower SLD in the presence of the native peptide as compared to the CHD-treated peptide may be attributed to greater hydration of the more positively charged native peptide, since water has a SLD of water is $-0.56 \times 10^{-6} \text{ \AA}^{-2}$ it would reduce the SLD of hydrated molecules. This proposition is based on observing the reflectivity curve in Figure 4-5 A; where it can be seen that the density of the lipid layer is decreased with CHD-treated clupeine (some parts of the d-PE:PG:CL peptide curve are lower than the pure lipid curve). However, this difference in the reflectivity profiles is not clearly seen in the presence of native clupeine (Figure 4.4 A). Furthermore, Lad et al. (2007) also reported that reflectivity profiles of the peptide melittin (2.8 kDa) adsorbed to d-DPPG monolayers were lower (less dense) than pure d-DPPG profiles. In addition, melittin was also found below the lipid layer rather than inserted in the lipid layer (Lad et al., 2007),

and in this regard the interactions of native and CHD- treated clupeine with the d-PE:PG:CL monolayer are similar to that of melittin. The difference in the fitted SLDs and the total adsorbed protein is almost two fold in the presence of the CHD-treated peptide which suggests the density of the material in the layer was different compared to the native peptide.

Certain characteristics of lipids and of CAPs have been shown to affect peptide adsorption to a lipid monolayer. For CAPs, the amphipathic structure, the molecular size, the net charge and conformational changes affect overall surface activity whereas for lipids, the length of the acyl chain, hydration and the nature of the head group are more important determinants of peptide-lipid interaction (Maget-Dana, 1999). However, unlike many other CAPs, clupeine is not amphipathic and lacks secondary structure due to the even distribution of positive charges along the peptide backbone (Bonora et al., 1979; Pink et al., 2013).

In examining the surface pressure and reflectivity data for the native and CHD-treated clupeine, there can be little doubt that both peptides interact to some degree with the model membranes, however, the CHD-treated peptide showed greater affinity for the lipid head group and more of the peptide was adsorbed in the peptide layer. The interfacial activity model proposed by Wimley (2011) although informative does not fully explain the peptide-lipid interactions of native and CHD-treated clupeine. Wimley (2011) defines interfacial activity as the ability of CAPs to enter the lipid bilayer and bring about changes in the vertical arrangement of lipids. This activity is also dependent on a physical-chemical balance between the peptides, membranes lipids and water (Rathinakumar and Wimley, 2008).

Interfacially active peptides are unlike other CAPs because they are not truly amphipathic but rather have hydrophobic segments interrupted by polar groups. Furthermore, Rathinakumar et al. (2009) explained that CAPs with a high abundance of arginine tend to function by the interfacial activity mechanism. However, clupeine has no hydrophobic domains (Pink et al., 2014), instead the native peptide has 20 arginine residues (of 30 residues), which means clupeine is protonated and positively charged in most biological environments. Based on the NR and XRR data presented the CHD-treated peptide more so than native clupeine was able to interact with lipid head groups in the lipid monolayer using hydrogen bonding between guanidinium groups, and affect lipid density. In the next chapter, the interactions of the native and CHD-treated peptides in bilayer systems which more closely represent the symmetry of the Gram-negative inner membrane will be examined.

CHAPTER 5: INTERACTIONS OF NATIVE AND CHD-TREATED CLUPEINE WITH GRAM-NEGATIVE MODEL BILAYERS

5.1 Abstract

Neutron reflectometry studies were used to better understand the nature of the interaction of native clupeine and CHD-treated clupeine (clupeine with 10% arginine modification (charge reduction) with 1,2-cylohexanedione) in deuterated-DPPC, 1,2-dipalmitoyl (d62)-sn-glycero-3-phosphocholine: DPPE, 1,2-dipalmitoyl--glycero-3-phosphoethanolamine: DPPG, 1,2-dipalmitoyl-sn-glycero-3-[phosphor-rac-1-glycerol]: CL, 1,1'2,2'-tetramyristoyl cardiolipin (DPPC:PE:PG:CL) and hydrogenated-DPPC:PE:PG:CL bilayer membrane systems. Models of the Gram-negative bilayers were supported on silicon blocks and were prepared using a combination of the Langmuir-Blodgett (LB) and Langmuir-Schaefer (LS) technique. Although asymmetric bilayers were formed, some lipid mixing was observed in the inner tail region ($\sim 69 \pm 0.24\%$ DPPC and $\sim 24 \pm 0.02\%$ PE:PG:CL) and in the outer tail region ($\sim 24 \pm 0.02\%$ DPPC and $\sim 56 \pm 0.01\%$ PE:PG:CL). The net effect of this interchange of lipids weakened the peptide-lipid interaction due to reduced negative charge in the outer lipid layer. The addition of CHD- treated clupeine resulted in a thicker peptide layer $11.04 \pm 5.99 \text{ \AA}$ compared to $4.15 \pm 2.93 \text{ \AA}$ in the presence of the native peptide. The use of the bilayer system enabled an improvement of the membrane models, however, there was no evidence that either peptide was able to translocate the biomembrane. This study has contributed to a better understanding of the interaction of native and CHD-treated clupeine in model biomembranes.

5.2 Introduction

Bacteria are of interest because of their beneficial and harmful effects. Some of their harmful effects include the emergence of antibiotic resistance, a problem which requires identifying new antimicrobial agents that have different modes of action from conventional antibiotics. CAPs (small, cationic peptides) have been studied as alternatives to conventional antibiotics because of their low toxicity and broad spectrum antimicrobial activity (Sevcsik et al. 2008).

Gram-negative bilayers form the basic structural framework for bacterial membranes and have been used extensively to study peptide-lipid interactions (Hughes et al., 2008). The Gram-negative cell envelope is a complex structure which consists of a distinct outer bilayer membrane which is composed of phospholipids on its inner leaflet and LPS on its outer leaflet (Figure 1-11). LPS is made up of three structural regions: (1) a hydrophobic region, lipid A; (2) a hydrophilic O-antigen disaccharide region; and (3) a core polysaccharide region that connects the two (Lohner and Blondelle, 2005; Clifton et al., 2015). Moving inwards past the outer membrane, a narrow space called the periplasm separates the outer and inner membranes and within the periplasm is found a thin peptidoglycan layer which helps to maintain the shape of the cell. Beyond the peptidoglycan layer is the inner membrane or cytoplasmic membrane, a simple phospholipid bilayer, which borders the cytoplasm, the site of all proteins synthesis regardless of their final cellular location (Lohner and Blondelle, 2005).

Some of the main mechanisms of action of CAPs against Gram-negative bacteria are based on interactions with the bilayer membrane. For example, in pore formation models CAPs interact with and bend the lipid bilayer forming a pore; in contrast, the

peptide completely coats the membrane and causes loss of membrane integrity in carpet models (Zhang et al., 2001). Other well-known effects of CAPs on bacterial membranes include membrane thinning and translocating across the bilayer without disruption (Lohner and Blondelle, 2005). The work presented in this thesis has focused on the antimicrobial interactions used by native and CHD-treated clupeine against the Gram-negative bacteria *E. coli* K-12 and *S. enterica* Typhimurium 14028. In chapter four, NR and XRR techniques were used to examine the interaction of each peptide in monolayers that represented the inner membrane of *E. coli*, PE:PG:CL (75:17:4 mole %); this molar ratio is also representative of the inner membrane of *S. Typhimurium* 14028 cells.

In this chapter, the interactions of the native and CHD-treated peptides were examined in a bilayer system that more closely represents the symmetry of the Gram-negative inner membrane. For this work a solid supported bilayer deposition approach was used which is described in the methods section below. The main objects of these experiments were: (1) to determine the structural changes in scattering length density (SLD), roughness and thickness of the lipid head group and acyl regions on addition of native and CHD-treated clupeine in model bilayer systems; and (2) to identify similarities and differences in native and CHD-treated clupeine interactions in the bilayer systems.

5.3 Materials and Methods

5.3.1 Materials

DPPE, 1,2-dipalmitoyl--glycero-3-phosphoethanolamine, MW 691.97 g/mol (zwitterionic and synthetic purity > 99%); DPPG, 1,2-dipalmitoyl-sn-glycero-3-[phosphor-rac-1-glycerol] (anionic sodium salt), MW 744.96 g/mol; and 1,1',2,2'-tetramyristoyl cardiolipin (anionic sodium salt), MW 1,285.62 g/mol, DPPC and tail

deuterated DPPC (d-PPC, 1,2-dipalmitoyl (d62)-sn-glycero-3-phosphocholine) were all purchased from Avanti Polar Lipids (Alabaster, AL, USA). Stock solutions of all the lipids were prepared using a 3:1 mixture of HPLC grade chloroform to methanol (Sigma-Aldrich, Oakville, ON, Canada) for the mixed lipid, a ratio of PE: PG: CL (79:17:4 mole %) was used and all the lipid samples were aliquoted and stored at -20°C. All the lipid samples were brought to room temperature before use.

Native clupeine (MW 4112 Da) was obtained from Sigma (clupeine sulfate, P4505, Sigma, Oakville, ON, Canada) and was used without further purification. The CHD-treated clupeine was prepared as outlined in Chapter 2 of this thesis. The peptide solutions were made using a 0.02 M Hepes buffer solution (pH 7) and were diluted to a final concentration of 0.48 μM .

5.3.2 Bilayer Deposition and Neutron Reflectometry Measurements

Gram-negative model, single bilayer membranes were prepared at the ISIS Biological Sample Laboratory (Rutherford, England) and the method used was similar to the one outlined by Clifton et al. (2013b). Neutron reflectivity (NR) measurements were carried out using the white beam SURF reflectometer, using neutron wavelengths from 0.5 to 6.5 Å and the collimated neutron beam was reflected from the silicon-liquid interface at different glancing angles of incidence 0.35Å, 0.65Å and 1.5Å.

An LB trough (KSV-Nima, Biolin Scientific, Finland) was cleaned three times with ultrapure water (Millipore, 18.2 M Ω cm⁻¹) and then a neutron flow-cell was placed at the bottom of the trough. Ultrapure water was pumped through the cell-base tubing using a syringe to ensure there were no air bubbles in the tubes and then the trough was

filled with 20 mM phosphates buffer (pH 7.0) A Piranha-cleaned ($\text{H}_2\text{O}_2/\text{H}_2\text{SO}_4/\text{H}_2\text{O}$ 1:4:1) silicon (SiO_2) crystal was then mounted onto the dipping mechanism (of the trough) in a vertical position and with the active face away from the center, and then the block was submerged under the buffer. The piranha cleaning treatment usually results in a natural oxide layer of 7-20 Å thickness and 3-5 Å roughness (Wacklin and Thomas, 2007).

Two bilayers were prepared and approximately 150 μL of tail-hydrogenated or deuterated 1,2-dipalmitoylphosphatidylcholine (h-DPPC and d-DPPC, Avanti polar lipids, Alabaster, AL, USA), 1 mg/mL in chloroform, was spread onto the clean water surface. After the solvent had evaporated the lipid was compressed to an initial pressure of 10 mN m^{-1} and then equilibrated for 15 min. After equilibrating, the lipid layer was compressed to 35 mN m^{-1} at a rate of 3 mm/min. Pressure-area isotherms were also recorded to confirm the homogeneity of the film (Appendix D, Figure D-3 and D-4). For LB deposition of the inner bilayer leaflet, the submerged silicon crystal was lifted through the air-water interface at a rate of 3 mm/min and at a constant pressure of 35 mN m^{-1} . The entire LB deposition procedure took 45 min (Figure D-1).

For LS transfer (Figure D-2), the trough was cleaned and a clean neutron flow-cell was placed in the bottom of the trough before it was filled with cold 20 mM Hepes buffer (pH 7.2). Approximately 150 μL of the lipid mix, PE:PG:CL (79:17:4 mole %) was used to form a monolayer on the water surface and after the solvent had evaporated, the monolayer was compressed to 35 mN m^{-1} . The silicon crystal containing the LB-deposited DPPC monolayer was placed on the dipping mechanism of the trough, in a position with the crystal face parallel to the water surface. The silicon crystal with the

deposited LB film was then dipped through the interface at a constant rate of 3 mm/min and lowered into the neutron flow-cell at the bottom of the trough (Figure D-5). Native and CHD-treated clupeine (0.48 μM) were added to the cell in a 20 mM Hepes buffer (pH 7). This buffer was used as it was the minimal composition required to keep the SLD (h/d) constant.

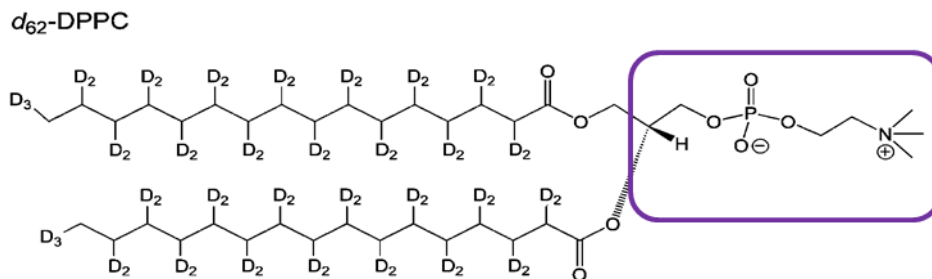


Figure 0-1 The structure of deuterated DPPC showing the alkyl chain region and the lipid head group containing the acyl carbonyls and the phosphate group.

5.3.3 Reflectivity Data Analysis

Neutron and x-ray reflectivity data were analyzed using a Matlab version of RasCal as described in section 4.3.5, and the SLDs of the lipids (head groups and tails), solvents and peptides were calculated using equation 4-1.

5.3.4 Bilayer NR Data Analysis:

Model biomembranes systems composed of either tail deuterated or tail hydrogenated DPPC as the inner leaflet and hydrogenated-PE:PG:CL (79:17:4 mole %) as the outer leaflet were prepared, then NR experiments were carried out using three

different solution subphases; (1) D₂O (100%, $\rho=6.35 \times 10^{-6} \text{ \AA}^{-2}$); (2) silicon matched water (SMW, 38% D₂O and 62% H₂O, $\rho=2.07 \times 10^{-6} \text{ \AA}^{-2}$); and (3) 100% water ($\rho=-0.56 \times 10^{-6} \text{ \AA}^{-2}$). Each deuterated and hydrogenated lipid bilayer was measured under all three isotopic contrasts (D₂O; SMW and H₂O) thus resulting in a total of six different reflectivity profiles. The large difference between the SLD for deuterated-DPPC ($7.45 \times 10^{-6} \text{ \AA}^{-2}$) and hydrogenated- DPPC ($-0.39 \times 10^{-6} \text{ \AA}^{-2}$) tail regions made it possible to determine structural parameters from the tail region within each individual bilayer.

Reflectivity data were obtained for the six contrasts before and after the addition of native and CHD-treated clupeine and the data were analyzed as described in Clifton et al. (2013) using a Matlab version of RasCal (version 1.1.2, Hughes, A., ISIS Spallation Neutron Source, Rutherford, Appleton Laboratory). The three membrane components in the bilayer were DPPC, PE:PG:CL and water and their individual contributions to the bilayer were determined from the fitted values obtained for the tail deuterated-DPPC SLDs in the three subphase mixtures (100% D₂O, SMW (30% D₂O and 100% water).

The SLD (ρ) of a given layer was related to the three membrane components by the following equation:

Equation 0-1

$$\rho = (\rho_{DPPC})(\phi_{DPPC}) + (\rho_{PE:PG:CL})(\phi_{PE:PG:CL}) + (\rho_{Water})(\phi_{Water})$$

Where ρ is the SLD of a given layer and ρ_{DPPC} , ρ_{PEPGCL} and ρ_{Water} represent the SLD of DPPC, PE:PG:CL and water respectively, while ϕ_{DPPC} , ϕ_{PEPGCL} and ϕ_{Water} represent the volume fractions of the same components. Because the DPPC and PE:PG:CL lipid tail regions do not contain labile hydrogens and would not undergo

solvent-contrast-related changes in SLD (Clifton et al., 2013b), the volume fraction of water was determined from the following equation:

Equation 0-2

$$\phi_{Water} = \frac{\rho_{water\ contrast1} - \rho_{water\ contrast2}}{\rho_{water1} - \rho_{water2}}$$

Where $\rho_{water\ contrast1}$ and $\rho_{water\ contrast2}$ represent the SLDs of the same layer in any two of the three contrasts (H₂O, SMW or D₂O) used, while $\rho_{water1} - \rho_{water2}$ represent the

SLDs of each solvent mixture. Once the volume fraction of water (ϕ_{Water}) was determined, then the DPPC fraction in the d-DPPC/h-PEPGCL bilayer system was determined using equation 5-2.

Equation 0-3

$$\rho - (\rho_{water}\phi_{water}) = (\rho_{DPPC\ tails})(\phi_{DPPC\ tails}) + (\rho_{PE:PG:CL\ tails})(\phi_{PE:PG:CL\ tails})$$

Equation 5-3 was used to find the value of $\rho - (\rho_{water}\phi_{water})$, which was needed in order to fully complete equation 5-4:

Equation 0-4

$$\phi_{DPPC\ tails} = \left(\frac{(\rho - (\rho_{(water)}\phi_{water}) - (\rho_{PE:PG:CL\ tails}(1 - \phi_{water})))}{(\rho_{d-DPPC\ tails} - \rho_{PE:PG:CL\ tails})} \right)$$

Once the relative contribution of the $\phi_{DPPC\ tails}$ were determined, then the relative contributions of the DP:PE:CL tails to the bilayer were determined by using equation 5-5:

Equation 0-5

$$\phi_{PE:PGCL} = 1 - (\phi_{DPPCtails} + \phi_{water})$$

5.4 Results

Table 5-1 shows the summary of the calculated SLD values for the PE:PG:CL lipid head group and tail and the native and CHD-treated clupeine, the data were summarized from Tables C1 to C3 (Appendix C). The SLD of the solvents used for this work are shown in Table 5-2. Figure 5-2 (A and B) shows the pressure area isotherms from the model bilayer system composed of a DPPC inner leaflet and a PE:PG:CL lipid mix in the outer leaflet, respectively.

The isotherm in Figure 5-2 B is similar to what was shown in Figure 4-1 B (chapter 4) even though the maximum pressure for the system was 35 mN m^{-1} as compared to 25 mN m^{-1} in the monolayer system. The surface pressure of 35 mN m^{-1} was chosen for these experiments since it allows the system to have a similar packing density to biological membranes (Brockman, 1999). Figure 5-2 A shows a different isotherm for the zwitterionic phospholipid, DPPC; here an increase in surface pressure in the GE phase was observed all the way to the condensed phase when the maximum surface pressure of 35 mN m^{-1} was achieved at $\sim 68 \text{ \AA}$. Figure 5-3 represents the SLD profile of the d-DPPC: h- PE:PG:CL lipids and the h-DPPC: h-PE:PG:CL lipids which shows the five-layer model that was used to describe the interfacial structure of the bilayer.

Table 0-1 Summary of the calculated scattering lengths, SLDs, molecular weights and molecular volumes and the ratios of PE:PG:CL (79:17:4 mole %) and native and CHD-treated clupeine used in this thesis.

Mixed Lipid PE:PG:CL (79:17:4)	Scattering Length Σb (10^{-3}\AA)	SLD (10^{-6}\AA^{-2})	Molecular Weight (g/mol)	Molecular Volume (\AA^3)
h-PE:PG:CL (head + tail)	0.339	0.300	720	1128
h-PE:PG:CL (hd. group)	0.598	2.059	273	288
d-PE:PG:CL tail	6.236	7.488	496	838
h-PE:PG:CL tail	-0.326	-0.394	434	838
Native clupeine	29.02	2.023	4200	14330
CHD-treated clupeine	29.02	2.023	4200	14330

Table 0-2 The SLDs of the solvents and solution sub-phases used in this study.

Solutions, Substrates and Peptides	Scattering Length Density (10^{-6}\AA^{-2})
20 mM Hepes buffer D ₂ O, pH 7.2	6.35
20 mM Hepes buffer SMW, pH 7.2	2.07
20 mM Hepes buffer H ₂ O, pH 7.2	-0.56
Silicon	2.07
Silicon oxide (SiO ₂)	3.41
h-PE:PG:CL	2.06
d-PE:PG:CL	7.49
h-PE:PG:CL	-0.39

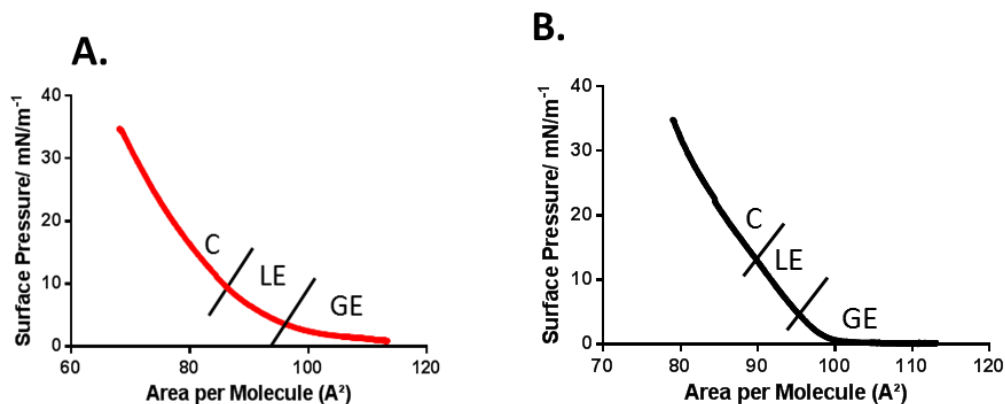


Figure 0-2 (A) The surface pressure area isotherm for DPPC used for the inner layer of the bilayer and (B) represents the surface pressure to area curve for PE:PG:CL mole% (79:17:4) used for the outer layer of the model bilayer prior to clupeine adsorption. The three typical phases shown are the gaseous extended phase (GE), the liquid extended phase (LE) and the condensed (C) phase.

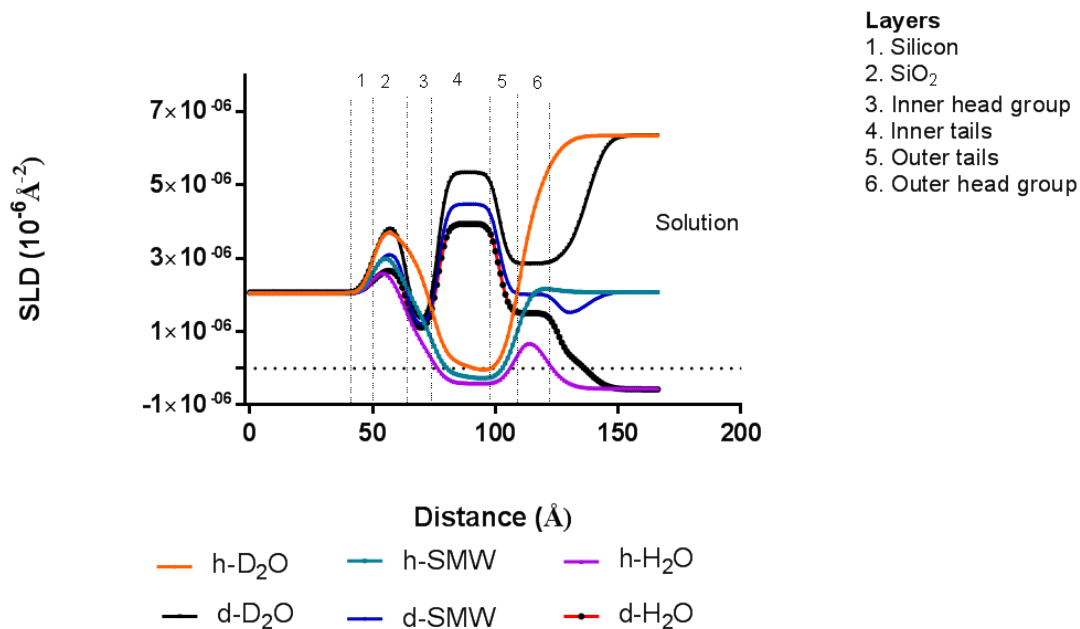


Figure 0-3 The SLD profile obtained from the bare d-DPPC:h-PE:PG:CL lipid contrasts in d-D₂O (black), d-SMW (blue) and d-H₂O (red) and the h-DPPC:h-PE:PG:CL lipid contrasts h-D₂O (orange), h-SMW (aqua blue) and h-H₂O (purple).

The layer closest to the silicon substrate was silicon dioxide and was described as layer 2, layer 3 was the head group of the inner lipid (DPPC), and layer 4 was described as the inner tail. The fifth layer was described as the outer tail (PE:PG:CL), whereas the sixth layer was described as the outer head group and represented the head group region of the mixed lipid. As expected, all the deuterated lipids had higher SLD values than the corresponding hydrogenated lipids which highlights the difference in nuclear scattering length between hydrogen (^1H , $-3.74 \times 10^{-6}\text{\AA}$) and its isotope deuterium (^2H , $6.64 \times 10^{-6}\text{\AA}$) (Le Brun et al., 2016).

The reflectivity profile obtained from fitting the bare d-DPPC, h-PE:PG:CL bilayer is shown in Figure 5-4, and of the three contrasts used, the adsorption of the deuterated lipid in the presence of D_2O showed the greatest increase in intensity of the reflected neutron beam. In NR, the signal depends on differences in the SLD of: (1) the layers in the model and (2) the solvents used. Water has a SLD of $-0.56 \times 10^{-6}\text{\AA}^{-2}$ whereas SMW with 38% D_2O has a higher SLD of $2.07 \times 10^{-6}\text{\AA}^{-2}$.

On the other hand, a fully deuterated solution has an SLD of $6.35 \times 10^{-6}\text{\AA}^{-2}$ thus the reflectivity data obtained in this study is in agreement with these principles. As in the other reflectivity profiles in this thesis, the data points with the associated error bars represent the experimental data whereas the solid lines represent the best model-to-data fit of the interface. During the fitting of these data the hydration, SLD and thickness parameters were fitted individually whereas the roughness parameters were linked for all the layers because they were assumed to be dependent on the roughness of the silicon block; the best-fit parameters are shown in Table 5.3.

In addition, the SLD values of the lipid head groups were set to be within the theoretical calculated ranges (Table 5.2) however, the SLD of the inner and outer tails were fixed at $7.45 \times 10^{-6} \text{ \AA}^{-2}$ and $-0.39 \times 10^{-6} \text{ \AA}^{-2}$, respectively. The best fit results are shown in Table 5.3 and here it was found that the inner and outer tails had similar thicknesses ($24.99 \pm 0.45 \text{ \AA}$ for the inner tail compared to $23.89 \pm 1.03 \text{ \AA}$, (for the outer tail). It is also of interest to note that the inner and outer head group thicknesses were also similar, $12.99 \pm 0.72 \text{ \AA}$ for the inner DPPC head group and $11.99 \pm 1.25 \text{ \AA}$ for the mixed PE:PG:CL head group.

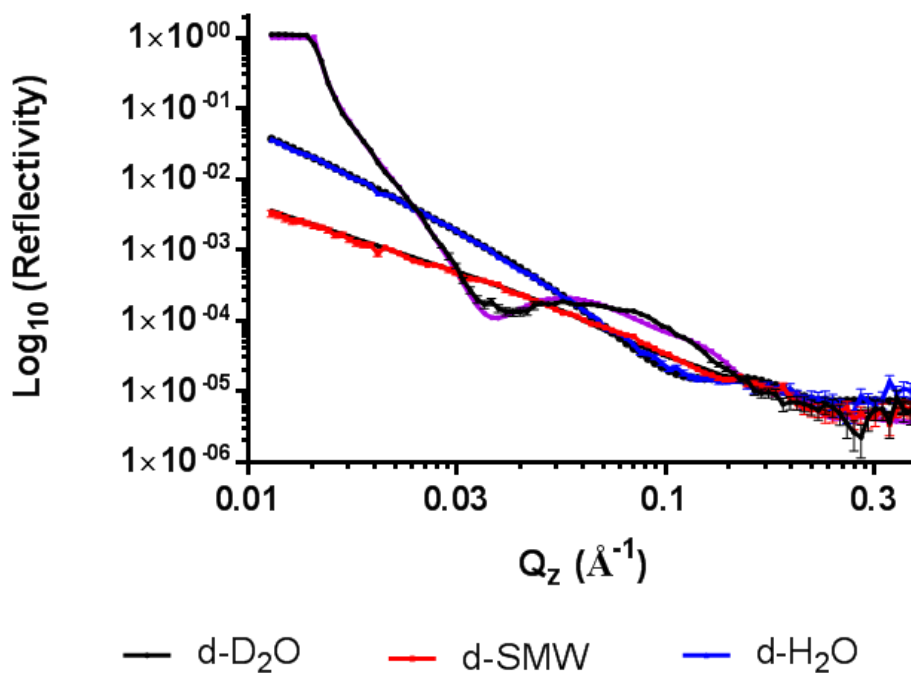


Figure 0-4 Reflectivity profile of bare d-DPPC:h-PE:PG:CL bilayer lipids in three contrasts, D₂O (black), SMW (red) and H₂O (blue) and the corresponding fits as lines, D₂O (purple), SMW (black), and H₂O (black).

The asymmetry of the deposited bilayer was determined by calculating the lipid composition in the outer and inner tail regions as described in section 5.3, and the head group hydration values were not taken into account, similar to the convention followed by (Clifton et al., 2013b). In the inner tail region, the volume fraction of DPPC was 0.69 ± 0.01 whereas the volume fraction of PE:PG:CL was 0.24 ± 0.02 for a combined lipid coverage of ~90%. Conversely, the volume fraction of PE:PG:CL in the outer lipid tail was 0.56 ± 0.01 compared to 0.24 ± 0.02 DPPC accounting for ~80% lipid coverage when the two lipid volume fractions were combined.

Table 0-3 Summary of structural parameters obtained for an asymmetrically deposited d-DPPC (inner leaflet) *E. coli* PE:PG:CL (outer leaflet) bilayer deposited on a silicon surface. These fits were repeated three times.

Layers	τ , Thickness (Å)	Φ_{DPPC}	$\Phi_{\text{PE:PG:CL}}$	Φ_{Water}	Roughness (Å)
Layer 2, Silicon oxide	11.1 ± 0.96	n.a.	n.a.	0.17 ± 0.04	3.99 ± 0.31
Layer 3, inner head group	12.99 ± 0.72			0.03 ± 0.04	Bilayer 3.03 ± 0.69
Layer 4, inner tails	24.99 ± 0.45	0.69 ± 0.01	0.24 ± 0.02	0.20 ± 0.02	
Layer 5, outer tails	23.89 ± 1.03	0.24 ± 0.02	0.56 ± 0.01	0.19 ± 0.03	
Layer 6, outer head group	11.99 ± 1.25			0.03 ± 0.04	

τ , represents layer thickness; Φ_{DPPC} , represents DPPC volume fraction; $\Phi_{\text{PE:PG:CL}}$, represents PE:PG:CL volume fraction.

Table E-1 (Appendix E) shows the percent hydration obtained in each layer and these values were used to calculate the volume fraction of water in the inner lipid and outer lipid area using equation 5-3. Figure 5.5 shows the reflectivity profile of the bare

hydrogenated lipids in three solvent contrasts, 100% D₂O, SMW (38% D₂O) and 100% H₂O, and the best fit parameters that describe these data are shown in Table 5.4. Similar to the deuterated lipids, the greatest reflectivity was observed in the presence of 100% D₂O. The hydrogenated lipids were also used to determine the changes in the bilayer in the presence of the two peptides; for this analysis the deuterated lipids were not used because they dominated the SLD profiles and subtle changes in SLD could not be distinguished. Before fitting these data the inner and outer tails were locked at their theoretical values and an additional layer was included in the model for the peptide as described by Dabkowska et al. (2009).

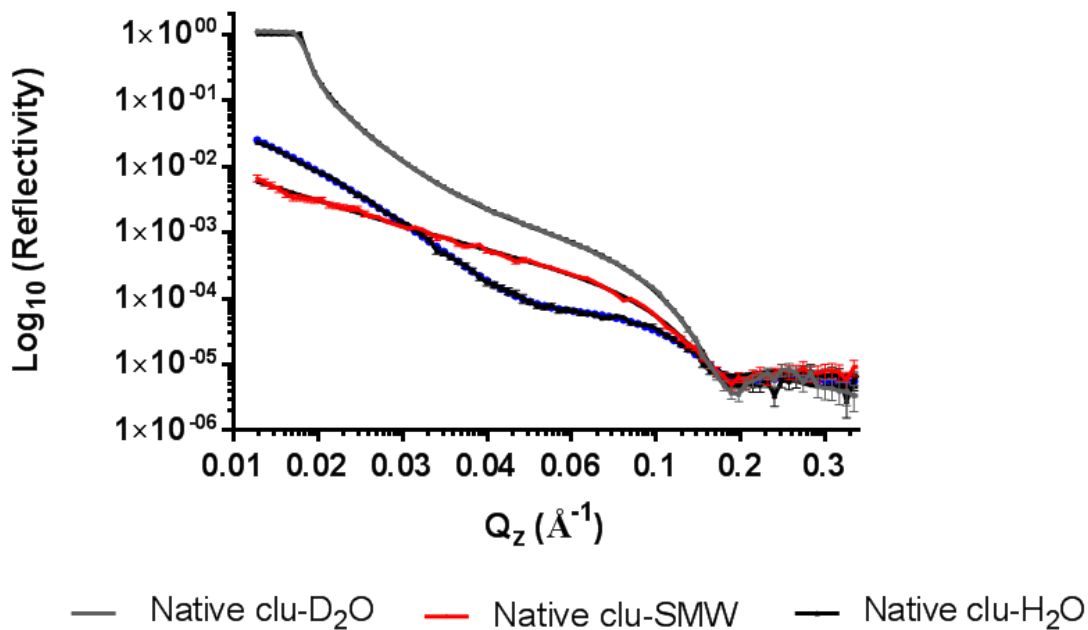


Figure 0-5 Reflectivity profile of bare h-DPPC:h-PE:PG:CL lipids in three contrasts; D₂O (blue), SMW (red) and H₂O (grey). The corresponding fits are shown as lines; D₂O (black), SMW, (black), and H₂O, (black).

On addition of native or CHD-treated clupeine, the thickness of the outer head group regions and their corresponding SLDs were allowed to vary as fitting parameters, however, it was assumed that no changes in the inner tails and inner head group regions of the bilayer would occur, thus these parameters were not fitted in the presence of the native or CHD-treated peptides.

Table 0-4 Parameters derived from fitting the bare h-DPPC:h-PE:PG:CL lipids. These fits were repeated three times.

Layers	τ , Thickness (Å)	SLD (10^{-6} \AA^{-2})	Roughness (Å)
Layer 1, Silicon oxide	11.9 ± 2.61	3.41	3.58 ± 0.95
Layer 2, inner head group	11.96 ± 3.28	1.53	Bilayer roughness = 4.99 ± 0.01
Layer 3, inner tails	15.69 ± 2.23	-0.39^{nf}	
Layer 4, outer tails	19.2 ± 0.89	-0.39^{nf}	
Layer 5, outer head group	7.94 ± 0.55	2.50	

Figure 5.6 compares the reflectivity of the hydrogenated lipids in the bilayer in the presence (B) and absence of native clupeine (A) and the parameters that describe this fit are shown in Table 5.5. The thickness of the silicon oxide layer was found to be 11.9 ± 2.61 with an interfacial roughness of $3.58 \pm 0.95 \text{ \AA}$ which was also used in the fits for the bilayer in the presence of CHD-treated clupeine (Tables 5.5 and 5.6). In the presence of native clupeine, the thickness of the peptide layer was found to be $4.15 \pm 2.93 \text{ \AA}$ with an increase in the outer head group thickness from 7.94 ± 0.55 to $8.52 \pm 0.04 \text{ \AA}$ (Table 5.4 and Table 5.5, respectively). In contrast, the CHD-treated clupeine formed a thicker peptide

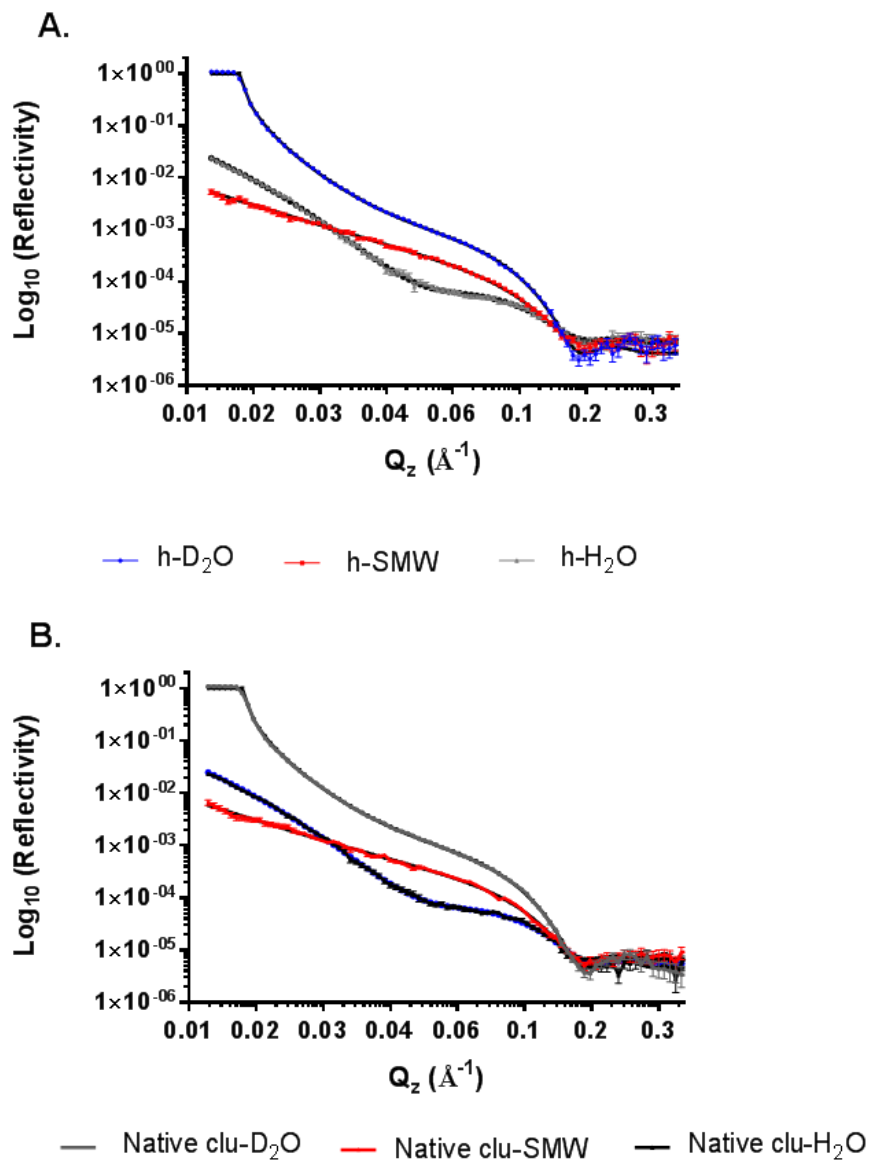


Figure 0-6 (A) Reflectivity profile of bare h-DPPC:h-PE:PG:CL bilayer lipids D_2O (blue), SMW (red) and H_2O (grey) and the corresponding fits all in black. (B) Native clupeine in three contrasts, D_2O (gray), SMW (red) and H_2O (black). The corresponding fits are shown as lines, D_2O (black), SMW (black), and H_2O (blue).

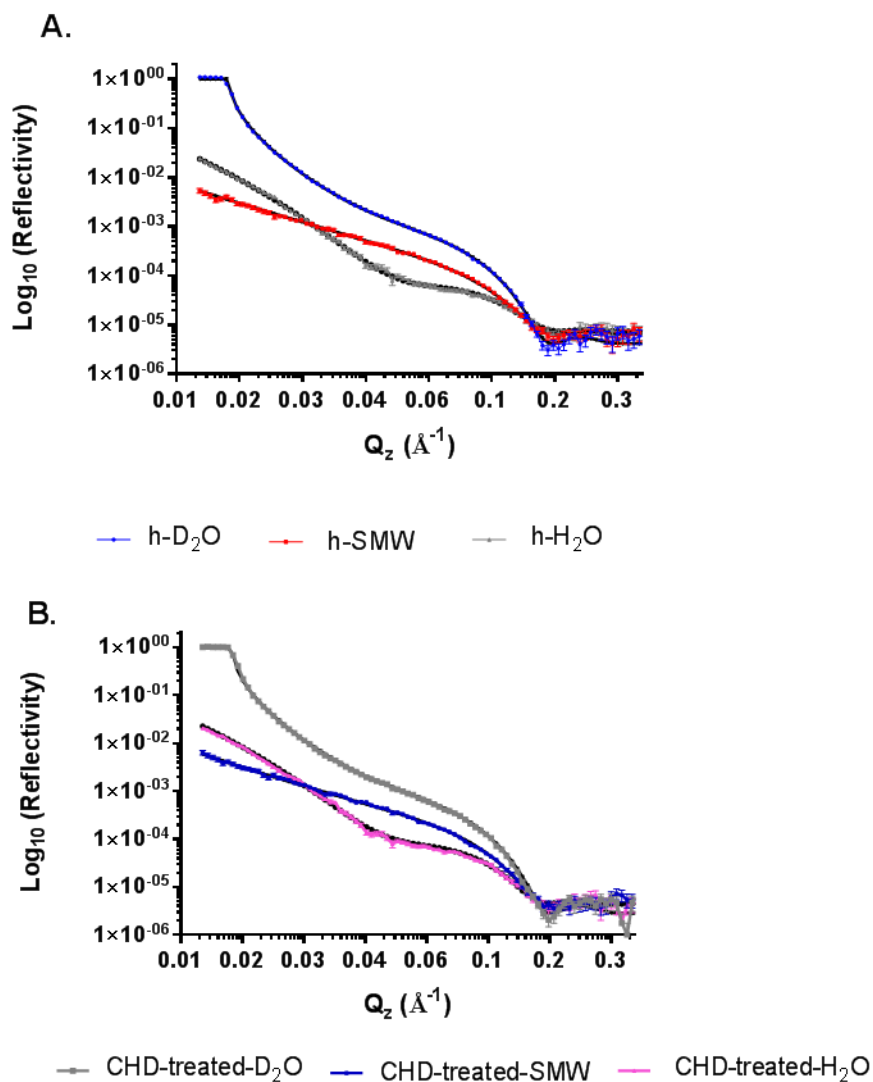


Figure 0-7 (A) Reflectivity profile of bare h-DPPC:h-PE:PG:CL bilayer lipids D₂O (blue), SMW (red) and H₂O (grey) and the corresponding fits, all in black. (B) Reflectivity profile of h-DPPC:h-PE:PG:CL bilayer lipids and CHD-treated clupeine in three contrasts, D₂O (gray), SMW (blue) and H₂O (pink). The corresponding model fits are shown as lines, all in black.

layer, $11.04 \pm 5.99 \text{ \AA}$ (Table 5.6), but the lipid head group thickness was lower in the presence of CHD-treated clupeine ($8.13 \pm 0.66 \text{ \AA}$) compared to when the bilayer was

exposed to native clupeine ($8.52 \pm 0.04 \text{ \AA}$) (Table 5.5). These differences were not statistically significant. In addition, in the presence of native clupeine, the peptide layer roughness was $3.15 \pm 2.65 \text{ \AA}$, whereas the roughness had increased to $6.91 \pm 1.6 \text{ \AA}$ in the presence of CHD-treated clupeine (Table 5.6). It is also noteworthy that an increase in the outer head group hydration occurred in the presence of both peptides, a 9% increase in the presence of native clupeine (from 0.18 to 0.27) and a 30% increase in the presence of CHD-treated clupeine (from 0.18 to 0.48) (Table 5-7).

Figure 5.8 shows the real space distribution of the fitted data as scattering length density versus distance across the interface for the bare bilayer (A) and in the presence of native clupeine (B), whereas Figure 5.9 shows a comparison of the bare bilayer (A) and in the presence of CHD-treated clupeine (B). The data illustrated in Figure 5.10 and Figure 5.11 represent the changes in reflectivity and SLD in the presence of native clupeine (H_2O contrast) and CHD-treated clupeine (H_2O contrast), respectively. Here only subtle changes in SLD were observed in the presence of both peptides in the head group regions (~ 106 to $\sim 120 \text{ \AA}$), head group SLD decreased from 2.5 to $2.2 \times 10^{-6} \text{ \AA}^{-2}$ or from 2.5 to $2.3 \times 10^{-6} \text{ \AA}^{-2}$ in the presence of native (Figure 5.10) or CHD-treated clupeine, respectively (Figure 5.11). The SLDs of the lipid region at distances of ~ 80 to $\sim 110 \text{ \AA}$ remained unchanged in all three solvents in the bare bilayer (Figure 5.8 A), and in the presence of the native peptide (Figure 5.8 B and Figure 5.10 B) or in the presence of the CHD-treated peptide (Figure 5.9 B and 5.11 B). Figure 5.10 (B) and Figure 5.11 (B) also clearly demonstrate the differences in the positive SLD of the inner head group region, and the negative SLD values of the inner tails. The NR profiles also demonstrate subtle

decreases in reflectivity in the presence of native (Figure 5-10 A) or CHD-treated clupeine (Figure 5-11 A).

Table 0-5 Parameters derived from fitting h-DPPC:h-PE:PG:CL lipids in the presence of native clupeine.

Layers	τ , Thickness (Å)	SLD (10^{-6} \AA^{-2})	Roughness (Å)
Layer 2, Silicon oxide	11.9 ± 2.61	3.41^{nf}	Silicon oxide = 3.58 ± 0.95
Layer 3, inner head group	11.96 ± 3.28	1.53^{nf}	Bilayer = 4.99 ± 0.01
Layer 4, inner tails	15.69 ± 2.23	-0.39^{nf}	
Layer 5, outer tails	19.2 ± 0.89	-0.39^{nf}	
Layer 6, outer head group	8.52 ± 0.04	2.17	
Native clupeine	4.15 ± 2.93		Peptide layer = 3.15 ± 2.65

*nf refers to non-fitted parameters.

Table 0-6 Parameters derived from fitting h-DPPC:h-PE:PG:CL bilayer lipids with CHD-treated clupeine.

Layers	τ , Thickness (Å)	SLD (10^{-6} \AA^{-2})	Roughness (Å)
Layer 2, Silicon oxide	11.9 ± 2.61	3.41^{nf}	Silicon oxide = 3.58 ± 0.95
Layer 3, inner head group	11.96 ± 3.28	1.53^{nf}	Bilayer roughness = 4.99 ± 0.01
Layer 4, inner tails	15.69 ± 2.23	-0.39^{nf}	
Layer 5, outer tails	19.2 ± 0.89	-0.39^{nf}	
Layer 6, outer head group	8.13 ± 0.66	2.27	
CHD-treated clupeine	11.04 ± 5.99		Peptide layer = 6.91 ± 1.6

*nf refers to non-fitted

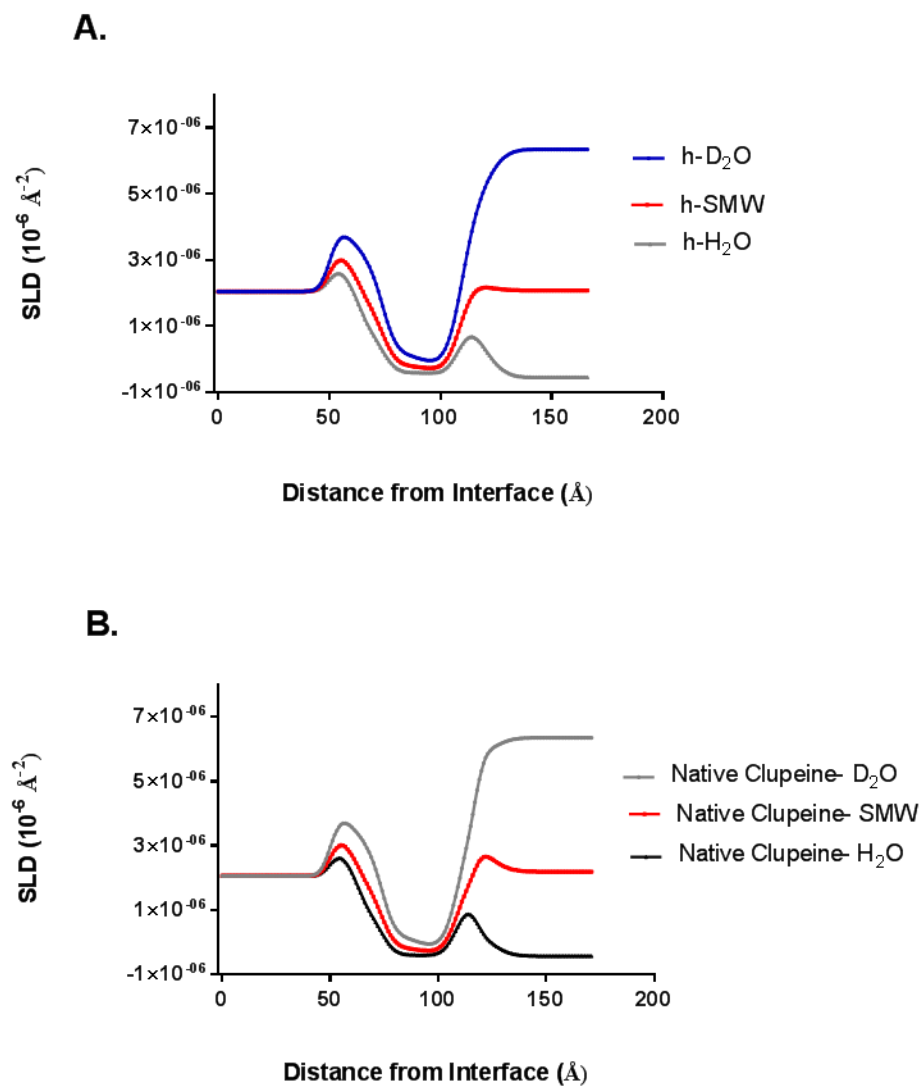


Figure 0-8 A comparison of the SLD profiles obtained for the bare h-DPPC:h-PE:PG:CL bilayer lipids (A) and in the presence of native clupeine (B).

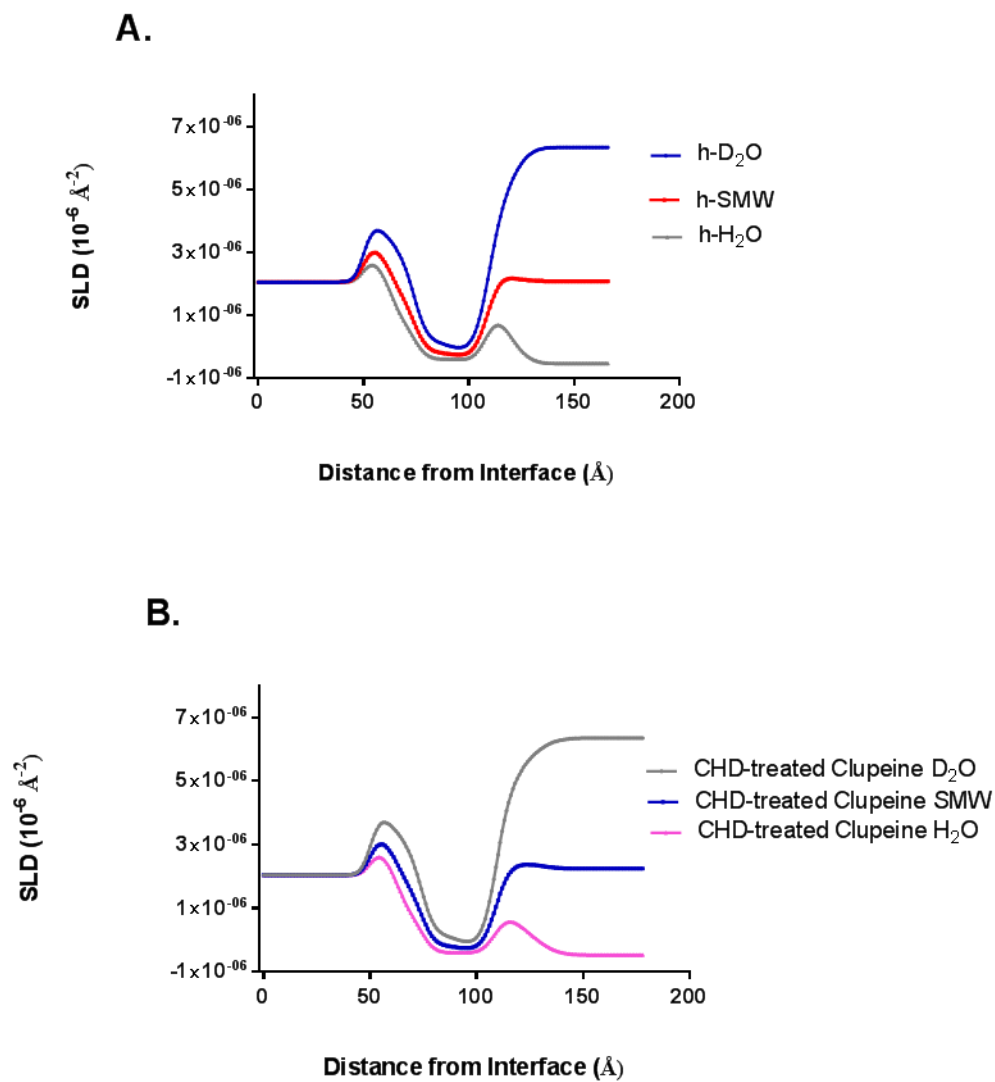


Figure 0-9 A comparison of the SLD profiles obtained for the bare h-DPPC:h-PE:PG:CL bilayer lipids (A) and in the presence of CHD-treated clupeine (B).

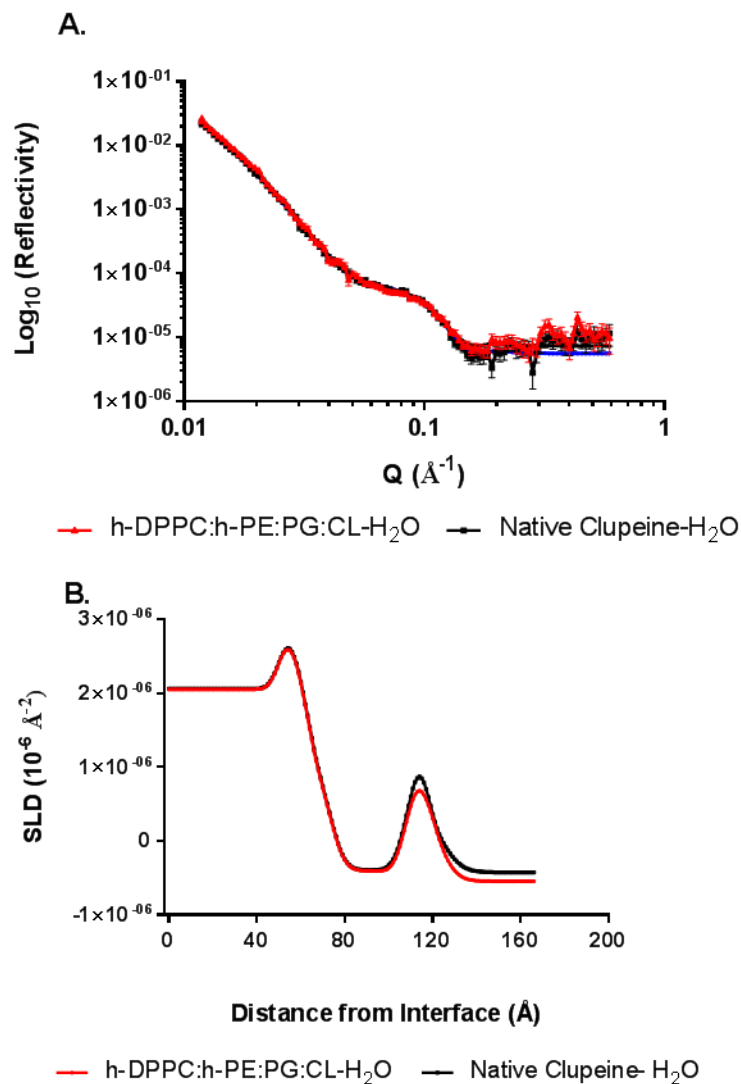


Figure 0-10 A comparison of the reflectivity curve obtained for the bare h-DPPC:h-PE:PG:CL bilayer lipids in H₂O in the presence of native clupeine in H₂O. The data are plotted as points with error bars and the fits are represented as a blue line (A). The corresponding SLD profiles that represent these data are shown in 5-10 (B).

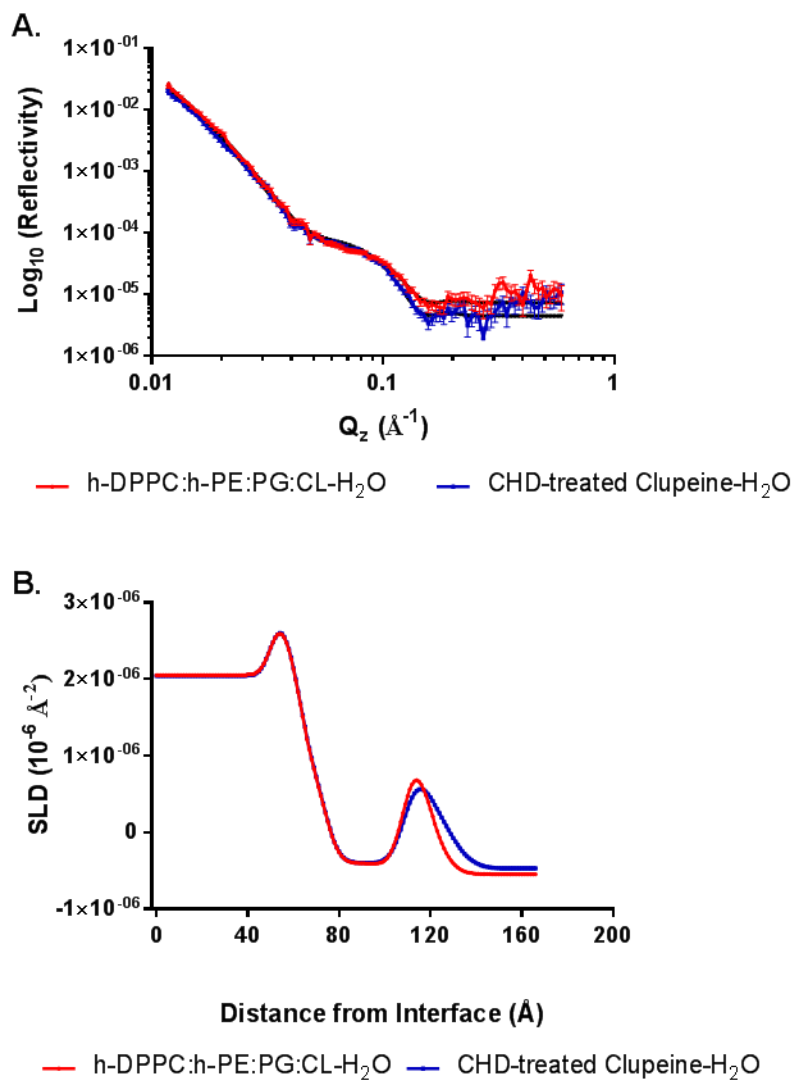


Figure 0-11 A comparison of the reflectivity curve obtained for the bare h-DPPC:h-PE:PG:CL bilayer lipids in H₂O in the presence of the CHD-treated clupeine. The data are plotted as points with error bars and the fits are represented as a black line (A). The corresponding SLD profiles that represent these data are shown in 5-11 (B).

Table 0-7 Best fit values and error estimates of asymmetrically deposited bare h-DPPC (inner leaflet) *E. coli* PE:PG:CL (outer leaflet) bilayer deposited on a silicon surface and the bilayer in the presence of native and CHD-treated clupeine.

Parameters of the Bilayer	Bare h-bilayer	h-bilayer + native clupeine	h-bilayer + CHD- treated clupeine
Oxide layer thickness (Å)	11.90 ± 2.61	nf	nf
Oxide layer hydration (%)	15.56 ± 2.39		
Oxide layer roughness (Å)	3.58 ± 0.95		
Inner head gp SLD (10 ⁻⁶ Å ⁻²)	1.53 ± 0.01	nf	nf
Inner head group hydration (%)	31.3 ± 5.49		
Inner head group thickness (Å)	11.95 ± 3.28		
Inner tail SLD (10 ⁻⁶ Å ⁻²)	-0.39	nf	nf
Inner tail hydration (%)	8.18 ± 1.53		
Inner tail thickness (Å)	15.69 ± 2.23		
Outer tail SLD (10 ⁻⁶ Å ⁻²)	-0.39	nf	nf
Outer tail hydration (%)	4.45 ± 0.93		
Outer tail thickness (Å)	19.21 ± 0.89		
Outer head gp SLD (10 ⁻⁶ Å ⁻²)	2.51 ± 0.30	2.17 ± 0.50	2.27 ± 0.48
Outer head group hydration (%)	17.9 ± 12.7	26.89 ± 5.51	48.21 ± 11.5
Outer head group thickness (Å)	7.94 ± 0.54	8.52 ± 0.04	8.13 ± 0.66
Bilayer roughness (Å)	4.99 ± 0.01	nf	nf
Clupeine hydration (%)	n.a.	48.81 ± 3.11	58.89 ± 14.5
Clupeine thickness (Å)	n.a.	4.15 ± 2.93	11.04 ± 5.99
Clupeine roughness (Å)	n.a.	3.15 ± 2.65	6.91 ± 1.60

nf = not fitted and n.a. = not applicable

5.5 Discussion

Neutron reflectometry studies were used to better understand the nature of the interaction of native and CHD-treated clupeine in d-DPPC:PE:PG:CL and h-DPPC:PE:PG:CL bilayer membrane systems. In biological membranes lipid asymmetry is important for many cellular functions such as lipid transport and membrane stability (Brown and Conboy 2011), thus establishing asymmetry is an important feature of model membranes. The model used to fit the reflectivity data from the deuterated lipids showed that it was possible to form asymmetrical bilayers, and the inner leaflet composition (~90% DPPC) was reasonably consistent with previous NR studies of DPPC-containing bilayers (Clifton et al., 2013b).

The incomplete bilayer coverage of the outer layer (~80% PE:PG:CL) may be attributed to imperfect speed and pressure used in LB deposition (Benz et al., 2004b; Hughes et al., 2008). One strategy proposed by Benz et al. (2004b) to overcome this shortcoming is to perform optimization studies to determine the ideal pressure and speed values for LB deposition. Furthermore, Hughes et al. (2008) also recommended that improving the uniformity of the supporting layer could also lead to better bilayer coverage.

Due to limited beamtime none of the optimization strategies described above were applied in these studies, however, the lipid volume fractions obtained fall within the acceptable range of what has been reported by Fernandez et al. (2013) to be sufficient coverage ($69 \pm 0.05\%$ to $83 \pm 0.07\%$) for studying mixed DMPC-anionic

dimyristoylphosphatidylglycerol (DMPG) and zwitterionic, dimyristoylphosphatidylcholine (DMPC)-supported bilayer membrane structures.

Based on the findings reported by Clifton et al. (2013) and Fernandez et al. (2013), it seems reasonable to assume that the bilayer coverage from this study was sufficient to characterize the interaction of native and charge-reduced clupeine with the d-DPPC:PE:PG:CL and h-DPPC:PE:PG:CL bilayer. Nevertheless, Barker et al. (2016) cautions that one of the main limitations associated with incomplete bilayer coverage are the challenges encountered in interpreting the NR data.

To further highlight this point, Koenig et al. (1996), and Wacklin and Thomas (2007) in their NR characterization of lipid bilayers adsorbed to silicon wafers, also emphasized that the average size of the covered region of the bilayer as well as the uncovered regions are crucial for data treatment. These points were taken into account during the fitting of the data, and similar to the study by Koenig et al. (1996) for the data analysis of these experiments it was also assumed that the fitted SLD values of the outer and inner lipid tail regions were an average over the pure hydrocarbon layer in the bilayer and the water layer in the uncovered regions.

In addition to asymmetry in the bilayer, some lipid mixing was also observed. For example, in the inner tail region, $\sim 69 \pm 0.24\%$ DPPC and $\sim 24 \pm 0.02\%$ PE:PG:CL were present whereas in the outer tail region, $24 \pm 0.02\%$ DPPC and $\sim 56 \pm 0.01\%$ PE:PG:CL were present. Bilayer lipid mixing or lipid translocation has been described by Kornberg and McConnell (1971), Gerelli et al. (2012), and Parisio et al. (2016) as lipid ‘flip-flop’, and some of these authors agree that it is difficult to do direct measurements of flip-flop mechanics, because depending on the method used, the data may not be consistent with

other findings. As a result, there has been an ongoing debate in the literature surrounding not just the time scale but also the occurrence and mechanisms of flip-flop in model membranes.

For example, Nakano et al. (2007) used small angle neutron scattering (SANS) to investigate the flip-flop mechanism in 1,2-dimyristoyl-sn-glycero-3-phosphocholine (DMPC), and 1,2-distearoyl-sn-glycero-3-phosphocholine (DSPC) vesicles and reported a flip-flop half-life of ~ 9 h at 30°C. However, Liu and Conboy (2005) used sum frequency vibrational spectroscopy to obtain a direct, kinetic measure of flip-flop mechanism and reported a half-life of ~3 min at 16°C. Furthermore, Gerelli et al. (2012) used NR to investigate the structural changes induced by lipid translocation, and reported no flip-flop process even after several hours. This discrepancy in the time scale using different methods forms a major part of the ongoing debate. In the present studies, no time scales were measured, however, there is sufficient evidence to suggest that lipid translocation (lipid flip-flop) in the bilayer occurred, and the inner lipid was still predominantly DPPC whereas the outer lipid was dominated by the mixed PE:PG:CL lipid (Table 5.3).

Although some of the features of the flip-flop mechanism remain unsettled in the literature, there is more agreement on what situations may lead to the occurrence of this phenomenon. Three conditions proposed by Gerelli et al. (2012) indicate that flip-flop occurs when: (1) bilayer components are in the liquid phase, (2) the packaging of one of the monolayers is not tight enough, or (3) when mechanical shock of lipids occurs during the LS stage of bilayer formation. Proposition one, although informative, does not accurately describe the state of the phospholipids used in these experiments, which were

in the gel or subgel phase (Clifton et al., 2013b). Based on the observations from this study, loose packing of the outer lipid layer or mechanical shock of the lipids during the LS stage of bilayer formation are more reasonable explanations for the occurrence of lipid flip-flop reported here.

The picture that emerged from the monolayer studies in Chapter 4, is one in which there was minimal interaction of both peptides with the PE:PG:CL monolayer with preferable interaction occurring with the mixed lipid head group and the formation of a protein layer either $15.27 \pm 0.07 \text{ \AA}$ thick in the presence of native clupeine (Table 4-3) or $17.56 \pm 0.05 \text{ \AA}$ in the presence of the CHD-treated peptide (Table 4-4). A combination of these findings along with other studies by Koenig et al. (2007), Wacklin and Thomas (2007), Dabkowska et al. (2009), and Kwaambwa et al. (2010) who all used NR to characterize the structure of lipid bilayers adsorbed to silicon wafers, have proven informative in providing a rationale for the choice of the model used in these studies and for the interpretation of the data.

There are several points to note during the fitting of the data; first, it was assumed that in the presence of the peptides there would be no change in the inner head group and inner tail regions of the bilayer thus these parameters were not fitted with the experimental data (Table 5.7). Similar to other studies by Fernandez et al. (2012) and Kwaambwa et al. (2010) this rationale was based on trying to find an adequate description of the data with a minimum number of parameters. A hydration parameter was assigned for each layer of the model and the upper and lower limits for the head group region were based on the theoretical calculations of each component in the head group (PE:PG:CL) in the ratio 79:17:4.

In addition, the hydrogenated lipid systems in the three contrasts (SMW, 100% H₂O and 38% D₂O) were fitted separately from the deuterated lipids since the former are best to assess the position of the peptides with respect to the interface (Clifton et al., 2013a). However, this approach has one weakness in that it cannot be determined where there has been flipping between the leaflets, consequently, the deuterated lipids were fitted separately to make this assessment. Lipid flipping that occurred between the leaflets was then taken into account when setting the limits for the inner and outer head group regions to ensure that the presence of either lipid especially in the outer head group region would be accommodated.

As noted in Chapter 4, for the CHD-treated peptide, the primary sequence was not known and there was uncertainty about the exact number of protons exchanged; as a result, the theoretical SLD of the CHD-treated peptide was assumed to be the same as the native peptide. Consequently, any differences in the 'dry' SLD which might have occurred with modifying the native clupeine to form CHD-treated clupeine would not have been accounted for in the calculations (Table 5-2). The obvious limitation with this assumption is accepting that the theoretical or 'dry' SLD values of both peptides would not change in different contrast solutions (H₂O, SMW and D₂O). Thus any differences in the 'dry' SLD which might have occurred with modifying the native clupeine to form CHD-treated clupeine would not have been accounted for in the calculations. Despite this limitation the model seems reasonable since only minimal changes in SLD were observed in the reflectivity and SLD profiles in the water contrasts (Figures 5.10 to 5.11) which are more sensitive to the lipid head group regions (Clifton et al., 2013b).

The minimal changes in the SLD profiles also indicate negligible changes in the density of the bilayer after exposure to the peptides. For example, in the outer lipid head group region there was a change in SLD from 2.5 to 2.2 or 2.3 $\times 10^{-6} \text{ \AA}^{-2}$ in the presence of native or CHD-treated clupeine, respectively. The decrease in SLD may be explained by lipid removal from the bilayer in the presence of the peptides. Lipid loss was also accompanied by an increase in hydration of the lipid head group, from $17.9 \pm 12.7\%$ on the bare bilayer compared to $26.9 \pm 5.5\%$ in the presence of native clupeine and $48.2 \pm 11.5\%$ in the presence of CHD-treated clupeine. The greater degree of hydration in the lipid head group region in the presence of CHD-treated clupeine compared to the native peptide is observed as a broader peak in Figure 5.11 B compared to Figure 5.10 B and may also indicate greater solvent penetration. These data may appear to weaken the assumption that the theoretical or 'dry' SLD of native and CHD-treated clupeine are the same; here again the small changes in SLD in the presence of the 100% H₂O contrast is evidence to support the validity of the model.

During fitting it is also advantageous to reduce the number of parameters (Nelson, 2006; Hughes et al., 2008), accordingly, for these studies, the bilayer roughness was shared between all the layers except the silicon oxide layer and the peptide layers which were assigned individual roughness and allowed to vary as fitting parameters (Table 5-7). The silicon oxide roughness obtained from these experiments was $3.58 \pm 0.94 \text{ \AA}$ which is within the acceptable range of 3-5 \AA (Wacklin and Thomas, 2007) and an oxide layer thickness of $11.9 \pm 2.61 \text{ \AA}$, which also falls within the normal range of 7- 20 \AA (Wacklin and Thomas, 2007). However, in the presence of the peptides it was necessary to include

an additional layer to represent the peptide layer which was consistent with earlier studies.

For example, this convention was used by Dabkowska et al. (2009) to examine the interaction of the membrane protein cytochrome-c in 1,2-dioleoyl-*sn*-glycerol-3-phosphatidylcholine (DPOC) and 1-palmitoyl-2-oleoyl-glycerol-3-phosphatidylserine (POPS) containing bilayers. Furthermore, Clifton et al. (2016) included an additional protein layer in NR experiments to examine the binding of the protein colicin N (ColN) to DPPC: LPS bilayer membranes. In both cases the fits were more reliable and realistic representations of the interactions of the peptides with the specific bilayer membranes.

In the presence of CHD-treated clupeine a thicker peptide layer was observed, 11.04 ± 5.99 Å compared to 4.15 ± 2.93 Å when the bilayer was exposed to native clupeine. The interaction of the cationic peptides with the bilayer may be related to the charge on the head groups in the outer lipid layer. The outer lipid bilayer was constructed from an uncharged zwitterionic lipid DPPE and the anionic lipids DPPG and CL in a ratio of (79:17:4) which means there could potentially be some electrostatic interaction with the cationic peptides and the anionic components of the outer lipid head group as proposed by Fernandez et al. (2012). However, with lipid flip-flop, more of the zwitterionic DPPC lipid would be brought in the outer lipid layer, thereby decreasing the concentration of the anionic lipids in the outer lipid layer. The net effect of this interchange of lipids would be a reduced negative charge in the outer lipid layer thus weaker interactions with the peptide due to weaker electrostatic attractions.

The importance of bilayer charge in mediating peptide interaction has been discussed by Vorobyov and Allen (2011) and overall it has been shown that adsorption of

cationic peptides to anionic bilayers is significantly higher than in zwitterionic membranes. Other researchers have reported evidence which is consistent with this observation. For instance, Strömstedt et al. (2010) investigated the interaction of peptides with anionic (DOPC/DOPA/cholesterol) and zwitterionic (DOPC/cholesterol) membranes and observed almost three-fold peptide adsorption for the anionic membrane.

The preferential interaction with anionic membranes was attributed to stronger electrostatic interaction between the peptide and the bilayer. In addition to electrostatic interaction, it should be emphasized that a balance between hydrophobic and electrostatic interactions results in more favourable peptide-lipid interaction. This proposition is based on observations made from the monolayer and bilayer studies (Chapters 4 and 5) in this thesis, and the data show that the slightly more hydrophobic, CHD-treated peptide exhibited greater binding to the lipid head region and the protein layer as compared to the native peptide.

Overall, although the interactions with the lipid head group and the thickness of the peptide layer was greater in the presence of the CHD-treated clupeine compared to the native peptide, it appears that neither peptide would be able to translocate the phospholipid bilayer. In this regard the conclusion from this study is similar to that of Pink et al. (2014) who reported the native peptide's inability to translocate bilayer membranes consisting primarily of bacterial phospholipids. However, the initial interactions observed with the lipid heads group and the protein layer formed in the presence of native and CHD-treated clupeine, may be attributed to the slightly different lipid composition used in this study (PE:PG:CL, 75:17: 4) compared to the PE:PG, 75:25 and 65:35 ratios used by Pink et al. (2014). Although Wimley's (2011) interfacial model

may be used to explain changes in lipid density in the monolayer studies from Chapter 4, the model cannot be used to explain the internalization of native clupeine observed by Pink et al. (2014) nor the lack of membrane translocation by native and CHD-treated clupeine observed in the model bilayer experiments from this study.

5.6 Summary of Biomembrane Experiments

In the present study, a small reduction in charge (10% arginine modification) was hypothesized to result in different interactions with hydrogenated and deuterated DPPC:PE:PG:CL biomembranes. Overall, there were some similarities and differences between the peptide interactions in the monolayer studies of Chapter 4 and the bilayer model membranes used in this chapter. Similar to the monolayer systems there was little adsorption into the lipid layers in the presence of either peptide in the bilayer systems, instead most of the peptide was adsorbed below the lipid layer, in a protein layer close to the bulk solution.

The model also showed the remainder of the peptide interacting with the outer lipid head group region and increasing the thicknesses of this layer. In both the peptide layer and the outer lipid head group region, the CHD-treated peptide had a greater interaction with the bilayer, however, there was a greater increase in head group hydration in the presence of this peptide resulting in an overall decrease in peptide concentration.

There were also minimal decreases in SLD which indicated minimal changes in the density of the bilayers in the presence of either peptide; here, a greater decrease in SLD was observed in the presence of the native peptide. In the monolayer studies it was possible to determine quantitative amounts of peptide in the lipid head group region and

in the peptide layer of the model, however, it was not possible to determine these peptide amounts for the bilayer system. This difference may be attributed to the inherent complexity of the bilayer model, a limitation which might make it less sensitive to small amounts of peptide penetration. In contrast, a monolayer has fewer layers in the fit which is more advantageous to differentiate between peptide and lipid components.

Another reason for observing less interaction in the bilayer system may be attributed to the substantial mixing of lipids between the two leaflets of the asymmetric layers, which reduced the overall charge of the outer layer thereby reducing the peptide-lipid interaction. Thus it seems reasonable to infer that preventing lipid flip-flop is an important criterion for optimum clupeine (native and CHD-treated) and Gram-negative membrane lipid interactions.

In summary, there were clear advantages to using both model biomembranes systems, however, the use of the bilayer systems enabled an improvement of the biomembrane models although the peptides were not able to translocate the biomembranes. Thus, the data obtained from both systems helped to better define the interactions of the native and CHD-treated peptide with model biomembranes.

CHAPTER 6: CONCLUSION

6.1 Summary and Conclusions

The work presented in this thesis has focused on determining whether native clupeine and CHD-treated clupeine have different modes of interaction with bacterial cells and model membranes. Accordingly, three main types of interactions were investigated: (1) the cytotoxicity of the native and CHD-treated peptide against *E. coli* K-12 and *S. enterica* Typhimurium 14028 cells and human red blood cells; (2) peptide-induced alterations in the expression of the bacterial outer membrane porin and protease genes (*ompF*, *ompC* and *ompT*, respectively) as well as the proteomic profile of outer membrane proteins and; (3) changes in the structure and composition of model biomembranes in the presence of the native and CHD-treated peptide.

Lower MIC values for native and CHD-treated clupeine were obtained for the *E. coli* K-12 strain (500 and 400 µg/mL, respectively) as compared to MIC values of 1250 µg/mL (for both peptides) obtained against the *S. enterica* Typhimurium 14028 strain, indicating differences in susceptibility. Although a significant difference ($P < 0.05$) in the percent hemolysis was observed in the presence of the native peptide ($0.36\% \pm 0.01$) versus CHD-treated peptide ($0.45\% \pm 0.01$), it should be noted that these values are still extremely low, since less than 0.5% of the erythrocytes were releasing hemoglobin. Overall, the SEM data revealed no visible signs of bacterial cell lysis after peptide treatment, however, fewer flagella were observed in the *S. enterica* Typhimurium 14028 strain after exposure to increasing concentrations of native and CHD-treated clupeine. Also, some cells appeared more elongated in the presence of CHD-treated clupeine.

In *E. coli* K-12 cells, native clupeine decreased and increased expression of the *ompF* and *ompC* genes, respectively, whereas the expression of both genes were down-regulated in the presence of the CHD-treated peptide. Little or no effect on *ompF* expression was observed at or below MIC levels of native and CHD-treated clupeine in *S. enterica* Typhimurium 14028 cells. This was in strong contrast to the up-regulation ($P < 0.05$) of *ompF* observed at the highest concentration of both peptides used (2500 $\mu\text{g/mL}$). In both test strains, the presence of the OmpA porin protein was identified. Increased OmpA expression was identified in *E. coli* K-12 cells especially in the presence of 1000 $\mu\text{g/mL}$ of native and CHD-treated clupeine. The latter observation was significant, since *E. coli* K-12 cells were more susceptible to CHD-treated clupeine and this protein was previously shown to play an important role in translocation across the outer membrane and in establishing the stability of cell membranes (Wang, 2002). The expression of GapA protein in *E. coli* K-12 cells was detected after exposure to the CHD-treated peptide but not to the native peptide. This observation is also important since GapA expression has been linked with several non-glycolytic roles in bacterial cells including oxidative stress (Aguilera et al., 2009). The expression of the OmpA porin protein and GapA observed in the presence of *E. coli* K-12 cells exposed to CHD-treated clupeine is a unique contribution of this study which further elucidates the interaction of the CHD-treated peptide with *E. coli* K-12 cells.

In Chapters 4 and 5, complementary techniques NR and XRR, were used to characterize structural changes in the Gram-negative model monolayer and bilayer membranes, in the presence of native and CHD-treated clupeine. This study contributes novel findings as these interactions, which to the best of our knowledge, are being

investigated here for the first time. The data obtained from these experiments have led to several conclusions. First, for the native peptide, there was very little interaction observed in the more complex bilayer model membranes, whereas in the monolayer system, there was evidence of peptide interaction with the lipid head group region and a peptide layer adsorbed below the monolayer. On the other hand, in the presence of the CHD-treated peptide, there was greater interaction with the lipid head group region and a more extended peptide layer was formed in the monolayer and bilayer systems compared to the native peptide. Second, in addition to the small size of the peptide (4.2 kDa), the complexity of the bilayer and lipid flip-flop appeared to quench the interactions of the peptides with the outer lipid head group region and made it more difficult to quantify penetration into the bilayer. In contrast, for the less complex monolayer system, quantitative amounts of peptides were determined as surface excess values in the presence of both peptides. Despite this advantage, one weakness of monolayer systems is that they represent a single layer (leaflet). Conversely, the use of bilayer systems in this study was advantageous, as they enabled an improvement of the biomembrane model system, since the latter more accurately represents the symmetry of the Gram-negative inner membrane.

6.2 Recommendations for Future Work

1. Determine MIC and MBC values for single *E. coli* K-12 and *S. enterica* Typhimurium 14028 *omp* mutants grown in the presence of native and CHD-treated clupeine. The mutant strains could then be exposed to more accurate MIC values following which qPCR studies would be carried out using the appropriate primers.

2. To complement the biomembrane studies done in Chapters 4 and 5, Transmission Electron Microscopy (TEM) could also be performed on the *E. coli* K-12 and *S. enterica* Typhimurium 14028 test strains to examine changes in the bacterial cell structure in the presence of the native and CHD-treated peptide. In addition, AFM studies would also allow real-time nanoscale imaging of bacterial surfaces under physiological conditions in the presence of the native and CHD-treated peptides.
3. Due to limited beamtime, optimization experiments to determine the ideal pressure and speed values for LB deposition were not performed for this work. Ideally, these experiments should be done to improve lipid coverage for the model bilayer membranes which would also decrease lipid flip-flop observed in the bilayer systems.
4. The efficacy of 10% CHD-treated clupeine as a food preservative should also be tested in a variety of food systems such as fish and fish products. Potter et al. (2005) tested the efficacy of both native and CHD-treated (14% and 23%) peptides in 2% milk and ground beef. Although several patents have described methods for preserving food by adding protamine from salmon (salmine) (Ueno et al., 1988; Ueno et al., 1990) clupeine has not been approved for food applications in Canada. If the efficacy of the peptides can be shown in specific foods, then the safety and toxicity of the peptides should also be investigated.
5. Studies to investigate the antimicrobial activity of other clupeine modifications such as clupeine analogues or synthetic peptides should be done. This technique is particularly advantageous because of its ability to identify which specific amino acid residues are responsible for antimicrobial activity and which sequence

substitutions result in the most effective antimicrobial activities. However, most of the studies which have incorporated the synthesis of CAP analogues were focused on studying bacterial pathogens causing communicable diseases (Giacometti et al., 2007; Strömstedt et al., 2009; Haney et al., 2009; and Cheng et al., 2009). It is also possible that these analogues would be less susceptible to proteases and could broaden the potential application of modified CAPs.

6.3 Final Comments

The work presented in this thesis has shown that the complementary techniques NR and XRR can be used to successfully describe the structural changes which occur in *E. coli* model membranes that are exposed to native or CHD-treated clupeine. Based on the model biomembrane studies, the native and CHD-treated clupeines are able to interact with the lipid head group and changed the density of the lipid layer. However, the peptides were not able to translocate the bacterial model membranes in the absence of any membrane proteins in the biomembrane models although the lipid head group interactions were greater in the presence of the CHD-treated peptide as compared to the native peptide.

Ultimately, the *E. coli* K-12 strain was more sensitive to the native and CHD-treated peptide as compared to the *S. enterica* Typhimurium 14028 strain. Overall, the OmpF and OmpC porins were down-regulated however, the potential importance of increased expression of the OmpA porin and the presence of the GapA protein in the presence of *E. coli* K-12 cells exposed to CHD-treated clupeine is twofold. First, increased levels of OmpA may satisfy an alternative channel requirement since OmpA provides structural integrity to the membrane and also functions in active and passive ion

transport. Second, the protein GapA has been linked to several non-glycolytic functions in bacterial cells including oxidative stress.

Although this study was specific to native and CHD-treated clupeine (10% arginine modification), these findings may have greater implications for improving our understanding of the effect of charge reduction on cationic ionic antimicrobial peptide interactions with Gram-negative bacteria. However, completion of some of the work suggested in section 6.2 would be required in order to further demonstrate the efficacy of native and CHD-treated clupeine before either peptide could be approved as potential food applications in Canada.

REFERENCES

- Ablain, W., Soulier, S., Causeur, D., Gautier, M. and Baron, F. (2009). A simple and rapid method for the disruption of *Staphylococcus aureus*, optimized for quantitative reverse transcriptase applications: application for the examination of Camembert cheese. *Dairy Science and Technology*, 89, 69–81.
- Abuillan, W., Schneck, E., Korner, A., Brandenburg, K., Gutschmann, T., Gill, T., Vorobiev, A., Konovalov, O., and Tanaka, M. (2013). Physical interactions of fish protamine and antiseptic peptide drugs with bacterial membranes revealed by combination of specular x-ray reflectivity and grazing-incidence x-ray fluorescence. *Physical Review*, 88, 1-11.
- Aguilera, L., Giménez, R., Badia, J., Aguilar, J., and Baldoma, L. (2009). NAD⁺-dependent post-translational modification of *Escherichia coli* glyceraldehyde-3-phosphate dehydrogenase. *International Microbiology*, 12, 187-192
- Alemu, K. (2014). Real-Time PCR and its application in plant disease diagnostics. *Advances in Life Science and Technology*, 39-49.
- Anaya-López, J., López-Meza, J., and Ochoa-Zarzosa, A. (2013) Bacterial resistance to cationic antimicrobial peptides. *Critical Reviews in Microbiology*, 39, 180-195.
- Ando, T., Yamasaki, M., Suzuki, K. (1973). Protamines. Isolation, characterization, structure and function. Berlin: Springer-Verlag 119 pages.
- Andrä, J., Jakovin, I., Grötzinger, J., Hecht, O., Krasnosdembskaya, A., Goldman, T., Gutschmann, T., and Leippe, M. (2008). Structure and mode of action of the antimicrobial peptide arenicin. *Biochemical Journal*, 410, 113-122.
- Andersen, J., Forst, S., Zhao, K., Inouye, M., and Delihias, N. 1989. The function of *micF* RNA: *micF* RNA is a major factor in the thermal regulation of OmpF protein in *Escherichia coli*. *Journal of Biological Chemistry*, 264, 17961-17970.

- Arnold, T., Nicklin, C., Rawle, J., Sutter, J., Bates, T., Nutter, B., McIntyre, G., Burt, B. (2012). Implementation of a beam deflection system for studies of liquid interfaces on Beamline I07 at Diamond. *Journal of Synchrotron Radiation*, 19, 408-416.
- Aspedon, A., and Groisman, E. (1996). The antibacterial action of protamine: evidence for disruption of cytoplasmic membrane energization in *Salmonella* Typhimurium. *Microbiology*, 142, 3389-3397.
- Bacalum, M. and Radu, M. (2015). Cationic Antimicrobial Peptides Cytotoxicity on Mammalian Cells: An Analysis Using Therapeutic Index Integrative Concept. *International Journal of Peptide Research and Therapeutics*, 21, 47-55.
- Bals, R., and Wilson, J. (2003). Cathelicidins – a family of multifunctional antimicrobial peptides. *Cellular and Molecular Life Sciences*, 60, 711- 720.
- Band, V., and Weiss, D. (2015). Mechanisms of antimicrobial peptide resistance in Gram-negative bacteria. *Antibiotics*, 4, 18–41.
- Baker, C., Banerjee, S. Tenover, F. (1994). Evaluation of Alamar colorimetric MIC method for antimicrobial susceptibility testing of Gram-negative bacteria. *Journal of Clinical Microbiology*, 32, 1261-67.
- Barker, R., McKinley, L., and Titmuss, S. (2016). Neutron Reflectivity as a tool for physics-based studies of model bacterial membranes, 261- 282. In: *Biophysics of Infection, Advances in Experimental Medicine and Biology*. Springer International Publishing, Switzerland.
- Belenky, P., and Collins, J. (2011). Antioxidant strategies to tolerate antibiotics. *Science*, 334:915–916.
- Benz, R. (1985). Porin from bacterial and mitochondrial outer membranes. *Critical Reviews in Biochemistry*, 19, 145-190.
- Benz, R. and Orlik, F. (2004a) Functional Reconstitution of Specific Porins. In: *bacterial and eukaryotic porins: structure, function, mechanism*, pp. 183- 212. R. Benz (Ed.). Weinheim, FRG. Wiley-VCH and Verlag.

- Benz, M., Gutschmann, T., Chen, N., Tadmor, R., Israelachvili, Jacob. (2004b). Correlation of AFM and SFA measurements concerning the stability of supported lipid bilayers. *Biophysical Journal*, 86, 870- 879.
- Benz, R., Schmid, A., and Hancock, R. (1985). Ion selectivity of Gram-negative bacterial porins. *Journal of Bacteriology*, 162, 722- 727.
- Bio-Rad Laboratories (2006) Real-time PCR application guide. Retrieved from: <http://www.gene-quantification.com/real-time-pcr-guide-bio-rad.pdf>
- Bonora, G., Ferrara, L., Paolillo, L., Toniolo, C., Trivellone, E. (1979). ¹³C Nuclear magnetic resonance of protamines. The three main components of clupeine. *European Journal of Biochemistry*, 93, 13–21.
- Born, M., and Wolf, E. (1970). Principles of Optics. Oxford, Pergamon Press.
- Brockman, H. (1999). Lipid Monolayers: why use half a membrane to characterize protein-membrane interactions? *Current Opinion in Structural Biology*, 9, 438–443.
- Brogden, K. (2005). Antimicrobial peptides: pore formers or metabolic inhibitors in bacteria? *Nature Reviews Microbiology*, 3, 238-250.
- Broniatowski, M., Mastalerz, P., Flasiński, M. (2015). Studies of the interactions of ursane-type bioactive terpenes with the model of *Escherichia coli* inner membrane -Langmuir monolayer approach. *Biochimica et Biophysica Acta*, 1848, 469–476.
- Brown, M., Collier, P., and Gilbert, P. (1990). Influence of growth rate on susceptibility to antimicrobial agents: Modification of the cell envelope and batch and continuous culture studies. *Antimicrobial Agents and Chemotherapy*, 34, 1623-1628.
- Brown, K., and Conboy, J. (2011). Electrostatic induction of lipid asymmetry. *Journal of the American Chemical Society*, 133, 8794- 8797.

- Brown, T. and Poon, T. (2005). *Introduction to organic chemistry* (Third Ed.) John Wiley & Sons, Inc.
- Brown, M., and Williams, P. (1985). Influence of substrate limitation and growth phase on sensitivity to antimicrobial agents. *Journal of Antimicrobial Chemotherapy*, 15, 7-14.
- Buckley, A., Webber, M., Cooles, S., Randall, L., La Ragione, R., Woodward, M., and Piddock, L. (2006). The AcrAB-TolC efflux system of *Salmonella enterica* serovar Typhimurium plays a role in pathogenesis. *Cell Microbiology*, 8, 847-56.
- Bustin, S., Benes, V., Garson, J., Hellems, J., Huggett, J., Kubista, M., Mueller, R., Nolan, T., Pfaffl, M., Shipley, G., Vandesompele, J., and Wittwer, C. (2009). The MIQE guidelines: minimum information for publication of quantitative real-time PCR experiments. *Clinical Chemistry*, 55, 611–22.
- Buttimor, R. (2005). Lipophilization of herring protamine to improve antimicrobial and emulsification properties. M.Sc. Thesis, Department of Food Science and Technology, Dalhousie University, Canada. Retrieved from ProQuest Dissertations and Theses Global.
- Capita, R. and Alonso-Calleja, C. (2013). Antibiotic-resistant bacteria: a challenge for the food industry. *Critical Reviews in Food Science and Nutrition*, 53, 11- 48.
- Carrica, M., Craig, P., García-Angulo, V., Aguirre, A., García-Véscovi, E., Goldbaum, F., and Cravero, S. (2011). YqiC of *Salmonella enterica* serovar Typhimurium is a membrane fusogenic protein required for mice colonization. *BMC Microbiology*, 11, 1-10.
- Chang, L., Lee, H., Chung, M., and Yang, V. (2005). PEG-modified protamine with improved pharmacological/ pharmaceutical properties as a potential protamine substitute: synthesis and *in vitro* evaluation. *Bioconjugate Chemistry*, 16, 147- 155.

- Chatterjee, S., and Chaudhuri, K. (2012). Gram-negative bacteria, the cell membranes. In: outer membrane vesicles of bacteria. pp.15 – 30. Springer Briefs in Microbiology, Springer.
- Cheng, J., Hale, J., Elliot, M., Hancock, R., and Straus, S. (2009). Effect of membrane composition on antimicrobial peptides Aurein 2.2 and 2.3 from Australian southern Bell frogs. *Biophysical Journal*, 96, 552–565.
- Ciumac, D., Campbell, R., Xu, H., Clifton, L., Hughes, A., Webster, J., Lu, J. (2017). Implications of lipid monolayer charge characteristics on their selective interactions with a short antimicrobial peptide. *Colloids and Surfaces B: Biointerfaces*, 150, 308–316.
- Clifton, L., Sanders, M., Hughes, A., Neylon, C., Frazier, R., and Green, R. (2011). Lipid binding interactions of antimicrobial plant seed defence proteins: puroindoline- α and β -purothionin. *Physical Chemistry Chemical Physics*, 13, 17153–17162.
- Clifton, L., Sanders, M., Kinane, C., Arnold, T., Edler, K., Neylon, C., Green, R., and Frazier, R. (2012). The role of protein hydrophobicity in thionin-phospholipid interactions: a comparison of $\alpha 1$ and $\alpha 2$ -purothionin adsorbed anionic phospholipid monolayers. *Physical Chemistry Chemical Physics*, 14, 13569–13579.
- Clifton, L., Neylon, C., and Lakey, J. (2013a). Examining protein-lipid complexes using neutron scattering. *Methods in Molecular Biology*, 974, 119-150.
- Clifton, L., Skoda, M., Daulton, E., Hughes, A., Le Brun, A., Lakey, J., Holt, S. (2013b) Asymmetric phospholipid: lipopolysaccharide bilayers; a Gram-negative bacterial outer membrane mimic. *Journal of the Royal Society Interface*, 10, 1-11.
- Clifton, L., Skoda, M., Le Brun, A., Ciesielski, F., Kuzmenko, I., Holt, S., Lakey, J. (2015). Effect of divalent cation removal on the structure of gram-negative bacterial outer membrane models. *Langmuir*, 31, 404–412.
- Clifton, L., Ciesielski, F., Skoda, M., Paracini, N., Holt, S., and Lakey, J. (2016). The effect of lipopolysaccharide core oligosaccharide size on the electrostatic binding

- of antimicrobial proteins to models of the Gram-negative bacterial outer membrane. *Langmuir*, 32, 3485–3494.
- Cohen, S., McMurray, L., and Levy, S. (1988) marA locus causes decreased expression of OmpF porin in multiple-antibiotic-resistant (Mar) mutants of *Escherichia coli*. *Journal of Bacteriology*, 170, 5416–5422.
- Confer, A., and Ayalew, S. (2015). The OmpA family of proteins: Roles in bacterial pathogenesis and immunity. *Veterinary Microbiology*, 163, 207–222.
- Cowan, S., Schirmer, T., Rummel, G., Steiert, M., Ghosh, R., Pauptit, R., Jansonius, J., and Rosenbusch, J. (1992). Crystal structures explain functional properties of two *E. coli* porins. *Nature*, 358, 727-733
- Dabkowska, A., Fragneto, G., Hughes, A., Quinn, P., and Lawrence, M. (2009). Specular neutron reflectivity studies of the interaction of Cytochrome c with supported phosphatidylcholine bilayers doped with phosphatidylserine. *Langmuir*, 25, 4203-4210.
- Danauskas, S. (2009). The Interaction of Amyloid Beta 40 Peptide with anionic phospholipid Langmuir monolayers. PhD Thesis, Department of Chemistry, the University of Chicago. Retrieved from ProQuest Dissertations and Theses Global.
- Dathe, M., and Wieprecht, T. (1999). Structural features of helical antimicrobial peptides: Their potential to modulate activity on model membranes and biological cells. *Biochimica et Biophysica Acta (BBA) - Biomembranes*, 1462 (1-2), 71-87.
- Davies, J., and Davies, D. (2010). Origins and evolution of antibiotic resistance. *Microbiology and Molecular Biology Reviews*, 74, 417–433.
- Davidson, P., Sofos, J., and Branen, A. (2005). Antimicrobials in foods. Third Edition Taylor and Francis group, CRC Press. pp. 721.
- Dawson, R., and Liu, C. (2008). Properties and Applications of antimicrobial peptides in biodefense against biological warfare threat agents. *Critical Reviews in Microbiology*, 34, 89-107.

- Del Nobile, M., Conte, A., Cannarsi, M., and Sinigaglia, M. (2009). Strategies for prolonging the shelf life of minced beef patties. *Journal of Food Safety*, 29, 14–25.
- Demkowicz, M., and Majewski, J. (2016). Probing interfaces in metals using neutron reflectometry. *Metals*, 6, 1- 17.
- Dowd, S., Killinger-Mann, K., Brashears, M., and Fralick, J. (2008). Evaluation of gene expression in a single antibiotic exposure-derived isolate of *Salmonella enterica* Typhimurium 14028 possessing resistance to multiple antibiotics. *Foodborne Pathogens and Disease*, 5, 205-21.
- Doyle, M., Steenson, L., and Meng, J. (2013). Bacteria in food and beverage production. In: Prokaryotes, applied bacteriology and biotechnology. Rosenberg, E., DeLong, E., Lory, S., Stackebrandt, E., and Thompson, F. (Ed.), 241- 256. Springer Berlin Heidelberg.
- Dwyer, D., Collins, J., Walker, G. (2015). Unraveling the physiological complexities of antibiotic lethality. *Annual Reviews in Pharmacology and Toxicology*, 55:313–332.
- Dumas, J., van Delden, C., Perron, K., and Kohler, T. (2006). Analysis of antibiotic resistance gene expression in *Pseudomonas aeruginosa* by quantitative real-time-PCR. *FEMS Microbiology Letters*, 254, 217–225.
- Eleaume, H., and Jabbouri, S. (2004). Comparison of two standardization methods in real-time quantitative RT-PCR to follow *Staphylococcus aureus* genes expression during *in vitro* growth. *Journal of Microbiological Methods*, 59, 363– 370.
- Eband, R. and Vogel, H. (1999). Diversity of antimicrobial peptides and their mechanisms of action. *Biochimica et Biophysica Acta*, 1462, 11- 28.
- Eband, RM., and Eband, RF. (2011). Bacterial membrane lipids in the action of antimicrobial agents. *Journal of Peptide Science*, 17, 298-305.

- Evers, F., Jeworrek, C., Weise, K., Tolan, M., and Winter, R. (2012). Detection of lipid raft domains in neutral and anionic Langmuir monolayers and bilayers of complex lipid composition. *Soft Matter*, 8, 2170- 2175.
- Falentin, H., Postollec, F., Parayre, S., Henaff, N., Le Bivic, P., Richoux, R., Thierry, A., Sohier, D. (2010). Specific metabolic activity of ripening bacteria quantified by real-time reverse transcription PCR throughout emmental cheese manufacture. *International Journal of Food Microbiology*, 144, 10–19.
- Fernandez, D., Le Brun, A., Whitwell, T., Sani, M., James, M., and Separovic, F. (2012). The antimicrobial peptide aurein 1.2 disrupts model membranes via the carpet mechanism. *Physical Chemistry Chemical Physics*, 14, 15739–15751.
- Fernandez, D., Brun, L., Lee, A., Tzong-Hsien, L., Bansal, P., Aguilar, M., James, M., and Separovic, F. (2013). Structural effects of the antimicrobial peptide maculatin 1.1 on supported lipid bilayers. *European Biophysical Journal*, 42, 47-59.
- Fleming A. (1929). On antibacterial action of culture of *Penicillium*, with special reference to their use in isolation of *B. influenzae*. *British Journal of Experimental Pathology*, 10, 226–236.
- Forst, S., Delgado, J., Ramakrishnan, G., and Inouye, M. (1988). Regulation of *ompC* and *ompF* expression in *Escherichia coli* in the absence of *envZ*. *Journal of Bacteriology*, 170, 5080-5085.
- Foster, J., and Spector, M. (1995). How *Salmonella* survive against the odds. *Annual Reviews in Microbiology*, 49, 145-74.
- Galdiero, S., Falanga, A., Cantisani, M., Taallo, R., Pepa, M., D’Orlando, V., and Galdier, M. (2012). Microbe-host interactions: structure and role of Gram-negative bacterial porins. *Current Protein and Peptide Science*, 13, 843- 854.
- Garavito, R., and Rosenbusch, J. (1986). Isolation and crystallization of bacterial porin. *Methods in Enzymology*, 125, 309 -328.

- Gautam, A., Vinson, H., Gibbs, P., Olet, S., and Barigye, R. (2011). Proteomic analysis of multidrug resistant *Escherichia coli* strains from scouring calves. *Veterinary Microbiology*, 151, 363- 371.
- GE Healthcare, (2014). Hi-Trap Columns Characteristics, 71-5017-51 AH, 1-28.
- Gerelli, Y., Porcar, L., and Fragneto, G. (2012). Lipid rearrangement in DSPC/DMPC bilayers: a neutron reflectometry study. *Langmuir*, 28, 15922–15928.
- Giacometti, A., Cirioni, O., Riva, A., Kamysz, W., Silvestri, C., Nadolski, P., Vittoria, A., Łukasiak, J., and Scalise, G. (2007). *In vitro* activity of Aurein 1.2 alone and in combination with antibiotics against Gram-positive *Nosocomial cocci*. *Antimicrobial Agents and Chemotherapy*, 51, 1494–1496.
- Gill, T., Singer, D., and Thompson, J. (2006). Purification and analysis of protamine. *Process Biochemistry*, 41, 1875–1882.
- Girard-Ergot, A., and Blum, L. (2007). Langmuir-Blodgett technique for synthesis of biomimetic lipid membranes In: Nanobiotechnology of biomimetic membranes. Martin, D. (Ed.) pp. 23- 62. New York, Springer.
- Gold, H., and Moellering, R. (1996). Antimicrobial-drug resistance. *The New England Journal of Medicine*, 335, 1445-1453.
- Gottschlich, G., Gravlee, G., and Georgitis, J., 1988. Adverse reactions to protamine sulfate during cardiac surgery in diabetic and non-diabetic patients. *Annals of Allergy, Asthma and Immunology*, 61, 277-287.
- Gray, G., O'Reilly, M., Muller, C., Watkins, I., and Lloyd, D. (2006). Low tyrosine content of growth media yields aflagellate *Salmonella enterica* serovar Typhimurium. *Microbiology*, 152, 23-28.
- Green, R., Su, T., Lu, J., Webster, J., and Penfold, J. (2000). Competitive adsorption of lysozyme and C12E5 at the air/liquid interface. *Physical Chemistry Chemical Physics*, 2, 5222-5229.

- Greenwood, D., Finch, R., Norby, S., and Whitley, R. (Eds.). (2003). Antibiotic and chemotherapy, anti-infective agents and their use in therapy. (8th Ed.). UK: Elsevier Health Sciences.
- Guénin, S., Melanie, M., Pelloux, J., Van Wuytswinkel, O., Bellini, C., and Gutierrez, L. (2009). Normalization of qRT-PCR data: the necessity of adopting a systematic, experimental conditions-specific, validation of references. *Journal of Experimental Botany*, 60, 487–493.
- Hajjar, E., Bessonov, A., Molitor, A., Kumar, A., Mahendran, K., Winterhalter, M., Pages, J., Ruggerone, P., and Ceccarelli, M. (2010). Toward screening for antibiotics with enhanced permeation properties through bacterial porins. *Biochemistry*, 49, 6928–6935.
- Hancock, R. and Fella, T. (1996). Cationic peptides. In: Biotechnology of antibiotics (Second Ed.). New York, Marcel Dekker, Inc.
- Hancock, R. (1997). Peptide antibiotics. *Lancet*, 349, 418–422.
- Hancock, R., and Lehrer, R. (1998). Cationic peptides: A new source of antibiotics. *Trends in Biotechnology*, 16 (2), 82-88.
- Hancock, R., and Diamond, G. (2000). The role of cationic antimicrobial peptides in innate host defences. *Trends in Microbiology*, 8, 402- 412.
- Hancock, R., and Rozek, A. (2002). Role of membranes in the activities of antimicrobial cationic peptides. *FEMS Microbiology Letters*, 206, 143- 149.
- Haney, E., Nazmi, K., Lau, F., Bolscher, J., and Vogel, H. (2009a). Novel lactoferrampin antimicrobial peptides derived from human lactoferrin, *Biochimie*, 91, 141–154.
- Haney, E. (2011). Structure-Function studies of antimicrobial peptides: Insights into their mechanism of action. PhD Thesis, Department of Biological Science, University of Calgary. Retrieved from ProQuest Digital Dissertations.
- Hartmann, M., Berditsch, M., Hawecker, J., Ardakani, M., Gerthsen, D., and Ulrich, A. (2010). Damage of the bacterial cell envelope by antimicrobial peptides

- Gramicidin S and PGLa as revealed by Transmission and Scanning Electron Microscopy. *Antimicrobial Agents and Chemotherapy*, 54, 3132–3142.
- Hawkey, P. (1998). The origins and molecular basis of antibiotic resistance. *British Medical Journal*, 317 (7159), 657-660.
- He, Q., and Li, J. (2007). Hydrolysis characterization of phospholipid monolayers catalyzed by different phospholipases at the air–water interface. *Advances in Colloid and Interface Science*, 131, 91–98.
- Health Canada, (2002). Impact on resistance and human health uses of antimicrobials in food animals in Canada: Impact on Resistance and Human Health. pp. 188.
- Heberle, F., Myles, D., and Katsarasa, J. (2015). Biomembranes research using thermal and cold neutrons. *Chemistry and Physics of Lipids*, 4392, 1- 10.
- Head, C., Tardy, A., and Kenney, L. (1998). Relative binding affinities of OmpR and OmpR-phosphate at the ompF and ompC regulatory sites. *Journal of Molecular Biology*, 281, 857–870.
- Hong, H., Szabo, G. and Tamm. L. (2006). Electrostatic couplings in OmpA ion-channel gating suggest a mechanism for pore opening. *Nature Chemical Biology*, 2, 627–635.
- Horrow, J., 1985. Protamine: a review of its toxicity. *Anesthesia and Analgesia*, 64, 348-361.
- Hoyle, D., Shaw, D., Knight, H., Davison, H., Pearce, M., Low, J., Gunn, G., and Woolhouse, M. (2004) Age-related decline in carriage of ampicillin-resistant *Escherichia coli* in young calves. *Applied Environmental Microbiology*, 70, 6927–6930.
- Hsieh, C., Sue, S., Lyu, P., and Wu, W. (1997). Membrane packing geometry of Diphytanoylphosphatidylcholine is highly sensitive to hydration: phospholipid polymorphism induced by molecular rearrangement in the head group region. *Biophysical Journal*, 73, 870-877.

- Hua, W., Xin-hong, L., Rui-xiang, Z., Li-dan, F., and Hua, L. (2008). Spectrophotometric determination of arginine in grape juice using 8-Hydroquinoline. *Agricultural Sciences in China*, 7, 1210-1215.
- Hughes, H., Howse, J., Dabkowska, A., Jones, R., Lawrence, M., and Roser, S. (2008). Floating lipid bilayers deposited on chemically grafted phosphatidylcholine surfaces. *Langmuir*, 24, 1989 – 1999.
- Hui, C., Guo, Y., He, Q., Peng, L., Wu, L., Cao, H., and Huang, S. (2010). *Escherichia coli* outer membrane protease OmpT confers resistance to urinary cationic peptides. *Microbiology and Immunology*, 54, 452–459.
- Im, W. (2002). Ion permeation and selectivity of OmpF porin: A theoretical study based on molecular dynamics, Brownian dynamics, and Continuum electrodiffusion theory. *Journal of Molecular Biology*, 322, 851-869.
- Im, W., and Roux, B. (2002). Ions and counterions in a biological channel: a molecular dynamics simulation of OmpF porin from *Escherichia coli* in an explicit membrane with 1 M KCl aqueous salt solution. *Journal of Molecular Biology*, 319, 1177–1197.
- Ishimura, M., Nishi, N., and Uedaira, H. (1991). Hydration of clupeine in solution. *International Journal of Peptide and Protein Research*, 37, 399-401.
- Islam, N., Itakura, T., Motohiro, T. (1984a). Antibacterial spectra and minimum inhibition concentration of Clupeine and Salmine sulfate. *Bulletin of the Japanese Society for the Science of Fish*, 50, 1705–1708.
- Islam, N., Motohiro, T., and Itakura, T. (1984b). The effects of pH, temperature, metal ions and organic matter on the bactericidal action of clupeine sulfate. *Bulletin of the Japanese Society of Scientific Fisheries*, 50, 811-815.
- Islam, N., Motohiro, T., and Itakura, T. (1985). Effects of pH, temperature, metal ions and organic matters on the bactericidal action of clupeine sulfate. *Bulletin of the Japanese Society for the Science of Fish*, 51, 811–815.

- Islam, D., Oda, H., and Motohiro, T. (1987). Changes in the cell morphology and the release of soluble constituents from washed cells of *Bacillus subtilis* by the action of protamine. *Nippon Suisan Gakkaishi*, 53, 297–303.
- Jap, B., and Walian, P. (1996). Structure and functional mechanism of porins. *Physiological Reviews*, 76, 1073 - 1088.
- Jarvik, T., Smillie, C., Groisman, E., and Ochman, H. (2010). Short-term signatures of evolutionary change in the *Salmonella enterica* Serovar Typhimurium 14028 genome. *Journal of Bacteriology*, 192, 560- 567.
- Jeffries, C., Graewert, M., Blanchet, C., Langley, D., Whitten, A., and Svergun, D. (2016). Preparing monodisperse macromolecular samples for successful biological small-angle X-ray and neutron-scattering experiments. *Nature Protocols*, 11, 2122- 2153.
- Jeffries, C., Graewert, M., Blanchet, C., Langley, D., Whitten, A., and Svergun, D. (2016). Preparing monodisperse macromolecular samples for successful biological small-angle x-ray and neutron scattering experiments. *Nature Protocols*, 11, 2122–2153.
- Jenssen, H., Hamill, P., and Hancock, R. (2006). Peptide antimicrobial agents. *Clinical Microbiology Reviews*, 19, 491–511.
- Jepson, A. (2014). *E. coli* motility and growth: a biophysical study. PhD Thesis, School of Physics, University of Edinburgh. Retrieved from <https://www.era.lib.ed.ac.uk>
- Johansen, C., Gill, T., and Abee, T. (1995). Antibacterial effect of protamine assayed by impedimetry. *Journal of Applied Bacteriology*, 78 (3), 297.
- Johansen, J., Gill, T., and Gram, L. (1996). Changes in cell morphology of *Listeria monocytogenes* and *Shewanella putrefaciens* resulting from the action of protamine. *Applied and Environmental Microbiology*, 62, 1058–1064.
- Johansen, C., Verheul, A., Gram, L., Gill, T., and Abee, T. (1997). Protamine-induced permeabilization of cell envelopes of Gram-positive and Gram-negative bacteria. *Applied and Environmental Microbiology*, 63, 1155–1159.

- Joo, S., Haozhong, S., Wang, J., and Zhu, L. (2013). Loss of osmoregulation of OmpC porin occurs if *Escherichia coli* are deficient in cAMP receptor protein. *Journal of Experimental Microbiology and Immunology*, 17, 78 – 82.
- Kaganer, V., Möhwald, H., and Dutta, P. (1999). Structure and phase transitions in Langmuir monolayers. *Reviews of Modern Physics*, 71, 779- 816.
- Kefala, G., Chihoon, A., Krupa, M., Esquivies, L., Innokentiy, M., Witek, K. and Senyon, C. (2010). Structures of the OmpF porin crystallized in the presence of foscholine-12. *Protein Science*, 19, 1117- 1125.
- Keymanesh, K., Soltani, S., and Sardari, S. (2009). Application of antimicrobial peptides in agriculture and food industry. *World Journal of Microbiology and Biotechnology*, 25, 933–944.
- Khalid, S., Bond, P., Carpenter, T, and Sansom, M. (2008). OmpA: gating and dynamics via molecular dynamics simulations. *Biochimica et Biophysica Acta*, 1778, 1871–1880.
- Kim, K., Aulakh, S., and Paetzel, M. (2012). The bacterial outer membrane β -barrel assembly machinery. *Protein Science*, 21, 751- 768.
- Kito, M. (1986). Chemical modification of proteins: Chemical and physical lipophilization of proteins. *Journal of the American Oil Chemists' Society*, 64, 1676-1681.
- Koenig, B., Krueger, S., Orts, W., Majkrzak, C., Berk, N., Silverton, J., and Gawrisch, K. (1996). Neutron reflectivity and atomic force microscopy studies of a lipid bilayer in water adsorbed to the surface of a silicon single crystal. *Langmuir*, 12, 1343–1350.
- Koli, P., Sudan, S., Fitzgerald, D., Adhya, S., and Kara, S. (2010). Conversion of commensal *Escherichia coli* K-12 to an invasive form via expression of a mutant histone-like protein. *Molecular Biology*, 2, 182- 193.

- Koluman, A., and Dikici, (2015). Antimicrobial resistance of emerging foodborne pathogens: Status quo and global trends. *Critical Reviews in Microbiology*, 39:1, 57-69.
- Komatsu, Y., Murakami, K., and Nishikawa, T. (1981). Penetration of moxalactam into its target proteins in *Escherichia coli* K-12: comparison of a highly moxalactam-resistant mutant with its parent strain. *Antimicrobial Agents and Chemotherapy*. 20: 613- 619.
- Kontani, M., Amano, A., Nakamura, T., Nakagawa, I., Kawabata, S., and Hamada, S. (1999). Inhibitory effects of protamines on proteolytic and adhesive activities of *Porphyromonas gingivalis*. *Infection and Immunity*, 4917–4920.
- Kornberg, R., and McConnell, H. (1971). Inside-outside transitions of phospholipids in vesicle membranes. *Biochemistry*, 10, 1111–1120.
- Kubista, M. (2014). Prime time for q-PCR: Raising the quality bar. *European Pharmaceutical Review*, 19, 63- 67.
- Kumar, A., Bhandari, A., and Krishnaswamy, S. (2015). Sequence and structural perspectives of bacterial β -stranded porins. *Protein and Peptide Letters*, 22, 1- 16.
- Kwaambwa, K., Helling, M., and Rennie A. (2010). Adsorption of a water treatment protein from *Moringa oleifera* seeds to a silicon oxide surface studied by neutron reflection. *Langmuir*, 26, 3902-3910.
- Lad, M., Birembaut, F., Frazier, R., and Green, R. (2005). Protein-lipid interactions at the air/water interface. *Physical Chemistry Chemical Physics*, 7, 3478- 3485.
- Lad, M., Birembaut, F., Clifton, L., Frazier, R., Webster, J., and Green, R. (2007). Antimicrobial peptide-lipid binding interactions and binding selectivity. *Biophysical Journal*, 92, 3575–3586.
- Laemmli, U. (1970). Cleavage of structural proteins during the assembly of the head of bacteriophage T4. *Nature*, 227, 680 – 685.

- Lahtinen, S., Gueimonde, M., Ouwehand, A., Reinikainen, J., Salminen, S. (2006). Comparison of four methods to enumerate probiotic bifidobacteria in a fermented food product. *Food Microbiology*, 23, 571–577.
- Langmuir, I. (1933). Surface Chemistry. *Chemical Reviews*, 13, 147–191.
- Lee, R., and Schnaitman, C. (1980). Comparison of outer membrane porin proteins produced by *Escherichia coli* and *Salmonella* Typhimurium. *Journal of Bacteriology*, 142, 1019-1022.
- Le Brun, A., Clifton, L., Halbert, C., Lin, B., Meron, M., Holden, P., Lakey, J., and Holt, S. (2013). Structural characterization of a model Gram-negative bacterial surface using lipopolysaccharides from rough strains of *Escherichia coli*. *Biomacromolecules*, 14, 2014–2022.
- Lefmann, K. (2007). Neutron Scattering: Theory, instrumentation, and simulation. Department of Materials Research Risø National Laboratory. Technical University of Denmark. Retrieved from: http://www.fys.ku.dk/~willend/Neutron1_4.pdf.
- Levy, S. (2002). The antibiotic paradox: how the misuse of antibiotics destroys their curative powers. Cambridge, MA. Perseus Publishing.
- Lin, X., Wang, C., Guo, C., Tiana, Y., Li, H., and Peng, X. (2012). Differential regulation of OmpC and OmpF by AtpB in *Escherichia coli* exposed to nalidixic acid and chlortetracycline. *Journal of Proteomics*, 75, 5898- 5910.
- Lipperheide, R., Kasper, J., Lee, H., and Reiss, G. (1997). The phase problem in neutron reflection. *Physica B*, 234-236, 1117-1119.
- Liu, J., and Conboy, J. (2005). 1,2-Diacyl-Phosphatidylcholine flip-flop measured directly by sum-frequency vibrational spectroscopy. *Biophysical Journal*, 89, 2522–2532.
- Liu, X., and Ferenci, T. (1998). Regulation of porin-mediated outer membrane permeability by nutrient limitation in *Escherichia coli*. *Journal of Bacteriology*, 180, 3917-3922.

- Llorens, J., Tormo, A., and Martinez-Garcia, E. (2010). Stationary phase in gram-negative bacteria. *FEMS Microbiology Review*, 34, 476–495.
- Loner, K., and Blondelle, S. (2005). Molecular mechanisms of membrane perturbation by antimicrobial peptides and the use of biophysical studies in the design of novel peptide antibiotics. *Combinatorial Chemistry and High Throughput Screening*, 8, 241-256.
- Lopez-Rubio, A., and Gilbert, E. (2009). Neutron scattering: a natural tool for food science and technology research. *Trends in Food Science and Technology*, 20, 576- 586.
- Luckey, M. (2008). Bundles and barrels. In: *Membrane structural biology: with biochemical and biophysical foundations*, pp 102–126. New York, Cambridge University Press.
- Maget-Dana, R. (1999). The monolayer technique: a potent tool for studying the interfacial properties of antimicrobial and membrane-lytic peptides and their interactions with lipid membranes. *Biochimica et Biophysica Acta*, 1462, 109 – 140.
- Mah, T., and O’Toole, G. (2001). Mechanisms of biofilm resistance to antimicrobial agents. *Trends in Microbiology*, 9, 34–39.
- Marr, A., Gooderham, W., and Hancock, R. (2006). Antibacterial peptides for therapeutic use: obstacles and realistic outlook. *Current Opinion in Pharmacology*, 6, 468-472.
- Matsuyama, S., Mizuno, T., and Mizushima, S. (1986). Interaction between two regulatory proteins in osmoregulatory expression of *ompF* and *ompC* genes in *Escherichia coli*: a novel *ompR* mutation suppresses pleiotropic defects caused by an *envZ* mutation. *Journal of Bacteriology*, 168, 1309-1314.
- Matsuzaki, K. (1999). Why and how are peptide-lipid interactions utilized for self-defense? Magainins and tachyplesins as archetypes. *Biochimica et Biophysica Acta*, 1462, 1- 10.

- McCarter, J., Stephens, D., Shoemaker, K., Rosenberg, S., Kirsch, J., and Georgiou, G. (2004). Substrate specificity of the *Escherichia coli* outer membrane protease OmpT. *Journal of Bacteriology*, 186, 5919–5925
- McClellan, D. (1930). The influence of testicular extract on dermal permeability and the response to vaccine virus. *The Journal of Pathology and Bacteriology*, 33:1045-1070.
- McLeod, G., and Spector, M. (1996). Starvation- and stationary-phase-induced resistance to the antimicrobial peptide Polymyxin B in *Salmonella typhimurium* is RpoS (σ) independent and occurs through both phoP-dependent and -independent pathways. *Journal of Bacteriology*, 178, 3683–3688.
- Means, G. and Feeney, R. (1971). Chemical modification of proteins, pp.254. San Francisco, Cambridge and London: Holden-Day, Inc.
- Means, G., and Feeney, R. (1998). Chemical modifications of proteins: A review. *Journal of Food Biochemistry*, 22, 399-425.
- Melo, M., Ferre, R. and Castanho, M. (2009). Antimicrobial peptides: linking partition, activity and high membrane-bound concentrations. *Nature Reviews Microbiology*, 9, 245-250.
- Mizuno, T., Chou, M., and Inouye, M. (1983). A comparative study on the genes for three porins of the *Escherichia coli* outer membrane. *The Journal of Biological Chemistry*, 258, 6932-6940.
- Mohan, M. (2010) Effects of protamine on *Pseudomonas aeruginosa* cell envelope components: surface remodelling. M.Sc. Thesis, Dalhousie University, Department of Process Engineering. Retrieved from ProQuest Dissertations and Theses Global.
- Moon, J., Henzler-Wildman, K., and Ramamoorthy, A. (2006). Expression and purification of a recombinant LL-37 from *Escherichia coli*. *Biochimica et Biophysica Acta*, 1758, 1351–1358.

- Morein, S., Andersson, S., Rilfors, L., and Lindblom, G. (1996). Wild-type *Escherichia coli* cells regulate the membrane lipid composition in a “Window” between Gel and Non-lamellar Structures. *The Journal of Biological Chemistry*, 271, 6801–6809.
- Mortimer, P. and Piddock, L. (1993). The accumulation of five antibacterial agents in porin-deficient mutants of *Escherichia coli*. *Journal of Antimicrobial Chemotherapy*, 32, 195-213.
- Nakae, T. (1976). Identification of the outer membrane protein of *E. coli* that produces transmembrane channels in reconstituted vesicle membranes. *Biochemical and Biophysical Research Communication*. 71, 877-884.
- Nakano, M.; Fukuda, M.; Kudo, T.; Endo, H.; Handa, T. (2007). Determination of Interbilayer and transbilayer lipid transfers by time-resolved small-angle neutron scattering. *Physical Review Letters*, 98, 238101-238104.
- Nakai, S., and Modler, R. (Eds.). (1996). Food proteins properties and characterization. United States of America: Wiley-VCH.
- Nikaido, H., Rosenberg, E., and Foulds, J. (1983). Porin channels in *Escherichia coli*: studies with beta-lactams in intact cells. *Journal of bacteriology*, 153, 232-240.
- Nikaido, H., and Vaara, M. (1985). Molecular basis of bacterial outer membrane permeability. *Microbiology Reviews*, 49, 1-32.
- Nikaido, H. (1994). Porins and specific diffusion channels in bacterial outer membranes. *The Journal of Biological Chemistry*, 269, 3905 – 3908.
- Nikaido, H. (2003). Molecular basis of bacterial outer membrane permeability revisited. *Microbiology and Molecular Biology Reviews*, 67, 593-656.
- Nelson, A. (2006). Co-refinement of multiple-contrast neutron/X-ray reflectivity data using MOTOFIT. *Journal of Applied Crystallography*, 39, 273–276.
- Neu, H. (1992). The crisis in antibiotic resistance. *Science*, 257 (5073), 1064-1073.

- Normark, B., and Normark, S. (2002). Evolution and spread of antibiotic resistance. *Journal of Internal Medicine*, 252 (2), 91-106.
- Oliveira, R., Schneck, E., Quinn, B., Konovalov, O., Brandenburg, K., Seydel, U., Gill, T., Hanna, C., Pink, D., Tanaka, M. (2009). Physical mechanisms of bacterial survival revealed by combined grazing-incidence X-ray scattering and Monte Carlo simulation. *Chimie*, 12, 209-217.
- Omardien, S., Brul, S., and Zaa, S. (2016). Antimicrobial activity of cationic antimicrobial peptides against Gram-positives: current progress made in understanding the mode of action and the response of bacteria. *Frontiers in Cell and Developmental Biology*, 4, 1-16.
- Page`s, J., Chloe, E., and Winterhalter, M. (2008). The porin and the permeating antibiotic: a selective diffusion barrier in Gram-negative bacteria. *Nature Reviews in Microbiology*, 6, 893–903.
- Pambou, E., Li, Z., Campana, M., Hughes, A., Clifton, L., Gutfreund, P., Foundling, J., Bell, G. and Lu, J. (2016). Structural features of reconstituted wheat wax films. *Journal of the Royal Society Interface*, 13, 1-12.
- Parisio, G., Ferrarini, A., and Sperotto, M. (2016). Model studies of lipid flip-flop in membranes. *International Journal of Advances in Engineering Sciences and Applied Mathematics*, 8, 134–146.
- Pasteur, L. and Lister, J. (1996). Germ theory and its application to medicine and on the antiseptic principle of the practice of surgery. H. C. (translator) Ernst, Eds. Prometheus Books, Amherst, New York. pp. 110-117.
- Pautsch, A., and Schulz, G. (2000). High-resolution Structure of the OmpA membrane domain. *Journal of Molecular Biology*, 298, 273 - 282.
- Penfold, J., and Thomas, R. (1990). Application of the specular refraction of neutrons to the study of surfaces and interfaces. *Journal of Physics: Condensed Matter*, 2, 1369-1412.

- Peschel, A. and Sahl, H. (2006). The co-evolution of host cationic antimicrobial peptides and microbial resistance. *Nature Reviews Microbiology*, 4, 529-536.
- Petty, M. (1996). Monolayer materials: In Langmuir-Blodgett films an introduction. Cambridge, pp. 65- 94. Cambridge University Press.
- Pfaffl, M. (2001). Relative quantification. In: Real-time PCR. Dorak, T. (Ed.). pp. 63- 82. International University Line.
- Pfaffl, M., Tichopad, A., Prgomet, C., and Neuvians, T. (2004). Determination of stable housekeeping genes, differentially regulated target genes and sample integrity: BestKeeper – Excel-based tool using pair-wise correlations. *Biotechnology Letters*, 26, 509–515.
- Pink, D., Truelstrup Hansen, L., Gill, T., Quinn, B., Jericho, M., and Beveridge, T. (2003). Divalent calcium ions inhibit the penetration of protamine through the polysaccharide brush of the outer membrane of Gram negative bacteria. *Langmuir*, 19, 8852–8858.
- Pink, D., Hasan, F., Quinn, B., Winterhalter, M., Mohan, M., and Gill, T. (2014). Interaction of protamine with gram-negative bacteria membranes: possible alternative mechanisms of internalization in *Escherichia coli*, *Salmonella* Typhimurium and *Pseudomonas aeruginosa*. *Journal of Peptide Science*, 20, 240–250.
- Pinto, M., Carvalho, A., Pires, S., Campus, A., Fonseca da Silva, H., Sobral, D., dePaula, J., and de lima Santos, A. (2011). The effects of nisin on *Staphylococcus aureus* count and the physicochemical properties of traditional Minas Serro cheese. *International Dairy Journal*, 21, 90–96.
- Potter, R., Truelstrup Hansen, L., and Gill, T. (2005). Inhibition of foodborne bacteria by native and modified protamine: Importance of electrostatic interactions. *International Journal of Food Microbiology*, 103, 23– 34.
- Powers, J. and Hancock, R. (2003). The relationship between peptide structure and antibacterial activity. *Peptides*, 24 (11), 1681-1691.

- Pratt, L., Hsing, W., Gibson, K., and Silhavy, T. 1996. From acid to osmZ: multiple factors influence synthesis of the OmpF and OmpC porins in *Escherichia coli*. *Molecular Microbiology*. 20 (5): 911- 917.
- Puente, J., Alvarez-Scherer, J., Gusset G., and Calva, E. (1989). Comparative analysis of the *Salmonella typhi* and *Escherichia coli ompC* genes. *Gene*, 83, 197- 206.
- Pynn, R. (1990). An introduction to neutron scattering. Los Alamos National Laboratory. Retrieved from:
https://neutrons.ornl.gov/sites/default/files/intro_to_neutron_scattering.pdf
- Pynn, R. (2009). Neutron Scattering - A Non-destructive microscope for seeing inside matter. In: Neutron applications in earth, energy and environmental sciences. Liang, L., Rinaldi, R., and Schober, H. (Ed.). pp. 15- 36. Springer.
- Ramani, N., Hedeshian, M., and Freundlich, M. (1994). micF antisense RNA has a major role in osmoregulation of OmpF in *Escherichia coli*. *Journal of Bacteriology*, 174, 5005-5010.
- Rantsiou, K., Alessandria, V., Urso, R., Dolci, P., Cocolin, L. (2008). Detection, quantification and vitality of *Listeria monocytogenes* in food as determined by quantitative PCR. *International Journal of Food Microbiology*, 121, 99–105.
- Rasmussen, R (2001) Quantification on the LightCycler. In: Meuer, S, Wittwer, C., Nakagawara, K. (Eds.). Rapid cycle real-time PCR, methods and applications, pp. 21-34. Heidelberg, Springer Press.
- Rathinakumar, R., and Wimley, W. (2008). Biomolecular engineering by combinatorial design and high throughput screening: small, soluble peptides that permeabilize membranes. *Journal of American Chemical Society*, 130, 9849–9858.
- Rathinakumar, R., Walkenhorst, W., and Wimley, W. (2009). Broad-spectrum antimicrobial peptides by rational combinatorial design and high-throughput screening: the Importance of interfacial activity. *Journal of American Chemical Society*, 131, 7609–7617.

- Reeves, P. (1979). The genetics of outer membrane proteins. In: M. Inouye. (Ed.) *Bacterial membranes: biogenesis and functions*, pp. 255-291. New York: Wiley-Interscience.
- Reusch, R. Insights into the structure and assembly of *Escherichia coli* outer membrane protein A. (2012). *FEBS Journal*, 279, 894–909.
- Rosenblatt-Farrell, N. (2009). The landscape of antibiotic resistance. *Environmental Health Perspectives*, 117, A245- A250.
- Roque, A., Ponte, I., and Suau, P. (2011). Secondary structure of protamine in sperm nuclei: an infrared spectroscopy study. *BioMed Central Structural Biology*, 11, 1-8.
- Roussel-Philippe, C., Pina, M., and Graille, K. (2000). Chemical lipophilization of soy protein isolates and wheat gluten. *European Journal of Lipid Science and Technology*, 2000, 97–101.
- Rucker, R. (1993). Chemical modifications of proteins in vivo: Selected examples important to cellular regulation. *The Journal of Nutrition*, 123 (6), 977.
- Ruggirello, M., Dolci, P., and Cocolin, C. (2014). Detection and viability of *Lactococcus lactis* throughout cheese ripening. *PLoS One*, 9, 1- 14.
- Ruiz, N., Kahne, D., and Silhavy, T. (2005). Advances in understanding bacterial outer-membrane biogenesis. *Nature Reviews Microbiology*, 4, 57 – 66.
- Saikaly, P., Barlaz, M., and de los Reyes III, F. (2007). Development of quantitative real-time PCR assays for detection and quantification of surrogate biological warfare agents in building debris and leachate. *Applied and Environmental Microbiology*, 73, 6557–6565.
- Sakaguchi, S., 1950. A new method for the colorimetric determination of arginine. *Journal of Biochemistry*, 37, 231– 236.

- Sanders, M., Clifton L., Frazier, R., and Green, R. (2016). Role of lipid composition on the interaction between a tryptophan-rich protein and model bacterial membranes. *Langmuir*, 32, 2050–2057.
- Santiviago, S., Toro, C., Hidalgo, A., Youderian, P., and Mora, G. (2003). Global regulation of the *Salmonella enterica* serovar Typhimurium major porin, OmpD. *Journal of Bacteriology*, 185, 5901–5905
- Sawyer, J., Martin, N., and Hancock, R. (1988) Interaction of macrophage cationic proteins with the outer membrane of *Pseudomonas aeruginosa*. *Infection and Immunity*, 56, 693- 698.
- Schibli, D., Epanand, R., Vogel, H., and Epanand, R. (2002). Tryptophan-rich antimicrobial peptides: comparative properties and membrane interactions. *Biochemistry and Cell Biology*, 80, 667–677.
- Sevcsik, E., Pabst, G., Richter, W., Danner, S., Amenitsch, H., Lohner, K. (2008). Interaction of LL-37 with model membrane systems of different complexity: influence of the lipid matrix. *Biophysical Journal*, 94:4688–4699.
- Shai, Y. (1999). Mechanism of the binding, insertion and destabilization of phospholipid bilayer membranes by alpha-helical antimicrobial and cell non-selective membrane-lytic peptides. *Biochimica et Biophysica Acta*, 1462, 55-70.
- Shevchenko, A., Tomas1, H., Havlis, J., Olsen, J., and Mann, M. (2006). In-gel digestion for mass spectrometric characterization of proteins and proteomes. *Nature Protocols*, 1, 2856- 2860.
- Singh, S., and Basu, S. (2004). Polarized neutron reflectometry at Dhruva reactor. *Pramana Journal of Physics*, 387-391.
- Singh, S., Miller, S., Williams, Y., Rudd, K., and Nikaido, H. (1996). Immunochemical structure of the OmpD porin from *Salmonella* Typhimurium. *Microbiology*, 142, 3201-3210.
- Singh, S., Williams, Y., Miller, S., and Nikaido, H. (2003). The C-Terminal domain of *Salmonella enterica* Serovar Typhimurium OmpA is an immunodominant antigen

in mice but appears to be only partially exposed on the bacterial cell surface. *Infection and Immunity*, 71, 3937–3946.

Sloan, K. (2005). Protamine's action against *Escherichia coli* depends upon outer membrane structure and electrostatic interactions. M.Sc. Thesis, University of Guelph.

Smith, S., Mahon, V., Lambert, M. and Fagan, R. (2007). A molecular Swiss army knife: OmpA structure, function and expression. *FEMS Microbiology Letters*, 273, 1–11.

Smith, J., and Yada, R. (1991). Lipophilization of *mucor miehei* aspartyl proteinase: Effect on structure-function and stability. *Journal of Food Biochemistry*, 15, 331–346.

Stanton, R. Glucose-6-Phosphate dehydrogenase, NADPH, and cell survival. (2012). *IUBMB Life*, 64, 362–369.

Straus, S., and Hancock, R. (2006). Mode of action of the new antibiotic for Gram-positive pathogens daptomycin: Comparison with cationic antimicrobial peptides and lipopeptides. *Biochimica et Biophysica Acta*, 1758, 1215–1223.

Strömstedt, A., Ringstad, L., Schmidtchen, L., Malmsten, M. (2010). Interaction between amphiphilic peptides and phospholipid membranes. *Current Opinion in Colloid and Interface Science*, 15, 467–478.

Stumpe, S., and Bakker, P. (1997). Requirement of a large K⁺-uptake capacity and of extracytoplasmic protease activity for protamine resistance of *Escherichia coli*. *Archives of Microbiology*, 167, 126–136.

Stumpe, S., Schmid, R., Stephens, D., Georgiou, G. and Bakker, E. (1998). Identification of OmpT as the protease that hydrolyzes the antimicrobial peptide protamine before it enters growing cells of *Escherichia coli*. *Journal of Bacteriology*, 180, 4002–4006.

Sugawara, E., and Nikaido, H. (1992). Pore-forming activity of OmpA protein of *Escherichia coli*. *Journal of Biological Chemistry*, 267, 2507–2511.

- Suzuki K, Ando T. Studies on Protamine: XVII. The complete amino acid sequence of clupeine YI. (1972). *Journal of Biochemistry*, 72, 1433–1446.
- Tenover, F. (2006) Mechanisms of antimicrobial resistance in bacteria. *American Journal of Medicine*, 119, S3–S10.
- Thomassin, J., Brannon, J., Gibbs, B., Gruenheid, S., and Le Mouala, H. (2012). OmpT outer membrane proteases of enterohemorrhagic and enteropathogenic *Escherichia coli* contribute differently to the degradation of human LL-37. *Infection and Immunity*, 80, 483–492.
- Thouzeau, C, Le Maho, Y., Froget, G., Sabatier, L., Le Bohec, C., Hoffmann, J., Bulet, P. (2003). Spheniscins, avian beta-defensins in preserved stomach contents of the king penguin, *Aptenodytes patagonicus*. *Journal of Biological Chemistry*, 278, 51053–51061.
- Toi, K., Bynum, E., Norris, E., and Itano, H. (1967). Studies on the chemical modification of arginine: 1. the reaction of 1,2-cyclohexanedione with arginine and arginyl residues of proteins. *The Journal of Biological Chemistry*, 242, 1036-1043.
- Tolong, (2004). Mechanisms of interaction of cationic antimicrobial peptides with the cytoplasmic membranes of *E. coli* and *S. Typhimurium*. M.Sc. Thesis, Dalhousie University, Department of Food Science and Technology.
- Truelstrup Hansen, L., and Gill, T. (2000). Solubility and antimicrobial efficacy of protamine on *Listeria monocytogenes* and *Escherichia coli* as influenced by pH. *Journal of Applied Microbiology*, 88, 1049 – 55.
- Truelstrup Hansen, L., Austin, J. and Gill, T. (2001). Antibacterial effect of protamine in combination with EDTA and refrigeration. *International Journal of Food Microbiology*, 66, 149-161.
- Tunio, S., Oldfield, Ala'Aldeen, D., Wooldridge, W., and Turner, D. (2010). The role of glyceraldehyde 3-phosphate dehydrogenase (GapA-1) in *Neisseria meningitidis* adherence to human cells. *BMC Microbiology*, 10, 280 – 290.

- Ueno, R., Fujita, Y., Yamamoto, M., and Kozakai, H. (1988). Multiplication inhibitor for *Bacillus cerus*. European patent application, 0372091. *European Patent Office*, Great Britain.
- Ueno, R., Fujita, Y., Nagamura, Y., Kamino, Y., and Tabata, A. (1989). Method for preserving food. European Patent Application 0372 091.
- Vandeputte-Rutten, L., Kramer, A., Kroon, J., Dekker, N., Egmond, M., and Gros, P. (2001). Crystal structure of the outer membrane protease OmpT from *Escherichia coli* suggests a novel catalytic site. *The EMBO Journal*, 20, 5033 – 5039.
- van der Heijden, J., Reynolds, L., Deng, W., Mills, A., Scholz, R., Imami, K., Foster, L., Duong, F., and Finlay, B. (2016). *Salmonella* rapidly regulates membrane permeability to survive oxidative stress. *Mbio American Society of Microbiology*, 7:e01238-16.
- Varik, V., Oliveira, S., Hauryliuk, V., and Tenson, T. (2016). Composition of the outgrowth medium modulates wake-up kinetics and ampicillin sensitivity of stringent and relaxed *Escherichia coli*. *Scientific Reports*, 6, 1-10.
- Verraes, C., Van Boxtael, S., Van Meervenne, E., Van Coillie, E., Butaye, P., Catry, B., Athénaïs de Schaetzen, M., Van Huffel, X., Imberechts, H., Dierick, K., Daube, G., Saegerman, C., De Block, J., Dewulf, J., and Herman, L. (2013). Antimicrobial resistance in the food chain: A Review. *International Journal of Environmental Research and Public Health*, 10, 2643-2669.
- Vinson, H., Gautam, A., Olet, S., Gibbs, P., and Barigye, R. (2010). Molecular analysis of porin gene transcription in heterogenotypic multidrug-resistant *Escherichia coli* isolates from scouring calves. *Journal of Antimicrobial Chemotherapy*, 65, 1926–1935.
- Vlieghe, P., Lisowski, V., Martinez, J., and Khrestchatisky, M. (2010). Synthetic therapeutic peptides: science and market. *Drug Discovery Today*, 15, 40-56.

- Vogel, C., and Marcotte, E. (2013). Insights into the regulation of protein abundance from proteomic and transcriptomic analyses. *Nature Reviews Genetics*, 13, 227–232.
- Vorobyov, I., and Allen, T. (2011). On the role of anionic lipids in charged protein interactions with membranes. *Biochimica et Biophysica Acta*, 1808, 1673–1683.
- Wacklin, H., Thomas, R. (2007). Spontaneous formation of asymmetric lipid bilayers by adsorption of vesicles. *Langmuir*, 23, 7644–7651.
- Wang, Y. (2002). The function of OmpA in *Escherichia coli*. *Biochemical and Biophysical Research Communications*, 292, 396–401.
- Wang, H., Liang, X., Zhao, R., Feng, L., and Li, H. (2008). Spectrophotometric determination of arginine in grape juice using 8-hydroquinoline. *Agricultural Sciences in China*, 10, 1210-1215.
- Wang, S., Zeng, X., Yang, Q., and Qiao, S. (2016). Antimicrobial peptides as potential alternatives to antibiotics in food animal industry. *International Journal of Molecular Sciences*, 17, 603-615.
- Warry, N., Mazanderani, S., and Sall, K. (2008). Controlling the growth rate of *Escherichia coli* by limiting the supply of carbon in an amylose-amylase nutrient system. *Journal of Experimental Microbiology and Immunology*, 12, 1-6.
- Weatherspoon-Griffin, N., Zhao, G., Kong, W., Kong, Y., Morigen, Andrews-Polymenis, H., McClelland, M., and Shi, Y. (2011). The CpxR/CpxA two-component system up-regulates two Tat-dependent peptidoglycan amidases to confer bacterial resistance to antimicrobial peptide. *The Journal of Biological Chemistry*, 286, 5529–5539.
- Weatherspoon-Griffin, N., Yang, D., Kong, W., Hua, Z., and Shi, Y. (2014). The CpxR/CpxA two-component regulatory system up-regulates the multidrug resistance cascade to facilitate *Escherichia coli* resistance to a model antimicrobial peptide. *The Journal of Biological Chemistry*, 289, 32571-32582.

- Weber, H., Engelmann, S., Becher, D., and Hecker, M. (2004). Oxidative stress triggers thiol oxidation in the glyceraldehyde-3-phosphate dehydrogenase of *Staphylococcus aureus*. *Molecular Microbiology*, 52, 133–140.
- Wiegand, I., Hilpert, K., and Hancock, R. (2008). Agar and broth dilution methods to determine the minimal inhibitory concentration (MIC) of antimicrobial substances. *Nature Protocols*, 3, 163-175.
- Wimley, W., (2010). Describing the mechanism of antimicrobial peptide action with the interfacial activity model. *American Chemical Society Chemical Biology*, 5, 905–917.
- Wimley, W., and Hristova, K. (2011). Antimicrobial Peptides: successes, challenges and unanswered questions. *Journal of Membrane Biology*, 239, 27–34.
- Wong, P., Nakamura, S., and Kitts, D. (2006). Functional and biological activities of casein glycomacropeptide as influenced by lipophilization with medium and long chain fatty acid. *Food Chemistry*, 97, 310-317.
- Wong, M., and Medrano, J. (2005). Real-time PCR for mRNA quantitation. *BioTechniques*, 39:75-85.
- Woolhouse, M., Webster, J., Domingo, E., Charlesworth, B., and Levin, B. (2002). Biological and biomedical implications of the co-evolution of pathogens and their hosts. *Nature Genetics*, 32, 569- 577.
- Woolhouse, M., Ward, M., van Bunnik, B., and Farrar, J. (2015). Antimicrobial resistance in humans, livestock and the wider environment. *Philosophical Transactions of the Royal Society*, B, 1-7.
- Wu, M., Maier, E., Benz, R., and Hancock, R. (1999). Mechanism of interaction of different classes of cationic antimicrobial peptides with planar bilayers and the cytoplasmic membrane of the *Escherichia coli*. *Biochemistry*, 38, 7235–7242.
- Yan, S. and Gilbert, J. (2004). Antimicrobial drug delivery in food animals and microbial food safety concerns: An overview of in vitro and in vivo factors potentially

- affecting the animal gut microflora. *Advanced Drug Delivery Reviews*, 56, 1497-1521.
- Yeaman, M. and Yount, N. (2003). Mechanism of antimicrobial peptide action and resistance. *Pharmacological Reviews*, 55, 27-55.
- Zasloff, M. 1987. Magainins, a class of antimicrobial peptides from *Xenopus* skin: isolation, characterization of two active forms, and partial cDNA sequence of a precursor. *Proceedings of the National Academy of Science, USA*. 84, 5449–5453.
- Zasloff, M. (2002). Antimicrobial peptides of multicellular organisms. *Nature*, 415, 389-395.
- Zhang L., Rozek A., and Hancock, R. Interaction of cationic antimicrobial peptides with model membranes. (2001). *The Journal of Biological Chemistry*, 276, 35714-35722.
- Zhu, X., Shan, A., Ma, Z., Xu, W., Wang, J., Chou, S., and Cheng, B. (2015). Bactericidal efficiency and modes of action of the novel antimicrobial peptide T9W against *Pseudomonas aeruginosa*. *Antimicrobial Agents and Chemotherapy*, 59, 3008 – 3017.
- Zhu, W., Smith, J., and Huang, C. (2009). Mass spectrometry-based label-free quantitative proteomics. *Journal of Biomedicine and Biotechnology*, 2010, 1-6.

APPENDICES

Appendix A: q-PCR

Table A-1. Precision of q-PCR reaction expressed as mean $C_q \pm SD$ (standard deviation) for target genes and reference genes from *E. coli* K-12 and *S. enterica* Typhimurium 14028 cells exposed to native clupeine. These experiments were repeated three times.

Genes of Interest	Mean $C_q \pm SD$
<i>E. coli</i> K-12 Native	
<i>ompF</i>	
Untreated	23.46 \pm 0.09
500 $\mu\text{g/mL}$	25.20 \pm 0.13
1000 $\mu\text{g/mL}$	22.10 \pm 0.21
1250 $\mu\text{g/mL}$	25.25 \pm 0.03
<i>ompC</i>	
Untreated	24.61 \pm 0.05
500 $\mu\text{g/mL}$	23.62 \pm 0.02
1000 $\mu\text{g/mL}$	21.99 \pm 0.05
1250 $\mu\text{g/mL}$	24.26 \pm 0.17
<i>ompT</i>	
Untreated	21.73 \pm 0.06
500 $\mu\text{g/mL}$	24.29 \pm 0.19
1000 $\mu\text{g/mL}$	22.10 \pm 0.39
1250 $\mu\text{g/mL}$	23.38 \pm 0.14
<i>rpoB</i>	
Untreated	23.73 \pm 0.12
500 $\mu\text{g/mL}$	23.79 \pm 0.08
1000 $\mu\text{g/mL}$	22.33 \pm 0.23
1250 $\mu\text{g/mL}$	24.56 \pm 0.19
<i>S. enterica</i> Typhimurium Native	
<i>ompF</i>	
Untreated	26.34 \pm 0.05
500 $\mu\text{g/mL}$	33.72 \pm 0.05
1250 $\mu\text{g/mL}$	25.14 \pm 0.07
2500 $\mu\text{g/mL}$	22.17 \pm 0.04
<i>ompC</i>	
Untreated	26.57 \pm 0.03
500 $\mu\text{g/mL}$	33.80 \pm 0.18
1250 $\mu\text{g/mL}$	28.56 \pm 0.27
2500 $\mu\text{g/mL}$	26.25 \pm 0.13

<i>rpoB</i>	
Untreated	26.59±0.12
500 µg/mL	33.13±0.14
1250 µg/mL	25.29± 0.16
2500 µg/mL	25.89±0.12

Table A-2. Precision of q-PCR reaction expressed as mean $C_q \pm$ SD (standard deviation) for target genes and reference genes from *E. coli* K-12 and *S. enterica* Typhimurium

14028 cells exposed to CHD-treated clupeine. These experiments were repeated three times.

Genes of Interest	Mean C_q ± SD
<i>E. coli</i> K-12 CHD-treated	
<i>ompF</i>	
Untreated	22.79 ± 0.11
400 µg/mL	23.37 ± 0.14
1000 µg/mL	24.44 ± 0.02
1250 µg/mL	26.31 ± 0.09
<i>ompC</i>	
Untreated	25.43 ± 0.16
400 µg/mL	25.57 ± 0.12
1000 µg/mL	25.54 ± 0.09
1250 µg/mL	25.75 ± 0.03
<i>ompT</i>	
Untreated	26.59 ± 0.05
400 µg/mL	33.13 ± 0.04
1000 µg/mL	25.29 ± 0.06
1250 µg/mL	25.89 ± 0.14
<i>rpoB</i>	
Untreated	22.67 ± 0.02
400 µg/mL	21.93 ± 0.11
1000 µg/mL	22.83 ± 0.04
1250 µg/mL	24.35 ± 0.18
<i>S. enterica</i> Typhimurium 14208	
CHD- treated	
<i>ompF</i>	
Untreated	25.55 ± 0.03
500 µg/mL	28.38 ± 0.17
1250 µg/mL	24.30 ± 0.19
2500 µg/mL	27.22 ± 0.16
<i>ompC</i>	
Untreated	24.66 ± 0.06
500 µg/mL	25.51 ± 0.16
1250 µg/mL	21.90 ± 0.09
2500 µg/mL	27.67 ± 0.14
<i>rpoB</i>	
Untreated	26.74 ± 0.10
500 µg/mL	27.36 ± 0.03
1250 µg/mL	24.54 ± 0.05
2500 µg/mL	29.98 ± 0.03

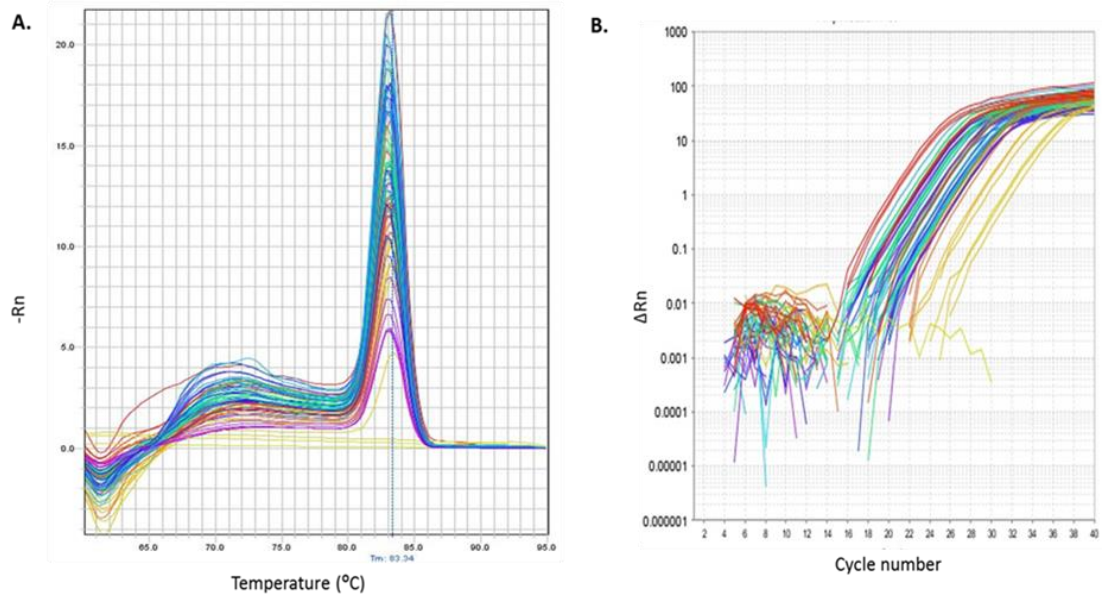


Figure A-1. (A) Example of a melt curve, and (B) an amplification plot for *E. coli ompF*.

Appendix B: Buffers and Reagents for Porin Protein Extraction

M9 Minimal growth media (modified from Sambrook et al., 1989; Forst et al., 1988):

5X Salt (20%):

- Add 160 mM Na₂HPO₄, 80 mM KH₂PO₄, 40 mM NaCl, 72 mM NH₄Cl, 0.8mM MgSO₄.7H₂O
- Glucose Salt Stock Solution:
 - 0.4% filter sterilized glucose solution.
- Thiamine, 2 µg/mL and Biotin, 0.008%.

Buffer for Washing Cells:

- 1mM EDTA (pH 7.0) or
- 10 mM Tris-HCl, pH 8.0

Buffer for Cell Lysis (pH, 8.0):

- 10 mM Tris-HCl
- 5% sucrose
- 0.1 M NaCl
- 3 mM NaN₃
- DNase 100 µL (stock conc. 1 mg/mL)
- 2 protease inhibitor tablets (Roche)

Buffer for DNase/RNase Treatment of Bacterial Cells (pH, 8.0)

- 10mM Tris-HCl
- 3 mM NaN₃
- 20 mM MgSO₄
- DNase 100 µL (stock conc. 1mg/mL)
- RNase 100 100 µL (stock conc. 1mg/mL)
- 1 protease inhibitor cocktail tablet (Roche) or 1 mM PMSF, phenylmethanesulfonylfluoride or phenylmethylsulfonyl fluoride, serine protease inhibitor).

Buffers for Detergent Extraction:

- (a) Pre-extraction of crude envelopes (pH, 8.0):
- 10 mM Tris-HCl

- 3 mM NaN₃
- 1 mM EDTA
- 3 mM DDT
- 0.5% octyl-POE (Poly (ethylene glycol) octyl ether)
- Leave overnight at 4°C or spin at 29,000 x g for 90 min (4°C).

(b) Buffer for Extraction of Porin Samples (pH, 8.0):

- 10mM Tris-HCl
- 3 mM NaN₃
- 1 mM EDTA
- 3 mM DDT (dithiothreitol, antioxidant used to stabilize enzymes and other proteins containing sulfhydryl groups)
- 3% O-POE

Buffers Used for Porin Protein Extraction

- **Citric Acid buffer:**
 - Add 0.1M citric acid A (21.01 g in 1000 mL) and 0.1 M sodium citrate B (29.41 g in 1000 mL), pH 3.46.
- **Dialysis buffer:**
 - Add citric acid buffer, pH 3.46
 - 150 mM NaCl
 - 1% O-POE
 - One hundred microliters of each protease inhibitor (Leupeptin hemisulfate salt; pepstatin and aprotinin).
- **Buffers Used for Cation Exchange:**
- **Buffer 1:**
 - Add citric acid buffer, pH 3.46
 - 1 M NaCl
 - 1% O-POE
 - 10 µL of each protease inhibitor (Leupeptin hemisulfate salt; pepstatin and aprotinin).
- **Buffer 2:**
 - Add citric acid buffer, pH 3.46
 - 185 mM NaCl

- 1% O-POE
 - 10 μ L of each protease inhibitor (Leupeptin hemisulfate salt; pepstatin and aprotinin).
-
- **Buffer 3 (Elution buffer):**
 - Add citric acid buffer, pH 4.81
 - 300 mM NaCl
 - 1% O-POE
 - 10 μ L of each protease inhibitor (Leupeptin hemisulfate salt; pepstatin and aprotinin).
-
- **Buffer 4 (Elution buffer):**
 - Add citric acid buffer, pH 4.81
 - 1M NaCl
 - 1% O-POE
 - 10 μ L of each protease inhibitor (Leupeptin hemisulfate salt; pepstatin and aprotinin).
-
- **Preparation of Protease Inhibitors:**
 - Pepstatin: 1 mg/mL in 10% (v/v) acetic acid in methanol
 - Aprotinin: 1 mg/mL in d-H₂O
 - Leupeptin: 0.2 mg/mL in d-H₂O.

Appendix C: NR and XRR

Synchrotron Facility

ISIS (NR) and Diamond Light Centre (XRR) (Rutherford Appleton Laboratory, Oxfordshire, UK) are institutions open to researchers interested in using synchrotron sources for experiments. The services offered at Diamond are free for researchers who are prepared to publish in the public domain. The first step involves applying for beamtime by submitting a proposal, which is assessed for technical feasibility, safety assessment and scientific merit. Proposals are reviewed and graded by review committees and if accepted users are awarded time on the instruments requested to carry out their experiments.

All successful proposals are assigned to a beam scientist who will guide their use of the equipment for the duration of the beamtime experiment, and the beamline scientist usually contacts the principal investigator to provide details of the experiment timeline and discuss any special sample preparation that might be needed on site for the experiments. Preparing for beamtime also involves registration of all the experimental team members and completing all the necessary safety tests and requirements (Figure C-1). Since most of the experiments were about three to four consecutive days, on site accommodation was available at Ridgeway House for all users and guests, and accommodation arrangements must be made before arriving on site. In addition, having at least three members on the team was also helpful for different shifts to prepare samples and collect data.

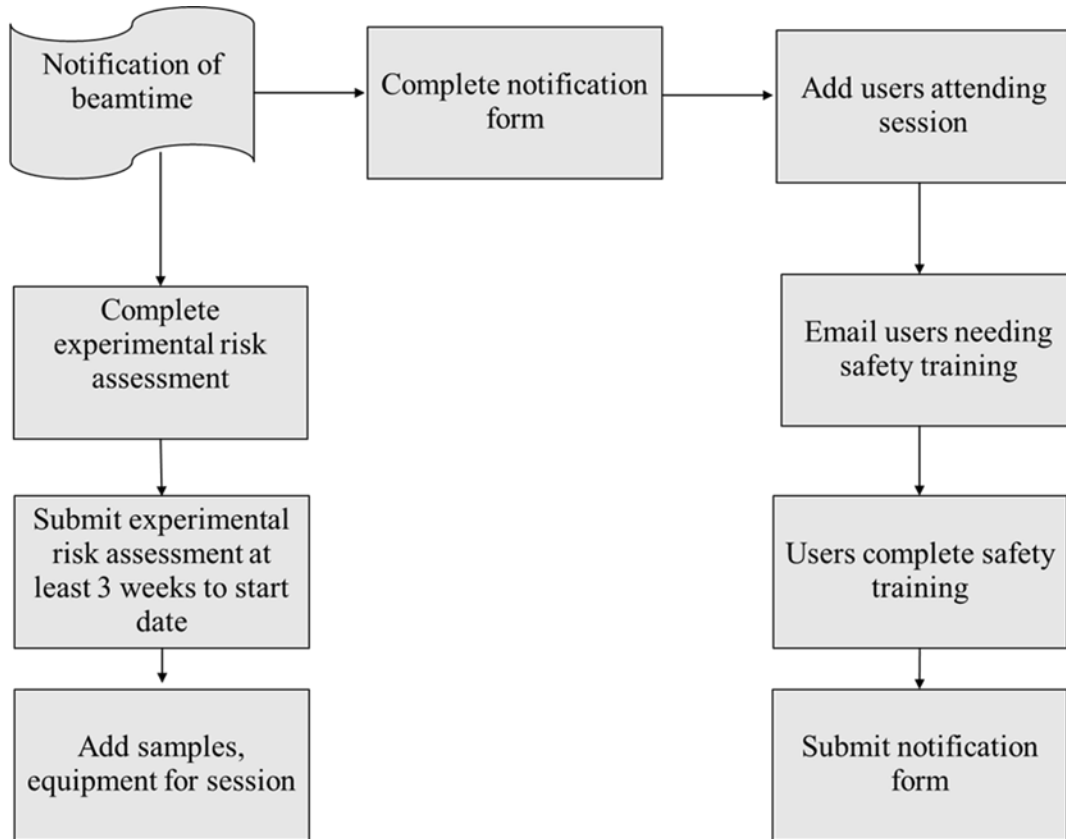


Figure C-1. Summary of some steps involved in preparing for beamtime experiments. <http://www.isis.stfc.ac.uk>

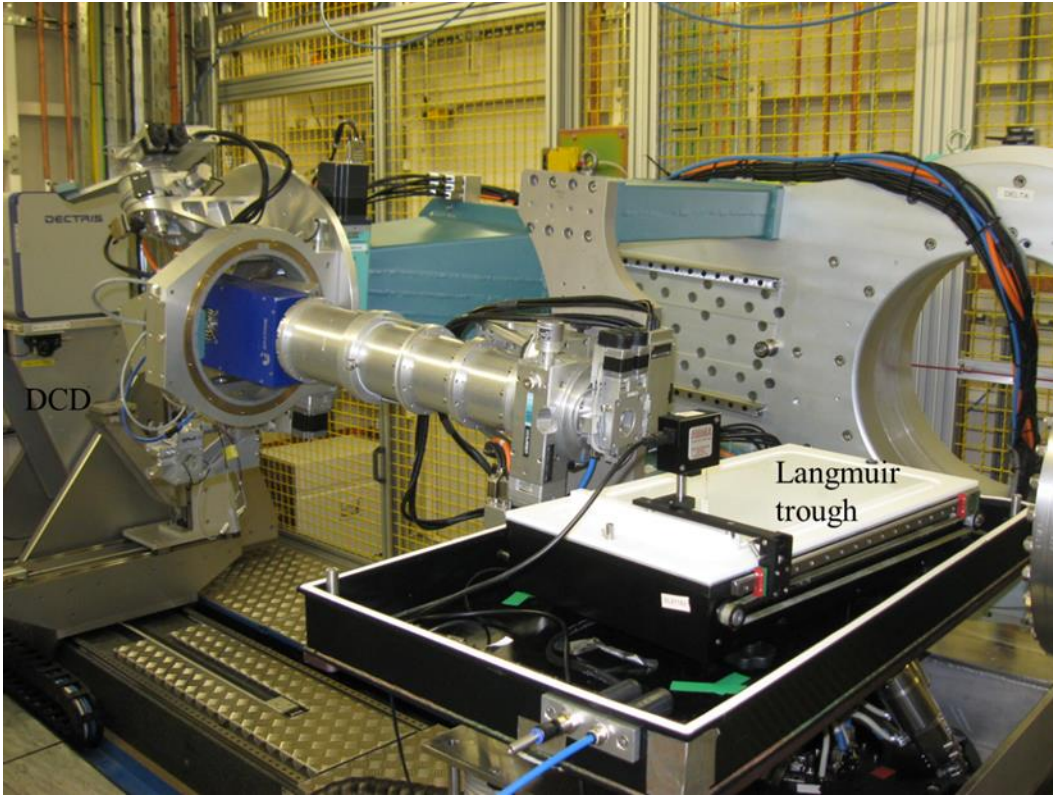


Figure C-2. Double Crystal Detector (DCD) and Langmuir trough setup for XRR experiment.

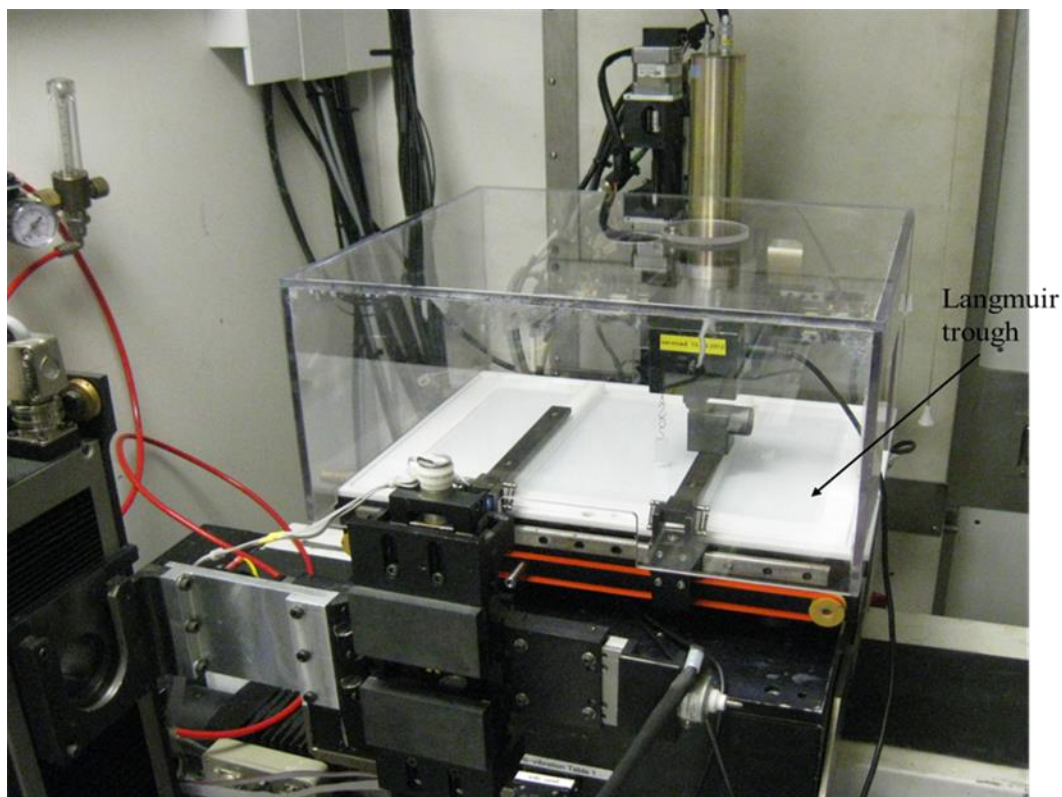


Figure C-3. Langmuir trough for NR experiment.

Table C-1. Calculated scattering lengths, scattering length densities, molecular weights and molecular volumes and the ratios of DPPG used in this thesis.

Lipid DPPG	Scattering length Σb (10^{-3} \AA)	SLD (10^{-6} \AA^{-2})	Molecular weight (g/mol)	Molecular Volume (\AA^3)
h-DPPG (lipid + tail)	0.3904	0.360	721	1093
h-DPPG head group	0.617	2.181	298	283
d-DPPG tail	6.130	7.540	484	813.4
h-DPPG tail	-0.324	-0.398	422	813.4
17% of h-DPPG (lipid + tail)	0.0663	0.0612	122.6	185.8
17% of h-DPPG (head group)	0.1049	0.3708	50.7	48.1
17% of h-DPPG tail	-0.055	-0.0677	71.3	138.3
17% of d-DPPG tail	1.0421	1.2818	82.3	138.3

Table C-2. Calculated scattering lengths, scattering length densities, molecular weights, molecular volumes and the ratios of DPPE used in this thesis.

Lipid DPPE	Scattering length $\sum b$ (10^{-3}\AA)	SLD (10^{-6}\AA^{-2})	Molecular weight (g/mol)	Molecular Volume (\AA^3)
h-DPPE (lipid + tail)	0.302	0.280	691	1097
h-DPPE head group	0.560	2.000	257	280
d-DPPE tail	6.130	7.540	484	813.4
h-DPPE tail	-0.324	-0.398	422	813.4
79% of h-DPPE (lipid + tail)	0.2356	0.2212	546	866.6
79% of h-DPPE (head group)	0.4424	1.580	203	221.2
79% of h-DPPE tail	-0.253	-0.314	333.4	642.6
79% of d-DPPE tail	4.843	5.957	382.4	642.6

Table C-3. Calculate scattering lengths, scattering lengths, scattering length densities, molecular weights, molecular volumes and the ratios of cardiolipin used in this thesis.

Lipid CL	Scattering length $\sum b$ (10^{-3}\AA)	SLD (10^{-6}\AA^{-2})	Molecular weight (g/mol)	Molecular Volume (\AA^3)
h-CL (head + tail)	0.85	0.45	1284	1880
h-CL head group	1.26	2.73	481	482
d-CL tail	8.79	6.20	790	1419
h-CL tail	-0.432	-0.304	728	1419
4% of h-CL (head + tail)	0.034	0.018	51.4	75.2
4% of h-CL head group	0.050	0.109	19.2	18.5
4% of h-CL tail	-0.017	-0.012	29.1	56.8
4% of d-CL tail	0.352	0.250	31.6	56.8

Appendix D: Bilayer Experiments

Langmuir-Blodgett/Schaeffer Deposition Procedure:

1. **Calibrate instrument with no sample on the water surface.**
 - a. Move detector to the center of the trough.
 - b. Detects water level in x and y direction.
 - c. Calibrate laser for optimal reflectivity off the water surface.

2. **Langmuir-Blodgett (vertical) dip:**
 - a. Place the neutron cell inside the trough and pump water through to remove air bubbles.
 - b. Check that the water is clean and open the barriers.
 - c. Attach the silicon block in a vertical position for the Blodgett dipping.
 - d. Submerge the block under water.
 - e. Check for any impurities and reset the pressure to zero.
 - f. Open barriers and deposit lipid to reach an initial pressure of $\sim 10 \text{ mNm}^{-1}$ and allow 10 to 15 min for the solvent to evaporate.
 - g. Compress the monolayer to $\sim 35 \text{ mNm}^{-1}$ and relax the monolayer and repeat 2 to 3 times.

When the pressure is stable start raising the block with a speed of $\sim 3 \text{ mm/min}$ (this takes about 45 min).

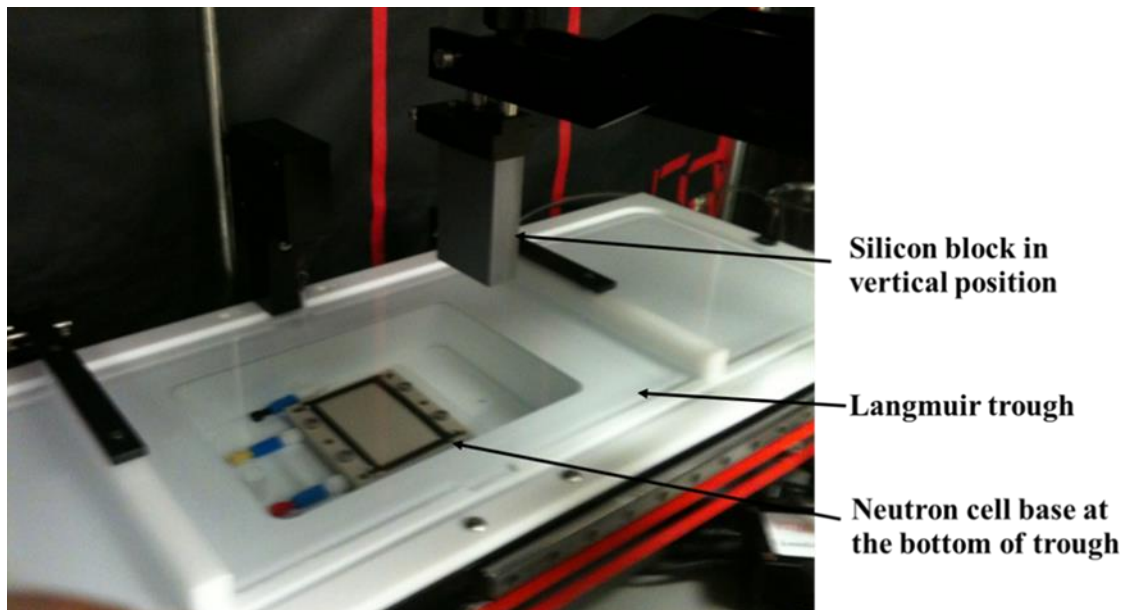
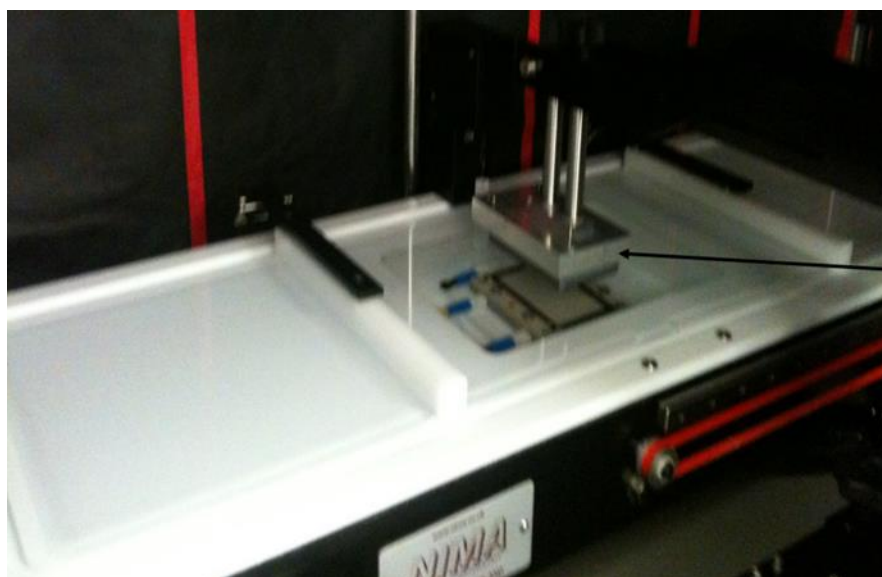


Figure D-1. Silicon block in vertical position for Langmuir-Blodgett dip.

3. Langmuir-Schaeffer (horizontal) dip:

- a. Set the dipper speed to 4 mm/min.
- b. Turn on Pressure Control at desired pressure.
- c. Start dipping the sample.
- d. When the block and holder is submerged – increase dipping speed and take the block and holder to the neutron cell.
- e. Unscrew the block holder (using a pair of pliers).
- f. Press the block gently against the cell with a screw-driver (via the hole in the holder) and raise the dipper to detach the block holder from the block.
- g. Attach the top of the cell onto the block.



**Silicon block
in horizontal position**

Figure D-2. Silicon block in horizontal position for Langmuir-Schaeffer dip.

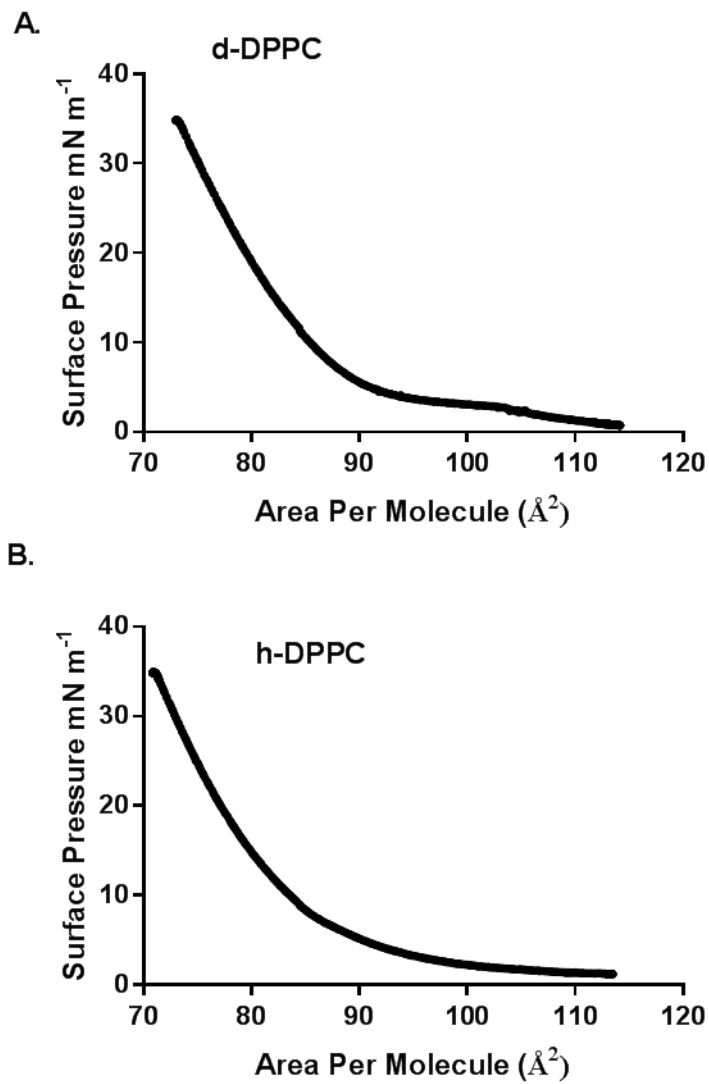


Figure D-3. Isotherms formed from deuterated (A) and hydrogenated (B) DPPC used in bilayer preparation.

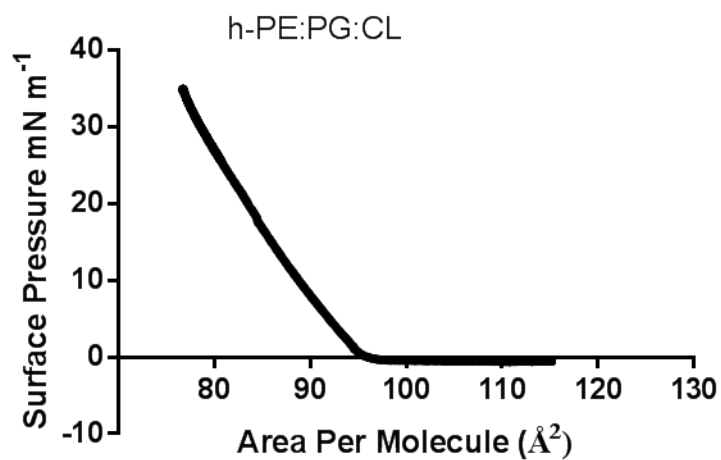


Figure D-4. Isotherm formed from h-PE:PG:CL mixed lipid used in the bilayer formation.

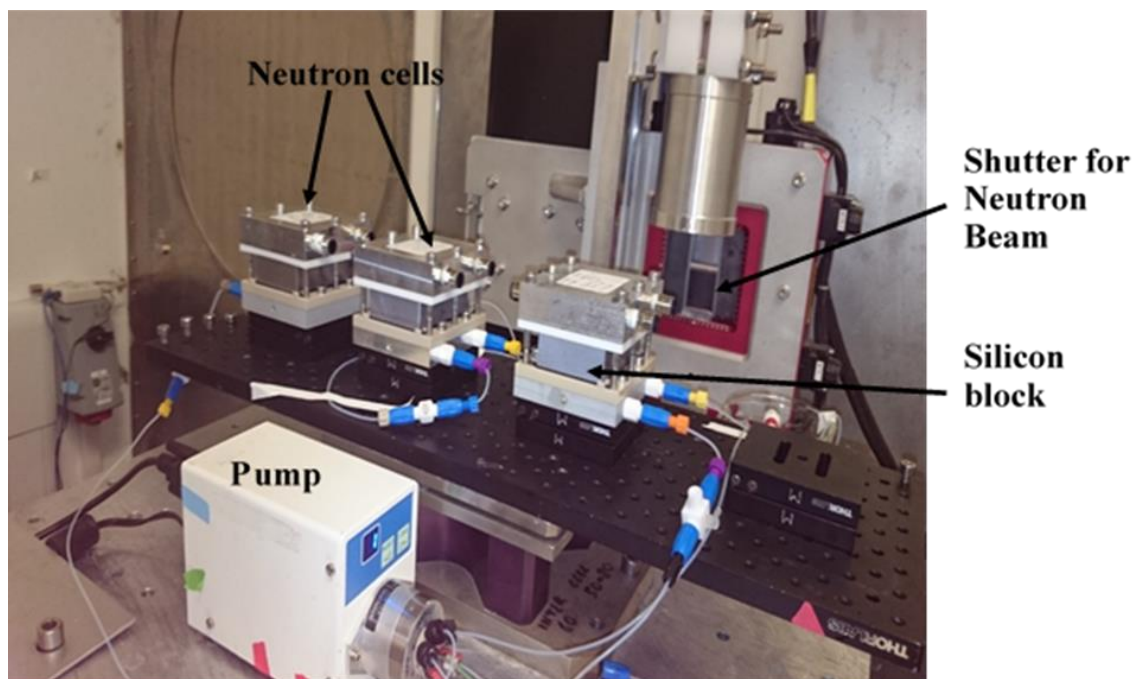


Figure D-5. Neutron sample flow cell containing DPPC:PE:PG:CL bilayer supported on silicon blocks. The flow cells are connected to a pump for the exchange of solutions.

Appendix E: Data Fitting

Fitting the Monolayer Data (NR and XRR):

All NR and XRR data were fitted using RasCal which is a MATLAB-based application developed specifically for NR and XRR data analysis (A. Hughes, ISIS Spallation Neutron Source, Rutherford, Appleton laboratory). The SLD values were set to be within the theoretical calculated ranges (Table 4-1). For the native peptide, the primary sequence was known and this was used to calculate the theoretical SLD of the native peptide using the online Biomolecular SLD calculator (<http://psldc.isis.rl.ac.uk/Psldc/>), the D₂O% of the solution was set to 8% for NRW and the percent of labile hydrogens that can exchange with the solution was set to 95%. However, for the CHD-treated peptide, the primary sequence was not known and there was uncertainty about the exact number of protons exchanged. As a result, the theoretical SLD of the CHD-treated peptide was assumed to be the same as the native peptide. Consequently, any differences in the ‘dry’ SLD which might have occurred with modifying the native clupeine to form CHD-treated clupeine would not have been accounted for in the calculations. The upper and lower limits for all the SLD values were set to the lowest theoretical SLD of the component to the highest theoretical SLD of the different components.

On the bare d-PE:PG:CL and h-PE:PG:CL monolayers, the roughness parameters were linked for all the layers including the XRR contrast and SLD, and thickness parameters were fitted individually, however, the roughness parameters were linked for all the layers. When fitting in the presence of the peptides it might have been possible to fit as a thick rough head group, however a protein layer, with its own thickness and

roughness parameters was added to the NR and XRR contrast. Similar to the bare monolayer, all the parameters were fitted and the best fit values are shown in Tables 4-2 to 4-4.

The experimental parameters were set up with separate backgrounds, scale factors and Qz shifts for the NR and XRR contrasts. In addition, separate SLD values were set for the bulk-out solutions and were appropriately assigned to each contrast since the SLD for the NRW ($0 \times 10^{-6} \text{ \AA}^{-2}$) and XRR water/buffer ($9.025 \times 10^{-6} \text{ \AA}^{-2}$) are very different. Taken together this approach helped to better constrain the fits and improve confidence in the interpretation of the data.

Fitting the Bilayer Data (NR):

A five-layer model was used to describe the interfacial structure of the bilayer. The layer closest to the silicon substrate was silicon dioxide and was described as layer 1, layer 2 was the head group of the inner lipid (DPPC), and layer 3 was described as the inner tail. The fourth layer was described as the outer tail (PE:PG:CL), whereas the fifth layer was described as the outer head group and represented the head group region of the mixed lipid (Figure 5-3). A hydration parameter was assigned for each layer of the model and the upper and lower limits for the head group region were based on the theoretical calculations of each component in the head group (PE:PG:CL) in the ratio 79:17:4.

During the fitting of the bilayer data the hydration, SLD and thickness parameters were fitted individually, whereas the roughness parameters were linked for all the layers because they were assumed to be dependent on the roughness of the silicon block. In

addition, the SLD values of the lipid head groups were set to be within the theoretical calculated ranges (Table 5.2). However, the SLD of the inner and outer tails were fixed at $7.45 \times 10^{-6} \text{ \AA}^{-2}$ and $-0.39 \times 10^{-6} \text{ \AA}^{-2}$, respectively.

The hydrogenated lipids were also used to determine the changes in the bilayer in the presence of the two peptides. For this analysis the deuterated lipids were not used because they dominated the SLD profiles and subtle changes in SLD could not be distinguished. Before fitting these data the inner and outer tails were locked at their theoretical values and an additional layer was included in the model for the protein as described by Dabkowska et al. (2009).

Table E-1. Best fit values and error estimates of asymmetrically deposited bare d-DPPC (inner leaflet) *E. coli* PE:PG:CL (outer leaflet) bilayer deposited on a silicon surface.

Parameters of the Bilayer	Bare d-bilayer
Oxide layer thickness (Å)	11.1 ± 0.96
Oxide layer hydration (%)	17.61 ± 4.62
Oxide layer roughness (Å)	3.99 ± 0.31
Inner head group SLD ($E^{-6} \text{ \AA}^{-2}$)	1.10 ± 0.01
Inner head group hydration (%)	3.06 ± 3.57
Inner head group thickness (Å)	12.99 ± 0.72
Inner tail SLD ($E^{-6} \text{ \AA}^{-2}$)	5.08 ± 0.12
Inner tail hydration (%)	20.19 ± 2.05
Inner tail thickness (Å)	24.99 ± 0.45
Outer tail SLD ($E^{-6} \text{ \AA}^{-2}$)	2.01 ± 0.20
Outer tail hydration (%)	19.45 ± 3.51
Outer tail thickness (Å)	23.89 ± 1.03
Outer head group SLD ($E^{-6} \text{ \AA}^{-2}$)	1.01 ± 0.16
Outer head group hydration (%)	37.79 ± 1.21
Outer head group thickness (Å)	11.99 ± 1.25
Bilayer roughness	3.03 ± 0.69

On addition of native or CHD-treated clupeine, the thickness of the outer head group regions and their corresponding SLDs were allowed to vary as fitting parameters.

However, it was assumed that no changes in the inner tails and inner head group regions of the bilayer would occur, thus these parameters were not fitted in the presence of the native or CHD-treated peptides (Table 5-7).